Modelling stromal-competent human lymph nodes *in vitro*

Andrew I. Morrison

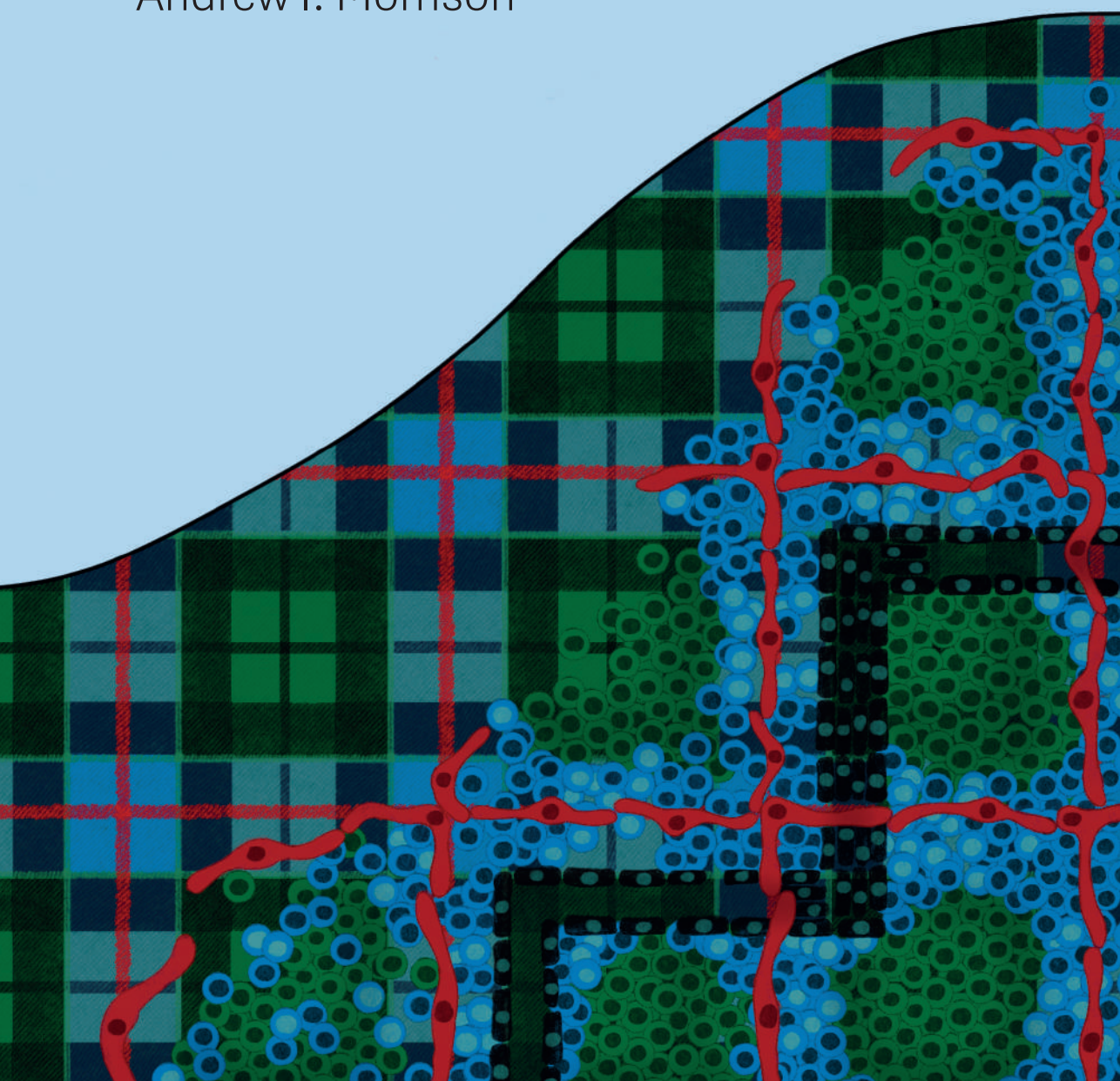

Modelling stromal-competent human lymph nodes *in vitro*

Andrew I. Morrison

ISBN: 978-94-6473-823-0
DOI: http://doi.org/10.5463/thesis.1221

Layout design: Sofa Pinni
Cover design: Ana Merino Vico
Printing: Ipskamp Printing Enschede

VRIJE UNIVERSITEIT

MODELLING STROMAL-COMPETENT HUMAN LYMPH NODES *IN VITRO*

ACADEMISCH PROEFSCHRIFT

ter verkrijging van de graad Doctor of Philosophy
aan de Vrije Universiteit Amsterdam,
op gezag van de rector magnificus
prof.dr. J.J.G. Geurts,
volgens besluit van de decaan
van de Faculteit der Geneeskunde
in het openbaar te verdedigen
op maandag 30 juni 2025 om 9.45 uur
in de universiteit

door

Andrew Ingram Morrison

geboren te Kirkcaldy, Verenigd Koninkrijk

promotoren:	prof.dr. R.E. Mebius
	prof.dr. S. Gibbs
copromotoren:	dr. C.M. de Winde
	dr. J.J. Koning
promotiecommissie:	prof.dr. T.D. de Gruijl
	dr. E.G.M. van Baarsen
	prof.dr. A.D. van der Meer
	dr. T. Cupedo
	dr. M. Coppola
	prof.dr. J.D. van Buul

Table of contents

1

General Introduction

The human immune system has evolved over time to ensure the continuous survival of the human race. It maintains global health by reducing morbidity and mortality, with individuals protected from infectious diseases, cancers, and other pathological conditions. The immune system is composed of an intricate arrangement of immune cells and organs that act efficiently to identify and eliminate bacteria, viruses and parasites, as well as distinguishing these pathogenic threats from the body's own cells. Furthermore, the immune system's adaptability is critical for the global success of vaccination, which has revolutionised world health with full eradication of smallpox[1] and near-eradication of other diseases like polio[2]. Beyond this, the immune system plays a pivotal part in the pathology of chronic conditions, including autoimmune disorders and allergies, as well as in the emerging fields of cancer immunotherapy and regenerative personalised medicines. In the face of societal challenges, such as antimicrobial resistance, pandemics and an aging population, understanding and enhancing immune functions are central to advancing healthcare and improving quality of life worldwide.

The human immune system contains around 1.8 trillion immune cells[3], comprising either the innate or adaptive branch of immunology. Innate immunity is the first line of defence, where a non-specific response is initiated to stop the spread of foreign pathogens. These cells include natural killer (NK) cells, neutrophils, dendritic cells (DC), macrophages and monocytes, which sense pathogenic challenge via pattern recognition receptors (PRRs)[4] and offer a quick immune response, such as phagocytosis. The adaptive immune response is the second line of defence, where a specific immune response is elicited after recognition of molecular fragments called antigens. T and B cells, collectively known as lymphocytes, offer long-lasting memory reactions to the same pathogenic threat, either through direct cell killing by T cells or neutralisation via immunoglobulin (antibody) production by B cells.

All immune cells are derived from, and matured in, primary lymphoid organs (Fig. 1). The bone marrow is the site of haematopoiesis and is where hematopoietic stem cells (HSCs) are generated, which can then differentiate into either common myeloid progenitor (innate) or lymphoid progenitor (adaptive) cells. This is also where B cells mature, whereas T cells undergo maturation in the thymus through processes that harbour T cells with functional potential (clonal selection) and eliminate self-reactive T cells (clonal deletion).

Secondary lymphoid organs include lymph nodes (LNs), tonsils, peyer's patches and spleen. They are a critical component of human immunology with ~500 LNs found throughout the body, located mainly in the abdomen, groin and thoracic cavity[5,6]. LNs are the place where lymphocytes are activated by antigen-presenting cells (APCs), as well as an important location for immune surveillance to monitor pathogens and abnormal/cancerous cells. As such, the LN functions essentially as a central hub for lymphocytes to undergo priming and antigen recognition, where specific immunological memory is generated for time-sensitive and long-lasting adaptive immune activity. Thus, understanding the biology of LN-related immune events is essential for developing innovative therapies and diagnostics to treat immune-related conditions and improve patient outcomes.

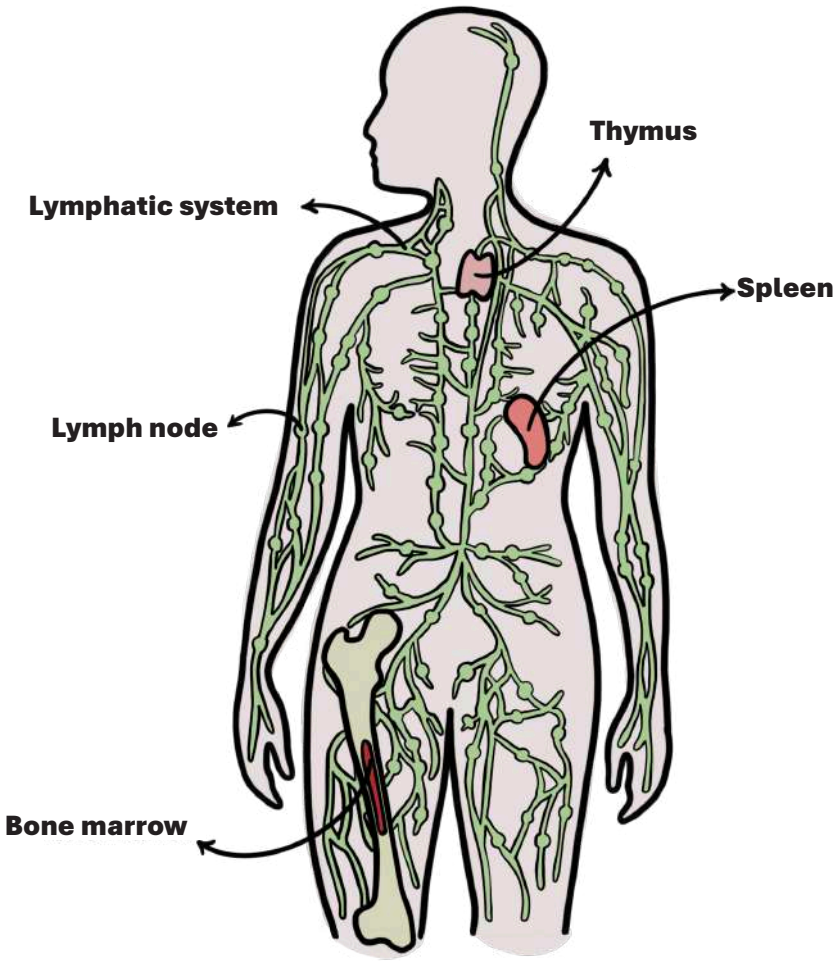

Fig. 1 - Artistic illustration of the immune system. Immune cells originate from primary lymphoid organs. The bone marrow is the first site of haematopoiesis and B cell development, and T cells further mature in the thymus. Secondary lymphoid organs include the lymph nodes and spleen to filter lymph and blood, respectively. Lymph nodes are featured in abundance throughout the lymphatic system, connected by a network of lymphatic vessels. This is where the adaptive immune response begins.

The structure and function of lymph nodes

Systemically, LNs are integrated within both the lymphatic and blood circulation. The lymphatic system is a network of lymphatic vessels that drain interstitial fluid, composed of water, electrolytes and nutrients, from all tissues and organs to prevent edema in steady-state conditions. During inflammation, interstitial fluid accumulates in tissue as exudate, a protein-rich liquid containing immune cells and waste products, which requires lymphatic drainage and filtration through the LNs[7]. Once in the lymphatic vessels, this fluid can be referred to as lymph, with 8-10 litres processed per day[8]. This is typically the route taken by soluble antigens, pathogens and innate immune cells, such as DCs and monocytes, to arrive in the LN via the afferent lymphatic vessels after activation in the periphery. Non-activated/naïve immune cells, like lymphocytes, enter the LN from the blood vasculature through specialised high endothelial venules (HEVs) after their development within primary lymphoid organs. Such processes happen regularly during homeostasis, but during infection or inflammation, the LNs can swell in size to accommodate the influx and proliferation of immune cells.

In this sense, LNs are a dense multi-cellular environment, with around 10^9 cells per gram of tissue[3] arranged in a specific structural organisation that facilitates optimal immune activity (Fig. 2). These include distinct domains for adaptive immune cells, such as B cell follicles in the LN cortex and T cell areas in the LN paracortex. The structural arrangement of these domains allows for an efficient immune response, as it ensures that the correct immune cells encounter each other at the right time and place, thereby improving response speed and specificity[9]. For example, the B cell follicles are generally located between the T cell area and LN subcapsular sinus (SCS) to facilitate antibody production. At one side, soluble antigens can be captured from the incoming lymph into the SCS for direct B cell recognition[10]. At the other end, activated $CD4^+$ T helper cells, from the nearby T cell area, can provide co-stimulatory molecules (e.g. CD40) and cytokines (such as interferon-γ (IFN-γ), interleukin-4 (IL-4) and transforming growth factor-β (TGF-β)) for B cells to assist with somatic hypermutation and isotype switching for high affinity antibody production[11]. This then leads to the formation of germinal centres (GCs) in the B cell follicles, where memory B cells reside and rapidly produce antibodies upon re-exposure to pathogens as part of the humoral immune response[12]. Similarly, the cell-mediated immune response occurs in the T cell area, where APCs bearing a foreign antigen on their major histocompatibility complex (MHC) can present and active cognate T cells[13]. This also requires co-stimulatory signals from both cells (CD80/86 on APCs with CD28 on T cells), as well as adhesion molecules and cytokines that skew the type of T cell response. This not only allows for enabling antibody secretion, but also for the elimination of intracellular (Th1 and $CD8^+$ T cell response) and extracellular pathogens (Th2 response), the clearance of bacteria and fungi (Th17 response), and prevents excessive immune activity by maintaining tolerance (Treg response)[14]. These cellular processes ensure that a tailored immune response is generated to efficiently counter a wide range of pathogenic threat, while still preserving immune homeostasis.

However, all of these cellular reactions depend on a group of non-hematopoietic cells that have yet to be mentioned until now. Hereby, introducing the immune maestros; the LN stromal cells (LNSCs).

Lymph node stromal cells: the immune architectures

LNSCs are historically categorised into mesenchymal fibroblastic reticular cells (FRCs), lymphatic endothelial cells (LECs), blood endothelial cells (BECs), and double negative cells (DNCs)[15]. LNSCs provide structural support to LNs and also facilitate cellular migration and anchorage for immune cells where needed. Furthermore, LNSCs produce immune cell survival factors, control lymphocyte proliferation, restrict self-reactive T cells and have the unique ability to present peripheral tissue antigens as a tolerogenic mechanism[16,17]. The development of LNSCs during LN organogenesis requires the lymphotoxin-β receptor (LTβR), which is expressed on non-hematopoietic cells. Knockout mouse models of LTβR have been shown not to develop LNs[18], similar to LTβR-deficient humans who have no tonsils or LNs[19]. More specifically, a multitude of studies performed with mouse models manipulating the LNSCs, such as ablation of FRCs, revealed the absence of homeostatic signals, disruption of stromal networks and HEVs, as well as hallmarks of autoimmunity, thereby resulting in an inability to mount an adaptive immune response[15,18,20-22]. Thus, LNSCs are required for correct immune functioning.

Fibroblastic reticular cells: chaperones of adaptive immunity

FRCs create the three-dimensional (3D) structural network throughout the LN[23] and promote cross-talk between DCs, T cells and B cells for immune activity[24] (Fig. 2 inset). LN FRCs have a unique transcriptional profile compared to fibroblasts from peripheral tissue, featuring an enrichment of genes associated with cytokine/chemokine pathways and antigen presentation[25-27], along with distinct functional properties described further below. Initially defined as podoplanin$^+$ (PDPN$^+$) cells in mice, new insights in humans have revealed a heterogenous profile of mesenchymal stromal cells with overlapping phenotypes between PDPN$^-$ and PDPN$^+$ FRCs[28]. These subdivision of FRCs were first identified in mice using single-cell RNA sequencing (scRNA-seq)[29], but recent human studies have unveiled a more heterogenous FRC diversity[28,30-35]. To date, the general classification of FRCs based on LN anatomical location include T cell zone FRCs (TRCs), B cell zone FRCs (BRCs), follicular dendritic cells (FDCs), marginal reticular cells (MRCs) and pericytes.

A range of specific FRC-functions have been discovered. Most notably, as mentioned above, FRCs can exclusively present peripheral tissue antigens to immune cells as a tolerogenic mechanism to restrict self-reactivity[36,37]. Dynamically, FRCs generate the cellular niches for B cells through B cell activating factor from the TNF family (BAFF) and CXC motif chemokine ligand 13 (CXCL13), and T cells through production of CC motif chemokine ligand 19 (CCL19), CCL21 and IL-7. Likewise, FRCs maintain homing of DC subsets and promote DC interactions with lymphocytes at the intrafollicular border[38]. As well as providing survival niches for plasma B cells[39], FRCs also create a conduit system through deposition of extracellular matrix proteins (ECM) for the rapid transport of <70 kDa molecules from the SCS into the LN paracortex[40-42]. This is not only important to prevent large molecules and pathogens from entering and disturbing the LN interior, but also to facilitate the delivery of cytokines/chemokines, nutrients and antigens directly to the paracortex for DC and incoming HEV-derived immune cell sampling[43]. FRCs are also responsible for LN swelling based on their interaction with

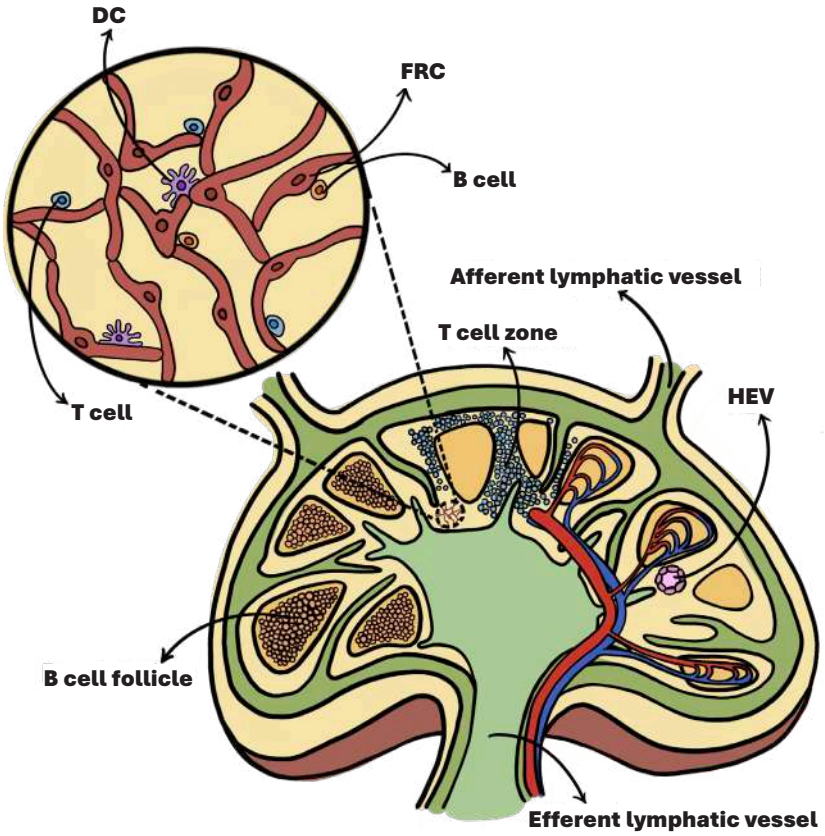

Fig. 2 - Artistic illustration of LN and FRCs. General overview of the LN interior, highlighting the B cell follicles and T cell zone areas, afferent and efferent lymphatic vessels, and high endothelial venules (HEVs). Pop out from the LN paracortex shows fibroblast reticular cells (FRCs) in a connected reticular network, supporting T, B and DC migration through the LN parenchyma.

DCs through the PDPN and C-type lectin-like receptor 2 (CLEC2) axis[44]. This is due to relaxation of the reticular network after actomyosin contractility in FRCs is downregulated, thereby inducing stretching of the LN to accommodate the influx of immune cells that boost an immune response[45]. In pathophysiology, homeostatic FRC function can become dysregulated. Autoimmune disorders, like rheumatoid arthritis (RA) are characterised by loss of tolerance. LN FRCs from RA patients displayed a lower induction of immunomodulatory molecules, such as the human leukocyte antigen-DR (HLA-DR) and programmed cell death ligand 1 (PD-L1), compared to healthy controls[46]. Likewise, changes to FRC phenotypes were observed in two distinct populations in melanoma[31] and remodelling of fibrous stromal tissue in follicular lymphoma[47].

In summary, these valuable functions not only highlight the importance of FRCs in dictating immune responses, but also their role in maintaining homeostatic mechanisms that can be unbalanced in disease settings.

Lymphatic endothelial cells: beacons of the lymphatic sea

The LECs of the LN can be generally distinguished from their BEC counterparts based on Prospero homeobox protein 1 (PROX1) and PDPN expression. They line the lymphatic vessels that drain interstitial fluid/exudate from tissue, with the resulting lymph then transported to the LNs. At the LN, LECs form sinus channels entering and exiting the LN (afferent and efferent lymphatic vessels, respectively), along the SCS, and across the LN parenchyma as an intertwined network (Fig. 3). For guiding immune cell migration, LECs secrete CCL21, which is detected by CC chemokine receptor type 7 (CCR7) on DCs[48] and thereby forms a chemotactic gradient for cell passage through the lymphatics and into the LN SCS. In addition to this, LN LECs also exhibit functional properties to optimise LN functioning, highlighting their distinct characteristics compared to other tissue LECs[26,49]. These include trapping and filtering lymph-borne molecules that arrive in the SCS[50], producing survival and proliferation signals for macrophages[51] and lymphocytes[52], and exhibiting antigen-presenting capabilities[36,53]. LECs are another heterogenous LNSC, with six subsets identified in humans based on anatomical location[54]. The main subsets include atypical chemokine receptor 4$^+$ (ACKR4$^+$) SCS ceiling LECs, TNF receptor superfamily member 9$^+$ (TNFRSF9$^+$) SCS floor LECs and macrophage receptor with collagenous structure$^+$ (MARCO$^+$) medullary LECs. While the complete purpose of these classification markers are yet to be fully elucidated, ACKR4 is well characterised for creating the chemokine gradient in the lymphatics, as it acts as a decoy receptor to scavenge CCL21[55]. In the LN SCS, LEC-secreted CCL21 further guides DC migration over the SCS floor LECs into the LN parenchyma[56]. From here, CCL21 and the other CCR7-ligand, CCL19, facilitate the guidance of APCs into the LN microdomains[48,57,58].

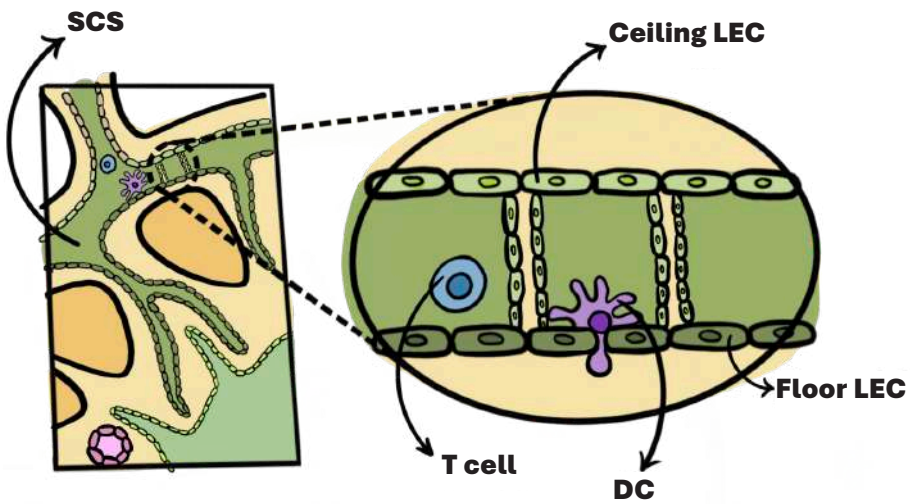

Fig. 3 - Artistic illustration of LECs within the LN. General overview of incoming afferent lymphatic vessel into the LN subcapsular sinus (SCS). Pop out from the SCS reveals LEC subtypes lining the ceiling and floor, supporting immune cell chemotaxis and transendothelial migration.

Human lymph node models

To study the LN in health and disease, and recapitulate such LN-related immune events, a biological system is required that can mimic features of the physiological microenvironment. Such *in vitro* models are termed microphysiological systems (MPS)[59]. MPS technology has been established to address the global demand for more humane models, which in turn can enhance the understanding of organ (patho)physiology and be further applied in disease modelling and drug development environments[60,61]. This is especially crucial given that animal models often have poor translational relevance to humans mainly due to species variation, *i.e.* immune cell subtype differences and limited representation of diseases[62], as well as other factors like low testing throughputs[59]. One such type of MPS platform is the organ-on-chip (OoC), which is a microfluidic device that strives to imitate native tissue/organ functions, such as dynamic, organisational and physiological responses, with control over mechanical parameters like flow rate, stretch and pressure. These small scale bioreactors allow the culture of cells, human biopsies or reconstructed organotypic tissues/organoids for extended periods of time[60]. The human immune system has now been recognised as an important factor in MPS development, but has yet to be fully recapitulated *in vitro* due to its intrinsic complexity. However, effort has been made to include the immune system as in the form of human LNs, which can be used to help further understand LN (patho)physiology[63] and study adaptive immune responses to tissue damage and infection[64]. MPS models have evolved for human LNs with a variety of static and dynamic elements, as well as recapitulating distinct aspects of immune functionality. The spectrum of human LN models can range from two-dimensional (2D) co-cultures of immune cells up to 3D microenvironments composed of biological-ECM or synthetic scaffolds, and further advanced into OoC systems where parameters like flow can be necessary for LN-relevant chemokines[65].

However, several pitfalls and shortcomings do still exist with such LN models, especially with the lack of LNSC integration as either individual cell types or unacknowledged in cell suspensions/tissue slices. Moreover, LN models that are 'organoid-like', meaning they are fully immunocompetent and display LN characteristics, have typically only focused on B cell-related humoral immune responses. As such, an overview of the latest LN models is presented in Table 1 below, categorised in order of increasing LN-like complexity from 2D cultures, 3D cultures, LN tissue slices, and OoC models either with specific immune cell types (partial) or tissue-derived cell suspensions (full). A more detailed summary about LN-on chip models, including information about microfluidic chip setups, can be found in **Chapter 2**[64], as well as from existing reviews[63,66,67].

Table 1 **Overview of human LN models.** ECM; extracellular matrix, LN; Lymph node, SCS; Subcapsular sinus, OoC; Organ-on-chip, 2D; two-dimensional, 3D; three-dimensional.

Complexity	Model	Features	Source	Limitations
2D cultures	Tonsil organoids in transwells	Plasmablast formation and antibody production against influenza virus[68] and vaccination[69] Follicular lymphoma treatment studies[70] Sex-specific lymphocyte responses[71]	Tonsils	No LNSCs No ECM Only humoral immune responses Static
3D cultures	B cell follicles in PEG-4MAL scaffold	De novo antibody formation, inhibition of regulatory pathways and immunodeficiency prediction in cancer patients[72]	Tonsils or PBMCs	No LNSCs Synthetic scaffold Only humoral immune responses Static
		Enhanced B-cell survival, proliferation, differentiation and antibody production[73]	PBMCs Tonsil-FRCs CD40L Cell lines	Synthetic scaffold Only humoral immune responses Static
Sliced tissue cultures	Explant lymphoid tissue in culture plate	Vaccine adjuvant testing on innate immune cells[74]	Axillary LNs	No LNSCs acknowledgement Static
		Stromal and immune responses to liposomal adjuvants, like TLR ligands[75]	Cystic LNs	Static
		FRC regulation of T cell stimulation[34]	Tonsils	Static
	SCS	Fluid flow regulates adhesive ligands for monocyte interactions[76]	Cell lines	No LNSCs No ECM No immune cells
Partial LN OoC models	Immune cell migration and interactions	Stromal-regulated DC and T cell migration in the LN paracortex[77]	PBMCs Cell lines	Only blood-derived immune cells LNSCs are cell lines No B cells
		Fluid flow negatively correlates with T cell egress, but positively with inflammatory cytokine secretion by stromal cells[78]	PBMCs Cell lines	Only blood-derived immune cells LNSCs are cell lines No B cells No ECM
		T cell-dependent interactions with B cells for antibody production[79]	Tonsils	Only blood-derived immune cells No LNSCs
Full LN OoC models	Lymphoid organs	Vaccine responses to hepatitis in a bioreactor device with antigen-specific DCs (TissUse)[80]	PBMCs	Only blood-derived immune cells No LNSCs
		Flow induced follicle formation and response to influenza[81] and COVID-19 vaccines (Emulate)[82]	PBMCs	Only blood-derived immune cells No LNSCs
		Long-term culture of high density lymphoid tissue for antibody responses[83]	Tonsils PBMCs	No LNSCs No ECM

Aim of this thesis

With the rapid progress in the global need for humane research, the immune system remains cemented as a critical factor that requires addressing and incorporation into animal-alternative models. While the LN itself acts essentially as the control centre of human immunology, and advancements in lymphoid organ models have shown promising developments, incorporation of the influential LNSCs has yet to be properly achieved. Therefore, this thesis aims to build a 3D LN model with a stromal cell backbone in both static and dynamic settings to mimic physiological LN functioning.

Chapter 2 provides a comprehensive overview of all single- and multi-OoC models that have incorporated the human immune system. This explores the level of immunocompetency for each OoC model with the use of innate and adaptive immune cells, while also discussing the current limitations, challenges and degrees of physiological improvements.

Before diving into the development of a LN model with an FRC component, **Chapter 3** outlines our initial efforts in examining whether it was possible to culture human LN-isolated FRCs *ex vivo*, and whether these FRCs could represent characteristics of human LNSCs subsets.

In **Chapter 4**, we investigate the possibility of constructing a human LN model using cultured FRCs to act as the foundation for DC integration. However, the LN contains a variety of immune cells, such as a plethora of lymphocyte and myeloid cell subsets. Therefore, in order to advance the two cell FRC-DC model into one reflecting a LN environment to study immune cell functionality, **Chapter 5** reports the incorporation of native LN-derived immune cells into a LN model, enriched with FRCs.

As mentioned, the LN is a dynamic environment characterised by immune cell trafficking, chemotactic gradients and cell-cell interactions. Static models fail to mimic these elements, which are pivotal in facilitating efficient and potent immune responses. Therefore, the last experimental study of this thesis, described in **Chapter 6**, aimed to bring the LN model into an OoC device and establish the lymphatic vasculature through the LN model using autologous LECs.

Finally, **Chapter 7** collectively discusses the key findings of each chapter to conclude this thesis.

References

[1] Fenner, F. The Eradication of Smallpox. *Impact Sci Soc* 38, 147-158 (1988).

[2] Lopez Cavestany, R. *et al.* The Last Mile in Polio Eradication: Program Challenges and Perseverance. *Pathogens* 13 (2024). https://doi.org/10.3390/pathogens13040323

[3] Sender, R. *et al.* The total mass, number, and distribution of immune cells in the human body. *Proc Natl Acad Sci U S A* 120, e2308511120 (2023). https://doi.org/10.1073/pnas.2308511120

[4] Janeway, C. A., Jr. Approaching the asymptote? Evolution and revolution in immunology. *Cold Spring Harb Symp Quant Biol* 54 Pt 1, 1-13 (1989). https://doi.org/10.1101/sqb.1989.054.01.003

[5] Hoorweg, K. & Cupedo, T. Development of human lymph nodes and Peyer's patches. *Semin Immunol* 20, 164-170 (2008). https://doi.org/10.1016/j.smim.2008.02.003

[6] Santambrogio, L. *Immunology of the Lymphatic System*. (Springer New York, NY).

[7] Fogh-Andersen, N., Altura, B. M., Altura, B. T. & Siggaard-Andersen, O. Composition of interstitial fluid. *Clin Chem* 41, 1522-1525 (1995).

[8] Michel, C. C. Microvascular permeability, ultrafiltration, and restricted diffusion. *Am J Physiol Heart Circ Physiol* 287, H1887-1888 (2004). https://doi.org/10.1152/classicessays.00012.2004

[9] Grant, S. M., Lou, M., Yao, L., Germain, R. N. & Radtke, A. J. The lymph node at a glance - how spatial organization optimizes the immune response. *J Cell Sci* 133 (2020). https://doi.org/10.1242/jcs.241828

[10] Pape, K. A., Catron, D. M., Itano, A. A. & Jenkins, M. K. The humoral immune response is initiated in lymph nodes by B cells that acquire soluble antigen directly in the follicles. *Immunity* 26, 491-502 (2007). https://doi.org/10.1016/j.immuni.2007.02.011

[11] Crotty, S. T Follicular Helper Cell Biology: A Decade of Discovery and Diseases. *Immunity* 50, 1132-1148 (2019). https://doi.org/10.1016/j.immuni.2019.04.011

[12] Cinti, I. & Denton, A. E. Lymphoid stromal cells-more than just a highway to humoral immunity. *Oxf Open Immunol* 2, iqab011 (2021). https://doi.org/10.1093/oxfimm/iqab011

[13] Bousso, P. T-cell activation by dendritic cells in the lymph node: lessons from the movies. *Nat Rev Immunol* 8, 675-684 (2008). https://doi.org/10.1038/nri2379

[14] Fu, H., Ward, E. J. & Marelli-Berg, F. M. Mechanisms of T cell organotropism. *Cell Mol Life Sci* 73, 3009-3033 (2016). https://doi.org/10.1007/s00018-016-2211-4

[15] Krishnamurty, A. T. & Turley, S. J. Lymph node stromal cells: cartographers of the immune system. *Nat Immunol* 21, 369-380 (2020). https://doi.org/10.1038/s41590-020-0635-3

[16] Lee, J. W. *et al.* Peripheral antigen display by lymph node stroma promotes T cell tolerance to intestinal self. *Nat Immunol* 8, 181-190 (2007). https://doi.org/10.1038/ni1427

[17] Turley, S. J., Fletcher, A. L. & Elpek, K. G. The stromal and haematopoietic antigen-presenting cells that reside in secondary lymphoid organs. *Nat Rev Immunol* 10, 813-825 (2010). https://doi.org/10.1038/nri2886

[18] Mebius, R. E. Organogenesis of lymphoid tissues. *Nat Rev Immunol* 3, 292-303 (2003). https://doi.org/10.1038/nri1054

[19] Ransmayr, B. *et al.* LTbetaR deficiency causes lymph node aplasia and impaired B cell differentiation. *Sci Immunol* 9, eadq8796 (2024). https://doi.org/10.1126/sciimmunol.adq8796

[20] Fletcher, A. L., Acton, S. E. & Knoblich, K. Lymph node fibroblastic reticular cells in health and disease. *Nat Rev Immunol* 15, 350-361 (2015). https://doi.org/10.1038/nri3846

[21] Denton, A. E., Roberts, E. W., Linterman, M. A. & Fearon, D. T. Fibroblastic reticular cells of the lymph node are required for retention of resting but not activated CD8+ T cells. *Proc Natl Acad Sci U S A* 111, 12139-12144 (2014). https://doi.org/10.1073/pnas.1412910111

[22] Cremasco, V. *et al.* B cell homeostasis and follicle confines are governed by fibroblastic reticular cells. *Nat Immunol* 15, 973-981 (2014). https://doi.org/10.1038/ni.2965

[23] Bajenoff, M. *et al.* Stromal cell networks regulate lymphocyte entry, migration, and territoriality in lymph nodes. *Immunity* 25, 989-1001 (2006). https://doi.org/10.1016/j.immuni.2006.10.011

[24] Li, L., Wu, J., Abdi, R., Jewell, C. M. & Bromberg, J. S. Lymph node fibroblastic reticular cells steer immune responses. *Trends Immunol* 42, 723-734 (2021). https://doi.org/10.1016/j.it.2021.06.006

[25] Buechler, M. B. *et al.* Cross-tissue organization of the fibroblast lineage. *Nature* 593, 575-579 (2021). https://doi.org/10.1038/s41586-021-03549-5

[26] Malhotra, D. *et al.* Transcriptional profiling of stroma from inflamed and resting lymph nodes defines immunological hallmarks. *Nat Immunol* 13, 499-510 (2012). https://doi.org/10.1038/ni.2262

[27] Valencia, J. *et al.* Characterization of human fibroblastic reticular cells as potential immunotherapeutic tools. *Cytotherapy* 19, 640-653 (2017). https://doi.org/10.1016/j.jcyt.2017.01.010

[28] Roet, J. E. G. *et al.* Human lymph node fibroblastic reticular cells maintain heterogeneous characteristics in culture. *iScience* 27, 110179 (2024). https://doi.org/10.1016/j.isci.2024.110179

[29] Rodda, L. B. *et al.* Single-Cell RNA Sequencing of Lymph Node Stromal Cells Reveals Niche-Associated Heterogeneity. *Immunity* 48, 1014-1028 e1016 (2018). https://doi.org/10.1016/j.immuni.2018.04.006

[30] Abe, Y. *et al.* A single-cell atlas of non-haematopoietic cells in human lymph nodes and lymphoma reveals a landscape of stromal remodelling. *Nat Cell Biol* 24, 565-578 (2022). https://doi.org/10.1038/s41556-022-00866-3

[31] Eom, J. *et al.* Distinctive Subpopulations of Stromal Cells Are Present in Human Lymph Nodes Infiltrated with Melanoma. *Cancer Immunol Res* 8, 990-1003 (2020). https://doi.org/10.1158/2326-6066.CIR-19-0796

[32] Park, S. M. *et al.* Sphingosine-1-phosphate lyase is expressed by CD68+ cells on the parenchymal side of marginal reticular cells in human lymph nodes. *Eur J Immunol* 44, 2425-2436 (2014). https://doi.org/10.1002/eji.201344158

[33] Severino, P. *et al.* Human Lymph Node-Derived Fibroblastic and Double-Negative Reticular Cells Alter Their Chemokines and Cytokines Expression Profile Following Inflammatory Stimuli. *Front Immunol* 8, 141 (2017). https://doi.org/10.3389/fimmu.2017.00141

[34] Knoblich, K. *et al.* The human lymph node microenvironment unilaterally regulates T-cell activation and differentiation. *PLoS Biol* 16, e2005046 (2018). https://doi.org/10.1371/journal.pbio.2005046

[35] Grasso, C. *et al.* Identification and mapping of human lymph node stromal cell subsets by combining single-cell RNA sequencing with spatial transcriptomics. *bioRxiv*, 2023.2008.2018.553530 (2023). https://doi.org/10.1101/2023.08.18.553530

[36] Fletcher, A. L. *et al.* Lymph node fibroblastic reticular cells directly present peripheral tissue antigen under steady-state and inflammatory conditions. *J Exp Med* 207, 689-697 (2010). https://doi.org/10.1084/jem.20092642

[37] Baptista, A. P. *et al.* Lymph node stromal cells constrain immunity via MHC class II self-antigen presentation. *Elife* 3 (2014). https://doi.org/10.7554/eLife.04433

[38] Kapoor, V. N. *et al.* Gremlin 1(+) fibroblastic niche maintains dendritic cell homeostasis in lymphoid tissues. *Nat Immunol* 22, 571-585 (2021). https://doi.org/10.1038/s41590-021-00920-6

[39] Huang, H. Y. *et al.* Identification of a new subset of lymph node stromal cells involved in regulating plasma cell homeostasis. *Proc Natl Acad Sci U S A* 115, E6826-E6835 (2018). https://doi.org/10.1073/pnas.1712628115

[40] Gretz, J. E., Norbury, C. C., Anderson, A. O., Proudfoot, A. E. & Shaw, S. Lymph-borne chemokines and other low molecular weight molecules reach high endothelial venules via specialized conduits while a functional barrier limits access to the lymphocyte microenvironments in lymph node cortex. *J Exp Med* 192, 1425-1440 (2000). https://doi.org/10.1084/jem.192.10.1425

[41] Nolte, M. A. *et al.* A conduit system distributes chemokines and small blood-borne molecules through the splenic white pulp. *J Exp Med* 198, 505-512 (2003). https://doi.org/10.1084/jem.20021801

[42] Roozendaal, R. *et al.* Conduits mediate transport of low-molecular-weight antigen to lymph node follicles. *Immunity* 30, 264-276 (2009). https://doi.org/10.1016/j.immuni.2008.12.014

[43] Palframan, R. T. *et al.* Inflammatory chemokine transport and presentation in HEV: a remote control mechanism for monocyte recruitment to lymph nodes in inflamed tissues. *J Exp Med* 194, 1361-1373 (2001). https://doi.org/10.1084/jem.194.9.1361

[44] Acton, S. E. *et al.* Podoplanin-rich stromal networks induce dendritic cell motility via activation of the C-type lectin receptor CLEC-2. *Immunity* 37, 276-289 (2012). https://doi.org/10.1016/j.immuni.2012.05.022

[45] de Winde, C. M. *et al.* Fibroblastic reticular cell response to dendritic cells requires coordinated activity of podoplanin, CD44 and CD9. *J Cell Sci* 134 (2021). https://doi.org/10.1242/jcs.258610

[46] Hahnlein, J. S. *et al.* Human Lymph Node Stromal Cells Have the Machinery to Regulate Peripheral Tolerance during Health and Rheumatoid Arthritis. *Int J Mol Sci* 21 (2020). https://doi.org/10.3390/ijms21165713

[47] Radtke, A. J. *et al.* Multi-omic profiling of follicular lymphoma reveals changes in tissue architecture and enhanced stromal remodeling in high-risk patients. *Cancer Cell* 42, 444-463 e410 (2024). https://doi.org/10.1016/j.ccell.2024.02.001

[48] Ulvmar, M. H. *et al.* The atypical chemokine receptor CCRL1 shapes functional CCL21 gradients in lymph nodes. *Nat Immunol* 15, 623-630 (2014). https://doi.org/10.1038/ni.2889

[49] Petrova, T. V. & Koh, G. Y. Organ-specific lymphatic vasculature: From development to pathophysiology. *J Exp Med* 215, 35-49 (2018). https://doi.org/10.1084/jem.20171868

[50] Kahari, L. *et al.* Transcytosis route mediates rapid delivery of intact antibodies to draining lymph nodes. *J Clin Invest* 129, 3086-3102 (2019). https://doi.org/10.1172/JCI125740

[51] Mondor, I. *et al.* Lymphatic Endothelial Cells Are Essential Components of the Subcapsular Sinus Macrophage Niche. *Immunity* 50, 1453-1466 e1454 (2019). https://doi.org/10.1016/j.immuni.2019.04.002

[52] Hara, T. *et al.* Identification of IL-7-producing cells in primary and secondary lymphoid organs using IL-7-GFP knock-in mice. *J Immunol* 189, 1577-1584 (2012). https://doi.org/10.4049/jimmunol.1200586

[53] Cohen, J. N. *et al.* Lymph node-resident lymphatic endothelial cells mediate peripheral tolerance via Aire-independent direct antigen presentation. *J Exp Med* 207, 681-688 (2010). https://doi.org/10.1084/jem.20092465

[54] Takeda, A. *et al.* Single-Cell Survey of Human Lymphatics Unveils Marked Endothelial Cell Heterogeneity and Mechanisms of Homing for Neutrophils. *Immunity* 51, 561-572 e565 (2019). https://doi.org/10.1016/j.immuni.2019.06.027

[55] Weber, M. *et al.* Interstitial dendritic cell guidance by haptotactic chemokine gradients. *Science* 339, 328-332 (2013). https://doi.org/10.1126/science.1228456

[56] Jalkanen, S. & Salmi, M. Lymphatic endothelial cells of the lymph node. *Nat Rev Immunol* 20, 566-578 (2020). https://doi.org/10.1038/s41577-020-0281-x

[57] Qu, C. *et al.* Role of CCR8 and other chemokine pathways in the migration of monocyte-derived dendritic cells to lymph nodes. *J Exp Med* 200, 1231-1241 (2004). https://doi.org/10.1084/jem.20032152

[58] Luther, S. A. *et al.* Differing activities of homeostatic chemokines CCL19, CCL21, and CXCL12 in lymphocyte and dendritic cell recruitment and lymphoid neogenesis. *J Immunol* 169, 424-433 (2002). https://doi.org/10.4049/jimmunol.169.1.424

[59] Marx, U. *et al.* Biology-inspired microphysiological systems to advance patient benefit and animal welfare in drug development. *ALTEX* 37, 365-394 (2020). https://doi.org/10.14573/altex.2001241

[60] Langhans, S. A. Three-Dimensional in Vitro Cell Culture Models in Drug Discovery and Drug Repositioning. *Front Pharmacol* 9, 6 (2018). https://doi.org/10.3389/fphar.2018.00006

[61] Pamies, D. *et al.* Recommendations on fit-for-purpose criteria to establish quality management for microphysiological systems and for monitoring their reproducibility. *Stem Cell Reports* 19, 1041 (2024). https://doi.org/10.1016/j.stemcr.2024.06.007

[62] Schinnerling, K., Rosas, C., Soto, L., Thomas, R. & Aguillon, J. C. Humanized Mouse Models of Rheumatoid Arthritis for Studies on Immunopathogenesis and Preclinical Testing of Cell-Based Therapies. *Front Immunol* 10, 203 (2019). https://doi.org/10.3389/fimmu.2019.00203

[63] Ozulumba, T., Montalbine, A. N., Ortiz-Cardenas, J. E. & Pompano, R. R. New tools for immunologists: models of lymph node function from cells to tissues. *Front Immunol* 14, 1183286 (2023). https://doi.org/10.3389/fimmu.2023.1183286

[64] Morrison, A. I., Sjoerds, M. J., Vonk, L. A., Gibbs, S. & Koning, J. J. In vitro immunity: an overview of immunocompetent organ-on-chip models. *Front Immunol* 15, 1373186 (2024). https://doi.org/10.3389/fimmu.2024.1373186

[65] Tomei, A. A., Siegert, S., Britschgi, M. R., Luther, S. A. & Swartz, M. A. Fluid flow regulates stromal cell organization and CCL21 expression in a tissue-engineered lymph node microenvironment. *J Immunol* 183, 4273-4283 (2009). https://doi.org/10.4049/jimmunol.0900835

[66] Wang, Q. *et al.* Lymph Node-on-Chip Technology: Cutting-Edge Advances in Immune Microenvironment Simulation. *Pharmaceutics* 16 (2024). https://doi.org/10.3390/pharmaceutics16050666

[67] Shanti, A., Hallfors, N., Petroianu, G. A., Planelles, L. & Stefanini, C. Lymph Nodes-On-Chip: Promising Immune Platforms for Pharmacological and Toxicological Applications. *Front Pharmacol* 12, 711307 (2021). https://doi.org/10.3389/fphar.2021.711307

[68] Wagar, L. E. *et al.* Modeling human adaptive immune responses with tonsil organoids. *Nat Med* 27, 125-135 (2021). https://doi.org/10.1038/s41591-020-01145-0

[69] Kastenschmidt, J. M. *et al.* Influenza vaccine format mediates distinct cellular and antibody responses in human immune organoids. *Immunity* 56, 1910-1926 e1917 (2023). https://doi.org/10.1016/j.immuni.2023.06.019

[70] Kastenschmidt, J. M. *et al.* A human lymphoma organoid model for evaluating and targeting the follicular lymphoma tumor immune microenvironment. *Cell Stem Cell* 31, 410-420 e414 (2024). https://doi.org/10.1016/j.stem.2024.01.012

[71] Mitul, M. T. *et al.* Tissue-specific sex differences in pediatric and adult immune cell composition and function. *Front Immunol* 15, 1373537 (2024). https://doi.org/10.3389/fimmu.2024.1373537

[72] Zhong, Z. *et al.* Human immune organoids to decode B cell response in healthy donors and patients with lymphoma. *Nat Mater* (2024). https://doi.org/10.1038/s41563-024-02037-1

[73] Braham, M. V. J. *et al.* A synthetic human 3D in vitro lymphoid model enhancing B-cell survival and functional differentiation. *iScience* 26, 105741 (2023). https://doi.org/10.1016/j.isci.2022.105741

[74] Stylianou, V. V. *et al.* Innate immune cell activation by adjuvant AS01 in human lymph node explants is age independent. *J Clin Invest* 134 (2024). https://doi.org/10.1172/JCI174144

[75] Fergusson, J. R. *et al.* Ex vivo Model of Functioning Human Lymph Node Reveals Pivotal Role for Innate Lymphoid Cells and Stromal Populations in Response to Vaccine Adjuvant. *bioRxiv*, 2024.2008.2021.608943 (2024). https://doi.org/10.1101/2024.08.21.608943

[76] Birmingham, K. G. *et al.* Lymph Node Subcapsular Sinus Microenvironment-On-A-Chip Modeling Shear Flow Relevant to Lymphatic Metastasis and Immune Cell Homing. *iScience* 23, 101751 (2020). https://doi.org/10.1016/j.isci.2020.101751

[77] Kwee, B. J., Mansouri, M., Akue, A. & Sung, K. E. On-chip human lymph node stromal network for evaluating dendritic cell and T-cell trafficking. *Biofabrication* 17 (2024). https://doi.org/10.1088/1758-5090/ad80ce

[78] Hammel, J. H. *et al.* Engineered human lymph node stroma model for examining interstitial fluid flow and T cell egress. *bioRxiv*, 2024.2012.2003.622729 (2024). https://doi.org/10.1101/2024.12.03.622729

[79] Zatorski, J. M. *et al.* Initiation of primary T cell—B cell interactions and extrafollicular antibody responses in an organized microphysiological model of the human lymph node. *bioRxiv*, 2025.2001.2012.632545 (2025). https://doi.org/10.1101/2025.01.12.632545

[80] Giese, C. *et al.* Immunological substance testing on human lymphatic micro-organoids in vitro. *J Biotechnol* 148, 38-45 (2010). https://doi.org/10.1016/j.jbiotec.2010.03.001

[81] Jeger-Madiot, R. *et al.* Modeling memory B cell responses in a lymphoid organ-chip to evaluate mRNA vaccine boosting. *J Exp Med* 221 (2024). https://doi.org/10.1084/jem.20240289

[82] Goyal, G. *et al.* Ectopic Lymphoid Follicle Formation and Human Seasonal Influenza Vaccination Responses Recapitulated in an Organ-on-a-Chip. *Adv Sci (Weinh)* 9, e2103241 (2022). https://doi.org/10.1002/advs.202103241

[83] Teufel, C. *et al.* Lymphoid-tissue-on-chip recapitulates human antibody responses in vitro. *bioRxiv*, 2025.2001.2014.632762 (2025). https://doi.org/10.1101/2025.01.14.632762

2

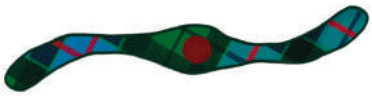

In Vitro Immunity: An Overview of Immunocompetent Organ-on-Chip Models

Andrew I. Morrison[1,2], Mirthe J. Sjoerds[1], Leander A. Vonk[1], Susan Gibbs[1,2,3], Jasper J. Koning[1,2]

[1] Amsterdam UMC location Vrije Universiteit Amsterdam, Molecular Cell Biology & Immunology, De Boelelaan 1117, Amsterdam, The Netherlands.

[2] Amsterdam institute for Infection and Immunity, Amsterdam, The Netherlands.

[3] Department of Oral Cell Biology, Academic Centre for Dentistry Amsterdam (ACTA), University of Amsterdam and Vrije Universiteit, Amsterdam, The Netherlands.

Front Immunol. 2024 May 21:15:1373186. DOI: 10.3389/fimmu.2024.1373186

Abstract

Impressive advances have been made to replicate human physiology *in vitro* over the last few years due to the growth of the organ-on-chip (OoC) field in both industrial and academic settings. OoCs are a type of microphysiological system (MPS) that imitates functional and dynamic aspects of native human organ biology on a microfluidic device. Organoids and organotypic models, ranging in their complexity from simple single-cell to complex multi-cell type constructs, are being incorporated into OoC microfluidic devices to better mimic human physiology. OoC technology has now progressed to the stage at which it has received official recognition by the Food and Drug Administration (FDA) for use as an alternative to standard procedures in drug development, such as animal studies and traditional *in vitro* assays. However, an area that is still lagging behind is the incorporation of the immune system, which is a critical element required to investigate human health and disease. In this review, we summarise the progress made to integrate human immunology into various OoC systems, specifically focusing on models related to organ barriers and lymphoid organs. These models utilise microfluidic devices that are either commercially available or custom-made. This review explores the difference between the use of innate and adaptive immune cells and their role for modelling organ-specific diseases in OoCs. Immunocompetent multi-OoC models are also highlighted and the extent to which they recapitulate systemic physiology is discussed. Together, the aim of this review is to describe the current state of immune-OoCs, the limitations and the future perspectives needed to improve the field.

Introduction

Disease is a major burden on society; economically, socially, physically and psychologically. Worldwide, over 7.6 million people die annually from transferable diseases, like influenza and COVID-19, and over 40 million people from non-transferable diseases, such as cancer and cardiovascular diseases[1]. Over the past decades, progress at healthcare organisations and pharmaceutical industries has advanced to such a level that many diseases can be prevented, controlled or even cured. Significant improvements have been made, with key driving factors including vaccination programs, innovative research on disease pathophysiology, discovery of new drug targets and advancements in toxicity screenings[2, 3]. Given the complexity of human physiology and ethical considerations, many human diseases have been investigated using animal models or *in vitro* cultures of human cells[4]. Animal studies have traditionally been the gold standard in the drug development process preceding clinical trials. While they have been recognised as a necessity for evaluating drug metabolism, toxicity and efficacy, they do have several drawbacks. These include poor translatability to humans, low reproducibility rates, high costs and a time-consuming nature[5]. Together, this results in around 90% of drug trials that are pre-screened in animals failing in humans due to differences with drug efficacy and toxicity effects[6]. In addition to in vivo models, conventional *in vitro* assays have been widely used for predictive drug testing. These make use of human cells derived from either fresh human tissues/organs, or immortalised cell lines cultured under static conditions[7]. However, such cultures generally lack the intricate three-dimensional (3D) multicellular organisation of a human organ, including vascularisation, which is complex to recreate in a static model. As such, this has led to the birth of MPS; a more realistic human physiological microenvironment represented in an *in vitro* setting.

Microphysiological systems and organ-on-chip platforms

MPS is a hypernym for *in vitro* models capable of replicating features of human physiology on a micro-scale that is biologically suitable for their intended function[8]. OoCs are a type of MPS platform in a microfluidic device that can control and allow the imitation of native tissue/organ functions such as dynamic, organisational and physiological responses. An OoC microfluidic device can act as a small scale bioreactor to maintain fresh human biopsies or reconstructed organotypic tissues/organoids for extended periods of time[9]. These microfluidic devices can enable additional mechanical parameters like flow rate, stretch and pressure, which are traditionally lacking in static two-dimensional (2D) and 3D cultures[10]. Such parameters allow constant supply of oxygen and nutrients to the organ models, as well as removal of toxic metabolites, while also facilitating cell migration and multi-organ crosstalk. The design of the microfluidic device varies based on the requirements for culturing single or multiple organ types within the device and the biological questions that need addressing[11, 12]. Examples of such microfluidic OoC platforms can be seen in Fig. 1. Typically, microfluidic devices are made from cell culture-compatible materials, namely polydimethylsiloxane (PDMS), and feature micro-channels for media flow and culture compartments that can be filled with cells, ECM-like gels, organotypic models or biopsies[13]. OoCs have been made in academic bioengineering laboratories and are also commercially available from industrial companies. Both sectors have generated promising results in

terms of modelling true human representative organ functions-on-chip. This includes toxicity screens performed during drug development and disease mechanisms that can be further understood to a deeper level than what is currently possible in animal models[14]. The more accurate portrayal of human physiology *in vitro* has led to official acknowledgement by the United States (US) FDA, who has authorised the "use of certain alternatives to animal testing" that includes OoC models to investigate the safety and effectiveness of a drug[15, 16].

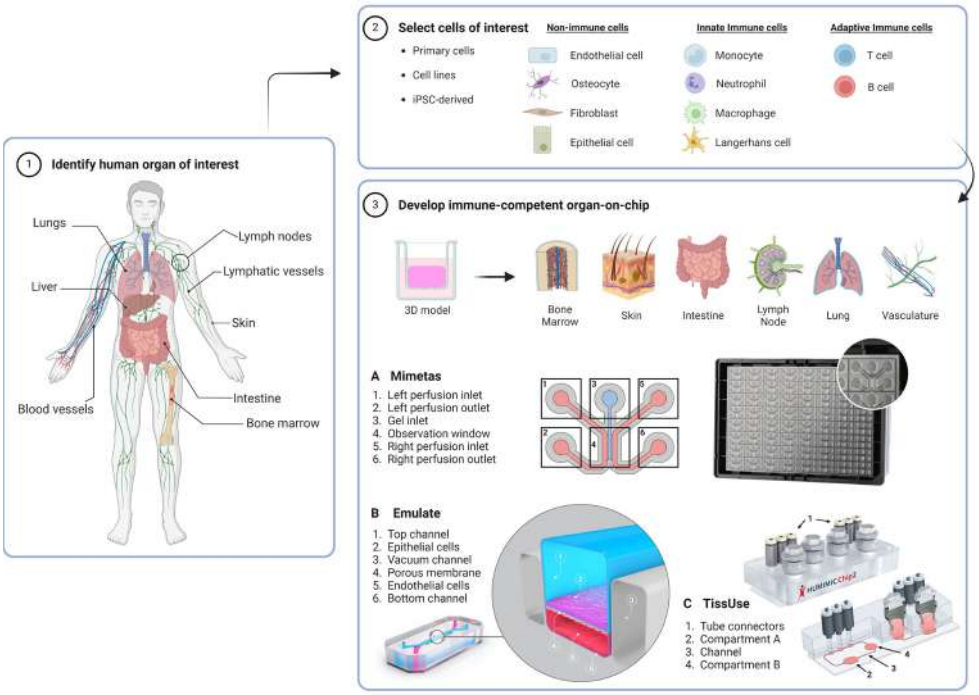

Fig. 1 - Workflow for generating an immunocompetent OoC. The human organ of interest (1) is modelled by using cells derived from either primary tissues or organs, cell lines or iPSCs (2) to make a 3D organotypic model that can be incorporated or built directly into an OoC microfluidic device (3). Dependent on organ anatomy and chip layout, single-OoCs are possible with various commercial chips companies, e.g. **(A)** Mimetas have a high-throughput 3-lane channel OrganoPlate® with 64-chips per plate, and **(B)** Emulate have a design that features a single chip with two channels separated by a porous membrane. **(C)** multi-OoCs are achievable through connection of multiple single-OoCs or within one microfluidic device, e.g. the setup of the TissUse HUMIMIC Chip2 where two (shown) or up to four compartments can house organotypic models or media reservoirs. Compartments can be connected by a channel, forming a continuous circuit with up to two separate circuits per chip. Chip images are courtesy of MIMETAS US Inc., Emulate Inc., and TissUse GmbH. Created with BioRender.com.

The necessity to incorporate the immune system

Although encouraging advancements have been made in OoC innovation, the inclusion of the immune system is still significantly lacking and is crucial for these models to reflect more optimally human physiology and disease[17–20]. The human immune system has a major underlying role in the pathophysiology of almost every disease, whether that be cancer[21], metabolic disease[22], infection[23] or autoimmunity [24]. The process by which the human body reacts to external or internal threat is called inflammation, and this can be an acute reaction, where unwanted pathogens, wound debris or toxins are swiftly removed, or chronic where the response persists for weeks or even years[25]. Inflammation in itself is an umbrella term for a cascade of events that result in the recruitment and activation of immune cells via release of pro- or anti-inflammatory mediators, such as lipids, cytokines and enzymes[26]. The landscape of these inflammatory mediators varies throughout different organs, resulting in organ-specific immune responses.

Immune cells develop within primary lymphoid organs and can then migrate through complicated blood and lymphatic vascular networks to secondary lymphoid organs and tissues. Lymphoid organs systemically co-operate with innate and adaptive immune cells, who can be migratory or tissue-resident[27]. Innate immunity is the first line of defence and includes cells such as dendritic cells (DC), macrophages, monocytes, neutrophils and mast cells from myeloid origin, and nature killer (NK) cells. These innate cells sense danger via pattern recognition receptors (PRRs)[28] and offer a quick immune response upon pathogenic challenge, such as phagocytosis and secretion of inflammatory cytokines. In contrast, T and B cells are the main subsets in adaptive immunity, which exhibit memory capabilities and are specific in their immune response. T cells become activated after the T cell receptor (TCR) recognises its cognate antigen in the lymph nodes via presentation by DCs using human leukocyte antigen class II (HLA) molecules. These molecules are composed of different subtypes, termed HLA-DR, -DP, -DQ. T cell activation also depends on co-stimulatory molecules, such as CD27 from T cells bound to CD80/CD86 on antigen presenting cells (APCs). Once T cells are activated, they can either stimulate other lymphocytes to respond to potential threat or directly eliminate the target through the release of cytotoxic proteins, like granzymes. B cells also become activated after stimulation from T-helper cells or via antigen recognition directly, and can produce antibodies to neutralise the pathogen and/or facilitate opsonisation; a specific type of directed phagocytosis.

Until now, innate immunity has been predominantly simulated in OoC platforms. Unlike adaptive immune cells, innate immune cells do not rely on HLA molecules for their activation. Complexity greatly increases when adaptive immune cells are to be used due to their associated HLA-molecules, which may result in immune cell activation when other HLA-mismatched cell types are also present in the platform. This undesirable effect, mirrors the phenomenon known as graft versus host disease (GVHD) which leads to organ rejection by the adaptive immune system[29]. In order to avoid cytotoxicity initiated by HLA-mismatch in OoC when investigating adaptive immune responses, all cell types should be derived from the same individual or at least be HLA-matched, introducing a major limitation of cell sourcing for current models. While efforts have been made by researchers to integrate immune cells into OoCs[30], development of human immunocompetent-organ models is needed to help us further understand how immune cells interact with organs during health and

disease. This is particularly important for understanding how drugs can influence these interactions (e.g. localised immunotherapies for treating autoimmune disorders or cancer).
Therefore, the aim of this review is to provide a comprehensive overview describing the extent in which the human immune system, specifically innate and adaptive immune cells, has been incorporated into both single- (Table 1) and multi-OoC (Table 2) models, and to discuss their current limitations and future perspectives. The focus is mainly on the body barriers (lung, skin, intestine and liver) and lymphoid organs.

Table 1 **Overview of immunocompetent single-organ-on-chip models.** P: primary, CL: cell line, IC: immune cell, SC: stromal cells, MD: microfluidic device, R: readout.

Organ	Simulated feature(s)	Cell types	Microfluidic device and readouts
Lung	Inflammation[39, 40, 42, 45] Cell crosstalk[33, 34, 37, 43, 44] SARS-CoV-2 [35-38, 41]	**IC:** (P) PBMCs[36, 39, 40], macrophages[35, 37], neutrophils[34, 41, 42], T cells[43, 44] **SC:** (P) alveolar epithelial cells [33-37, 40, 43-45], microvascular ECs[33, 35, 37, 39, 41, 43-45], lung fibroblasts[42], HUVECs[39, 42], airway epithelial cells[41, 42]	**MD:** commercial OoC (Emulate)[33-35, 37, 38, 40, 41, 43-45] and in-house[36, 39, 42], unidirectional open systems **R:** IC migration and adhesion, cytokine secretion, gene and protein expression, barrier permeability, metabolomics and proteomics
Skin	Barrier function[48] Wound healing[50] Inflammation[49, 51, 55] Adipose[54]	**IC:** (P) PBMCs[54], macrophages [50], T cells[49], neutrophils[49] (CL) U937-monocytes[48], HL-60 cells[51] **SC**: (P) keratinocytes[48, 55], fibroblasts[50, 51, 55], HUVECs[50], ECs[54] (CL) HaCaT cells[49-51]	**MD:** in-house[48-51, 54, 55], dynamic open/closed systems **R:** barrier function (microscopy, electrical resistance and fluorescent tracers), inflammation (cytokine secretion), viability, cell-cell interactions, IC phenotype and migration
Intestine	Host immune-microbiome interactions[58-60, 62] Barrier function[66] IC migration[63] Inflammation[44, 61, 64, 65, 69, 70]	**IC:** (P) PBMCs[60], monocyte/macrophages[61, 64], moDCs[63], neutrophils[66] (CL) THP-1 cells[65, 66, 70], MUTZ-3-DC precursors[65], U937 cells **SC:** (P) HUVECs[61, 70], microvascular ECs[44, 60], organoids/iPSC[38, 63, 64, 69, 70] (CL) epithelial cells (Caco-2), HT-29-MTX-12 cells[65],	**MD:** in-house[61-63,70] and commercial OoC (Emulate[38, 58, 59], ChipShop[60], and Mimetas [64,66,69]), unidirectional/ bidirectional/dynamic open/closed systems **R:** barrier function (permeability), cell viability, bacterial activity, gene and protein expression, cytokine secretion, transcriptomics
Liver	Inflammation[72-77] IC infiltration[72]	**IC:** (P) PBMC-isolated macrophages[72], Kupffer cells **SC:** (P) Hepatocytes, HUVECs[72] (CL) stellate cells LX-2[72, 74], HepaRG [77]	**MD:** in-house[75], commercial OoC (CNbio[76, 77], Emulate[74], Mimetas[73], ChipShop[72]), unidirectional/ bidirectional/dynamic open/closed systems **R:** IC migration, cell-cell interactions, gene and protein expression, cytokine secretion, metabolomics, cell viability

Bone Marrow	Haematopoiesis and niche formation[80, 81, 84]	**IC:** (P) HSPCs, BMNCs [83], $CD34^+$ progenitors[82, 83] (CL) SUP-B15[85] **SC:** (P) BMSCs, MSCs, HUVECs [82], osteoblasts[82]	**MD**: in-house[80-82, 85] and commercial (TissUse[84] and Emulate[83]) OoC, dynamic/unidirectional closed/open systems **R**: cell survival and phenotype, cell-cell/matrix interactions, gene and protein expression, cytokine secretion, oxygen consumption
	Bone marrow and cancer cell interactions[82, 85]		
	Shwachman–Diamond syndrome[83]		
Lymph Node	IC interaction and trafficking[90, 92, 98]	**IC:** (P) PBMCs[87-90], DCs[98], moDCs[88], T cells[98], (CL) MUTZ-3 cells[90], THP-1 cells[91, 93], Jurkat cells[91, 92] **SC**: (CL) fibroblasts[98]	**MD**: in-house[87, 90-93, 98] and commercial (Emulate[89], TissUse[88]) OoC, unidirectional/dynamic open/closed systems **R**: DC maturation and migration, T cell activation, cell adhesion, antigen-specific antibody secretion, cytokine production and permeability
	Cellular organization[89, 91]		
	Antigen-antibody responses[87, 88]		
	Cancer metastasis[93]		
Spleen	Blood filtration[94, 95]	**IC**: (CL) THP-1 cells[96] **Other**: RBCs	**MD:** in-house[94-96] **R:** cell viability, morphology, metabolomics, mechanical parameters, microscopy
	Sickle-cell disease[96]		
Vasculature	Blood and lymph vessel-IC interaction[101, 102]	**IC:** (P) PBMCs[104], T cells[101-103, 105, 106], neutrophils[107-109], moDCs[110], (CL) THP-1 cells[103] **SC:** (P) HUVECs[101, 103, 106, 107], (CL) HMEC-1 ECs[102] **Cancer cells:** (CL) melanoma A375 cells[102], breast cancer cells[103]	**MD**: in-house[103-106, 108-110] and commercial (Mimetas[101, 102, 107]) OoC, dynamic/bidirectional open systems **R**: DC maturation and migration, T cell activation, Cell adhesion, antigen-specific antibody secretion, cytokine production and permeability
	IC migration and infiltration[105-107, 110]		
	Cancer metastasis [103, 108, 109, 111-114]		

Organ barriers

Tissue barriers (e.g. lung, skin and intestine) play a vital role in maintaining systemic homeostasis by protecting internal organs from direct environmental assault, such as pathogens. In this way, the tissue barriers preserve organ functions and provide a robust defence against immunological challenges. Additionally, although the human liver is not directly connected and exposed to the external environment, it is an immune-rich tissue that acts as a checkpoint for the clearance of foreign intestine-derived antigens before they can enter the systemic blood stream[105]. Therefore, characteristics of single organ barriers-on-chip with an immune component, including the liver, are summarised in Table 1 and are further described in the following text below.

Lung

The first OoC model to be established, which represented a more complex human micro-physiology, compared to what could be achieved in static models, was a model of the lung[10]. The airways are prone to infection and inflammation and therefore have numerous mechanisms for protection such as; mucus surfactant for trapping foreign particles, epithelial cell barriers and resident immune cell

populations, where the most prevalent are the alveolar macrophages[106].

The lung-on-chip mirrors human physiology by replicating essential tissue characteristics, including dynamic airway movements, surfactant release, the alveolar-capillary interface, airway inflammation and incorporation of blood vessels[42]. Such chip models contain an air-liquid interface (ALI) and are generally constructed in two-channel microfluidic devices. These channels can house primary lung alveolar epithelial cells and pulmonary microvascular endothelial cells (ECs) on either side to simulate an epithelial barrier, separated by a porous membrane. A standard configuration of a lung-on-chip is illustrated in Fig. 1, which shows a design associated with the Emulate lung-on-chip system.

Incorporation of immune cells into existing lung-on-chips has been used mainly for disease models, namely that of the lung's response to SARS-CoV-2 from the COVID-19 global pandemic, but also inflammatory diseases like asthma[38]. The most common approach to introduce immunity involves the use of peripheral blood mononuclear cells (PBMCs) obtained from buffy coats, which consist predominantly of T cells and different proportions of B cells, NK cells, monocytes and DCs. PBMCs can be administered into the vascular endothelial lined channels of the chip, simulating the circulation of immune cells from blood. In the context of a lung-on-chip exposure to SARS-CoV-2, PBMC-derived macrophages were found to contribute towards a SARS-CoV-2 induced interferon β (IFNβ) inflammatory response. The use of an inhibitor targeting the type 1 IFN intracellular pathway demonstrated the capability to alleviate the inflammation-on-chip, bringing the IFNβ levels down to those observed in an uninfected chip[36]. Additionally, macrophages were recorded to have the ability to phagocytose SARS-CoV-2 damaged ECs[35]. Furthermore, a severe immune overreaction, known as a cytokine storm, was modelled when SARS-CoV-2 infected patient samples were tested on a lung-on-chip, where the high cytokine levels were suppressed after monoclonal antibody treatment[37]. In addition, clinically relevant SARS-CoV-2 treatments demonstrated drug efficacy by reducing viral load and inflammation on a lung-on-chip when PBMCs were present, indicating a benefit for the use of immune cells[43].

While most disease-related inflammatory lung-on-chip models focus on SARS-CoV-2, other viral infections have also been studied. PBMCs in a lung-on-chip model of rare acute respiratory distress syndrome (ARDS) displayed extravasation from one chip channel to another that was dependent on the presence of an endothelial barrier, ECM density/stiffness, and the flow profile[31]. Bidirectional flow delayed the extravasation of immune cells compared to unidirectional flow, highlighting the importance of organ-specific dynamic flow conditions. Another study focusing on influenza virus-induced endothelial inflammation found that the number of PBMCs adhering to the lung-on-chip's endothelium was 100 times higher compared to uninfected chips[32], demonstrating their capability to react to pathogenic challenges.

In addition to PBMCs, single immune cell populations have also been brought into lung-on-chips. For instance, neutrophils, a major component of the lung's innate immune system[42], have displayed migratory chemotactic properties across the EC barrier to epithelial cells upon Influenza A exposure in lung-on-chips[39], as well as in fibrotic lung-chips[33]. Next to this, T cells are the predominant adaptive immune cell present in the airways and consist of mainly tissue resident memory T cells. When applied to lung-on-chips in a pool of PBMCs, activated T cells also had a migratory capacity towards

epithelial cells upon inflammation using different viruses[39]. Since T cells have a prominent role in recognising infected cells or cancer cells, effort has been made to increase their killing capability via multiple mechanisms, including the generation of bi-specific antibodies[40]. The safety efficacy of a bi-specific antibody coupling CD3+ T cells to tumour antigens has been evaluated using an alveolus-on-chip, highlighting the practical use of such a model in the toxicology field[41]. T cells also have a pathophysiological role in asthma, and while T cells have not yet been used in asthma-on-chip, interleukin (IL)-13 was used to represent a T-helper cell type 2 suited microenvironment in a microfluidic device that replicated clinical data in terms of mucociliary clearance and increased mucus secretion[34].

In summary, immunocompetent lung-on-chips have rapidly evolved, heightened by the COVID-19 pandemic, and have started to characterise the role of immune cells in viral and bacterial infections and their effect on epithelial and ECs. There is still a need for further representation of the innate and adaptive immune system in these chips, particularly for more inflammatory diseases such as respiratory allergies to elucidate the role of allergen-related immune cells i.e., mast cells, and for understanding drug mechanisms.

Skin

The skin is another protective barrier against external pathogens, chemicals and physical stimuli. It consists of two main layers; the epidermis and the dermis. The epidermis is composed of highly specialised keratinocytes, melanocytes and immune cells, such as Langerhans cells (LCs). The dermis is a fibroblast-populated ECM compartment containing the vasculature and immune cells such as dermal DCs, T cells and macrophages[107]. These skin immune cells exist in either resident or migratory populations, where upon tissue damage the APCs (LCs and DCs) become activated and migrate towards the skin-draining lymph nodes through the lymphatic vasculature.

A major characteristic of *in vitro* human organotypic skin models is their exposure to the air from the epidermis side, known as the ALI, which promotes spontaneous epidermal differentiation and stratification. Nutrients are supplied via culture medium in contact with the basal layer of the epidermis in reconstructed human epidermal (RhE) models or via the dermis side in full-thickness reconstructed human skin (RhS) models. RhS are typically bi-layered structures with keratinocytes seeded on top of a fibroblast-populated collagen-based 3D matrix[108]. This design offers several advantages over ex vivo skin biopsies, e.g. prolonged culture duration with defined cell types present and can be readily used for safety/risk assessment, wound healing, drug delivery and allergen induced inflammation/disease. However, immunocompetent skin-on-chip models are still in their infancy and relatively simple in terms of their cellular setup.

One of the first reported immunocompetent skin-on-chip models was developed using epidermal keratinocytes, cultured together with the U937 monocyte-like cell line under dynamic flow. The model showed improved keratinocyte tight junction formation and general long term cell survival[44]. Such immunocompetent skin-on-chips have evolved further by the addition of dermal fibroblasts with PBMC-derived T cells[47] or human umbilical vein endothelial cells (HUVECs) with macrophages[46] to simulate a vascular channel. These immune cell additions facilitate the study of tissue infiltration,

cytokine production and dynamic cell-cell interactions that more closely resemble normal native skin processes. In addition, vascularised skin-on-chip models have demonstrated neutrophil migration from endothelium to dermis upon ultraviolet (UV) radiation exposure[48], further show-casing the ability to recapitulate dermatology-based phenomenon. Increased complexity of skin-on-chip has been described to include neopapillae into the dermis hydrogel, which are precursors of the hair follicle[109], but this has yet to include immune cells.

The pathophysiology of numerous skin related-diseases show immune cell involvement. For example, the addition of an adipocyte layer to RhS model has displayed an essential role in stabilising the metabolic properties of the skin[110], and as such, obesity has been mimicked with immune cell incorporation into a white adipose tissue (WAT)-on-chip[45]. Adipocytes and ECs were isolated from skin biopsies and co-cultured in a chip with the same patient derived PBMCs, namely CD14+ monocytes and T cells. The addition of these immune cells to the model could recapitulate endocrine and immunomodulatory WAT functions. For more inflammatory and allergy-associated skin diseases-on-chip, incorporation of immune cells has yet to be achieved. However, potential does exist to address these disease mechanisms. For example, atopic dermatitis (AD) was modelled on chip using the disease-relevant cytokines IL-4 and IL-13. This resulted in tissue dehydration, keratin exfoliation and suppression of barrier-related genes[49].

In summary, skin-on-chip models have been comprehensively characterised and demonstrate robust properties in comparison to native human skin, albeit still lacking key features such as adipocyte layers, glands, nerves and growth of hair follicles. However, their immune-compatibility is still in its initial phases, primarily relying on the use of innate immune cells.

Intestine (Gut)

Like the skin and airways, the intestine (gut) is a barrier organ that is constantly in contact with external stimuli, harbouring a microbe dense microenvironment to fine tune a balance between tissue homeostasis and pathogenic infection. Hence, this is why the gut houses an extensive population of resident immune cells in the body. These immune cells can be found in an area of connective tissue called the lamina propria that house a plethora of e.g. macrophages, T cells and DCs[111, 112]. The intestinal architecture contains villi, which are small projections of epithelium extending into the lumen to increase the surface area for nutrient uptake. The majority of gut-on-chips have overlapping attributes with lung-on-chips, such as inclusion of vacuum chambers to replicate peristaltic movement and chip-channels separated with a semi-porous membranes or ECM-rich hydrogel to enable culture of human intestine (or colon) epithelial cells and ECs (Fig. 1).

Immune cells of myeloid origin have generally been used in multiple gut-on-chip models. Similar to skin-on-chip models, the first immunocompetent gut-on-chip model introduced the monocyte cell line U937, perfused through a two-channel chip containing the epithelial cell line CaCo-2. After lipopolysaccharide (LPS) or tumour necrosis factor alpha (TNFα) exposure to trigger inflammation, the epithelium increased barrier permeability and induced immune activation[44]. To date, gut-on-chip models have become more complex by the addition of HUVECs for the endothelial compartment, and gut commensal microbiome components such as probiotic bacterial strains as detailed below.

Gut-on-chip co-cultures with microbial species have included either complete PBMCs or PBMC-isolated macrophages/DCs perfused through endothelial channels to study several different parameters, such as microbe-dependent tissue inflammation, damage and cell differentiation (50–52). Such addition of immune cells in these experiments have displayed protective properties of the endothelium, as the ECs were normally subjected to inflammation-associated tissue damage from the microbial species when immune cells were not present.

The major chronic inflammatory disease associated with the gut is inflammatory bowel disease (IBD), encompassing conditions like ulcerative colitis and Crohn's disease. This condition poses significant challenges for individuals, which is why gut-on-chip models are an appealing choice for IBD disease modelling and testing drug efficacy. When epithelial barriers are damaged, it leads to leaky gut, allowing pathogens to enter the bloodstream. In the context of gut-on-chips, IBD has been recapitulated through combinations of inflammatory cytokines, E. coli or LPS, and has involved the use of monocyte-derived DCs, macrophages, and PBMCs[53, 54, 56]. More specifically, after cytokine exposure, pro-inflammatory M1 macrophage differentiation occurred via crosstalk with epithelial cells[55] and the monocyte cell lines THP-1 and MUTZ-3 were able to provoke synergistic inflammation through increase in IL-8 secretion in a chip[58]. The theme of gut inflammation has extended to the use of neutrophils in an LPS-induced gut-on-chip, which mimics epithelial damage by neutrophil invasion and inflammatory crosstalk between resident and circulating immune cells[57].

Interestingly, there has been limited incorporation of adaptive immune cells in gut-on-chip models. One study has explored the safety and efficacy of T cell bi-specific antibodies targeting tumour antigens, which was conducted in parallel with an alveolus-on-chip model, as previously mentioned[40, 41]. Nonetheless, for an incapacitating disease like IBD, the addition of immune cells, such as macrophages, and inflammatory mediators to the intestine-on-chips recapitulates a physiologically-relevant disease setting. This is particularly relevant since IBD patients have a higher abundance of macrophages and inflamed epithelium compared to healthy individuals[113, 114]. Notably, models of the human intestine have a well distinguished organoid profile, whether derived from patient samples or induced pluripotent stem cell (iPSCs). Such organoids are now being cultured in gut-on-chip models that have an immune-like environment, such as iPSC-derived gut-like tubules that secrete IL-6 and IL-8 under an inflammatory stimulus[60]. Likewise, a vascularised colon organoid demonstrated monocyte adherence to ECs, which then transmigrated towards the epithelium to undergo macrophage differentiation[59]. To summarise these immune gut-on-chip studies, it becomes apparent that they have predominantly featured innate immune cells over adaptive immune cells. This is reasonable given their prominent involvement in gut-related diseases to a certain extent. However, it is worth noting that the gut contains a substantial population of T cells, which play a foundational role in other gut disorders, like Crohn's and celiac disease. Our intestine is influential to general health, so it would be pivotal to include adaptive immunity into future gut-on-chip models.

Liver

As stated in the introduction to the organ barriers, the liver is included in this review. The liver directly receives intestine draining-blood from the portal vein and thereby can act as a barrier to systemic infection. Since it is crucial for filtering blood and metabolising drugs and toxins which have bypassed the lymph node and spleen, this makes it an ideal organ for on-chip immunotoxicity testing. The liver is an immune privileged organ, with specialised resident macrophages known as Kupffer cells[115]. Liver-on-chip models normally use primary human hepatocytes, but the inclusion of immune cells at the single-OoC level are still lacking and are in a relative infant state. Such liver-on-chips can be used to study hepatocyte differentiation and culture stability e.g. LPS-induced inflammation with PBMC-derived macrophages resulted in macrophage polarisation to a M2 phenotype and demonstrated their adhesive properties and infiltration into hepatic cell channels on the chip[61]. Inclusion of Kupffer cells allow for a more physiological immune model, where their use has been validated in a liver-chip as a hepatotoxic screening platform based on metabolic readouts[62, 63]. These Kupffer cells have also been administered to study liver-related diseases on chip, such as advanced stages of non-alcoholic fatty liver disease (NAFLD), where exposure to an overload of long-chain free fatty acids induced pro-inflammatory biomarkers that could then be attenuated with drug application, indicating a proof-of-concept for hepatotoxicity testing of drugs[64]. Likewise, in a liver-on-chip model of hepatitis, the Kupffer cells responded to LPS and hepatitis B virus (HBV) infection by secreting pro-inflammatory molecules associated with the disease[65]. Additionally, glucocorticoids were assessed on liver-on-chips containing Kupffer cells to evaluate their anti-inflammatory properties[66]. Henceforth, it is clear that so far only innate immunity is partially represented in liver-on-chip models with the use of Kupffer cells. Integration of other innate immune cells to represent liver functioning is still required for future studies.

Lymphoid vasculature and organs

Lymphoid organs are a crucial component of the human immune system and distributed throughout the body to regulate and support immune responses. These specialised organs are integral in the production, maturation and activation of various immune cells. This all begins in the primary lymphoid organs and proceeds to the secondary lymphoid organs, which are strategically located to drain interstitial fluid from tissue. These secondary lymphoid organs play a fundamental role in immune surveillance, tissue specific immunity and memory responses.

The trafficking of immune cells between organs and tissues takes place in blood and lymphatic vessels, which serve as a key structural element for systemic immunology e.g. to guide immune cells from the tissue into secondary lymphoid organs and to direct them to the sites of inflammation. Since it is evident that vessel-on-chip has almost unlimited potential for its integration into the OoC field amongst numerous scientific disciplines[116, 117], this review focusses only on literature which includes vessel-on-chip to study immune cell migration. As such, features of lymphoid organs- and immunocompetent vasculature-on-chip are summarised together in Table 1 and discussed in detail below.

Primary lymphoid organs

In comparison to other organ models, lymphoid organ-on-chip models are distinctive for their abundance of immune cells since they play a primary role in regulating our immune system. The bone marrow and thymus are essential constituents of our immune system. Innate immune cells arise in the bone marrow and mature in tissue. Adaptive immune cells stem from the bone marrow, functionally mature in the thymus and differentiate in the lymph nodes. In this review, we focus on bone marrow-on-chip models for immune cells, as immunocompetent thymus-on-chips are yet to be developed.
The bone marrow is a complex organ that consists of several unique niches with differing microenvironments of ECM structures to perform several functions, namely erythropoiesis, myelopoiesis and lymphopoiesis. The first bone marrow-on-chip model was created by implanting a PDMS device into the bone marrow of mice, loaded with bone marrow-stimulating growth factors. The device was then explanted after 8 weeks of growth and maintained for up to seven days ex vivo. The model, albeit using mice in this study, was shown to accurately mimic physiological niches in the bone marrow and was later used in drug toxicity tests[67]. Progress without using animal material for bone marrow niches are now widely modelled on chip. Numerous studies have recreated the endosteal niche, located at the surface of the bone for hematopoietic stem and progenitor cell (HSPC) differentiation, on chip to highlight the importance of mesenchymal stromal cell adhesion and cytokine secretion for CD34+ HSPCs maintenance and haematopoiesis[68, 70, 71]. Currently, one bone marrow-on-chip study has demonstrated the formation of macrophage colonies from HSPCs[69] and, to date, the generation of further immune cell subsets are yet to be recapitulated.
One of the most studied diseases on bone marrow-chips is bone marrow cancer. As the bone marrow is closely situated to the blood supply, cancers that develop in the bone marrow can be prone to metastasis. This proximity provides a route for cancer cells to enter the bloodstream, facilitating their travel to distant organs and the subsequent formation of secondary tumours. This is particularly perilous, as the spread of cancer cells can impact the normal functioning of various organs. Cancer cells have been included in bone marrow-on-chips to study tumour migration, indicating preferential metastasis to different niches[71]. Moreover, anti-leukaemia drugs have been screened in bone marrow-on-chips. Here, the 3D microenvironment was deemed to protect the cancer cells from drug-induced apoptosis compared to 2D cultures[72], highlighting the advantages of chip models for the study of drug efficacy. In addition to bone marrow cancer-on-chip, the genetic disease Shwachman–Diamond syndrome (SDS) was emulated on chip, where mechanisms of the disease pathophysiology were revealed to indicate association with neutrophil maturation impairment[70].
The modelling of bone marrow-on-chip is a complex task since the bone marrow features an intricate organisation of different compartments, each with their own functions. Future improvements could be made by demonstrating haematopoiesis for multiple immune cell subsets and/or the inclusion of lymphoid progenitors. Further development of these models is crucial in our understanding of the bone marrow microenvironment.

Secondary lymphoid organs

Secondary lymphoid organs are strategically located throughout the body and are inter-connected by a network of lymphatic vessels that transport lymph-fluid drained from the peripheral tissues. These organs include lymph nodes, tonsils, spleen and peyer's patches. Their key feature is a complex multicellular environment that is organised into special niches by lymph node stromal cells (LNSCs), and this is where the adaptive immune response is orchestrated[118]. Due to the involvement of secondary lymphoid organs in the pathophysiology of inflammatory diseases and tumour metastasis, recreating an organotypic lymph node environment that encompasses every biological process is challenging. While there is a lot of complexity to immunological processes within lymph nodes, the majority of models have used PBMC-derived moDCs, T cells and B cells to investigate immune cell clustering. This research has included dynamic perfusion with adaptive immune readouts such as plasma cell differentiation, antigen-specific antibody formation and cytokine productions[76–78]. Furthermore, imitation of immune cell chemotaxis across lymph nodes has extended to include DC maturation and migration in the direction of flow to T cell compartments[73, 79]. DC migration could be standardised using the commercially available drug hydroxychloroquine, which induced reactive oxygen species in T cells on the chip[74]. Cell-cell interactions have also been explored by investigating adhesion molecules in a subcapsular sinus model[80], although the extent of this cellular characterisation remains somewhat limited.

The spleen is another secondary lymphoid organ which, unlike the lymph node, filters blood. Initial efforts have been made to recapitulate core spleen-functions, such as blood filtration, from perfusion of ex-vivo spleen tissue[81] and spleen-on-chip devices using red blood cells (RBCs)[82]. Intriguingly, macrophages were used in a spleen-on-chip model of sickle cell disease that revealed differences in their phagocytic capabilities between sickled red RBCs and non-sickled RBCs, under hypoxia[83]. In spite of the fact that robust spleen features have been well-characterised with immune cells-on-chip, the technical developments to advance spleen-on-chip models are still at an early stage. For example, further studies to recreate immune cell behaviour with spleen-on-chip are required to more accurately portray splenic tissue biology, as well as using such models to better investigate infectious diseases, like visceral leishmaniasis[119].

The challenges of modelling secondary lymphoid organs, the lymph node in particular, lies in their complexity. A vital feature across all lymph node-on-chip models to date is their lack of stromal cells, in contrast to other tissue/organ models-on-chip, which all contained a stromal component, as detailed above. Currently, there is one chip model has included fibroblast reticular cells (FRCs) from a cell line source[75], which showcased DC and T cell migration towards this FRC compartment. There is clearly an unmet need for incorporation of these FRCs, given their role in not only shaping immune responses within the lymph node[120], but also their importance for immune cell survival and functioning in a 3D environment[121]. Considering the abundance of lymph nodes in the human body and their central role in continuous filtration of interstitial fluid containing toxins, metabolites, and immune cells from large organ barriers (such as skin), lymph nodes are an ideal candidate for incorporation into multi-OoCs. Combined with other organ models, this can allow the recreation of a systemic immune response *in vitro*, as depicted in the schematic of Fig. 2.

Vasculature

Blood and lymphatic vessels play an important role in immunological processes by trafficking immune cells between organs, tissue and the lymphatic system. Blood vessels allow for the transport and circulation of a plethora of lymphocytes from primary lymphoid organs into secondary lymphoid organs via high endothelial venules, as well as multiple other organs and tissue types. Lymphatic vessels drain interstitial fluid, which contains waste metabolites, pathogens and activated APCs, from all tissue to secondary lymphoid organs through afferent lymphatic vessels, for filtration and to initiate adaptive immunity. Once primed in secondary lymphoid organs, immune cells leave through efferent lymphatic vessels, and re-join the peripheral circulation. Therefore, without vasculature, it is not possible for a systemic immune response to occur. Vascularisation of organ models within microfluidic devices has become somewhat of a hot topic in the OoC field. This includes the integration of ECs under a single organotypic model and/or the seeding of ECs in vessel-like compartments entering or leaving the organ model. These models can provide insight into significant parameters such as blood and lymphatic vessel permeability of endothelial walls, shear stress, vessel formation and inflammatory responses, such as cytokine production. In addition, immune cell migration and cancer metastasis can also be modelled. Typically, the configurations of vessels-on-chip involves a primary microfluidic channel that can be populated with ECs, allowing immune cells to be administered through this channel. ECs can form lumen-like structures, which are often surrounded by a matrix containing stimulants or even tumour cells.

As such, vascular inflammation-on-chip with immune cell migration revealed that cytokine-stimulated PBMCs could change EC barrier properties, such as affecting EC morphology and upregulation of certain adhesion molecules[84]. Similarly, T cells were characterised on their response to chemotactic gradients and shown to interact with ECs through transmigration into ECM hydrogels[85–87]. The versatility of T cells was explored in other vascularised OoCs to highlight their functionality against tumour cells[88, 89]. Another immune cell type regularly integrated into vessels-on-chip is the neutrophil. It has been shown that ECM components can dictate their migration capacities[90]. Neutrophils were shown to exacerbate tumour cell metastasis in an ovarian cancer-on-chip device, indicating their unique role in cancer progression, which may have been overlooked in standard static cultures[91]. A similar result was also observed with LPS-stimulated neutrophils that disrupted EC barriers and enhanced tumour cell extravasation[92]. Likewise, APC characteristics could be recapitulated with vessels-on-chip, where DCs exhibited their antigen capturing and presenting ability along a chemotactic gradient[93] and macrophages exhibited phagocytic capacities[94]. M1 macrophages were also seen significantly inhibited tumour-induced angiogenesis on chip[95]. These cellular functions even extended to NK cells, which underwent trans-endothelial migration and killed tumour cells on chip[96]. Further NK cell killing properties were also displayed through trans-endothelial migration into breast cancer spheroids-on-chip[97]. In summary, there are numerous prospects to explore immune cell migration through vessels-on-chip. While it is already at a promising stage, this could be better accomplished by defining the use of blood ECs (BECs) or lymphatic ECs (LECs) for showing specific immune processes. As such, vessels-on-chip possesses unlimited potential for integration into pre-existing organ models and multi-OoC devices, aiming to truthfully replicate a systemic immune response *in vitro* (Fig. 2).

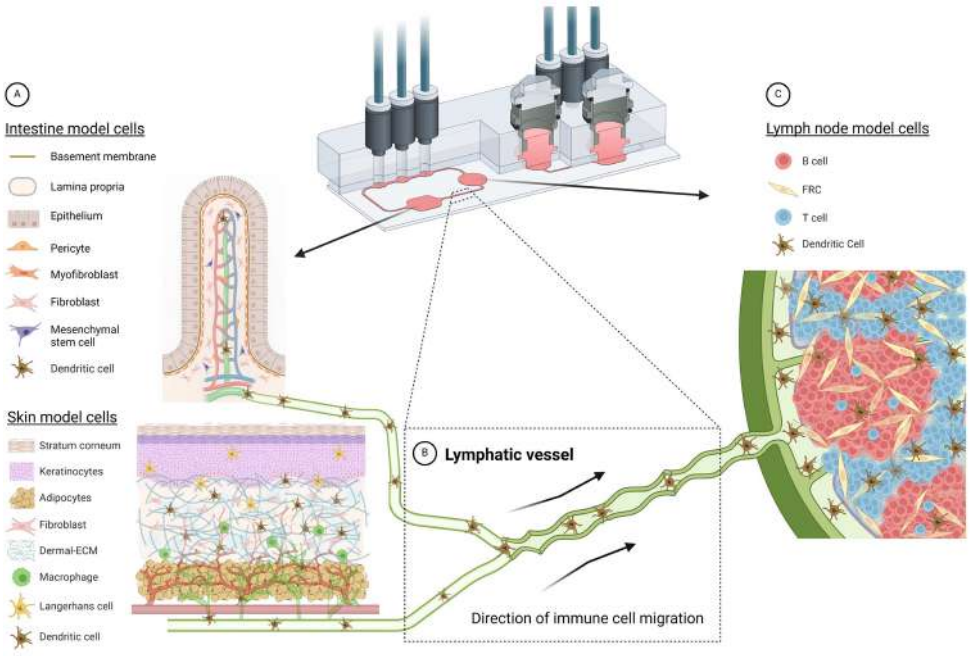

Fig. 2 - Schematic illustration of a potential organ-draining lymph node-on-chip. Exemplar use of a TissUse multi-OoC device to demonstrate immune cell migration between an organotypic skin or intestine model **(A)** through lymphatic vasculature **(B)** to an organotypic lymph node model **(C)**. This is representative of a standard immune response, where skin Langerhans cells and skin/intestine dendritic cells can become activated in the epidermis or dermis/lamina propria, respectively, due to either allergen/bacterial exposure, injury or disease. APC migrate into the lymphatic vessels for their journey to the lymph node for antigen presentation to the adaptive immune cells. Such a response can be possible using multi-OoCs, as well as other types of organ-crosstalk models. Chip image is courtesy of TissUse GmbH. Image of intestine model is credited to and adapted from[122]. Created with BioRender.com.

Multi-organ-on-chip

The systemic physiological nature of the human immune response ensures a coordinated, total-body defence against a variety of health threats, like infections, cancer and toxic substances. This is why multi-OoCs have been developed. The arrangement of multi-OoCs can either be one microfluidic device that contains multiple interconnected organ models via channels and chambers, or multiple separate single-OoC microfluidic devices that are externally connected through tubing. The goal of such an integrated system, even without immune cells, offers a beneficial predictive value for drug safety and toxicity testing at a more systemic physiological level[123]. From an immunology perspective *in vitro*, the potential of multi-OoCs are ideal for replicating dynamic immune cell migration between human organs to initiate tissue-specific immune responses. A comprehensive summary of all multi-OoC attributes with immune cells is displayed in Table 2, visualised in Fig. 2, 3, and elaborated upon below.

Human-on-chip

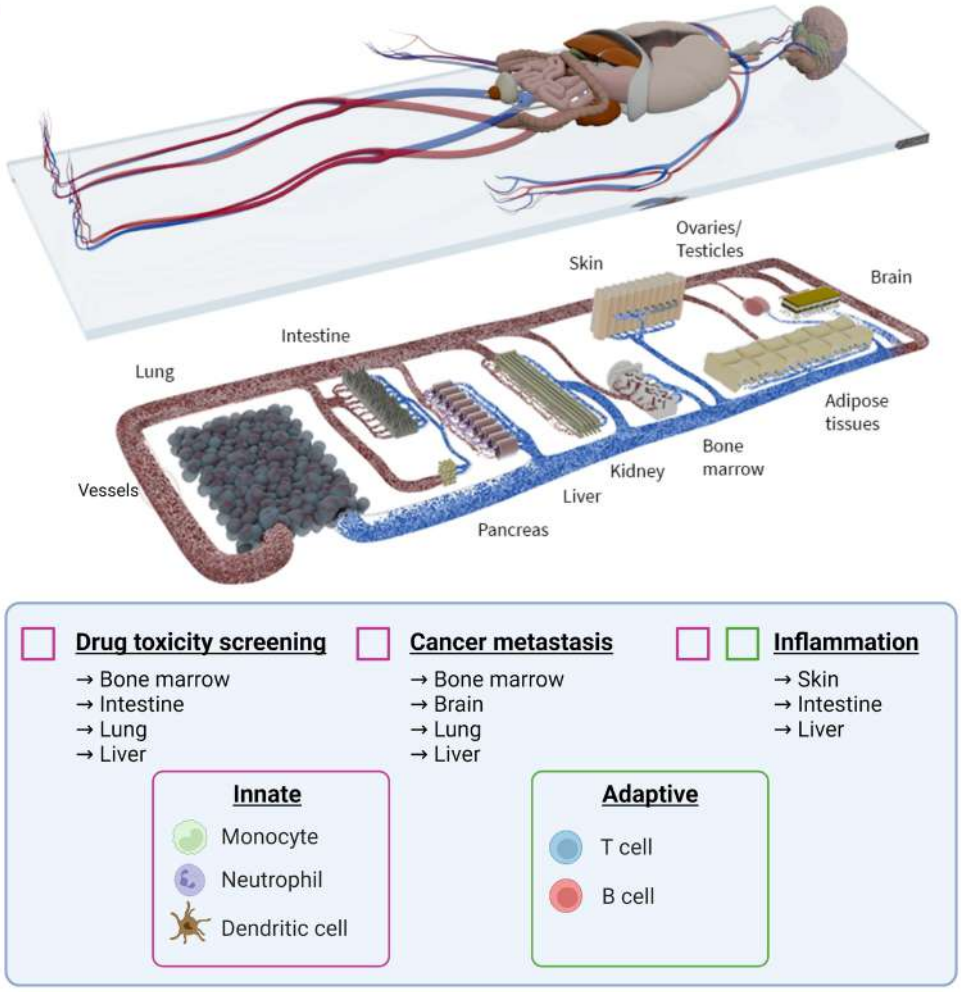

Fig. 3 - Schematic overview of a human-on-chip design from all possible immunocompetent multi-OoCs. Immune cells (innate and adaptive) are colour-coded to show the combinations to which they are currently used in various biological processes and applications. Connecting and expanding such multi-OoCs would create the ability to recapitulate human physiology in an *in vitro* setting, albeit on a more simplified level. Image is courtesy of TissUse GmbH. Created with BioRender.com.

Table 2. **Overview of all immunocompetent multi-organ-on-chip models.** P: primary, CL: cell line, IC: immune cell, SC: stromal cell, MD: microfluidic device, R: read-out

Organ	Simulated feature(s)	Cell types	Microfluidic device and readouts
Gut/Skin[119]	Gut inflammation and lipid uptake on skin	**IC:** (P) macrophages **SC:** (P) dermal fibroblasts, keratinocytes (CL) Caco-2 cells	**MD:** in-house **R:** cell viability, metabolite production, cytokine/chemokine secretion, permeability and immunofluorescence
Liver/Gut[116, 117]	Inflammation mediated modulation of drug disposition.	**IC:** (P) Kupffer cells, DCs, T cells[117] **SC:** (P) hepatocytes (CL) Caco-2 cells and HT29-MTX[116]	**MD:** in-house **R:** cytokine/chemokine secretion and gene expression
Skin/Gingiva[118]	Nickel induced inflammation	**IC:** (CL) LCs **SC:** (P) keratinocytes, fibroblasts	**MD:** commercial HUMIMIC multi-OoC (TissUse), dynamic system
Lung/BBB[120]	Lung cancer metastasis to the brain	**IC:** (CL) THP-1 monocytes **SC:** (CL) lung cancer cells, fibroblast, ECs, epithelial cells, astrocytes, ECs	**MD:** in-house **R:** barrier integrity and permeability, immunofluorescence and cytokine/chemokine secretion and gene expression
Lung/Liver/Heart[121]	Drug toxicity screening	**IC:** (P) Kupffer cells **SC:** (P) hepatic stellate cells, hepatocytes, iPSC-derived cardiomyocytes, cardiac fibroblasts, ECs, stromal mesenchymal cells, bronchial epithelial cells	**MD:** in-house **R:** barrier function (microscopy, electrical resistance and fluorescent tracers), inflammation (cytokine secretion), viability, metabolite secretion
Gut/Liver/Kidney/Bone Marrow[123]	First pass metabolism, PK and toxicity.	**IC:** (P) CD34+ progenitor cells	**MD:** in-house **R:** viability and cell tracking by immunofluorescence

At a two-organ immunocompetent multi-OoC level, crosstalk between the gut and liver during LPS-induced inflammation was recreated by administering DCs to the gut compartment and Kupffer cells to the liver model. Here, the upregulation of immune pathway genes and pro-inflammatory cytokines was detected when the immune cells were present in each organ compartment[99]. In a separate gut-liver axis study, the addition of circulating T cells enhanced IBD-like conditions on the multi-OoC, enhancing its practical use for a disease-based model[100]. In another study, the skin was separately combined in two multi-OoCs devices, such as connection to gingiva[101] and the gut[98]. The skin-gingiva

organotypic model on chip mimicked a clinical case study where topical allergen exposure to the gingiva resulted in activation of a skin immune response, as illustrated by LC migration in the skin model thus representing a systemic inflammatory response. The gut-skin multi-OoC assessed the downstream effect of fatty acid absorption by the gut model on skin inflammation, where macrophages increased nitric oxide uptake, associated with a pro-inflammatory response. Next to this, a lung-blood brain barrier (BBB) multi-OoC was developed containing monocytes to study the epigenetics of non-small cell lung cancer. The outcome was a consistent data profile between mice and patient studies, indicating an accurate proof-of-principle set up that does not require animal models[102]. A singular immunocompetent three-organ multi-OoCs has been developed, where lung-liver-heart organs were connected through external tubing linking microreactors. Using liver Kupffer cells, cardiotoxicity was to be mediated by pro-inflammatory cytokine secretion after inducing toxicity to the lung model with bleomycin, a chemotherapy antibiotic[103]. Four-organ multi-OoCs have demonstrated crosstalk among organs in both lung-brain-bone-liver and gut-liver-kidney-bone marrow multi-OoCs. The lung-brain-bone-liver multi-OoC showcased immune involvement, where monocytes seeded in the lung tissue differentiated to M2 macrophages after tumour cell introduction. This provoked transmigration of cancer cells into other tissues and inflicted damage on the astrocytes (brain tissue), osteocytes (bone tissue) and hepatocyte (liver tissue) organ compartments[124]. The gut-liver-kidney-bone marrow multi-OoC used CD34+ progenitor immune cells to represent the bone marrow and study metabolomics with pharmacodynamic and pharmacokinetic parameters. However, such readouts were not immunology-related[104]. In summary, immunocompetent multi-OoCs are still in their initial stages of development, predominantly featuring innate over adaptive immune cells. Multi-OoCs represent the ultimate frontier in replicating systemic immunological processes in an in vitro environment. It is evident that progress is being made in the immunotoxicity field, but the path ahead is long and numerous challenges still need to be overcome.

Conclusion and perspectives

OoCs are crucial for advances in studying immunity *in vitro*. However, scientists are challenged by the most optimal chip design, fabrication and implementation to address biological questions. Human immunology is complicated on a physiological level and this review has aimed to summarise the extent of which the immune system has been recapitulated into OoC models.

In general, the innate branch of the immune system has most frequently been included into single- and multi-OoC compared to adaptive immune cells. From a logical perspective, these innate cells are the first line of defence against external pathogens, disease and inflammation, and therefore offer an unspecific and diligent response that may be easier to model. Such immune cells are readily available through PBMC-isolation from blood donors or as cell lines, allowing practical universal benefits and a somewhat unlimited source of cells. However, as we learn more about tissue microenvironments, the importance of tissue-specific immune cells becomes apparent and must be considered. This

for example includes the liver Kupffer cells or skin LCs, which each exhibit specific environmental profiles that dictate their tissue functioning.

While adaptive immune cells have been employed sparingly in non-lymphoid OoCs, these cells present a genuine assessment of functional specificity due to their long-lasting and memory-like properties representing the adaptive immune response. Once successfully integrated and thoroughly evaluated, this development will mark a significant step towards systemic immunology *in vitro*, further complementing areas such as disease modelling, drug testing and personalised medicine. As OoCs become more and more advanced and complicated, this will allow the opportunity to use tissue-specific cells that can either be obtained from biopsies or more appealingly; iPSCs. The strength of using iPSC-derived immune cells above primary cells or cell lines will be that they will enable donor-matched autologous cell types to be integrated into OoCs, thus bypassing the allogenic responses in a donor HLA-mismatch, a vital hurdle for immune modelling. However, the current limitations with iPSCs include the incomplete maturation status of the differentiated cells, unknown ability to skew towards tissue specificity and, especially in the immunology field, their unknown ability to generate diverse repertoires of T and B cells. The origin of these cell types can naturally raise complex questions concerning whether an individual's sex, age or lifestyle choice might influence their functionality in an OoC, especially considering how our immune system alters over time under the influence of epigenetic factors[125].

As mentioned above, OoCs still lack the inclusion of all organ-specific cells. This is where the organoid field can act as a promising tool for creating models of the immune system for organ-on-chip. Such examples include kidney organoid-on-chip[126] and BBB-on-chip[127], which both feature T cells that demonstrate tumour eradication and adhesion, extravasation, and migration under inflammatory conditions. Additionally, a primary NK cell model has illustrated dynamic extravasation into a physically separated tumour cell niche on a microfluidic device[128], indicating that immune cell migration can be recapitulated without using an actual organ model on the chip. For immune organs, human tonsil organoids have been established to show early promise for modelling vaccine efficacy[129] and a lymphoma microenvironment[130]. However, these tonsil models do not feature or acknowledge stromal cells, which are integral for lymphoid organ functioning as alluded to earlier. In future studies, we anticipate a greater shift towards making these organoid models into more immunology based-on-chip. The gold standard consideration is to what extent one must delicately balance the complexity and simplicity of the biological and technical OoC design. For example, a liver-on-chip was able to detect close to 90% of drug-induced liver toxicity in patients, a result that went completely under the radar in an animal model[131 132]. While this liver-on-chip did not include immune cells, it is just one initial example of the potential promise that immunocompetent OoCs will have in superiority over animal experiments. Likewise, the very first lung-on-chip, developed by Emulate, mimicked lung pathology to a level that was never observed before in an *in vitro* setting[42]. Not to mention, the technical design of such microfluidic devices must be considered for adding an immune element. The 3D environment of tissue models, whether that be built around biological or synthetic scaffolds, need to mimic the correct ECM of the native organ[133], and should be bio-compatible and spatially suitable for bringing into a microfluidic compartment[134]. Care must also be taken in regards to the properties of such

biomaterials on immune cell sensitivity. For example, hydrogel components like fibrinogen can modulate immune cell behaviour in either a suppressive or supportive manner[135, 136]. Other factors such as the mechanical stimuli within the microfluidic device, such as shear stress, flow rate etc., and the type of experimental readouts, such as in-line or end-point sampling, must all be acknowledged when studying human immunology.

How far this work can progress into human immunology-on-chip, rather than multi-OoCs, is somewhat of a paradoxical outstanding question that only time will tell if it will be a tangible possibility or whether it is even needed. The recent approval by the US FDA for OoCs to be used in pre-clinical testing[15] has complemented the progress of this field which works towards efficient standardisation and safe robust use of such chips, as well as incorporating the immune system. This has already seen a benefit from a drug repurposing perspective, as a human lung-on-chip accelerated the discovery of a novel class of RNA-based therapeutics, where a pathological role of receptor found on lung alveolar cells was identified in viral infections[32]. Such an avenue is also highly appealing for big pharma, as it has been reported that OoCs could reduce up to 26% of the costs for each drug that is approved[137], therefore applicable companies with the appropriate resources can invest to scale up OoC research, and in turn save finances, accelerate drug development and deliver the promise of personalised medicine in the near future[138, 139].

In conclusion, improvements of immunocompetent single-OoC and multi-OoC models are critical for their utilisation in both the fundamental research and drug development field. The closer these models come to accurately represent physiological systemic processes, the more widely available and applicable they will become. In this way, they will play a pivotal role in the need to study human diseases in more physiologically relevant models.

Contributions

AM: Conceptualization, Writing – original draft. MS: Writing – original draft. LV: Writing – original draft. SG: Conceptualization, Funding acquisition, Supervision, Writing – review & editing. JK: Conceptualization, Supervision, Writing – review & editing.

Acknowledgments

We would like to extend our appreciation to Emulate Inc., MIMETAS US Inc., and TissUse GmbH for granting us permission to use their images in this review.

References

[1] World Health O. WHO methods and data sources for country-level causes of death 2000-2019 2020 [Available from: https://www.who.int/data/gho/data/themes/mortality-and-global-health-estimates/ghe-leading-causes-of-death.

[2] Pognan F, Beilmann M, Boonen HCM, Czich A, Dear G, Hewitt P, et al. The evolving role of investigative toxicology in the pharmaceutical industry. Nat Rev Drug Discov. 2023;22(4):317-35.

[3] Lindstrand A, Cherian T, Chang-Blanc D, Feikin D, O'Brien KL. The World of Immunization: Achievements, Challenges, and Strategic Vision for the Next Decade. J Infect Dis. 2021;224(12 Suppl 2):S452-S67.

[4] Weaver RJ, Valentin JP. Today's Challenges to De-Risk and Predict Drug Safety in Human "Mind-the-Gap". Toxicol Sci. 2019;167(2):307-21.

[5] Leenaars CHC, Kouwenaar C, Stafleu FR, Bleich A, Ritskes-Hoitinga M, De Vries RBM, Meijboom FLB. Animal to human translation: a systematic scoping review of reported concordance rates. J Transl Med. 2019;17(1):223.

[6] Sun D, Gao W, Hu H, Zhou S. Why 90% of clinical drug development fails and how to improve it? Acta Pharmaceutica Sinica B. 2022.

[7] Zhao C. Cell culture: in vitro model system and a promising path to in vivo applications. J Histotechnol. 2023;46(1):1-4.

[8] Marx U, Akabane T, Andersson TB, Baker E, Beilmann M, Beken S, et al. Biology-inspired microphysiological systems to advance patient benefit and animal welfare in drug development. ALTEX. 2020;37(3):365-94.

[9] Langhans SA. Three-Dimensional in Vitro Cell Culture Models in Drug Discovery and Drug Repositioning. Front Pharmacol 2018;9(6).

[10] Huh D, Hamilton GA, Ingber DE. From 3D cell culture to organs-on-chips. Trends Cell Biol. 2011;21(12):745-54.

[11] Leung CM, de Haan P, Ronaldson-Bouchard K, Kim G-A, Ko J, Rho HS, et al. A guide to the organ-on-a-chip. Nature Reviews Methods Primers. 2022;2(1):33.

[12] Cao UMN, Zhang Y, Chen J, Sayson D, Pillai S, Tran SD. Microfluidic Organ-on-A-chip: A Guide to Biomaterial Choice and Fabrication. Int J Mol Sci. 2023;24(4).

[13] Wu Q, Liu J, Wang X, Feng L, Wu J, Zhu X, et al. Organ-on-a-chip: recent breakthroughs and future prospects. BioMed Eng OnLine. 2020.

[14] Sharifi F, Su Htwe S, Righi M, Liu H, Pietralunga A, Yesil-Celiktas O, et al. A Foreign Body Response-on-a-Chip Platform. Advanced Healthcare Materials. 2019;8(4):1801425-.

[15] Federal Food D, and Cosmetics Act S.5002 - FDA Modernization Act 2.0 2022 [Available from: https://www.congress.gov/bill/117th-congress/senate-bill/5002.

[16] Han JJ. FDA Modernization Act 2.0 allows for alternatives to animal testing. Artif Organs. 2023;47(3):449-50.

[17] Morsink MAJ, Willemen NGA, Leijten J, Bansal R, Shin SR. Immune Organs and Immune Cells on a Chip: An Overview of Biomedical Applications. Micromachines (Basel). 2020;11(9):849.

[18] Polini A, Del Mercato LL, Barra A, Zhang YS, Calabi F, Gigli G. Towards the development of human immune-system-on-a-chip platforms. Drug Discov Today. 2019;24(2):517-25.

[19] Maharjan S, Cecen B, Zhang YS. 3D Immunocompetent Organ-on-a-Chip Models. Small Methods. 2020;4(9):2000235-.

[20] Michaels YS, Buchanan CF, Gjorevski N, Moisan A. Bioengineering translational models of lymphoid tissues. Nature Reviews Bioengineering. 2023.

[21] Hiam-Galvez KJ, Allen BM, Spitzer MH. Systemic immunity in cancer. Nat Rev Cancer. 2021;21(6):345-59.

[22] Zmora N, Bashiardes S, Levy M, Elinav E. The Role of the Immune System in Metabolic Health and Disease. Cell Metab. 2017;25(3):506-21.

[23] Sattler S. The Role of the Immune System Beyond the Fight Against Infection. Adv Exp Med Biol. 2017;1003:3-14.

[24] Saferding V, Bluml S. Innate immunity as the trigger of systemic autoimmune diseases. J Autoimmun. 2020;110:102382.
[25] Oronsky B, Caroen S, Reid T. What Exactly Is Inflammation (and What Is It Not?). Int J Mol Sci. 2022;23(23).
[26] Chen L, Deng H, Cui H, Fang J, Zuo Z, Deng J, et al. Inflammatory responses and inflammation-associated diseases in organs. Oncotarget. 2018;9(6):7204-18.
[27] McDaniel MM, Meibers HE, Pasare C. Innate control of adaptive immunity and adaptive instruction of innate immunity: bi-directional flow of information. Curr Opin Immunol. 2021;73:25-33.
[28] Janeway CA, Jr. Approaching the asymptote? Evolution and revolution in immunology. Cold Spring Harb Symp Quant Biol. 1989;54 Pt 1:1-13.
[29] Magenau J, Runaas L, Reddy P. Advances in understanding the pathogenesis of graft-versus-host disease. Br J Haematol. 2016;173(2):190-205.
[30] Van Os L, Engelhardt B, Guenat OT. Integration of immune cells in organs-on-chips: a tutorial. Front Bioeng Biotechnol. 2023;11:1191104.
[31] Stamataki Z, Swadling L. The liver as an immunological barrier redefined by single-cell analysis. Immunology. 2020;160(2):157-70.
[32] Snyder ME, Farber DL. Human lung tissue resident memory T cells in health and disease. Curr Opin Immunol. 2019;59:101-8.
[33] Huh D, Matthews BD, Mammoto A, Montoya-Zavala M, Hsin HY, Ingber DE. Reconstituting organ-level lung functions on a chip. Science. 2010;328(5986):1662-8.
[34] Benam KH, Villenave R, Lucchesi C, Varone A, Hubeau C, Lee HH, et al. Small airway-on-a-chip enables analysis of human lung inflammation and drug responses in vitro. Nat Methods. 2016;13(2):151-7.
[35] Domizio JD, Gulen MF, Saidoune F, Thacker VV, Yatim A, Sharma K, et al. The cGAS-STING pathway drives type I IFN immunopathology in COVID-19. Nature. 2022;603(7899):145-51.
[36] Zhang M, Wang P, Luo R, Wang Y, Li Z, Guo Y, et al. Biomimetic Human Disease Model of SARS□CoV□2□ Induced Lung Injury and Immune Responses on Organ Chip System. Advanced Science. 2021;8(3).
[37] Thacker VV, Sharma K, Dhar N, Mancini G-F, Sordet-Dessimoz J, McKinney JD. Rapid endotheliitis and vascular damage characterize SARS-CoV-2 infection in a human lung-on-chip model. EMBO reports. 2021;22(6):e52744-e.
[38] Bein A, Kim S, Goyal G, Cao W, Fadel C, Naziripour A, et al. Enteric Coronavirus Infection and Treatment Modeled With an Immunocompetent Human Intestine-On-A-Chip. Frontiers in Pharmacology. 2021;12.
[39] van Os L, Yeoh J, Witz G, Ferrari D, Krebs P, Chandorkar Y, et al. Immune cell extravasation in an organ-on-chip to model lung inflammation. Eur J Pharm Sci. 2023;187:106485.
[40] Bai H, Si L, Jiang A, Belgur C, Zhai Y, Plebani R, et al. Mechanical control of innate immune responses against viral infection revealed in a human lung alveolus chip. Nature Communications. 2022;13(1):1-17.
[41] Si L, Bai H, Rodas M, Cao W, Oh CY, Jiang A, et al. A human-airway-on-a-chip for the rapid identification of candidate antiviral therapeutics and prophylactics. Nature Biomedical Engineering. 2021;5(8):815-29.
[42] Mejías JC, Nelson MR, Liseth O, Roy K. A 96-well format microvascularized human lung-on-a-chip platform for microphysiological modeling of fibrotic diseases. Lab on a Chip. 2020;20(19):3601-11.
[43] Kerns SJ, Belgur C, Petropolis D, Kanellias M, Barrile R, Sam J, et al. Human immunocompetent Organ-on-Chip platforms allow safety profiling of tumor-targeted T-cell bispecific antibodies. eLife. 2021;10.
[44] Kerns JS, Belgur C, Kanellias M, Manatakis DV, Barrile R, Tien-Street W, et al. Safety Profiling of Tumor-targeted T Cell-Bispecific Antibodies with Alveolus Lung- and Colon-on-Chip. Bio Protoc. 2023;13(1).
[45] Nawroth JC, Lucchesi C, Cheng D, Shukla A, Ngyuen J, Shroff T, et al. A microengineered airway lung chip models key features of viral-induced exacerbation of asthma. American Journal of Respiratory Cell and Molecular Biology. 2020;63(5):591-600.
[46] Zhang C, Merana GR, Harris-Tryon T, Scharschmidt TC. Skin immunity: dissecting the complex biology

of our body's outer barrier. Mucosal Immunol. 2022;15(4):551-61.
[47] Rodrigues Neves C, Gibbs S. Progress on Reconstructed Human Skin Models for Allergy Research and Identifying Contact Sensitizers. Curr Top Microbiol Immunol. 2021;430:103-29.
[48] Ramadan Q, Ting FC. In vitro micro-physiological immune-competent model of the human skin. Lab Chip. 2016;16(10):1899-908.
[49] Ren X, Getschman AE, Hwang S, Volkman BF, Klonisch T, Levin D, et al. Investigations on T cell transmigration in a human skin-on-chip (SoC) model. Lab Chip. 2021;21(8):1527-39.
[50] Biglari S, Le TYL, Tan RP, Wise SG, Zambon A, Codolo G, et al. Simulating Inflammation in a Wound Microenvironment Using a Dermal Wound-on-a-Chip Model. Adv Healthc Mater. 2019;8(1):e1801307.
[51] Kwak BS, Jin SP, Kim SJ, Kim EJ, Chung JH, Sung JH. Microfluidic skin chip with vasculature for recapitulating the immune response of the skin tissue. Biotechnology and Bioengineering. 2020;117(6):1853-63.
[52] Vahav I, Thon M, van den Broek LJ, Spiekstra SW, Atac B, Lindner G, et al. Proof-of-Concept Organ-on-Chip Study: Topical Cinnamaldehyde Exposure of Reconstructed Human Skin with Integrated Neopapillae Cultured under Dynamic Flow. Pharmaceutics. 2022;14(8).
[53] Jager J, Vahav I, Thon M, Waaijman T, Spanhaak B, de Kok M, et al. Reconstructed Human Skin with Hypodermis Shows Essential Role of Adipose Tissue in Skin Metabolism. Tissue Eng Regen Med. 2024;21(3):499-511.
[54] Rogal J, Roosz J, Teufel C, Cipriano M, Xu R, Eisler W, et al. Autologous Human Immunocompetent White Adipose Tissue-on-Chip. Adv Sci (Weinh). 2022;9 (18):e2104451.
[55] Kim K, Kim H, Sung GY. An Interleukin-4 and Interleukin-13 Induced Atopic Dermatitis Human Skin Equivalent Model by a Skin-On-A-Chip. International Journal of Molecular Sciences. 2022;23(4):2116-.
[56] Chassaing B, Kumar M, Baker MT, Singh V, Vijay-Kumar M. Mammalian gut immunity. Biomed J. 2014;37(5):246-58.
[57] Mowat AM, Agace WW. Regional specialization within the intestinal immune system. Nat Rev Immunol. 2014;14(10):667-85.
[58] Kim HJ, Ingber DE. Gut-on-a-Chip microenvironment induces human intestinal cells to undergo villus differentiation. Integr Biol (Camb). 2013;5(9):1130-40.
[59] Kim HJ, Li H, Collins JJ, Ingber DE. Contributions of microbiome and mechanical deformation to intestinal bacterial overgrowth and inflammation in a human gut-on-a-chip. Proc Natl Acad Sci U S A. 2016;113(1):E7-15.
[60] Maurer M, Gresnigt MS, Last A, Wollny T, Berlinghof F, Pospich R, et al. A three-dimensional immunocompetent intestine-on-chip model as in vitro platform for functional and microbial interaction studies. Biomaterials. 2019;220:119396.
[61] Jing B, Xia K, Zhang C, Jiao S, Zhu L, Wei J, et al. Chitosan Oligosaccharides Regulate the Occurrence and Development of Enteritis in a Human Gut-On-a-Chip. Front Cell Dev Biol. 2022;10:877892.
[62] Shin W, Kim HJ. Intestinal barrier dysfunction orchestrates the onset of inflammatory host-microbiome cross-talk in a human gut inflammation-on-a-chip. Proc Natl Acad Sci U S A. 2018;115(45):E10539-E47.
[63] Cherne MD, Sidar B, Sebrell TA, Sanchez HS, Heaton K, Kassama FJ, et al. A Synthetic Hydrogel, VitroGel® ORGANOID-3, Improves Immune Cell-Epithelial Interactions in a Tissue Chip Co-Culture Model of Human Gastric Organoids and Dendritic Cells. Frontiers in Pharmacology. 2021;12:707891-.
[64] Beaurivage C, Kanapeckaite A, Loomans C, Erdmann KS, Stallen J, Janssen RAJ. Development of a human primary gut-on-a-chip to model inflammatory processes. Scientific Reports. 2020;10(1):1-16.
[65] Gijzen L, Marescotti D, Raineri E, Nicolas A, Lanz HL, Guerrera D, et al. An Intestine-on-a-Chip Model of Plug-and-Play Modularity to Study Inflammatory Processes. SLAS Technol. 2020;25(6):585-97.
[66] Gjorevski N, Avignon B, Gerard R, Cabon L, Roth AB, Bscheider M, Moisan A. Neutrophilic infiltration in organ-on-a-chip model of tissue inflammation. Lab Chip. 2020;20(18):3365-74.
[67] Zhu W, Yu J, Nie Y, Shi X, Liu Y, Li F, Zhang XL. Disequilibrium of M1 and M2 macrophages correlates with

the development of experimental inflammatory bowel diseases. Immunol Invest. 2014;43(7):638-52.
[68] Lissner D, Schumann M, Batra A, Kredel LI, Kuhl AA, Erben U, et al. Monocyte and M1 Macrophage-induced Barrier Defect Contributes to Chronic Intestinal Inflammation in IBD. Inflamm Bowel Dis. 2015;21(6):1297-305.
[69] Naumovska E, Aalderink G, Wong Valencia C, Kosim K, Nicolas A, Brown S, et al. Direct On-Chip Differentiation of Intestinal Tubules from Induced Pluripotent Stem Cells. Int J Mol Sci. 2020;21(14).
[70] Rajasekar S, Lin DSY, Abdul L, Liu A, Sotra A, Zhang F, Zhang B. IFlowPlate-A Customized 384-Well Plate for the Culture of Perfusable Vascularized Colon Organoids. Adv Mater. 2020;32(46):e2002974.
[71] Kubes P, Jenne C. Immune Responses in the Liver. Annu Rev Immunol. 2018;36:247-77.
[72] Groger M, Rennert K, Giszas B, Weiss E, Dinger J, Funke H, et al. Monocyte-induced recovery of inflammation-associated hepatocellular dysfunction in a biochip-based human liver model. Sci Rep. 2016;6(1):21868.
[73] Bircsak KM, DeBiasio R, Miedel M, Alsebahi A, Reddinger R, Saleh A, et al. A 3D microfluidic liver model for high throughput compound toxicity screening in the OrganoPlate(R). Toxicology. 2021;450:152667.
[74] Jang KJ, Otieno MA, Ronxhi J, Lim HK, Ewart L, Kodella KR, et al. Reproducing human and cross-species drug toxicities using a Liver-Chip. Sci Transl Med. 2019;11(517).
[75] Freag MS, Namgung B, Reyna Fernandez ME, Gherardi E, Sengupta S, Jang HL. Human Nonalcoholic Steatohepatitis on a Chip. Hepatol Commun. 2021;5(2):217-33.
[76] Ortega-Prieto AM, Skelton JK, Wai SN, Large E, Lussignol M, Vizcay-Barrena G, et al. 3D microfluidic liver cultures as a physiological preclinical tool for hepatitis B virus infection. Nature Communications. 2018;9(1):1-15.
[77] Sarkar U, Rivera-Burgos D, Large EM, Hughes DJ, Ravindra KC, Dyer RL, et al. Metabolite profiling and pharmacokinetic evaluation of hydrocortisone in a perfused three-dimensional human liver bioreactor. Drug Metab Dispos. 2015;43(7):1091-9.
[78] Moses SR, Adorno JJ, Palmer AF, Song JW. Vessel-on-a-chip models for studying microvascular physiology, transport, and function in vitro. Am J Physiol Cell Physiol. 2021;320(1):C92-C105.
[79] Pollet A, den Toonder JMJ. Recapitulating the Vasculature Using Organ-On-Chip Technology. Bioengineering (Basel). 2020;7(1).
[80] Torisawa YS, Spina CS, Mammoto T, Mammoto A, Weaver JC, Tat T, et al. Bone marrow-on-a-chip replicates hematopoietic niche physiology in vitro. Nat Methods. 2014;11(6):663-9.
[81] Nelson MR, Ghoshal D, Mejias JC, Rubio DF, Keith E, Roy K. A multi-niche microvascularized human bone marrow (hBM) on-a-chip elucidates key roles of the endosteal niche in hBM physiology. Biomaterials. 2021;270:120683.
[82] Glaser DE, Curtis MB, Sariano PA, Rollins ZA, Shergill BS, Anand A, et al. Organ-on-a-chip model of vascularized human bone marrow niches. Biomaterials. 2022;280:121245.
[83] Chou DB, Frismantas V, Milton Y, David R, Pop-Damkov P, Ferguson D, et al. On-chip recapitulation of clinical bone marrow toxicities and patient-specific pathophysiology. Nat Biomed Eng. 2020;4(4):394-406.
[84] Sieber S, Wirth L, Cavak N, Koenigsmark M, Marx U, Lauster R, Rosowski M. Bone marrow-on-a-chip: Long-term culture of human haematopoietic stem cells in a three-dimensional microfluidic environment. J Tissue Eng Regen Med. 2018;12(2):479-89.
[85] Bruce A, Evans R, Mezan R, Shi L, Moses BS, Martin KH, et al. Three-Dimensional Microfluidic Tri-Culture Model of the Bone Marrow Microenvironment for Study of Acute Lymphoblastic Leukemia. PLoS One. 2015;10(10):e0140506.
[86] Krishnamurty AT, Turley SJ. Lymph node stromal cells: cartographers of the immune system. Nature Immunology. 2020;21:369-80.
[87] Giese C, Demmler CD, Ammer R, Hartmann S, Lubitz A, Miller L, et al. A human lymph node in vitro--challenges and progress. Artif Organs. 2006;30(10):803-8.

[88] Giese C, Lubitz A, Demmler CD, Reuschel J, Bergner K, Marx U. Immunological substance testing on human lymphatic micro-organoids in vitro. J Biotechnol. 2010;148(1):38-45.

[89] Goyal G, Prabhala P, Mahajan G, Bausk B, Gilboa T, Xie L, et al. Ectopic Lymphoid Follicle Formation and Human Seasonal Influenza Vaccination Responses Recapitulated in an Organ-on-a-Chip. Advanced Science. 2022;9(14):2103241-.

[90] Mitra B, Jindal R, Lee S, Xu Dong D, Li L, Sharma N, et al. Microdevice integrating innate and adaptive immune responses associated with antigen presentation by dendritic cells. RSC Adv. 2013;3(36):16002-10.

[91] Shanti A, Samara B, Abdullah A, Hallfors N, Accoto D, Sapudom J, et al. Multi-Compartment 3D-Cultured Organ-on-a-Chip: Towards a Biomimetic Lymph Node for Drug Development. Pharmaceutics 2020, Vol 12, Page 464. 2020;12(5):464-.

[92] Hallfors N, Shanti A, Sapudom J, Teo J, Petroianu G, Lee S, et al. Multi-Compartment Lymph-Node-on-a-Chip Enables Measurement of Immune Cell Motility in Response to Drugs. Bioengineering (Basel). 2021;8(2):19.

[93] Birmingham KG, O'Melia MJ, Bordy S, Reyes Aguilar D, El-Reyas B, Lesinski G, Thomas SN. Lymph Node Subcapsular Sinus Microenvironment-On-A-Chip Modeling Shear Flow Relevant to Lymphatic Metastasis and Immune Cell Homing. iScience. 2020;23(11):101751.

[94] Buffet PA, Milon G, Brousse V, Correas JM, Dousset B, Couvelard A, et al. Ex vivo perfusion of human spleens maintains clearing and processing functions. Blood. 2006;107(9):3745-52.

[95] Rigat-Brugarolas LG, Elizalde-Torrent A, Bernabeu M, De Niz M, Martin-Jaular L, Fernandez-Becerra C, et al. A functional microengineered model of the human splenon-on-a-chip. Lab Chip. 2014;14(10):1715-24.

[96] Qiang Y, Sissoko A, Liu ZL, Dong T, Zheng F, Kong F, et al. Microfluidic study of retention and elimination of abnormal red blood cells by human spleen with implications for sickle cell disease. Proc Natl Acad Sci U S A. 2023;120(6):e2217607120.

[97] de Melo CVB, Hermida MD, Mesquita BR, Fontes JLM, Koning JJ, Solca MDS, et al. Phenotypical Characterization of Spleen Remodeling in Murine Experimental Visceral Leishmaniasis. Front Immunol. 2020;11:653.

[98] Kwee BJ, Akue A, Sung KE. On-chip human lymph node stromal network for evaluating dendritic cell and T-cell trafficking. bioRxiv. 2023:2023.03.21.533042.

[99] Grasso C, Pierie C, Mebius RE, van Baarsen LGM. Lymph node stromal cells: subsets and functions in health and disease. Trends Immunol. 2021;42(10):920-36.

[100] Morrison AI, Mikula AM, Spiekstra SW, de Kok M, Affandi AJ, Roest HP, et al. An Organotypic Human Lymph Node Model Reveals the Importance of Fibroblastic Reticular Cells for Dendritic Cell Function. Tissue Eng Regen Med. 2023.

[101] Ehlers H, Nicolas A, Schavemaker F, Heijmans JPM, Bulst M, Trietsch SJ, van den Broek LJ. Vascular inflammation on a chip: A scalable platform for trans-endothelial electrical resistance and immune cell migration. Front Immunol. 2023;14:1118624.

[102] de Haan L, Suijker J, van Roey R, Berges N, Petrova E, Queiroz K, et al. A microfluidic 3D endothelium-on-a-chip model to study transendothelial migration of T cells in health and disease. International Journal of Molecular Sciences. 2021;22(15).

[103] Aung A, Kumar V, Theprungsirikul J, Davey SK, Varghese S. An Engineered Tumor-on-a-Chip Device with Breast Cancer–Immune Cell Interactions for Assessing T-cell Recruitment. Cancer Research. 2020;80(2):263-75.

[104] Lin F, Butcher EC. T cell chemotaxis in a simple microfluidic device. Lab Chip. 2006;6(11):1462-9.

[105] Pavesi A, Tan AT, Koh S, Chia A, Colombo M, Antonecchia E, et al. A 3D microfluidic model for preclinical evaluation of TCR-engineered T cells against solid tumors. JCI Insight. 2017;2(12).

[106] Paek J, Park SE, Lu Q, Park KT, Cho M, Oh JM, et al. Microphysiological Engineering of Self-Assembled and Perfusable Microvascular Beds for the Production of Vascularized Three-Dimensional Human

Microtissues. ACS Nano. 2019;13(7):7627-43.
[107] Riddle RB, Jennbacken K, Hansson KM, Harper MT. Endothelial inflammation and neutrophil transmigration are modulated by extracellular matrix composition in an inflammation-on-a-chip model. Scientific Reports. 2022;12(1):1-14.
[108] Surendran V, Rutledge D, Colmon R, Chandrasekaran A. A novel tumor-immune microenvironment (TIME)-on-Chip mimics three dimensional neutrophil-tumor dynamics and neutrophil extracellular traps (NETs)-mediated collective tumor invasion. Biofabrication. 2021;13(3):035029-.
[109] Chen MB, Hajal C, Benjamin DC, Yu C, Azizgolshani H, Hynes RO, Kamm RD. Inflamed neutrophils sequestered at entrapped tumor cells via chemotactic confinement promote tumor cell extravasation. Proc Natl Acad Sci U S A. 2018;115(27):7022-7.
[110] Parlato S, De Ninno A, Molfetta R, Toschi E, Salerno D, Mencattini A, et al. 3D Microfluidic model for evaluating immunotherapy efficacy by tracking dendritic cell behaviour toward tumor cells. Scientific Reports. 2017;7(1):1-16.
[111] Boussommier-Calleja A, Atiyas Y, Haase K, Headley M, Lewis C, Kamm RD. The effects of monocytes on tumor cell extravasation in a 3D vascularized microfluidic model. Biomaterials. 2018;198:180-93.
[112] Bi Y, Shirure VS, Liu R, Cunningham C, Ding L, Meacham JM, et al. Tumor-on-a-chip platform to interrogate the role of macrophages in tumor progression. Integr Biol (Camb). 2020;12(9):221-32.
[113] Song J, Choi H, Koh SK, Park D, Yu J, Kang H, et al. High-Throughput 3D In Vitro Tumor Vasculature Model for Real-Time Monitoring of Immune Cell Infiltration and Cytotoxicity. Frontiers in Immunology. 2021;12:3848-.
[114] Ayuso JM, Truttschel R, Gong MM, Humayun M, Virumbrales-Munoz M, Vitek R, et al. Evaluating natural killer cell cytotoxicity against solid tumors using a microfluidic model. Oncoimmunology. 2019;8(3):1553477.
[115] Sung JH. Multi-organ-on-a-chip for pharmacokinetics and toxicokinetic study of drugs. Expert Opin Drug Metab Toxicol. 2021;17(8):969-86.
[116] Chen WLK, Edington C, Suter E, Yu J, Velazquez JJ, Velazquez JG, et al. Integrated gut/liver microphysiological systems elucidates inflammatory inter-tissue crosstalk. Biotechnol Bioeng. 2017;114(11):2648-59.
[117] Trapecar M, Communal C, Velazquez J, Maass CA, Huang YJ, Schneider K, et al. Gut-Liver Physiomimetics Reveal Paradoxical Modulation of IBD-Related Inflammation by Short-Chain Fatty Acids. Cell Syst. 2020;10(3):223-39 e9.
[118] Koning JJ, Rodrigues Neves CT, Schimek K, Thon M, Spiekstra SW, Waaijman T, et al. A Multi-Organ-on-Chip Approach to Investigate How Oral Exposure to Metals Can Cause Systemic Toxicity Leading to Langerhans Cell Activation in Skin. Frontiers in Toxicology. 2022;0:70-.
[119] Lee HR, Sung JH. Multi-Organ-on-a-Chip for Realization of Gut-Skin Axis. Biotechnology and Bioengineering. 2022.
[120] Liu W, Song J, Du X, Zhou Y, Li Y, Li R, et al. AKR1B10 (Aldo-keto reductase family 1 B10) promotes brain metastasis of lung cancer cells in a multi-organ microfluidic chip model. Acta Biomater. 2019;91:195-208.
[121] Skardal A, Murphy SV, Devarasetty M, Mead I, Kang HW, Seol YJ, et al. Multi-tissue interactions in an integrated three-tissue organ-on-a-chip platform. Scientific Reports. 2017;7(1):1-16.
[122] Xu Z, Li E, Guo Z, Yu R, Hao H, Xu Y, et al. Design and Construction of a Multi-Organ Microfluidic Chip Mimicking the in vivo Microenvironment of Lung Cancer Metastasis. ACS Appl Mater Interfaces. 2016;8(39):25840-7.
[123] Herland A, Maoz BM, Das D, Somayaji MR, Prantil-Baun R, Novak R, et al. Quantitative prediction of human pharmacokinetic responses to drugs via fluidically coupled vascularized organ chips. Nat Biomed Eng. 2020;4(4):421-36.
[124] Cisneros B, Garcia-Aguirre I, Unzueta J, Arrieta-Cruz I, Gonzalez-Morales O, Dominguez-Larrieta JM, et al. Immune system modulation in aging: Molecular mechanisms and therapeutic targets. Front

Immunol. 2022;13:1059173.
[125] Kroll KT, Mata MM, Homan KA, Micallef V, Carpy A, Hiratsuka K, et al. Immune-infiltrated kidney organoid-on-chip model for assessing T cell bispecific antibodies. Proc Natl Acad Sci U S A. 2023;120(35):e2305322120.
[126] Nair AL, Groenendijk L, Overdevest R, Fowke TM, Annida R, Mocellin O, et al. Human BBB-on-a-chip reveals barrier disruption, endothelial inflammation, and T cell migration under neuroinflammatory conditions. Frontiers in Molecular Neuroscience. 2023;16.
[127] Marzagalli M, Pelizzoni G, Fedi A, Vitale C, Fontana F, Bruno S, et al. A multi-organ-on-chip to recapitulate the infiltration and the cytotoxic activity of circulating NK cells in 3D matrix-based tumor model. Front Bioeng Biotechnol. 2022;10:945149.
[128] Wagar LE, Salahudeen A, Constantz CM, Wendel BS, Lyons MM, Mallajosyula V, et al. Modeling human adaptive immune responses with tonsil organoids. Nat Med. 2021;27(1):125-35.
[129] Kastenschmidt JM, Schroers-Martin JG, Sworder BJ, Sureshchandra S, Khodadoust MS, Liu CL, et al. A human lymphoma organoid model for evaluating and targeting the follicular lymphoma tumor immune microenvironment. Cell Stem Cell. 2024;31(3):410-20 e4.
[130] Ewart L, Apostolou A, Briggs SA, Carman CV, Chaff JT, Heng AR, et al. Performance assessment and economic analysis of a human Liver-Chip for predictive toxicology. Commun Med (Lond). 2022;2(1):154.
[131] Nahle Z. A proof-of-concept study poised to remodel the drug development process: Liver-Chip solutions for lead optimization and predictive toxicology. Front Med Technol. 2022;4:1053588.
[132] Kutluk H, Bastounis EE, Constantinou I. Integration of Extracellular Matrices into Organ-on-Chip Systems. Adv Healthc Mater. 2023;12(20):e2203256.
[133] Danku AE, Dulf EH, Braicu C, Jurj A, Berindan-Neagoe I. Organ-On-A-Chip: A Survey of Technical Results and Problems. Front Bioeng Biotechnol. 2022;10:840674.
[134] Bu W, Wu Y, Ghaemmaghami AM, Sun H, Mata A. Rational design of hydrogels for immunomodulation. Regen Biomater. 2022;9:rbac009.
[135] Pereira RVS, EzEldeen M, Ugarte-Berzal E, Martens E, Malengier-Devlies B, Vandooren J, et al. Physiological fibrin hydrogel modulates immune cells and molecules and accelerates mouse skin wound healing. Front Immunol. 2023;14:1170153.
[136] Franzen N, van Harten WH, Retel VP, Loskill P, van den Eijnden-van Raaij J, M IJ. Impact of organ-on-a-chip technology on pharmaceutical R&D costs. Drug Discov Today. 2019;24(9):1720-4.
[137] Sunildutt N, Parihar P, Chethikkattuveli Salih AR, Lee SH, Choi KH. Revolutionizing drug development: harnessing the potential of organ-on-chip technology for disease modeling and drug discovery. Front Pharmacol. 2023;14:1139229.
[138] Ingber DE. Human organs-on-chips for disease modelling, drug development and personalized medicine. Nat Rev Genet. 2022;23(8):467-91.
[139] Asal M, Rep M, Bontkes HJ, van Vliet SJ, Mebius RE, Gibbs S. Towards Full Thickness Small Intestinal Models: Incorporation of Stromal Cells. Tissue Eng Regen Med. 2024;21(3):369-77.

3

Human lymph node fibroblastic reticular cells maintain heterogeneous characteristics in culture

Janna E.G. Roet[1,2,†], Andrew I. Morrison[1,2,†], Aleksandra M. Mikula[1,2,3,†], Michael de Kok[1,2], Daphne Panocha[1,2,3], Henk P. Roest[4], Luc J.W. van der Laan[4], Charlotte M. de Winde[1,2,3], Reina E. Mebius[1,2,3]

[1] Amsterdam UMC location Vrije Universiteit Amsterdam, Molecular Cell Biology & Immunology, De Boelelaan 1117, Amsterdam, The Netherlands;

[2] Amsterdam Institute for Immunology and Infectious diseases, Amsterdam, The Netherlands;

[3] Cancer Center Amsterdam, Cancer Biology & Immunology, Amsterdam, The Netherlands.

[4] Erasmus MC Transplant Institute, University Medical Center Rotterdam, Department of Surgery, Dr. Molewaterplein 40, 3015 GD, Rotterdam, The Netherlands;

[†]Equal contribution

iScience. 2024 Jul 19; 27(7): 110179. DOI: 10.1016/j.isci.2024.110179

Summary

Fibroblastic reticular cells (FRCs) are mesenchymal stromal cells in human lymph nodes (LNs) playing a pivotal role in adaptive immunity. Several FRC subsets have been identified, yet it remains to be elucidated if their heterogeneity is maintained upon culture. Here, we established a protocol to preserve and culture FRCs from human LNs and characterized their phenotypic profile in fresh LN suspensions and upon culture using multispectral flow cytometry. We found nine FRC subsets in fresh human LNs, independent of donor, of which four persisted in culture throughout several passages. Interestingly, the historically FRC-defining marker podoplanin (PDPN) was not present on all FRC subsets. Therefore, we propose that CD45negCD31neg human FRCs are not restricted by PDPN expression, as we found CD90, BST1, and CD146/MCAM to be more widely expressed. Together, our data provide insight into FRC heterogeneity in human LNs, enabling further investigation into the function of individual FRC subsets.

Introduction

Human lymph nodes (LNs) are strategically positioned throughout the body, allowing cells and antigens from the tissues to enter via lymphatic vessels, while naive lymphocytes enter from the bloodstream by means of specialized endothelial cells forming high endothelial venules (HEVs). Through their lymphatic drainage, LNs function as a filter for tissues, allowing the generation of immune responses upon tissue damage or infection. Within LNs, a high level of organization provides distinct domains for adaptive immune cells, with B cell follicles in the cortex and T cell areas in the paracortex[1,2]. Upon presentation of antigen by dendritic cells (DCs) to lymphocytes, the adaptive immune response is initiated. These cellular interactions are influenced by LN stromal cells (LNSCs) that not only provide structural support to LNs but also facilitate cellular migration and anchorage where needed. They also control lymphocyte proliferation, restrict self-reactive T cells, and produce immune cell survival factors[3,4]. Thus, non-hematopoietic LNSCs are central to the final outcome of adaptive immune responses.

LNSCs are traditionally subdivided into four main groups using three cell surface markers: CD45, CD31, and podoplanin (PDPN). Cells that express the platelet endothelial cell adhesion molecule CD31/PECAM-1 are from endothelial origin and are either blood endothelial cells (BECs) or lymphatic endothelial cells (LECs), where LECs in addition express the glycoprotein marker PDPN. LNSCs derived from mesenchymal lineage are CD31^{neg} and have been termed either double-negative cells (DNCs) or, when they express PDPN, fibroblastic reticular cells (FRCs). Further subdivision of FRCs based on anatomical location within LNs and phenotypic markers defined T cell zone FRCs (TRCs), B cell zone FRCs (BRCs), pericytes, marginal reticular cells (MRCs), as well as follicular dendritic cells (FDCs)[2,3]. Single-cell RNA sequencing (scRNA-seq) of both mouse and human LNSCs indicated even more heterogeneity among these stromal cell subsets[5,6,7,8,9,10,11]. This notion allowed for further definition and identification of their specific roles in regulating the immune response. Distinct functions have been identified for FRC subsets, ranging from the generation of micro-domains for the spatial organization and homeostasis of DC subsets[9,12], providing survival niches for macrophage subsets and plasma B cells[13,14], acting as a conduit system for small molecules[15,16], and forming a cellular interaction niche for B cells, T cells, and DCs at the follicular border[5,17,18,19]. These functional analyses of FRC subsets have mostly been carried out using cell-specific mutations in mice.

For human FRC subsets, determining these cellular functions requires characterization of stromal cells in vitro in two-dimensional (2D) and three-dimensional (3D) systems by means of blocking and directed mutagenesis studies to determine cell-specific functions. Several reports have shown that, in addition, PDPN^{neg} mesenchymal stromal cells with similar characteristics to PDPN^{+} FRCs can be found in human LNs[20,21]. While PDPN is used historically as the hallmark FRC marker, this is mostly based on its broad expression on mesenchymal stromal cells within mouse LNs. However, the definition of FRCs has changed over the years, ranging from fibroblasts in the T cell area[22] to all PDPN-expressing mesenchymal cells in mouse LNs[23]. A substantial portion of mesenchymal stromal cells within human LNs lacks this expression when freshly isolated[20,21]. Therefore, we here aim to further standardize the currently available methods for isolation and culture of LN-derived

CD45^{neg}CD31^{neg} mesenchymal stromal cells, which we collectively define as FRCs for this study. We assess their phenotypic profile by multispectral flow cytometry to allow the analyses of distinct cellular subsets for future studies.

Hereto, we reproduced and improved the isolation of FRCs from healthy human LN tissue[24,25] for *ex vivo* analysis of fresh FRCs and in vitro-cultured FRCs. We assessed their phenotypic profile using high-dimensional analysis on cell surface proteins that could potentially distinguish various types of FRCs. Based on pseudotime analysis recently performed on human FRCs[9], as well as RNA and protein data from recent publications, we selected the following membrane markers: ACKR4, BST1, CD146, CD21, CD271, CD34, CD90, PDPN, and VCAM1[5,6,9,20,21,26,27]. We analyzed expression of these markers using multispectral flow cytometry and our in-house developed unbiased approach to correct for the great heterogeneity in autofluorescence (AF) found in both fresh and cultured FRCs[28]. Upon analysis of CD45^{neg}CD31^{neg} cells in fresh human LNs, nine heterogeneous FRC clusters were identified across all human LN donors. Of these, four clusters remained throughout several culture passages, while four new clusters emerged upon FRC expansion *in vitro*. Our findings advance the knowledge of FRC heterogeneity in healthy human LNs and identify which subsets are maintained in in vitro cultures. This offers a valuable starting point for their prospective use in functional assays to uncover the role of FRC subsets in human immunity.

Key resources table

Reagent or Resource	Source	Identifier
Antibodies		
anti-ACKR4/CCRL1- BV650	BD Biosciences	Cat# 747804; RRID:AB_2872268
anti-BST1/CD157- BV750	BD Biosciences	Cat# 747147; RRID:AB_2871891
anti-CD146- BV711	BioLegend	Cat# 361032; RRID:AB_2800998
anti-CD21- PE-Dazzle594	BioLegend	Cat# 354922; RRID:AB_2750243
anti-CD235a- eFluor450	ThermoFisher Scientific	Cat# 48-9987-42; RRID:AB_2574141
anti-CD271- PerCP-Cy5.5	BioLegend	Cat# 345112; RRID:AB_11204075
anti-CD31/PECAM-1- BV605	BioLegend	Cat# 303122; RRID:AB_2562149
anti-CD34- PE-Cy7	BioLegend	Cat# 343516; RRID:AB_1877251
anti-CD45- eFluor450	Thermo Fisher Scientific	Cat# 48-0459-42; RRID:AB_2016677
anti-CD90/Thy1- BV785	BioLegend	Cat# 328142; RRID:AB_2734318
anti-PDPN- Alexa Fluor 647	BioLegend	Cat# 337008; RRID:AB_2162063
anti-VCAM1/CD106- BV421	BioLegend	Cat# 305816; RRID:AB_2832596
Biological samples		
Lymph node of donor #1 (female, 83 years old)	Erasmus MC, Rotterdam	N/A
Lymph node of donor #2 (female, 16 years old)	Erasmus MC, Rotterdam	N/A
Lymph node of donor #3 (female, 21 years old)	Erasmus MC, Rotterdam	N/A

Reagent or Resource	Source	Identifier
Lymph node of donor #4 (female, 53 years old)	Erasmus MC, Rotterdam	N/A
Lymph node of donor #5 (male, 75 years old)	Erasmus MC, Rotterdam	N/A
Lymph node of donor #6 (female, 25 years old)	Erasmus MC, Rotterdam	N/A
Lymph node of donor #7 (male, 16 years old)	Erasmus MC, Rotterdam	N/A
Lymph node of donor #8 (male, 28 years old)	Erasmus MC, Rotterdam	N/A
Lymph node of donor #9 (female, 33 years old)	Erasmus MC, Rotterdam	N/A
Lymph node of donor #10 (male, 53 years old)	Erasmus MC, Rotterdam	N/A
Chemicals, peptides, and recombinant proteins		
Belzer UW® Cold Storage Solution	Bridge to Life, University of Wisconsin	
RPMI 1640 Medium	Gibco	Cat# 11875093
Dispase II	Sigma-Aldrich	Cat# 04942078001
Collagenase P	Sigma-Aldrich	Cat# 11213857001
DNAse I	Sigma-Aldrich	Cat# 11284932001
EDTA	Sigma-Aldrich	Cat# 03677
Foetal calf serum	Corning	Cat# 35-079-CV
Dulbecco's Modified Eagle Medium (DMEM), high glucose	Gibco	Cat# 11965092
Penicillin/Streptomycin/Glutamine	Capricorn Scientific	Cat# PS-B
Insulin/Transferrin/Selenium	Gibco	Cat# 41400045
Trypsin	Gibco	Cat# 15400-054
Brilliant Stain Buffer	BD Biosciences	Cat# 563794
Critical commercial assays		
LIVE/DEAD™ Fixable Blue Dead Cell Stain Kit	ThermoFisher Scientific	Cat# L34961
MojoSortTM Human CD45 Nanobeads	BioLegend	Cat# 480029
Software and algorithms		
Multibatch Cytometry Data Integration for Optimal Immunophenotyping (iMUBAC)	Ogishi et al.[32]	https://github.com/casanova-lab/iMUBAC
R (version 4.2)	The R Foundation	https://www.rproject.org/
Harmony (version 0.2.1)	Korsunsky et al.[41]	https://github.com/immunogenomics/harmony
OMIQ	Dotmatics	www.omiq.ai
FlowJoTM Software (version 10.10)	BD Biosciences	https://www.flowjo.com
Graphpad Prism 9	GraphPad Software	https://www.graphpad.com
Image J	National Institutes of Health	https://imagej.net

Reagent or Resource	Source	Identifier
Slingshot	Kapoor et al.[9] Street et al.[42]	https://github.com/kstreet13/slingshot)
Seurat	Stuart et al.[43]	http://www.satijalab.org/seurat)

Experimental model and study participant details

Tissue collection

Human LNs were obtained from donors and patients from both sexes during liver transplant procedures performed at the Erasmus MC, Rotterdam, The Netherlands, in accordance to the Medical Ethical Committee (Medisch Ethische Toetsings Commissie; METC) of Erasmus MC (MEC-2014-060). All patients (liver transplant recipients) gave written informed consent to use their donor tissue. The LNs were resected along the hepatic artery and portal vein in the porta hepatis from donor livers and diseased patient explant livers. Donor age and sex are shown in the key resources table, and extended donor characteristics can be found in Table S1. Further information regarding donor ethnicity, race, ancestry and socioeconomic has not been documented upon collection of the tissues. LNs were transported in Belzer University of Wisconsin (UW) cold storage solution (Bridge to Life Ltd., London, England, UK) and processed within 72 hours of surgery.

Cell culture

To allow for an efficient and selective outgrowth of FRCs from LN cell suspensions, a seeding density of 1.25 x 10^6 cell suspension per cm^2 was used on culture flasks that were coated with 2 µg/cm2 collagen from calf skin (Sigma-Aldrich). Culture media comprised of DMEM with 10% FCS, 2% Penicillin/Streptomycin/Glutamine and 1% Insulin/Transferrin/Selenium. After three days, lymphocytes were washed away with PBS to allow for optimal FRC growth. This process of washing away floating cells from the same flask was repeated twice per week during medium refreshments. Upon confluence, cells were harvest with PBS supplemented with 0.05% trypsin and 5 mM EDTA for up to 5 minutes maximum. Trypsin was neutralised using culture medium (as above), and FRCs were passaged or collected for flow cytometry analysis. FRCs were used up to and including passage 6 for all individual experiments.

Method details

Enzymatic digestion of human lymph nodes

Human LNs were enzymatically digested, where modifications were made to the time of each digestion cycle (4 x 10 minute intervals) compared to earlier protocols[24,25]. In short, LNs were minced and subsequently digested with an enzyme mixture containing RPMI-1640 medium with 2.4 mg/

ml Dispase II, 0.6 mg/ml Collagenase P and 0.3 mg/ml DNase I (all from Sigma-Aldrich, St. Louis, MO, USA). To prevent over-digestion and neutralise the digestion enzymes after each cycle, isolated cells were collected in ice-cold phosphate-buffered saline (PBS) supplemented with 2% foetal calf serum (FCS) and 5 mM EDTA, and spun down at 300 g for 4 minutes at 4°C. The cell pellet was re-suspended in 1 ml Dulbecco›s Modified Eagle Medium (DMEM) (Gibco, Grand Island, NY, USA) supplemented with 10% FCS, 2% Penicillin/Streptomycin/Glutamine and 1% Insulin/Transferrin/Selenium (Gibco). After the last digestion cycle, all collected cells were filtered through a 100 µM filter and counted. The obtained human LN cell suspension was either cryopreserved, enriched for $CD45^{neg}$ cells or cultured to grow out FRCs.

Enrichment of $CD45^{neg}$ cells

LN suspensions were enriched for $CD45^{neg}$ (stromal) cells by negative selection using MojoSort™ Human CD45 Nanobeads (BioLegend, San Diego, CA, USA). The manufacturer's protocol was followed, with the addition of a fluorescently-labelled antibody against CD45 during the CD45 Nanobeads incubation step to enhance the CD45 signal for flow cytometry. The $CD45^{neg}$ enriched LN cell suspension was further processed for characterisation by flow cytometry.

Multispectral flow cytometry

Cell suspensions were stained in a 96-well U bottom plate at 4°C for multispectral flow cytometry analysis. Cells were firstly washed with PBS and stained with a fixable viability dye (LIVE/DEAD™ Fixable Blue Dead Cell Stain Kit, 1:1000, cat. no. L34961, Invitrogen, Paisley, Scotland, UK) for 10 minutes at 4°C. Next, cells were washed with PBS containing either 0.1 % bovine serum albumin (BSA) or 2% FCS (referred to as FACS buffer) prior to Fc-receptor blocking using 10 % normal human serum in FACS buffer, mixed 1:1 with Brilliant Stain Buffer (BSB) (563794, BD Biosciences, Franklin Lakes, NJ, USA). Cells were then incubated with directly-labelled antibodies diluted in blocking buffer and BSB in the following dilutions: anti-ACKR4/CCRL1- 1:100, anti-BST1/CD157-1:200, anti-CD146-1:100, anti-CD21-1:50, anti-CD235a-1:10, anti-CD271-1:100, anti-CD31/PECAM-1-1:100, anti-CD34-1:100, anti-CD45-1:100, anti-CD90/Thy1-1:100, anti-PDPN-1:50, anti-VCAM1/CD106-1:200. After staining, cells were washed two times with FACS buffer and fixed with 2% PFA for 15 minutes at 4°C in the dark, and washed two times with FACS buffer. Samples, single stains on beads and for some markers (PDPN, BST1 and CD90) single stains on cells as well as Fluorescence Minus One (FMO) controls were acquired on Aurora 5-laser Flow Cytometer (Cytek, Amsterdam, The Netherlands). For highly AF samples, area scaling factor was adjusted across all lasers.

Multispectral flow cytometry data analysis

First, the heterogeneous and bright AF spectra seen in LNSCs were extracted according to our in-house developed analysis pipeline[28]. In short, all different AF clusters of the unstained samples were identified in an unbiased method, and their unique AF spectra were used during the unmixing to extract the AF from the full stained samples. This workflow was performed for every new batch acquired.

To test reproducibility of our FRC isolation protocol, LNSCs were derived from ten human LN donors and used in the different experiments (Table S1). For objective inter-batch comparison, data were corrected using the iMUBAC method[32]. All files were pre-processed by gating on the cells of interest, *i.e.* live $CD45^{neg}CD235a^{neg}CD31^{neg}$ cells. Doublet exclusion was omitted due to morphology of human LNSCs affecting the FSC, based on brightfield images acquired on CytPix Attune Flow Cytometer (Thermofisher, Waltham, MA, USA) (Fig. S6).

Next, batch correction was performed for all files combined, both fresh and cultured LNSCs, as we assumed that minimal biological variability would be present between the samples. The expression values for all markers were batch-corrected with Harmony (version 0.2.1)[41], as part of the iMUBAC pipeline[32] in R (version 4.2), using the same parameters as their example script and using each marker directly as an input for batch correction, resulting in the corrected expression values (CEV) per marker. MaxN was chosen based on the minimum number of available cells per batch. The effect of batch correction was visualised using uniform manifold approximation and projection (UMAP) (Fig. S7A, S7C). Using the online analysis software OMIQ (www.omiq.ai, Boston, MA, USA), dimensional reduction (Opt-SNE) was performed separately on the batch-corrected freshly digested LNSCs or batch-corrected cultured FRCs. Different clusters were manually gated based on the expression of different markers.

Data were visualised using OMIQ for the Opt-SNEs, FlowJot™ Software (v10.7, TreeStar, Ashland, OR, USA) for density dot plots, and Graphpad Prism 9 software (GraphPad Software Inc., San Diego, CA, USA) for bar graphs and heatmaps.

Brightfield imaging

Human LN cell suspension cultures were assessed for selective outgrowth of FRCs identified on morphological changes. Brightfield images were acquired on consecutive days using a microscope (Zeiss AX10, Jena, Germany) equipped with a high-resolution camera (Canon EOS 100D, Tokyo, Japan). The images were processed with ImageJ software.

Pseudotime analysis

To identify the position of the FRC markers on the pseudotime axis of human FRC ($CD45^{neg}CD31^{neg}PDPN^{+}$) scRNAseq dataset [9] (E-MTAB-10206), we reconstructed the trajectory using the Slingshot algorithm as described by[9,42]. First, the Harmony algorithm was used for batch correction between three donors. Next, the Slingshot algorithm was run on the corrected dimensional reduction from Harmony, resulting in a pseudotime score per cell. For visualisation in a heatmap, the cells were ordered based on their pseudotime scores. Markers for each cluster were calculated using the FindAllMarkers function in Seurat[43] with default parameters and visualised in a heatmap together with the FRC cell surface markers that could be used for flow cytometry analysis (Table S2) and that were present in the dataset.

Quantification and statistical analysis

Statistical analysis was performed using unpaired student's T-test or two-way ANOVA followed by Tukey's multiple comparison test in GraphPad Prism 9 software (GraphPad Software Inc., San Diego, CA, USA).*$p < 0.05$, **$p < 0.01$.

Results

Reproducible methods for isolation, enrichment, and culture of FRCs from human LNs

The percentage of FRCs in human LNs is very low (1%–5%) making it a challenge to characterize the phenotypic profiles of the different FRC subsets. Here, we established a protocol to enrich human LNSCs from LN suspensions and to expand FRCs by culturing LN suspensions. To obtain single-cell suspensions from human LNs, we modified the enzymatic digestion protocols published before[24,25] (Fig. 1A). In short, LNs were minced and subsequently digested with a mixture of three enzymes (Collagenase P, Dispase II, and DNase I). To prevent over-digestion and improve LNSC yield, we performed digestion in 4 cycles of 10 min with gentle shaking of the tube after 5 min, to increase the FRC yield (Fig. S1A). After each digestion cycle, the cell suspension was transferred to a buffer containing FCS and EDTA to inhibit enzyme activity and, in contrast to previous protocols, immediately spun down and re-suspended in DMEM-based FRC culture media (in contrast to other medium as mentioned in previous protocols[24,25]). After digestion, on average, 5% of the cells from the LN cell suspension were identified as $CD45^{neg}CD235a^{neg}$ stromal cells (Fig. 1B,1C).

To allow a detailed characterization of these LNSCs, $CD45^{neg}$ stromal cells were enriched to, on average, 60% of the cell suspension using CD45-negative bead selection (Fig. 1C), which did not affect PDPN expression (Fig. S1B). LNSCs can be divided into four main subtypes, based on the expression of the endothelial cell marker CD31 and the glycoprotein PDPN (Fig. 1B)[26,29]. The CD31-expressing endothelial cells can be divided into LECs ($CD31^{+}PDPN^{+}$) and BECs ($CD31^{+}PDPN^{neg}$), while mesenchymal subsets, called FRCs, can be divided based on the expression of PDPN into $CD31^{neg}PDPN^{+}$ cells and DNCs ($CD31^{neg}PDPN^{neg}$). The proportions of these subsets remained the same after $CD45^{neg}$ cell enrichment of the LN cell suspension (Fig. 1D).

In order to selectively grow out FRCs, the freshly digested human LN cell suspensions were cultured in collagen type I-coated flasks. After 2–3 days, lymphocytes suspended in the culture flasks were carefully rinsed away. This process of washing away floating cells was consistently repeated twice per week during media refreshments to promote the adherence of cells exhibiting an elongated morphology, i.e., a distinctive characteristic of FRCs (Fig. 1E). Using these methods we were able to isolate, culture, and expand FRCs, with most of the cells being attached in a confluent flask at the end of the first culture passage (passage 0) (Fig. S1C). There was minimal endothelial stromal cell contamination in passage 2, 4, and 6, as the average percentages of $CD31^{+}PDPN^{neg}$ cells were 0.78%, 0.49% and 0.22%, respectively, and the average percentages of CD31+PDPN+ cells were 0.60%, 0.58%, and 0.28%, respectively (Fig. S1D).

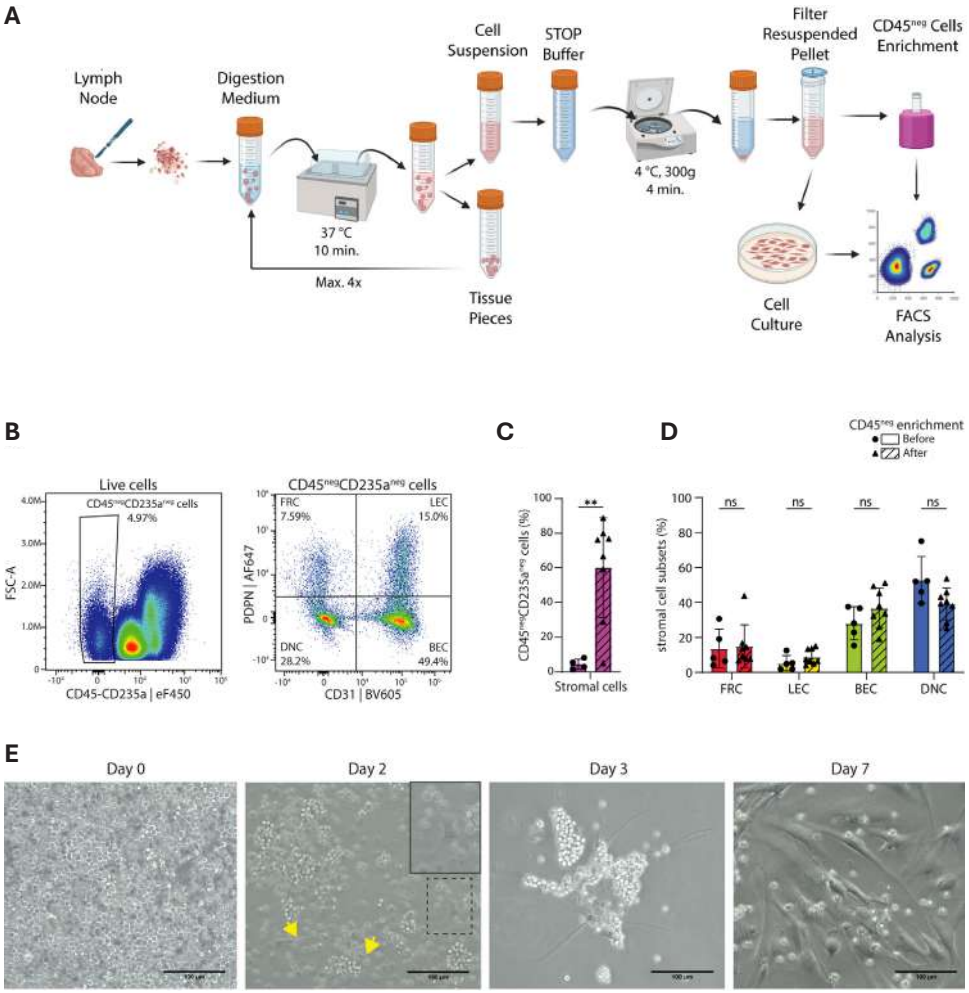

Fig. 1 - Isolation and CD45neg enrichment for culture of stromal cells from fresh human LNs. (A) Schematic representation of the method used to isolate stromal cells from fresh human LNs and the next steps including CD45neg cell enrichment by CD45-negative bead selection or culturing *in vitro*, after which the cells are characterized by spectral flow cytometry (FACS analysis). **(B)** Representative density plot showing the gating strategy for CD45negCD235aneg cells and subsequently the gating used to determine the four main subtypes of LNSCs based on the expression of PDPN and CD31. **(C)** Percentage of CD45negCD235aneg stromal cells in the LN cell suspension before (n = 4) and after (n = 8) CD45neg enrichment. Data represent total mean percentage ±SEM. Unpaired Student's t test, $^{**}p < 0.01$. **(D)** Distribution of the four main LN stromal cell subsets before (n = 5) and after (n = 8) CD45neg enrichment. Data represent total mean percentage ±SEM. Two-way ANOVA with multiple comparison Tukey's test, not significant (ns). **(E)** Representative images of FRC expansion from an LN cell suspension, from day 0, 2, 3, and 7. Scale bar represents 100 µm. See also Fig. S1 for cell characteristics of the improved digestion protocol and Table S1 for donor information. FSC, forward scatter; eF, eFluor; BV, Brilliant Violet; FRC, fibroblastic reticular cell; LEC, lymphatic endothelial cell; BEC, blood endothelial cell; DNC, double-negative cell. Created with BioRender.com.

Identification of cell membrane markers to distinguish various subsets of FRCs

Recent studies using scRNA-seq, flow cytometry, and/or imaging have shown that various FRC subsets can be distinguished depending on their marker expression profiles. Based on protein and RNA expression data from mouse LNSCs, PDPN[26],BST1[26],CD21[27],VCAM1[27],CD34[5],and ACKR4[6] have all been described as markers for multiple stromal cell subtypes with different localizations and functions within the LN. Additional markers have been described for human LN FRCs, namely CD90[30], CD146[20], and CD271[31]. For example, PDPN$^+$BST1$^+$CD146$^+$CD271$^+$ cells can be referred to as T-zone FRCs, whereas CD271$^+$ cells, along with CD21$^+$ and VCAM1$^+$ cells, have been used to identify FDCs within the B cell follicles. CD34$^+$ stromal cells are located in the LN capsule and medullary vessel adventitia, and ACRK4$^+$ stromal cells are located within the subcapsular sinus[20,21].Moreover, re-analyzing the pseudotime analysis of human LN FRCs based on scRNA-seq[9],the FRC marker profiles are expressed along the complete pseudotime axis (Fig. 2). This suggests that these markers can be used to identify FRC subsets present at different pseudotime stages, and therefore we decided to include them in our analysis.

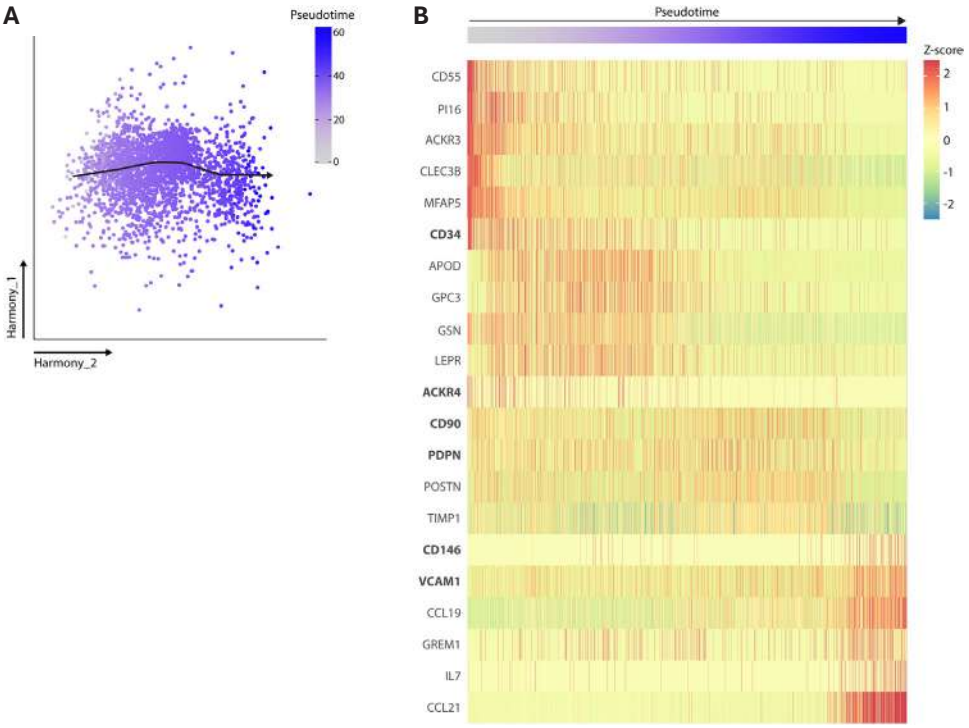

Fig. 2 - Pseudotime analysis of human LN FRCs. (A) Trajectory analysis of human FRCs (CD45^{neg}CD31^{neg}PDPN$^+$) with slingshot obtained from Kapoor[9]. **(B)** Heatmap displaying the average expression of indicated genes, including the FRC cell surface markers that we used in this study for flow cytometry analysis, along the pseudotime trajectory as shown before[9].

Similar FRC subsets are present in freshly isolated human LNs from multiple donors

For the characterization of freshly isolated FRCs, we performed multispectral flow cytometry analysis of four human LNs (donors 1–4, Table S1) using the FRC markers described earlier: BST1, CD34, PDPN, CD146, CD271, CD90, VCAM1, CD21, and ACKR4 [5,6,20,21,26,27]. AF extraction was performed according to the method developed in our lab[28], and we selected live $CD45^{neg}CD235a^{neg}CD31^{neg}$ cells. To eliminate batch effects, data were corrected according to the integration of multibatch cytometry (iMUBAC) workflow[32]. Next, dimensional reduction and gating based on the expression of the selected FRC markers (Fig. 2) identified nine FRC clusters (Fig. 3A, S2, and S3; Table S2), which were all present in the fresh cell suspensions of the four LN donors (Fig. S3B).

To better visualize and quantify the median corrected expression value (CEV) of each marker per cluster, a heatmap was generated based on cells from all donors (Fig. 3B). The highest median CEV was that of the marker CD90, which was highly expressed across the majority of clusters, apart from low expression in cluster 1, 7, and 9. This pattern of expression was similar to that of BST1, although BST1 CEV was overall lower. Interestingly, expression of PDPN, a historically known FRC-defining marker[26,29], was only expressed in two clusters, 4 and 6. Of these $PDPN^+$ subsets, cluster 4 co-expressed BST1, CD90, and CD34, and cluster 6 co-expressed BST1, CD90, and CD146. Additionally, $CD34^+$ cells were mostly found in clusters 2, 3, and 4, and $CD146^+$ cells were present in clusters 1, 2, 5, 6, and 8. Of note, cluster 7 was the only cluster to show $VCAM1^+$ cells with co-expression of BST1 and ACKR4.

We next sought to investigate the contribution of each cluster per donor, and this revealed a consistent percentage of cluster contributions across all donors from freshly isolated $CD31^{neg}$ cell populations (Fig. 3C). However, in one donor (donor 2), there was a higher abundance of clusters 4 ($CD34^+PDPN^+CD90^+$) and 7 ($PDPN^{neg}CD90^{neg}VCAM1^+$) compared to the other donors, and this was compensated with less cells belonging to cluster 3 ($CD34^+PDPN^{neg}CD90^+$) and 8 ($PDPN^{neg}CD90^+$), albeit not statistically significant. Together, based on a selection of nine membrane markers, we identified nine different FRC clusters in fresh cell suspensions of human LNs, and this heterogeneity was consistent over all donors tested.

FRC subset heterogeneity is maintained in culture throughout different passages

To investigate if heterogeneity of FRCs is maintained upon *in vitro* culture and over time, we cultured and expanded FRCs from LN cell suspensions from six different donors (donors 5–10, Table S1) and performed multispectral flow cytometry analysis after passage 2, 4, and 6 in the same way as the fresh LN cell suspensions. Using dimensional reduction (Opt-SNE), we identified eight FRC clusters in cultured FRCs (Fig. 4A, S2, and S4). Based on the data from marker profiles of fresh FRCs (Fig. 3), we observed a conservation of clusters 1, 3, 8, and 9 and a loss of clusters 2, 4, 5, 6, and 7. Interestingly, we identified the emergence of four new clusters: cluster 10 ($VCAM1^+CD90^+BST1^+CD146^+$,$PDPN^+$), cluster 11 ($CD90^+BST1^+CD34^+CD146^+PDPN^{neg}$), cluster 12 ($CD90^+BST1^+CD146^+PDPN^+$), and cluster 13 ($CD90^+BST1^+CD34^+CD146^+PDPN^+$) (Fig. 4A; Table S2).

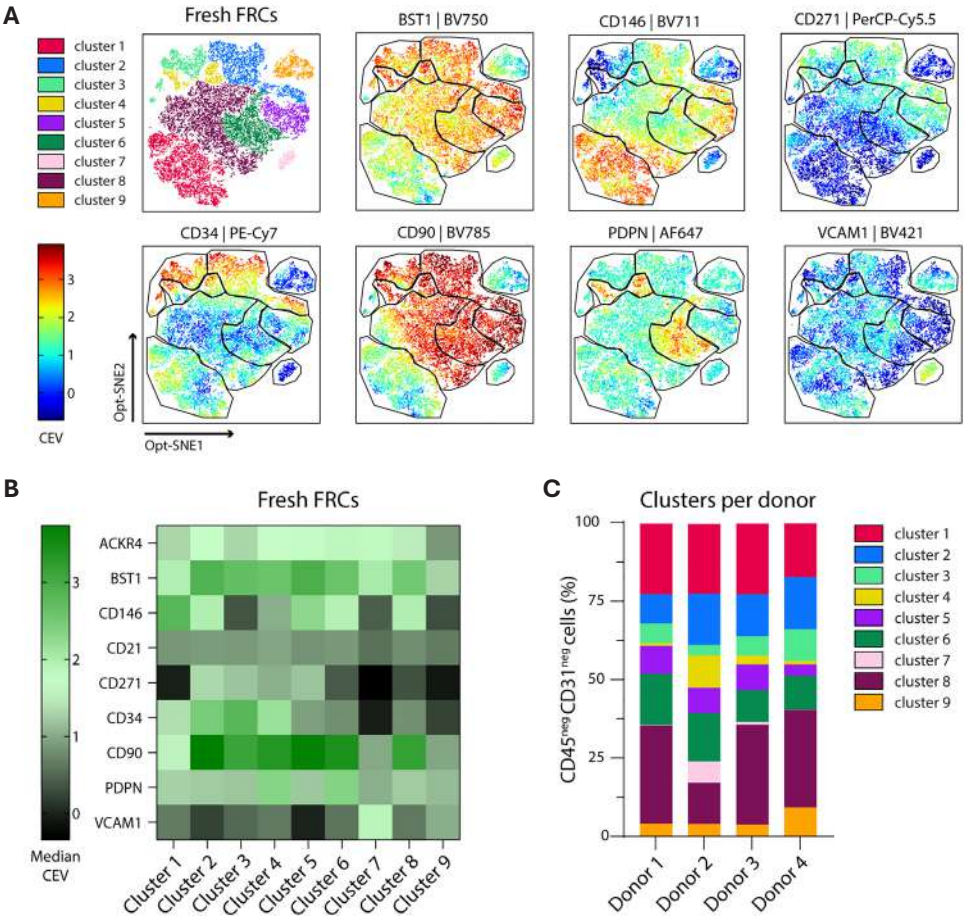

Fig. 3 - High-dimensional analysis of FRCs in fresh human LN cell suspensions. (A) Based on Opt-SNE visualization, we identified nine distinct clusters of fresh FRC subsets, gated from live, CD45^{neg}CD31^{neg} cells. Scale bar represents median correction expression value (CEV) from −0.7 to 3.9. Data represent an overlay of four human LN donors (Table S1). **(B)** Heatmap displaying median CEV of each marker per cluster shown in A. **(C)** Contribution of clusters (shown in A) to overall CD45^{neg}CD31^{neg} cell populations by donor. See also Fig. S2 for the gating strategy of the identified clusters, Fig. S3 for Opt-SNEs of additional markers and per donor visualization, Table S1 for donor information, and Table S2 for key markers per cluster.

Next, we generated a heatmap from all donors and combined passages to visualize how the expression of markers deviates per cluster (Fig. 4B). The expression of CD90, which was the most prolific marker expressed on FRCs in fresh human LNs (Fig. 3), remained highly abundant across most clusters, as well as in the four new clusters (10, 11, 12, and 13) (Fig. 4B). This trend was also seen for BST1^{+} and CD146^{+} cells. Furthermore, we noticed the appearance of PDPN^{+} cells in the new clusters 10, 12, and 13 (Fig. 4B). In addition, we identified a new VCAM1^{+} cluster (10) co-expressing BST1, PDPN, CD90, and CD146 (Fig. 4B), while the VCAM1^{+} FRCs (cluster 7, Fig. 3) in *ex vivo* human LNs only co-expressed BST1 and ACKR4.

We next determined the contributions of each cluster per donor across all passages. All donors contributed to all clusters (Fig. 4C). However, there was a significant difference between donors for cluster 1 ($CD146^+$), 8 ($CD90^+BST1^+$), and 9 (negative for all) (Fig. S4B, S4C). Subsequently, we questioned whether all passages contributed uniformly to different clusters. We observed no significant differences in cluster dominance between passages 2, 4, and 6 (Fig. 4D). However, cluster 1 ($CD146^+$) showed a higher contribution in passage 4 and 6 when compared to passage 2, and this was compensated with more cells belonging to cluster 10 ($VCAM1^+CD90^+BST1^+CD146^+PDPN^+$) in passage 2 (Fig. 4D). Together, these data indicate that the heterogeneous FRC phenotype found in human LNs is highly maintained throughout culture irrespective of passage, with a broad overlap of FRC clusters between freshly digested human LNs and cultured cells, and with a consistent homogeneity among all donors.

Discussion

Here, we provide an updated protocol for isolation and culture of mesenchymal stromal cells from human LNs, which we here collectively call FRCs. This protocol is adapted from previously published protocols for mouse and human LNs[25] and human tonsils[24]. Furthermore, we characterized FRC subsets *ex vivo* and at different passages upon culturing and found that FRC heterogeneity is maintained *in vitro*. We observed some differences between FRC clusters *ex vivo* and in culture, as previously reported[21]. However, changes in expression of markers on LNSC subsets upon culture cannot discriminate whether functionally distinct FRC subsets are lost upon *in vitro* culture or whether they undergo differentiation resulting in expression of additional surface markers.

Based on mouse data, mesenchymal stromal cells can be distinguished from endothelial cells based on lack of CD31 expression[26,29]. Within the mesenchymal fraction of murine stromal cells, FRCs are characterized as high PDPN-expressing cells ($PDPN^{++}$), which separate them from a heterogeneous population of $CD31^{neg}PDPN^{neg}$ cells (DNCs)[26,29]. In our data, we find only two $PDPN^+$ clusters (out of nine) in the $CD31^{neg}$ fraction in human LNs. However, we find five $CD90^+$ clusters, of which only two are co-expressing PDPN, suggesting that not all FRCs in human LNs express PDPN, in contrast to mouse LNs. Indeed, Knoblich et al. also found $CD90^+PDPN^{neg}$ cells in freshly isolated human LNs[21], and CD90 has been used as human FRC marker by others[9,20,30,33]. As such, we conclude that characterization of human $CD45^{neg}CD31^{neg}$ FRCs should not be restricted to only PDPN expression as, in addition to CD90, we also found BST1 and CD146/MCAM to be more widely expressed.

However, we also found $CD90^{neg/dim}$ populations that lacked CD146, CD34, PDPN, and BST1, which could indicate that these are the cells originally classified as DNCs[26,29]. Recently, CD21 was proposed to further distinguish FRCs from DNCs in the $CD31^{neg}$ fraction of human LN suspensions[34]. However, in our studies, we did detect some $CD21^+$ cells in fresh LN cell suspensions, but they did not form a separate CD21-expressing cluster, neither in fresh LNs nor in cultured FRCs. Likewise, the mesenchymal cell marker CD271, originally detected in splenic FRCs[31], was detected at low levels in fresh LNs, but later lost in cultured FRCs.

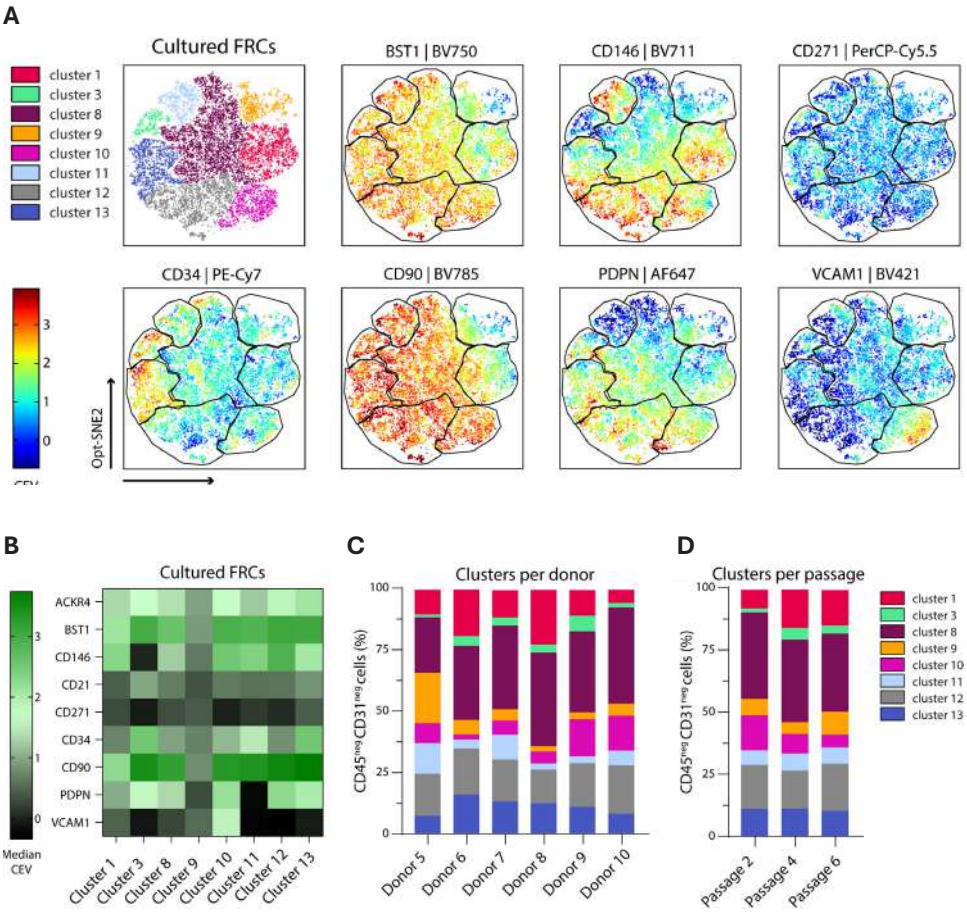

Fig. 4. High-dimensional analysis of cultured FRCs (A) Based on Opt-SNE visualization, we identified eight distinct clusters of FRC subsets throughout culture, gated from live, $CD45^{neg}CD31^{neg}$ cells. Scale bar represents median correction expression value (CEV) from −0.7 to 3.9. Data represent an overlay of six human LN donors (Table S1), passages 2, 4, and 6 combined. **(B)** Heatmap displaying median CEV of each marker per cluster shown in A. **(C and D)** Contribution of clusters to overall $CD45^{neg}CD31^{neg}$ cell populations by either **(C)** donor (mean of all passages combined) or **(D)** passage number (mean of all six donors combined). See also Fig. S2 for gating strategy of the identified clusters, Fig. S4 for Opt-SNEs of additional markers, per donor and per passage visualization, Table S1 for donor information, and Table S2 for key markers per cluster.

Using scRNA-seq, nine and twelve mesenchymal stromal cells clusters were defined in mouse LNs[5,9] and five in human LNs[9]. Based on protein expression of key surface markers (BST1, CD146, CD34, CD90, PDPN, and VCAM1), we found nine clusters in fresh human LNs. Of these, four were also present in cultured FRCs, as well as four new clusters (Table S2). We found three CD34$^+$ clusters (clusters 2–4) in fresh LNs, which is in line with two *CD34*$^+$ clusters found by Kapoor et al. using transcriptomics[9]. A ccording to their pseudotime analysis, CD34-expressing FRCs would form the subset that is placed at the beginning of this trajectory and could thus be the more immature FRC subset present within human LNs[9]. However, they did not observe co-expression of *CD34* and *CD90* mRNA, whereas in our data all three CD34$^+$ clusters co-express CD90 at protein level, which is in line with published flow cytometry data of CD34$^+$ LNSCs[20]. We speculate that *CD34* mRNA is not newly synthesized upon FRC maturation but that CD34 protein expression remains stable. Future research is necessary to test this hypothesis; for example, cellular indexing of transcriptomes and epitopes-sequencing (CITE-Seq) could be used to directly compare scRNA-seq and protein datasets.

We also define a CD90$^+$BST1$^+$CD146$^+$CD271$^+$PDPN^{neg} cluster (cluster 5) in human LNs. These cells are most likely pericytes, which are located around blood vasculature controlling endothelial barrier integrity, based on the phenotypic similarity described earlier for human LN pericytes[20]. Interestingly, we completely lose this cluster upon culture, which indicates that pericytes require other conditions to maintain their characteristic phenotype in culture. Perhaps that co-culture with BECs, which were not present in our cultures (Fig. S1D), may allow sufficient cellular interaction needed to mimic and maintain their LN niche.

We found one cluster highly expressing VCAM1 and BST1 (cluster 7) in *ex vivo* FRCs. FDCs, an FRC subset present in B cell follicles, express high VCAM1[34], but we did not observe CD21 co-expression in these cells, nor throughout their culture period (Fig. S2A). Upon culture, we observed a VCAM1$^+$ cluster co-expressing BST1 and PDPN as well as CD90 and CD146. We also detected this FRC phenotype in an organotypic human LN model in which we identified these FRCs as supporting stromal cell type for DCs[35]. These FRCs also expressed *GREM1* mRNA[35] and are thus likely to represent the *GREM1*$^+$ *VCAM1*$^+$ FRCs that provide a niche maintaining LN-resident DCs[9]. To more accurately define the other FRC clusters we found in this study, future work needs to elucidate the transcriptome, functionality, and secretome of these cells.

Interestingly, we observed five PDPN$^+$ clusters in cultured FRCs compared to two clusters expressing PDPN in *ex vivo* human LNs. Increased PDPN expression is a hallmark of fibroblast activation, for example, described to occur upon wound healing [36], during an immune response[37] or in cancer[38]. Potentially, the culture medium or growing cells on plastic may induce FRC activation. Furthermore, we expanded and cultured FRCs on collagen type I, which may result in the selective expansion of FRC subsets or induce FRC differentiation. It would be interesting to further investigate phenotypes of FRCs grown on other ECM types, e.g., either single ECM proteins or human LN-derived ECM[39,40], and compare whether these new culturing methods result in the outgrowth of different subsets or the differential contribution of other subsets to the overall stromal cells grown *in vitro*.

Other micro-environmental factors may also influence the observed FRC phenotypes. Here, we have analyzed FRCs from liver-draining LNs, but LNs from other locations in the body, draining other organs,

may potentially have different or additional FRC subsets. Additionally, FRCs normally reside in a 3D reticular network, while here they were taken out of this 3D structure for analysis in a single-cell suspension or after 2D culture. We have recently shown that co-culturing FRCs with DCs in a hydrogel induces a DC-supporting phenotype[35], which provides a starting point for future investigations of FRC phenotypes in 3D models mimicking the human LN.

Since the markers we used to distinguish these FRC subsets were based on existing datasets, we also took into account the antibody fluorophore availability based on the high AF profile seen in spectral flow cytometry, for which we have developed an analysis pipeline to extract AF spectra[28]. Spectral flow cytometry allows for analysis of more markers than conventional flow cytometry and can also distinguish various AF signals. However, the number of markers that can be analyzed with spectral flow cytometry is limited by availability of antibodies with correct fluorophores and study of multiple markers on the same cell. The latter depends on the type of cell, density of the marker, chosen fluorophore, and co-expression/co-localization of the marker on the cell surface. When adding additional markers to the antibody panel used in this manuscript, it would be recommended to avoid fluorophores that overlap with channels where high AF is detected (Fig. S5).

In summary, this study shows that there are various FRC subsets present in human LNs, of which the majority is preserved upon *in vitro* culture, but culture conditions may also induce functionally relevant new FRC subsets. The heterogeneity of FRC subsets defined here in human LNs and in cultured FRCs provides a better understanding of LNSC subtypes and allows the opportunity of sorting specific subsets for future investigations of FRC functionality in homeostasis, disease, and broader immunological research applications.

Limitations of the study

This study analyzes the phenotypic profile of freshly isolated *ex vivo* FRCs and *in vitro*-cultured FRCs. The main limitation of this work is the small number of stromal cells from the LN material. In human LNs, there is a low abundance of LNSCs (on average 5% of the total LN cell population) of which around 35% are $CD45^{neg}CD31^{neg}$ cells. As such, we could not use the same LN material to compare freshly isolated *ex vivo* FRCs with *in vitro*-cultured FRCs from the same donor. Ideally, to assess whether marker expression is changed upon culture, e.g., gain of PDPN or loss of CD271, FRC subsets should be sorted from fresh LN cell suspensions and their marker profile in culture tracked over time. All donors for *ex vivo* analysis were female, but for the cultured FRCs we had both female and male donors. We did not observe FRC cluster variation across the different donors, indicating a homogeneity that we would also expect for fresh FRCs between the two sexes.

For the *in vitro*-cultured FRCs, we analyzed passages 2, 4, and 6. We could not analyze earlier passages, as we needed to expand FRCs up to passage 2 in order to have enough cells to perform phenotypic analysis, continue the culture to analyze higher passages, and freeze cells as backup. Moreover, we did not analyze higher passages, since no phenotypic changes between passages 2, 4, and 6 were observed.

Acknowledgments

The authors would like to thank and acknowledge the expert help of the Microscopy & Cytometry Core Facility at Amsterdam UMC (location Vrije Universiteit Amsterdam). We thank BioLegend for advice on initial antibody panel design, and Alberta Paul (Cytek) for advice on and help with improved and extended antibody panel design for multispectral flow cytometry of lymph node stromal cells. We thank Kimberley Ober and Dr. Monique Verstegen from the Erasmus MC, Rotterdam, for sample logistics. J.E.G.R. is supported by a gravitation 2013 BOO grant financed by the Dutch Research Council (NWO) as part of the Institute for Chemical Immunology (ICI; 024.002.009). A.I.M. is supported by European Union's Horizon 2020 research and innovation program under grant agreement no. 847551 ARCAID. A.M.M. is supported by NWO ZonMw TOP Grant (91217014). D.P. is supported by NWO Lymph-Chip (1292.19.019). L.J.W.v.d.L. is supported by funding from the Convergence Health Technology Flagship grant (Organ Transplantation) and Medical Delta program grant (Regenerative Medicine 4D). C.M.d.W. is supported by Cancer Center Amsterdam (grant no. CCA2019-9-57 and CCA2020-9-73) and the Dutch Cancer Foundation (KWF; Young Investigator Grant no. 2022-4 EXPL/14641). Graphical abstract and Fig. 1A were created using BioRender.com.

Author contributions

Conceptualization: C.M.d.W. and R.E.M.; methodology: J.E.G.R., A.I.M., A.M.M., M.d.K., C.M.d.W., and R.E.M.; investigation: J.E.G.R., A.I.M., A.M.M., and D.P.; validation: J.E.G.R., A.I.M., A.M.M., and C.M.d.W.; software: J.E.G.R., M.d.K., and C.M.d.W.; data curation: J.E.G.R., A.I.M., A.M.M., and C.M.d.W.; writing: J.E.G.R., A.I.M., A.M.M., C.M.d.W., and R.E.M.; supervision: C.M.d.W. and R.E.M.; funding acquisition: C.M.d.W. and R.E.M.; ethical approval and donor information: L.J.W.v.d.L. and H.P.R. All authors have read and agreed to the published version of the manuscript.

References

[1] Mueller, S.N., and Germain, R.N. (2009). Stromal cell contributions to the homeostasis and functionality of the immune system. Nat Rev Immunol *9*, 618-629. 10.1038/nri2588.

[2] Fletcher, A.L., Acton, S.E., and Knoblich, K. (2015). Lymph node fibroblastic reticular cells in health and disease. Nat Rev Immunol *15*, 350-361. 10.1038/nri3846.

[3] Krishnamurty, A.T., and Turley, S.J. (2020). Lymph node stromal cells: cartographers of the immune system. Nat Immunol *21*, 369-380. 10.1038/s41590-020-0635-3.

[4] Grasso, C., Pierie, C., Mebius, R.E., and van Baarsen, L.G.M. (2021). Lymph node stromal cells: subsets and functions in health and disease. Trends Immunol *42*, 920-936. 10.1016/j.it.2021.08.009.

[5] Rodda, L.B., Lu, E., Bennett, M.L., Sokol, C.L., Wang, X., Luther, S.A., Barres, B.A., Luster, A.D., Ye, C.J., and Cyster, J.G. (2018). Single-Cell RNA Sequencing of Lymph Node Stromal Cells Reveals Niche-Associated Heterogeneity. Immunity *48*, 1014-1028 e1016. 10.1016/j.immuni.2018.04.006.

[6] Takeda, A., Hollmen, M., Dermadi, D., Pan, J., Brulois, K.F., Kaukonen, R., Lonnberg, T., Bostrom, P., Koskivuo, I., Irjala, H., et al. (2019). Single-Cell Survey of Human Lymphatics Unveils Marked Endothelial Cell Heterogeneity and Mechanisms of Homing for Neutrophils. Immunity *51*, 561-572 e565. 10.1016/j.immuni.2019.06.027.

[7] Brulois, K., Rajaraman, A., Szade, A., Nordling, S., Bogoslowski, A., Dermadi, D., Rahman, M., Kiefel, H., O'Hara, E., Koning, J.J., et al. (2020). A molecular map of murine lymph node blood vascular endothelium at single cell resolution. Nat Commun *11*, 3798. 10.1038/s41467-020-17291-5.

[8] Fujimoto, N., He, Y., D'Addio, M., Tacconi, C., Detmar, M., and Dieterich, L.C. (2020). Single-cell mapping reveals new markers and functions of lymphatic endothelial cells in lymph nodes. PLoS Biol *18*, e3000704. 10.1371/journal.pbio.3000704.

[9] Kapoor, V.N., Muller, S., Keerthivasan, S., Brown, M., Chalouni, C., Storm, E.E., Castiglioni, A., Lane, R., Nitschke, M., Dominguez, C.X., et al. (2021). Gremlin 1(+) fibroblastic niche maintains dendritic cell homeostasis in lymphoid tissues. Nat Immunol *22*, 571-585. 10.1038/s41590-021-00920-6.

[10] Abe, Y., Sakata-Yanagimoto, M., Fujisawa, M., Miyoshi, H., Suehara, Y., Hattori, K., Kusakabe, M., Sakamoto, T., Nishikii, H., Nguyen, T.B., et al. (2022). A single-cell atlas of non-haematopoietic cells in human lymph nodes and lymphoma reveals a landscape of stromal remodelling. Nat Cell Biol *24*, 565-578. 10.1038/s41556-022-00866-3.

[11] Grasso, C., Roet, J., Graça, C.G.d., Semmelink, J.F., Remmerswaal, E., Jongejan, A., Moerland, P.D., Mebius, R.E., and Baarsen, L.G.M.v. (2023). Identification and mapping of human lymph node stromal cell subsets by combining single-cell RNA sequencing with spatial transcriptomics. bioRxiv, 2023.2008.2018.553530. 10.1101/2023.08.18.553530.

[12] Gerner, M.Y., Kastenmuller, W., Ifrim, I., Kabat, J., and Germain, R.N. (2012). Histo-cytometry: a method for highly multiplex quantitative tissue imaging analysis applied to dendritic cell subset microanatomy in lymph nodes. Immunity *37*, 364-376. 10.1016/j.immuni.2012.07.011.

[13] Mondor, I., Baratin, M., Lagueyrie, M., Saro, L., Henri, S., Gentek, R., Suerinck, D., Kastenmuller, W., Jiang, J.X., and Bajenoff, M. (2019). Lymphatic Endothelial Cells Are Essential Components of the Subcapsular Sinus Macrophage Niche. Immunity *50*, 1453-1466 e1454. 10.1016/j.immuni.2019.04.002.

[14] Huang, H.Y., Rivas-Caicedo, A., Renevey, F., Cannelle, H., Peranzoni, E., Scarpellino, L., Hardie, D.L., Pommier, A., Schaeuble, K., Favre, S., et al. (2018). Identification of a new subset of lymph node stromal cells involved in regulating plasma cell homeostasis. Proc Natl Acad Sci U S A *115*, E6826-E6835. 10.1073/pnas.1712628115.

[15] Gretz, J.E., Norbury, C.C., Anderson, A.O., Proudfoot, A.E., and Shaw, S. (2000). Lymph-borne chemokines and other low molecular weight molecules reach high endothelial venules via specialized conduits while a functional barrier limits access to the lymphocyte microenvironments in lymph node cortex. J Exp Med *192*, 1425-1440. 10.1084/jem.192.10.1425.

[16] Nolte, M.A., Belien, J.A., Schadee-Eestermans, I., Jansen, W., Unger, W.W., van Rooijen, N., Kraal, G., and Mebius, R.E. (2003). A conduit system distributes chemokines and small blood-borne molecules through the splenic white pulp. J Exp Med *198*, 505-512. 10.1084/jem.20021801.

[17] Li, J., Lu, E., Yi, T., and Cyster, J.G. (2016). EBI2 augments Tfh cell fate by promoting interaction with IL-2-quenching dendritic cells. Nature *533*, 110-114. 10.1038/nature17947.

[18] Lu, E., Dang, E.V., McDonald, J.G., and Cyster, J.G. (2017). Distinct oxysterol requirements for positioning naive and activated dendritic cells in the spleen. Sci Immunol *2*. 10.1126/sciimmunol.aal5237.

[19] Baptista, A.P., Gola, A., Huang, Y., Milanez-Almeida, P., Torabi-Parizi, P., Urban, J.F., Jr., Shapiro, V.S., Gerner, M.Y., and Germain, R.N. (2019). The Chemoattractant Receptor Ebi2 Drives Intranodal Naive CD4(+) T Cell Peripheralization to Promote Effective Adaptive Immunity. Immunity *50*, 1188-1201 e1186. 10.1016/j.immuni.2019.04.001.

[20] Eom, J., Park, S.M., Feisst, V., Chen, C.J., Mathy, J.E., McIntosh, J.D., Angel, C.E., Bartlett, A., Martin, R., Mathy, J.A., et al. (2020). Distinctive Subpopulations of Stromal Cells Are Present in Human Lymph Nodes Infiltrated with Melanoma. Cancer Immunol Res *8*, 990-1003. 10.1158/2326-6066.CIR-19-0796.

[21] Knoblich, K., Cruz Migoni, S., Siew, S.M., Jinks, E., Kaul, B., Jeffery, H.C., Baker, A.T., Suliman, M., Vrzalikova, K., Mehenna, H., et al. (2018). The human lymph node microenvironment unilaterally regulates T-cell activation and differentiation. PLoS Biol *16*, e2005046. 10.1371/journal.pbio.2005046.

[22] Farr, A.G., Berry, M.L., Kim, A., Nelson, A.J., Welch, M.P., and Aruffo, A. (1992). Characterization and cloning of a novel glycoprotein expressed by stromal cells in T-dependent areas of peripheral lymphoid tissues. J Exp Med *176*, 1477-1482. 10.1084/jem.176.5.1477.

[23] Link, A., Hardie, D.L., Favre, S., Britschgi, M.R., Adams, D.H., Sixt, M., Cyster, J.G., Buckley, C.D., and Luther, S.A. (2011). Association of T-zone reticular networks and conduits with ectopic lymphoid tissues in mice and humans. Am J Pathol *178*, 1662-1675. 10.1016/j.ajpath.2010.12.039.

[24] Bar-Ephraim, Y.E., Konijn, T., Gonultas, M., Mebius, R.E., and Reijmers, R.M. (2016). A Reproducible Method for Isolation and In Vitro Culture of Functional Human Lymphoid Stromal Cells from Tonsils. PLoS One *11*, e0167555. 10.1371/journal.pone.0167555.

[25] Fletcher, A.L., Malhotra, D., Acton, S.E., Lukacs-Kornek, V., Bellemare-Pelletier, A., Curry, M., Armant, M., and Turley, S.J. (2011). Reproducible isolation of lymph node stromal cells reveals site-dependent differences in fibroblastic reticular cells. Front Immunol *2*, 35. 10.3389/fimmu.2011.00035.

[26] Link, A., Vogt, T.K., Favre, S., Britschgi, M.R., Acha-Orbea, H., Hinz, B., Cyster, J.G., and Luther, S.A. (2007). Fibroblastic reticular cells in lymph nodes regulate the homeostasis of naive T cells. Nat Immunol *8*, 1255-1265. 10.1038/ni1513.

[27] Allen, C.D., and Cyster, J.G. (2008). Follicular dendritic cell networks of primary follicles and germinal centers: phenotype and function. Semin Immunol *20*, 14-25. 10.1016/j.smim.2007.12.001.

[28] Roet, J.E.G., Mikula, A.M., Kok, M.d., Chadick, C.H., Vallejo, J.J.G., Roest, H.P., Laan, L.J.W.v.d., Winde, C.M.d., and Mebius, R.E. (2023). Unbiased method for spectral analysis of cells with great diversity of autofluorescence spectra. bioRxiv, 2023.2007.2028.550943. 10.1101/2023.07.28.550943.

[29] Fletcher, A.L., Lukacs-Kornek, V., Reynoso, E.D., Pinner, S.E., Bellemare-Pelletier, A., Curry, M.S., Collier, A.R., Boyd, R.L., and Turley, S.J. (2010). Lymph node fibroblastic reticular cells directly present peripheral tissue antigen under steady-state and inflammatory conditions. J Exp Med *207*, 689-697. 10.1084/jem.20092642.

[30] Park, S.M., Angel, C.E., McIntosh, J.D., Brooks, A.E., Middleditch, M., Chen, C.J., Ruggiero, K., Cebon, J., and Rod Dunbar, P. (2014). Sphingosine-1-phosphate lyase is expressed by CD68+ cells on the parenchymal side of marginal reticular cells in human lymph nodes. Eur J Immunol *44*, 2425-2436. 10.1002/eji.201344158.

[31] Steiniger, B.S., Wilhelmi, V., Seiler, A., Lampp, K., and Stachniss, V. (2014). Heterogeneity of stromal cells in the human splenic white pulp. Fibroblastic reticulum cells, follicular dendritic cells and a third

superficial stromal cell type. Immunology *143*, 462-477. 10.1111/imm.12325.

[32] Ogishi, M., Yang, R., Gruber, C., Zhang, P., Pelham, S.J., Spaan, A.N., Rosain, J., Chbihi, M., Han, J.E., Rao, V.K., et al. (2021). Multibatch Cytometry Data Integration for Optimal Immunophenotyping. J Immunol *206*, 206-213. 10.4049/jimmunol.2000854.

[33] Severino, P., Palomino, D.T., Alvarenga, H., Almeida, C.B., Pasqualim, D.C., Cury, A., Salvalaggio, P.R., De Vasconcelos Macedo, A.L., Andrade, M.C., Aloia, T., et al. (2017). Human Lymph Node-Derived Fibroblastic and Double-Negative Reticular Cells Alter Their Chemokines and Cytokines Expression Profile Following Inflammatory Stimuli. Front Immunol *8*, 141. 10.3389/fimmu.2017.00141.

[34] Mourcin, F., Verdiere, L., Roulois, D., Amin, R., Lamaison, C., Sibut, V., Thamphya, B., Pangault, C., Monvoisin, C., Huet, S., et al. (2021). Follicular lymphoma triggers phenotypic and functional remodeling of the human lymphoid stromal cell landscape. Immunity *54*, 1901. 10.1016/j.immuni.2021.07.018.

[35] Morrison, A.I., Mikula, A.M., Spiekstra, S.W., de Kok, M., Affandi, A.J., Roest, H.P., van der Laan, L.J.W., de Winde, C.M., Koning, J.J., Gibbs, S., and Mebius, R.E. (2023). An Organotypic Human Lymph Node Model Reveals the Importance of Fibroblastic Reticular Cells for Dendritic Cell Function. Tissue Eng Regen Med. 10.1007/s13770-023-00609-x.

[36] Honma, M., Minami-Hori, M., Takahashi, H., and Iizuka, H. (2012). Podoplanin expression in wound and hyperproliferative psoriatic epidermis: regulation by TGF-beta and STAT-3 activating cytokines, IFN-gamma, IL-6, and IL-22. J Dermatol Sci *65*, 134-140. 10.1016/j.jdermsci.2011.11.011.

[37] de Winde, C.M., Makris, S., Millward, L.J., Cantoral-Rebordinos, J.A., Benjamin, A.C., Martinez, V.G., and Acton, S.E. (2021). Fibroblastic reticular cell response to dendritic cells requires coordinated activity of podoplanin, CD44 and CD9. J Cell Sci *134*. 10.1242/jcs.258610.

[38] Quintanilla, M., Montero-Montero, L., Renart, J., and Martin-Villar, E. (2019). Podoplanin in Inflammation and Cancer. Int J Mol Sci *20*. 10.3390/ijms20030707.

[39] Choi, Y.S., Jeong, E., Lee, J.S., Kim, S.K., Jo, S.H., Kim, Y.G., Sung, H.J., Cho, S.W., and Jin, Y. (2021). Immunomodulatory Scaffolds Derived from Lymph Node Extracellular Matrices. ACS Appl Mater Interfaces *13*, 14037-14049. 10.1021/acsami.1c02542.

[40] van Tienderen, G.S., van Beek, M.E.A., Schurink, I.J., Rosmark, O., Roest, H.P., Tieleman, J., Demmers, J., Muntz, I., Conboy, J., Westergren-Thorsson, G., et al. (2022). Modelling metastatic colonization of cholangiocarcinoma organoids in decellularized lung and lymph nodes. Front Oncol *12*, 1101901. 10.3389/fonc.2022.1101901.

[41] Korsunsky, I., Millard, N., Fan, J., Slowikowski, K., Zhang, F., Wei, K., Baglaenko, Y., Brenner, M., Loh, P.R., and Raychaudhuri, S. (2019). Fast, sensitive and accurate integration of single-cell data with Harmony. Nat Methods *16*, 1289-1296. 10.1038/s41592-019-0619-0.

[42] Street, K., Risso, D., Fletcher, R.B., Das, D., Ngai, J., Yosef, N., Purdom, E., and Dudoit, S. (2018). Slingshot: cell lineage and pseudotime inference for single-cell transcriptomics. BMC Genomics *19*, 477. 10.1186/s12864-018-4772-0.

[43] Stuart, T., Butler, A., Hoffman, P., Hafemeister, C., Papalexi, E., Mauck, W.M., 3rd, Hao, Y., Stoeckius, M., Smibert, P., and Satija, R. (2019). Comprehensive Integration of Single-Cell Data. Cell *177*, 1888-1902 e1821. 10.1016/j.cell.2019.05.031.

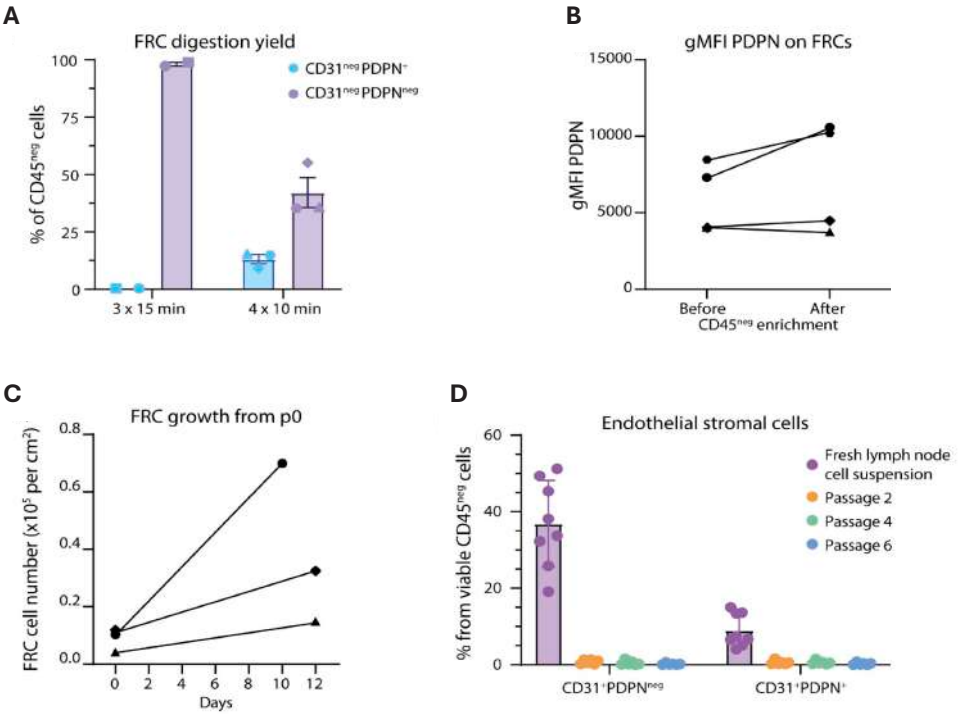

Fig. S1 - Cell characteristics of improved digestion protocol, related to Fig. 1. (A) Bar graph visualising the percentage of CD31^{neg}PDPN+ and CD31^{neg}PDPN^{neg} cells from CD45^{neg} cells after 3 digestion rounds of 15 minutes or after 4 digestion rounds of 10 minutes. **(B)** Geometric mean fluorescent intensity of PDPN on FRCs before or after CD45^{neg} enrichment. Shapes represent four different donors. **(C)** FRC growth from passage 0, visualised as FRC cell number per cm^2 on day 0 within the lymph node cell suspensions and after 10 or 12 days in culture. The three different symbols correspond to three different donors. **(D)** Bar graph visualising the percentage of endothelial stromal cells from viable CD45^{neg} cells within the fresh lymph node cell suspensions or after culture at passage 2, 4 and 6. For panels A and D, the mean is visualised with error bars representing standard deviations.

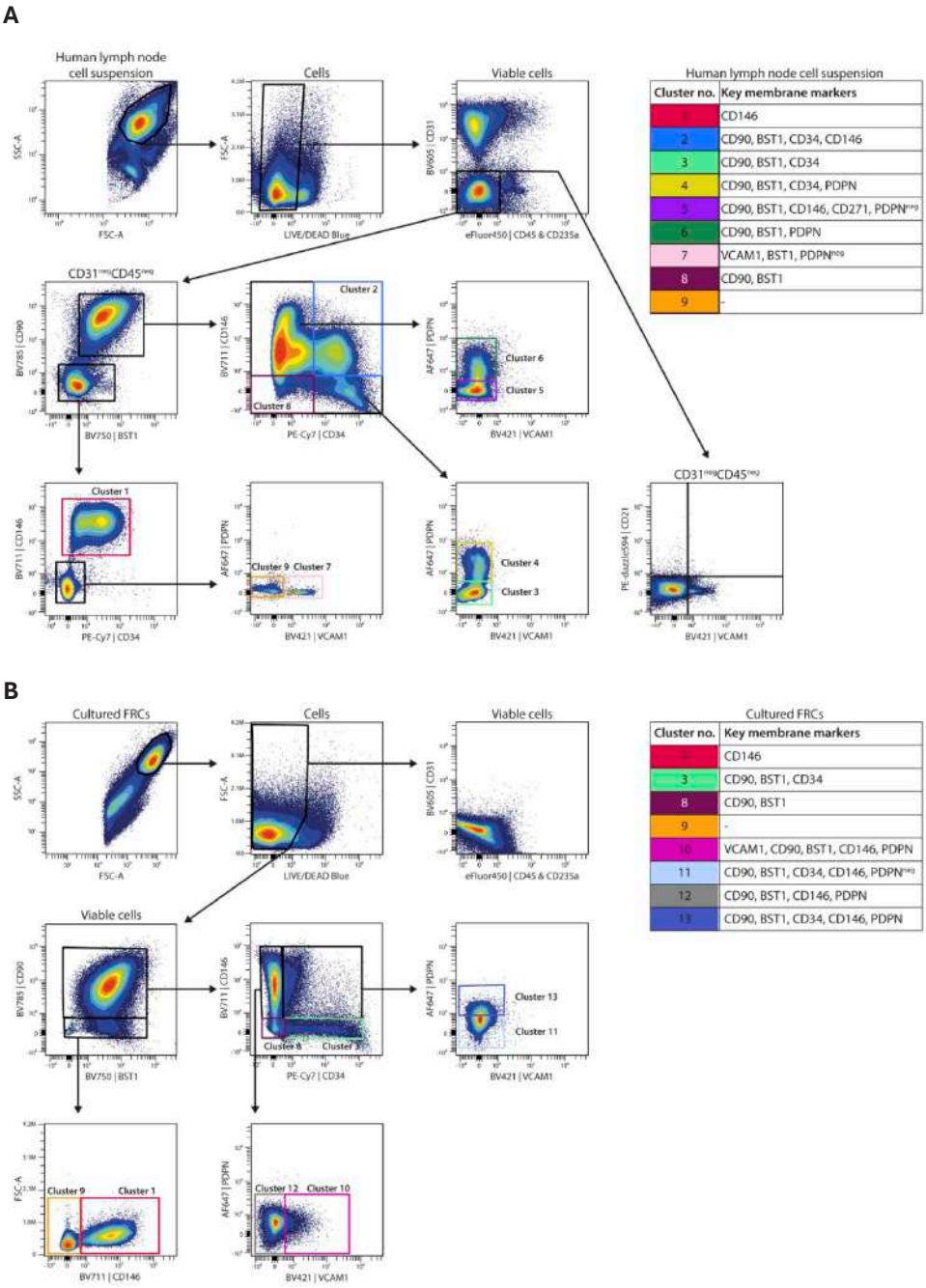

Fig. S2 - Gating strategy of clusters within human LN cell suspensions and cultured FRCs, related to Fig. 3 , 4. (A) Gating strategy and key membrane markers of the clusters identified within CD31^{neg}CD45^{neg} cells from human LN cell suspensions, related to Fig. 3. Contour plots shown from one representative donor. **(B)** Gating strategy and key membrane markers of the clusters identified within CD31^{neg}CD45^{neg} cells from cultured FRCs, related to Fig. 4. Contour plots shown from one representative donor.

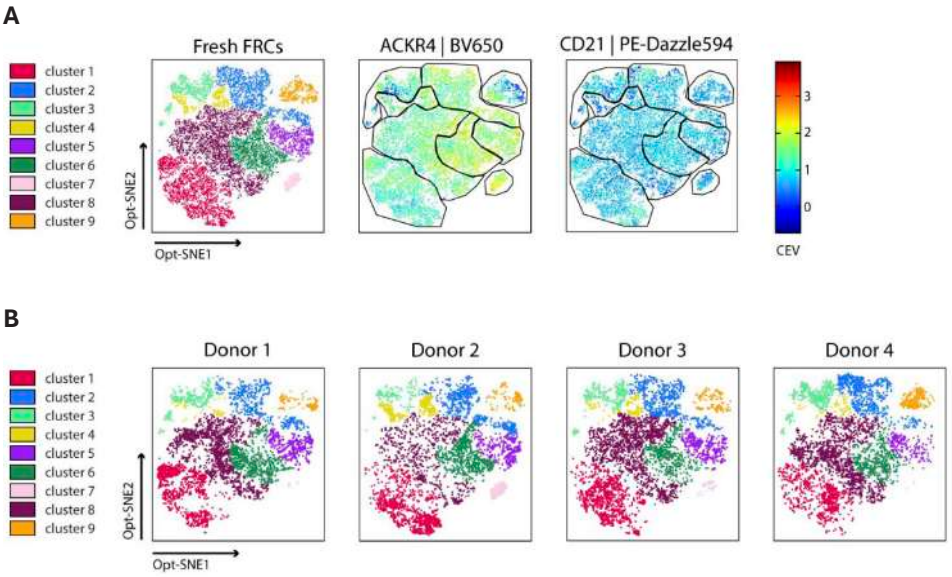

Fig. S3 - High dimensional analysis of FRCs in fresh human LN cell suspensions, related to Fig. 3. (A) Based on Opt-SNE visualisation, we identified nine distinct clusters of fresh LNSC subsets, gated from live, CD45^{neg}CD31^{neg} cells. Scale bar represents median correction expression value (CEV) from -0.7 to 3.9. Data represents an overlay of four independent human LN donors (Table S1). **(B)** Opt-SNE per human LN donor of the nine distinct clusters of fresh LNSC subsets.

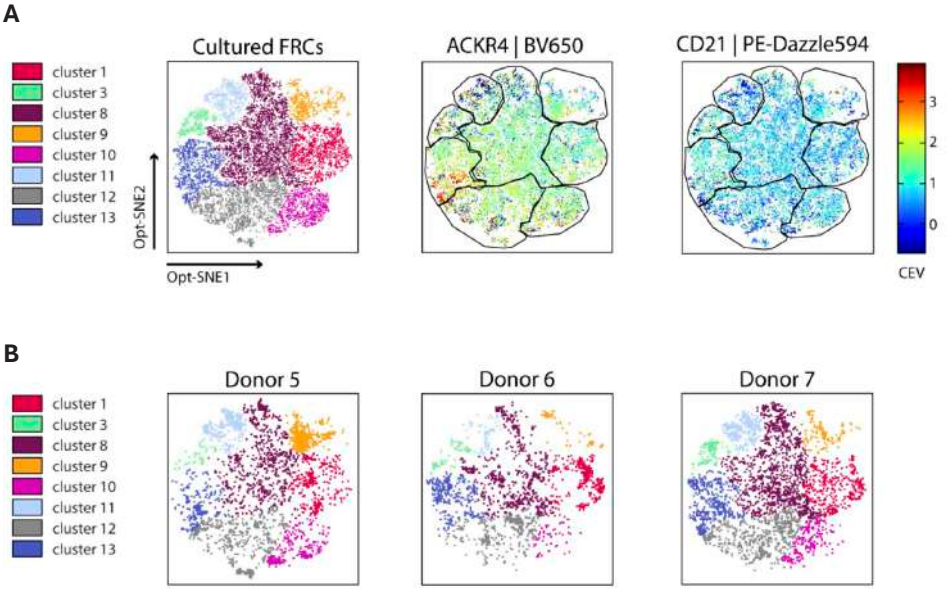

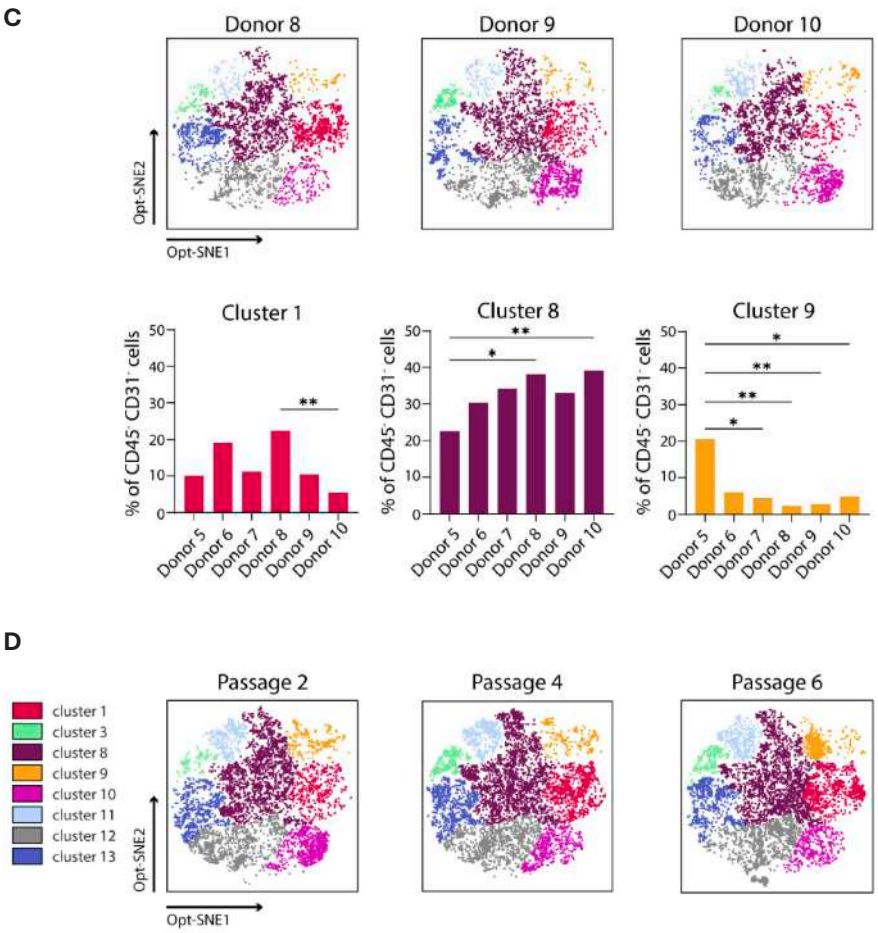

Fig. S4. High dimensional analysis of cultured FRCs, related to Fig. 4. (A) Based on Opt-SNE visualisation, we identified eight distinct clusters of FRC subsets throughout culture, gated from live, CD45^{neg}CD31^{neg} cells. Scale bar represents median correction expression value (CEV) from -0.7 to 3.9. Data represents an overlay of six human LN donors (Table S1), passages 2, 4 and 6 combined. **(B)** Opt-SNE per human LN donor of the eight distinct clusters of cultured FRCs, passages 2, 4 and 6 combined. **(C)** Significant different clusters between donors are represented per cluster. Two-way ANOVA with Tukey's multiple comparison test, *p < 0.05 and **p < 0.01. **(D)** Opt-SNE per passage of the eight distinct clusters of cultured FRCs, six human LN donors combined.

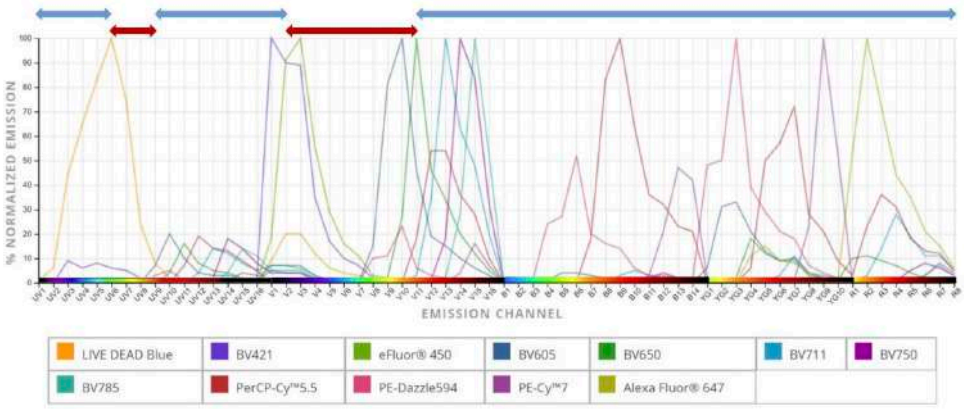

Fig. S5 - Spectra of the fluorophores of the antibody panel, related to STAR Methods. This image shows the spectra of fluorophores of the antibody panel used in this manuscript (made with Cytek® Spectrum Viewer). The red arrows above the graph indicate areas in the spectrum with high autofluorescence of human FRCs, and the blue arrows indicate areas in the spectrum with low autofluorescence of human FRCs. When adding extra markers to the panel, we recommend to choose fluorophores emitted in channels with low autofluorescence (blue arrows).

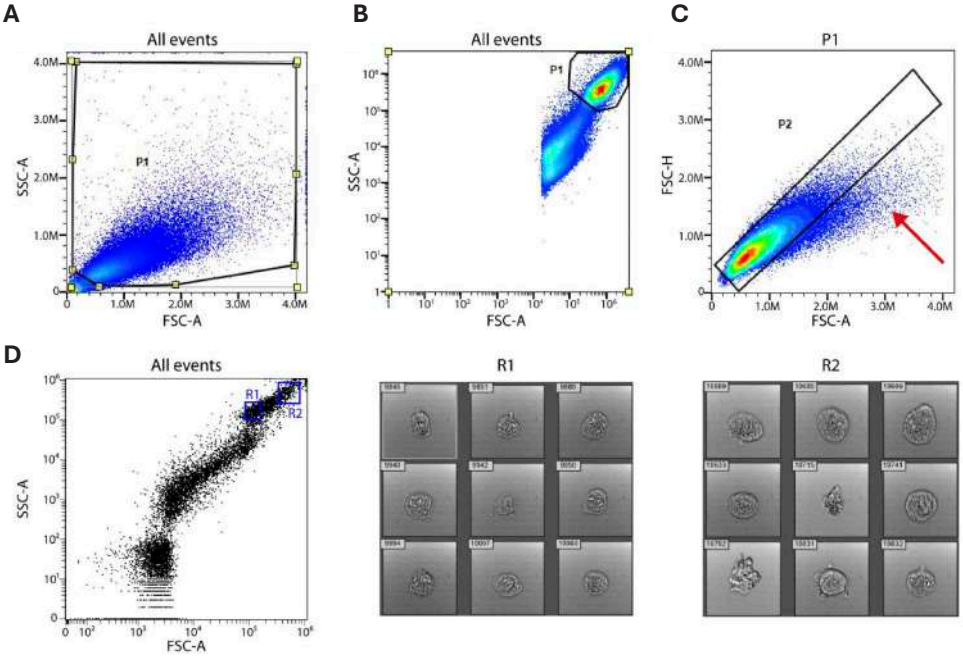

Fig. S6 - Morphology of cultured human FRCs affects the positioning of events on forward (FSC) and side (SSC) scatter, related to STAR Methods. Gating strategy for selection of human LN stromal cells (gate P1) in **(A)** linear and **(B)** logarithmic scale. **(C)** Red arrow shows single cells deviating from linearity. **(D)** Images of individual human FRCs acquired on CytPix flow cytometer. The blue squares indicate the area of zoom in of single events depicted by brightfield images on the right. FSC and SSC are in log scale.

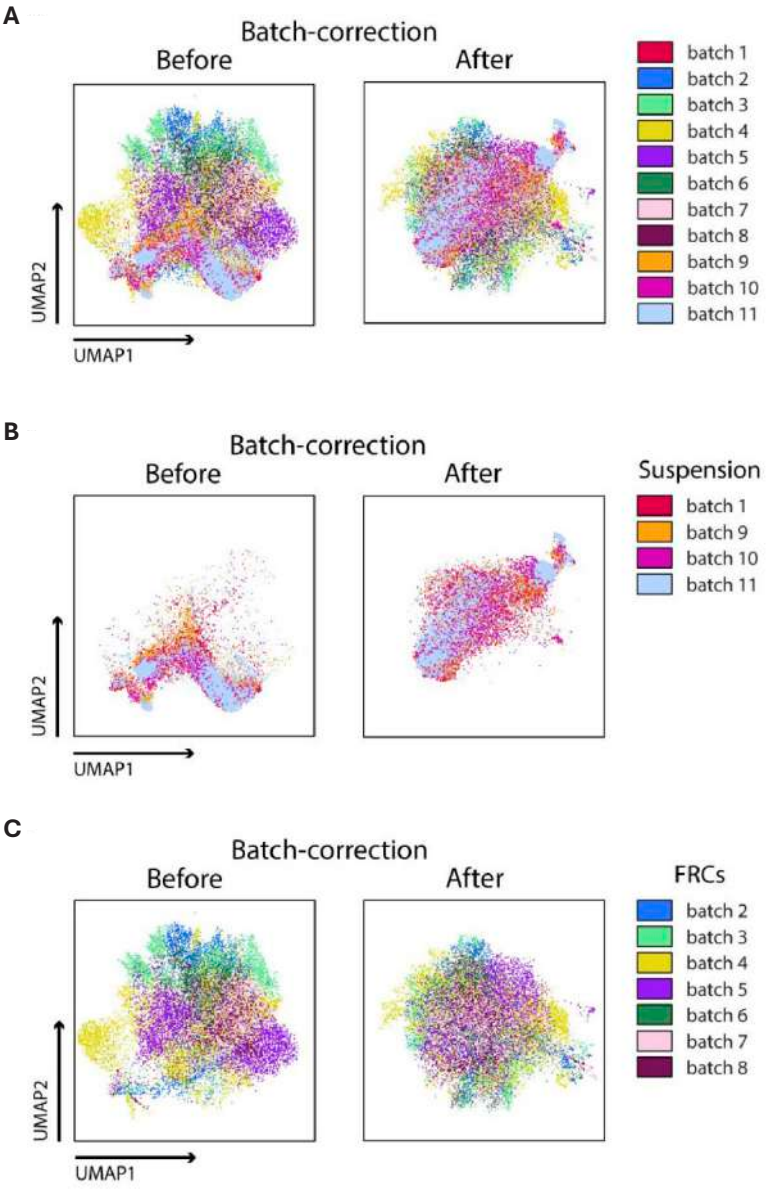

Fig. S7. Visualisation of batch correction, related to STAR Methods. (A) UMAP visualisation of the different batches before and after iMUBAC batch correction. **(B)** UMAP visualisation of the batches of fresh LN cell suspensions before and after iMUBAC batch correction. **(C)** UMAP visualisation of the batches of cultured FRCs before and after iMUBAC batch correction.

Table S1 **Human lymph node donor characteristics, related to Fig. 1, 3 & 4.** F: Female, M: Male, DBD: Donation after Brain Death, DCD: Donation after Circulatory Death., DLT, Donation after Liver Transplantation.

#	Sex	Age	Donor type	Underlying liver disease	Used in Fig.
1	F	83	DBD	None	1 & 3
2	F	16	DBD	None	1 & 3
3	F	21	DBD	None	1 & 3
4	F	53	DBD	None	1 & 3
5	M	75	DCD	None	4
6	F	25	DLT	Wilson's disease	4
7	M	16	DCD	None	4
8	M	28	DCD	None	4
9	F	33	DCD	None	4
10	M	53	DBD	None	4

Table S2 **Summary of FRC subsets present in *ex vivo* and cultured human LNSC samples.** Related to Fig. 3, 4.

Cluster no.	Present ex vivo?	Present in culture?	Key membrane markers
1	Yes	Yes	CD146
2	Yes	-	CD90, BST1, CD34, CD146
3	Yes	Yes	CD90, BST1, CD34
4	Yes	-	CD90, BST1, CD34, PDPN
5	Yes	-	CD90, BST1, CD146, CD271, PDPN^{neg}
6	Yes	-	CD90, BST1, PDPN
7	Yes	-	VCAM1, BST1, PDPN^{neg}
8	Yes	Yes	CD90, BST1
9	Yes	Yes	-
10	-	Yes	VCAM1, CD90, BST1, CD146, PDPN
11	-	Yes	CD90, BST1, CD34, CD146, PDPN^{neg}
12	-	Yes	CD90, BST1, CD146, PDPN
13	-	Yes	CD90, BST1, CD34, CD146, PDPN

4

An Organotypic Human Lymph Node Model Reveals the Importance of Fibroblastic Reticular Cells for Dendritic Cell Function

Andrew I. Morrison[1,2], Aleksandra M. Mikula[1,2], Sander W. Spiekstra[1,2], Michael de Kok[1,2], Alsya J. Affandi[1,2,3], Henk P. Roest[4], Luc J.W. van der Laan[4], Charlotte M. de Winde[1,2,3], Jasper J. Koning[1,2], Susan Gibbs[1,2,5], Reina E. Mebius[1,2]

[1] Amsterdam UMC location Vrije Universiteit Amsterdam, Molecular Cell Biology & Immunology, De Boelelaan 1117, Amsterdam, The Netherlands.

[2] Amsterdam institute for Infection and Immunity, Amsterdam, The Netherlands.

[3] Cancer Center Amsterdam, Amsterdam, The Netherlands

[4] Erasmus MC Transplant Institute, University Medical Center Rotterdam, Department of Surgery, Dr. Molewaterplein 40, 3015GD, Rotterdam, The Netherlands.

[5] Department Oral Cell Biology, Academic Centre for Dentistry Amsterdam (ACTA), University of Amsterdam and Vrije Universiteit, Amsterdam, The Netherlands.

Tissue Eng Regen Med. 2024 Apr;21(3):455-471. DOI: 10.1007/s13770-023-00609-x

Abstract

Background:

Human lymph node (HuLN) models have emerged with invaluable potential for immunological research and therapeutic application given their fundamental role in human health and disease. While fibroblastic reticular cells (FRCs) are instrumental to HuLN functioning, their inclusion and recognition of importance for organotypic *in vitro* lymphoid models remain limited.

Methods:

Here, we established an *in vitro* three-dimensional (3D) model in a collagen-fibrin hydrogel with primary FRCs and a dendritic cell (DC) cell line (MUTZ-3 DC). To study and characterise the cellular interactions seen in this 3D FRC-DC organotypic model compared to the native HuLN; flow cytometry, immunohistochemistry, immunofluorescence and cytokine/chemokine analysis were performed.

Results:

FRCs were pivotal for survival, proliferation and localisation of MUTZ-3 DCs. Additionally, we found that CD1a expression was absent on MUTZ-3 DCs that developed in the presence of FRCs during cytokine-induced MUTZ-3 DC differentiation, which was also seen with primary monocyte-derived DCs (moDCs). This phenotype resembled HuLN-resident DCs, which we detected in primary HuLNs, and these $CD1a^-$ MUTZ-3 DCs induced T cell proliferation within a mixed leukocyte reaction (MLR), indicating a functional DC status. FRCs expressed podoplanin (PDPN), CD90 (Thy-1), CD146 (MCAM) and Gremlin-1, thereby resembling the DC supporting stromal cell subset identified in HuLNs.

Conclusion:

This 3D FRC-DC organotypic model highlights the influence and importance of FRCs for DC functioning in a more realistic HuLN microenvironment. As such, this work provides a starting point for the development of an *in vitro* HuLN.

Introduction

In humans, lymph nodes (LNs) are secondary lymphoid organs that possess a fundamental role in orchestrating the adaptive immune response. Strategically positioned throughout the human body, they drain interstitial fluid from all tissue and have a highly specialised architectural organisation that is strictly regulated by non-hematopoietic stromal cells to facilitate multicellular interactions within anatomical niches[1, 2].

Lymph node stromal cells (LNSCs) have the ability to directly shape the immune responses through lymphocyte communication[3, 4] and can be categorised into various subsets based on their origin, location and function[5, 6]. Among these subsets, fibroblastic reticular cells (FRCs) are present in the paracortex area, also known as the T cell zone, as well as in the B cell follicles, where they are termed follicular dendritic cells (FDCs). FRCs in the paracortex form a three-dimensional (3D) scaffold that supports immune cell functioning, such as dendritic cell (DC) entry, migration and antigen presentation to T cells[7, 8, 9].

DCs exhibit heterogeneous characteristics that divides their status as either plasmacytoid DCs (pDCs) or conventional DCs (cDCs)[10], which can all be found in the LN after their extravasation from blood or lymphatic vessels. These DC subsets have been further identified in distinct niches within the paracortex, where type 1 cDCs (cDC1; $CD11c^+CD141^+$) localise to the central paracortical region and are biased to antigen cross-presentation within MHC class I (MHC-I) molecules to $CD8^+$ T cells, while type 2 cDCs (cDC2; $CD11c^+CD1c^+$) are found underneath the subcapsular sinus, in the interfollicular area and in the B/T zone border for antigen presentation in MHC class II (MHC-II) to $CD4^+$ T cells[11, 12, 13]. Furthermore, DCs can be classified as LN-resident or migratory based on their antigen sampling capabilities and homeostatic locations[14, 15].

It has been shown that FRCs are necessary for the maintenance of DCs in LNs, as ablation of the FRC network in mice depleted DC populations[16] and, moreover, the FRC subset expressing Gremlin-1 (GREM1) was shown to be essential for survival of tissue-resident cDCs[17].

The development of human LN (HuLN) organotypic models offers attractive benefits for human immunity, whether that be for therapeutic application in immunotoxicology studies or translational experiments to more precisely elucidate the behaviour of immune cells in a realistic *in vitro* microenvironment[18]. Progress towards 3D HuLN organotypic models has incorporated elements like extracellular matrix (ECM)-based hydrogels and dynamic flow on microfluidic organ-on-chip devices that are typically omitted from, and not possible with, traditional two-dimensional (2D) cell co-cultures.

To date, 3D models of HuLNs have demonstrated flow-induced B cell follicle formation with blood-derived lymphocytes capable of producing antibodies upon antigen exposure[19] and, similarly, tonsil-derived organoids in transwell cultures resulted in antibody production[20]. In addition, tissue slices have demonstrated migration and activation of immune cells *in vitro*, yet this has been primarily performed with murine LNs[21] and tonsil slices with human material[22]. However, a common feature among most of these models is the lack of stromal cells, which have been minimally addressed in a synthetic *in vitro* B cell follicle model[23] and an organ-on-chip model to study DC and T cell migration towards FRCs[24], despite their importance for LN biology.

Here, we aimed to construct a 3D FRC-DC organotypic model to recapitulate and characterise the cellular interactions that take place within the paracortical region of the native HuLN. We isolated FRCs from HuLNs and generated a 3D hydrogel co-culture with MUTZ-3, a well characterised plastic DC-like cell line previously used in immunocompetent organotypic models, such as reconstructed human skin and oral mucosa[25,26,27].

This model uncovers the critical role of FRCs for DC functioning within a 3D environment that mimics the HuLN. Moreover, it establishes the foundations for building an *in vitro* HuLN with potential for future advancements, including the integration of additional immune cell populations and incorporated into dynamic microfluidic platforms, such as (multi)-organ-on-chips, to study a systemic immune response and crosstalk between other organotypic tissue models.

Materials and methods

Cell isolation and culture

Enzymatic digestion of human lymph nodes

HuLNs were obtained from donors during liver transplant procedures at Erasmus MC, Rotterdam, The Netherlands. Tissue was transported in University of Wisconsin (UW, Bridge to Life Ltd. Belzer Cold Storage Solution, London, UK) preservation solution and processed within 72 h of surgery. For a complete overview, characteristics of human donors are shown in Table 1. Isolation of HuLN immune and stromal cells was achieved through enzymatic tissue digestion, as previously described[28], where modifications were made to the time of each digestion cycle (4 × 10 min intervals). The enzyme mixture contained RPMI-1640 with 2.4 mg/ml Dispase II, 0.6 mg/ml Collagenase P and 0.3 mg/ml DNase I (all from Sigma-Aldrich, St. Louis, MO, USA). To prevent over-digestion and stop the enzyme reaction after each digestion cycle, ice cold PBS supplemented with 2% foetal calf serum (FCS) and 5 mM EDTA was used to wash the isolated cells, after which they were spun down at 300 G for 4 min at 4 °C. Cell pellet was re-suspended in 1 ml of DMEM with 10% FCS, strained through a 100 µM filter, and counted. The HuLN cell suspension was either cryopreserved or cultured as described below.

Culture of primary fibroblastic reticular cells

LN cell suspensions were plated at a minimum concentration of 20×10^6 cells in a T-25 flask at 37 °C and 5% CO_2. To selectively grow out FRCs, flask surface was coated with 2 µg/cm^2 collagen from calf skin (Sigma-Aldrich) and FRCs were cultured in FRC medium, defined as DMEM with 10% FSC, 2% Penicillin/Streptomycin/Glutamine and 1% Insulin Transferrin Selenium (Gibco, Grand Island, NY, USA). After three days, lymphocytes were washed away with PBS to allow optimal stromal cell growth. Upon confluence, cells were passaged and harvested with 0.5% Trypsin + 5 mM EDTA. FRCs were used up to passage 8 for all individual experiments.

Table 1 Human lymph node donor details

Donor	HLA-type	Sex	Age
#1	A2 A9 A24 B8 B35 Bw4 Bw6 Cw4 Cw7 DR3 DR17 DR5 DR11 DR52 DQ2 DQ3 DQ7	F	71
#2	A2 A19 A29 B12 B44 B21 B49 Bw4 Cw7 Cw16 DR4 DR7 DR53 DQ2 DQ3 DQ8	M	84
#3	A1 A1 B7 B8 Bw6 Cw7 Cw15 DR3 DR17 DR5 DR12 DR52 DQ2 DQ3 DQ7	F	50
#4	A2 A11 B12 B44 B22 B55 Bw4 Bw6 Cw3 Cw9 Cw5 DR4 DR6 DR14 DR52 DR53 DQ1 DQ5 DQ3 DQ8	M	59
#5	A3 A9 A24 B15 B62 B35 Bw6 Cw3 Cw10 Cw4 DR1 DR4 DR53 DQ1 DQ5 DQ3 DQ8	F	46
#6	A1 A2 B5 B51 B8 Bw4 Bw6 Cw5 Cw7 DR3 DR17 DR5 DR11 DR52 DQ2 DQ3 DQ7	M	21
#7	A1 A11 B8 B12 B44 Bw4 Bw6 Cw5 Cw7 DR3 DR17 DR6 DR14 DR52 DQ1 DQ5 DQ2	F	60
#8	A2 A19 A29 B12 B44 B35 Bw4 Bw6 Cw4 Cw16 DR6 DR14 DR7 DR52 DR53 DQ1 DQ5 DQ2	M	57

Culture of MUTZ-3 dendritic cell line

The MUTZ-3 progenitor cell line (Deutsche Sammlung von Mikroorganismen und Zellkulturen [DSMZ], Braunschweig, Germany) was cultured as previously described[29]. MUTZ-3 progenitor cells were differentiated into MUTZ-3 DCs by supplementing minimal essential media-alpha (MEM-α; Gibco) containing 20% v/v FCS, 1% Penicillin/Streptomycin, 2 mM L-glutamine (Gibco), 50 μM 2-β mercaptoethanol (Merck, Whitehouse Station, NY, USA), 100 ng/ml recombinant human granulocyte macrophage-colony stimulating factor (rhGM-CSF; Biosource, International Inc, Camarillo, CA, USA), 10 ng/ml interleukin-4 (IL-4; BioVision, Waltham, MA, USA) and 2.5 ng/ml tumour necrosis factor-alpha (TNF-α; Strathmann Biotec, Hamburg, Germany) for seven days. Cells were cultured at 37 °C and 5% CO_2, and used before passage 30 for all experiments. In experiments where MUTZ-3 DCs cells were fluorescently labelled, CellTracker Orange CMTMR (Invitrogen, Paisley, Scotland, UK) was used at a volume of 2.5 μl per 1 × 10^6 cells in serum-free medium for 15 min at 37 °C, after which the cells were washed with the relevant cell media.

Generation of monocyte-derived dendritic cells

Human $CD14^+$ monocytes were selected using magnetic activated cell sorting (MACS) with $CD14^+$ magnetic beads from peripheral blood mononuclear cells (PBMCs) as previously described[30]. Monocytes were cultured in RPMI-1640 with HEPES and L-glutamine (BioWhittaker, Lonza, Verviers, Belgium) supplemented with 10% heat inactivated fetal calf serum (FCS, HyClone; GE Healthcare, Chicago, IL, USA), 50 µM β-mercaptoethanol (Merck), 100 IU/ml sodium-penicillin (Gibco), 100 µg/ml streptomycin (Gibco), and 2 mM L-glutamine (Gibco). For monocyte-derived dendritic cell (moDC) generation, monocyte culture medium stated above was supplemented with 100 ng/ml rhGM-CSF and 10 ng/ml IL-4 for seven days.

Construction of 3D FRC-DC organotypic model

The 3D FRC-DC organotypic model was constructed in 12-well transwells (0.4 µm pore size; Corning, NY, USA) by mixing rat-tail collagen type I (3 mg/ml end concentration) in Hank's Balanced Salt Solution (HBSS without Ca and Mg; Gibco) 1:1 with fibrinogen from human plasma (Enzyme research laboratories, cat no: FIB 1, South Bend, IN, USA) (1 mg/ml end concentration). After optimising cell density to maintain maximum cell viability with limited hydrogel shrinkage, FRCs were added at a final cell density of 2.0×10^5 cells per gel. The FRC co-cultures with either MUTZ-3 progenitor cells, MUTZ-3 DCs or primary monocytes were mixed at a 1:1 cell ratio with a final total cell concentration of 4.0×10^5 cells per gel. Thrombin (0.5 U/ml; Merck KGaA, Darmstadt, Germany) was added to each gel to allow for fibrin formation and hydrogels were polymerised for 1.5 h at 37 °C and 5% CO_2. FRC medium was added both above and below the hydrogel, and was refreshed every 2–3 days while culture supernatant was stored at −20 °C. At the end of the culture period, hydrogels were either fixed for histological analysis or enzymatically digested to a single cell suspension for flow cytometry using 0.8 mg/ml Dispase II, 0.2 mg/ml Collagenase P and 0.1 mg/ml DNase I for 1 h at 37 °C, after which the reaction was stopped with ice cold PBS containing 2% FCS and 5 mM EDTA.

Flow cytometry

Cell suspensions were stained in a 96-well U bottom plate at 4 °C for flow cytometric analysis. Cells were firstly washed with FACS buffer containing PBS, 0.1% bovine serum albumin (BSA) and 0.05% NaN_3, and stained with a fixable viability dye (Live/Dead Fixable Blue; L34961, Invitrogen) for 10 min at 4 °C. Fc-receptor blocking was performed using 10% normal human serum and cells were then incubated with directly-labelled antibodies. An overview of all antibodies used can be found in Table 2. After staining, cells were fixed with 2% PFA (diluted in PBS) for 10 min, washed and acquired on the Aurora 4-Laser multispectral flow cytometer (CYTEK, Amsterdam, The Netherlands). Autofluorescence (AF) correction of cells was performed as previously described[31]. Data analysis was carried out using FlowJo (v10.7, TreeStar, Ashland, OR, USA) or OMIQ (Boston, MA, USA).

Table 2 Antibodies used for flow cytometry (FACS), Immunohistochemistry (IHC) and Immunofluorescence (IF)

Target	Fluorochrome	Species	Clone	Cat. no	Manufacturer	Assay
CD1a	eFluor450	Mouse	HI149	48-0019-42	Invitrogen	FACS
CD1c	PerCP-eFluor710	Mouse	L161	46-0015-41	Invitrogen	FACS
CD11c	BV650	Mouse	3.9	301,638	Biolegend	FACS
CD31	BV605	Mouse	WM59	303,122	Biolegend	FACS
CD45	eFluor450	Mouse	HI30	48-0459-42	Invitrogen	FACS
CD45	BUV395	Mouse	HI30	563,791	BDBiosciences	FACS
CD83	APC-Vio770	n/a	REA714	130-110-506	Miltenyi	FACS
CD86	PE-Vio770	n/a	REA968	130-116-162	Miltenyi	FACS
CD90	BV785	Mouse	5E10	328,142	Biolegend	FACS
CD141	PE-Cy7	Mouse	M90	344,109	Biolegend	FACS
CD146	BV711	Mouse	P1H12	361,032	Biolegend	FACS
CLEC2	PE	Mouse	AYP1	372,003	Biolegend	FACS
DC-SIGN	FITC	Mouse	DCN46	551,264	BDBiosciences	FACS
HLA-DR	PerCP-Cy5.5	Mouse	L243	307,629	Biolegend	FACS
PDPN	Alexa Fluor 647	Rat	NC-08	337,008	Biolegend	FACS
CD45	–	Mouse	2B11 + PD7/26	MO701	Dako	IHC
Vimentin	–	Mouse	V9	Sc-6260	Santa Cruz	IHC
CD3	Alexa Fluor 488	Mouse	UCHT1	300,415	BioLegend	IF
CD11c	–	Mouse	S-HCL-3	371,502	Biolegend	IF
HLA-DR	–	Mouse	TAL1b5	M0746	Dako	IF
Ki67	–	Mouse	MIB-1	M7240	Dako	IF
PDPN	–	Mouse	n/a	11–003	AngioBio	IF
Vimentin	Alexa Fluor 488	Mouse	091D3	677,809	Biolegend	IF

Immunohistochemical and immunofluorescence staining

Human lymph node tissue

LNs were cryopreserved by fixing with 4% PFA for 15 min at room temperature (RT), followed by sequential incubation with 15% and 30% sucrose. Tissue was embedded in OCT compound (Sakura Finetek, Alphen aan den Rijn, The Netherlands), frozen on liquid nitrogen and stored at −70 °C. Cryosections of 5 µm were fixed in acetone for 10 min, air-dried and then blocked for 20 min with PBS containing 1% BSA and 10% normal goat serum. Sections were stained with primary antibody for 60 min, washed and, if needed, stained with a secondary antibody for 30 min. Sections were mounted with mounting medium containing DAPI (Abcam, Cambridge, UK) and stored at 4 °C until acquisition. Images were acquired using a fluorescent microscope (Axiolmager, Zeiss, Jena, Germany).

3D FRC-DC organotypic model

Hydrogel pieces were fixed in 4% PFA for histology. For paraffin embedding, samples were dehydrated, embedded in paraffin and cut at 5 µm sections for morphological (hematoxylin and eosin, H&E), immunohistochemical (IHC) and immunofluorescent (IF) analysis. Sections were deparaffinised and immersed in 0.01 M sodium citrate buffer (pH 6.0) for 15 min at 100 °C for antigen retrieval, followed by slowly cooling to RT. Sections were then washed with PBS, blocked for 20 min with 10% normal human serum and stained for 1 h with primary antibodies, followed by a secondary antibody conjugate for 30 min, if necessary.

3D light sheet microscopy imaging

For 3D light sheet imaging, hydrogels were fixed in 4% EM-grade formaldehyde (VWR, Radnor, PA, USA) for 15 min at RT, washed in PBS containing 0.05% NaN_3, stained with Vimentin-Alexa Fluor 488 (clone O91D3; BioLegend, San Diego, CA, USA) and cleared according to the iDISCO protocol, modified to a 24 h antibody incubation period [32]. Cleared samples were acquired using the light sheet Ultramicroscope (La Vision BioTec, Bielefeld, Germany) and 3D analysis was conducted using Imaris (version 9 or higher; Oxford Instruments, Abingdon, UK).

Cytokine/chemokine detection in culture supernatants

Hydrogel supernatants were pooled from the top and bottom of the transwell, and analysed for the presence of cytokines and chemokines using cytokine bead arrays (Human Essential Immune Response and Custom LEGENDplex panel; BioLegend), according to the manufacturer's instructions. Acquisition was performed on AttuneNxT (ThermoFisher, Waltham, MA, USA) and protein concentrations were determined using the LEGENDplex Data Analysis Software Suite (BioLegend).

Mixed lymphocyte reaction: T cell proliferation assay

Total $CD4^+$ T cells were isolated from a buffy coat (Sanquin, Amsterdam, The Netherlands) using

$CD4^+$ negative selection beads (Miltenyi Biotec, Bergisch Gladbach, Germany). Isolated T cells were labelled with 3 µM of CFSE for 7 min at 37 °C in PBS containing 5% FCS. Cells were washed and left for a further 15 min in the dark at RT. CFSE-labelled T cells were then washed and co-cultured with a single cell suspension of differentiated MUTZ-3 DCs and FRCs harvested from the digested 3D FRC-DC organotypic model after seven days, or MUTZ-3 DCs alone without FRCs after a seven day differentiation in 2D 12-well plates. Cells and culture supernatants were collected and refreshed at day three and day six to assess T cell proliferation via flow cytometry (Aurora 4L) and protein secretion (BioLegend, LEGENDplex), as detailed above.

Quantitative polymerase chain reaction

mRNA of cultured HuLN FRCs and MUTZ-3 DCs were isolated using Trizol (Invitrogen) followed by cDNA synthesis using RevertAid First Strand cDNA Synthesis Kit (ThermoFisher) according to the manufacturers' instruction. RNA and cDNA concentrations and quality were measured with a NanoPhotometer (Implen, Munich, Germany). The reaction mix consisted of Fast SYBR Green Master Mix (Applied Biosystems, Waltham, MA, USA), 300 nM of primer, cDNA and DEPC-Treated Water (Invitrogen) with a total volume of 10 µl. Relative changes in mRNA levels were calculated with the $2^{-\Delta\Delta Ct}$ method, using S18 as the housekeeping gene for normalisation. The GREM1 primer had the following sequence; fw: TCATCAACCGCTTCTGTTACGGC, rev: CAGAAGGAGCAGGACTGAAAGG.

Statistical analysis

All data are presented as mean ± standard error of the mean (SEM). All HuLN tissue material, FRCs and immune cells were derived from different donors resulting in the use of eight HuLN donors spread across all experiments (to reduce donor variation). Statistical analysis was performed by means of either unpaired t test, 2way ANOVA, Kruskal–Wallis test or Wilcoxon test using GraphPad Prism 9 software (GraphPad Software Inc., San Diego, CA, USA). Differences were considered to be significant when $p < 0.05$. For heatmap analysis, the pheatmap and ggbetweenstats functions of the R packages *prettyheatmap* and *ggstatsplot* (version 0.11.0) were used under R (version 4.2.1) respectively.

Results

FRCs enhance MUTZ-3 DC localisation and survival in the 3D FRC-DC organotypic model

DCs can be found within the T cell area of a HuLN and are often seen in close contact with FRCs for their survival[17]. In order to generate a biologically relevant 3D model containing LN FRCs and DCs, we first visualised the spatial relationship of DCs relative to FRCs in a HuLN. Hereto, we performed immunofluorescence analysis on primary HuLNs to identify the localisation of FRCs and DCs. $CD11c^+$ DCs were broadly distributed across the paracortex area, indicated by the presence of $CD3^+$ cells, and in close proximity to $PDPN^+$ cells, a marker used to identify FRCs (Fig. 1A).
We next aimed to model the FRC-DC localisation in an *in vitro* 3D HuLN model. FRCs and MUTZ-3

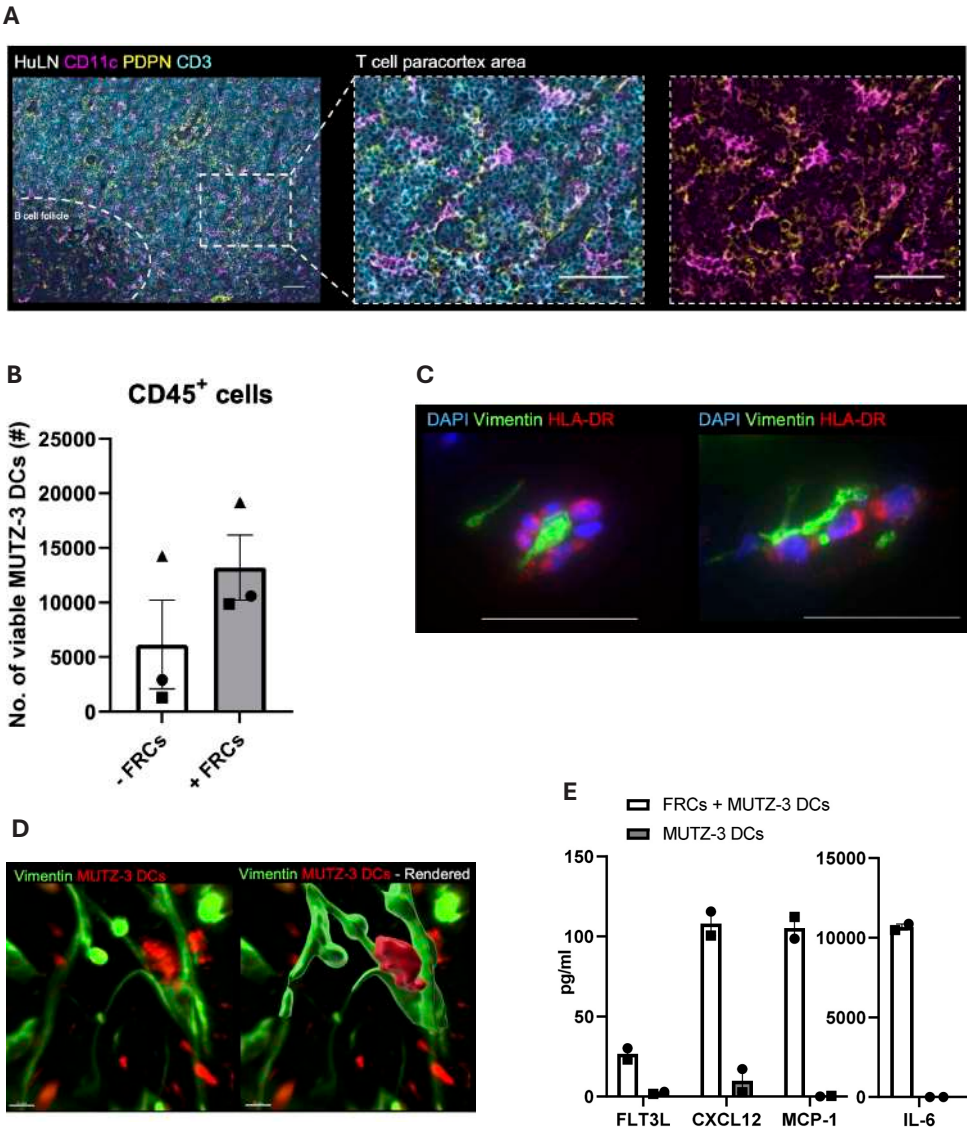

Fig. 1 - The 3D FRC-DC organotypic model benefits cell-cell interactions as seen in native HuLNs. **(A)** Cryosections of HuLN stained for DCs (CD11c, magenta), FRCs (PDPN, yellow) and T cells (CD3, cyan). Scale bar = 50 µm. **(B)** Viability of MUTZ-3 DCs harvested from hydrogel after two days -/+ FRCs. Each shape represents an independent experiment and a different FRC donor if applicable. Results are shown as mean ± SEM; *n* = 3 independent experiments performed in duplicate. **(C)** Paraffin section of hydrogel show MUTZ-3 DCs (HLA-DR, red) localisation with FRCs (Vimentin, green) after a one week co-culture. Scale bar = 50 µm. **(D)** Ultra microscope light sheet analysis identifies labelled MUTZ-3 DCs (red) with elongated FRCs (Vimentin, green) after a one week co-culture. Scale bar = 50 µm. **(E)** Cytokine / chemokine analytes detected in the hydrogel medium after a one week culture. Each shape represents an independent experiment and a different FRC donor if applicable. Results are shown as mean ± SEM; *n* = 2 independent experiments performed in duplicate.

DCs were cultured in a collagen-fibrin hydrogel, either mixed at a 1:1 cell ratio or added individually. In the absence of FRCs, we observed a reduced viability of MUTZ-3 DCs harvested as early as two days in the hydrogel in comparison to MUTZ-3 DCs with FRCs (Fig. 1B). After one week in culture, most FRCs were elongated with a reticular morphology and surrounded by HLA-DR$^+$ MUTZ-3 DCs (Fig. 1C). Further analysis using light sheet fluorescence microscopy displayed physical interaction and anchorage of MUTZ-3 DCs to elongated FRCs (Fig. 1D).
In the supernatants of hydrogels containing FRCs and MUTZ-3 DCs, we found increased levels of DC-related analytes fms-related tyrosine kinase 3 ligand (FLT3L), c-x-c motif chemokine ligand-12 (CXCL12), monocyte chemoattractant protein-1 (MCP-1/CCL2) and interleukin-6 (IL-6), in contrast to the hydrogels containing only MUTZ-3 DCs (Fig. 1E).
These findings suggest that FRCs provide MUTZ-3 DC survival signals and the 3D FRC-DC organotypic model mimics the spatial distribution of FRCs and DCs observed in the paracortex of primary HuLNs.

FRCs influence the proliferation of MUTZ-3 progenitors in the 3D FRC-DC organotypic model

We next aimed to determine the impact of FRCs in the 3D FRC-DC organotypic model on MUTZ-3 progenitor cells, which represent an earlier stage preceding their differentiation to DCs. These MUTZ-3 progenitor cells can act as equivalents to human monocytes or precursor DCs, which are found to interact with FRCs in the native HuLN[14]. After a one week hydrogel co-culture with MUTZ-3 progenitor cells, we found the presence of FRCs to be beneficial for MUTZ-3 progenitor cell survival and proliferation, as a 23-fold higher number of CD45$^+$ cells were recovered when MUTZ-3 progenitor cells were with FRCs in the hydrogel (Fig. 2A).
We analysed the protein levels in the supernatant of the models and found no FLT3L, but increased levels of CXCL12 and significantly higher levels of MCP-1 and IL-6 in the co-culture, compared to MUTZ-3 progenitors alone (Fig. 2B). Upon histological analysis of hydrogel cross sections, H&E staining revealed areas of dense cellular niches which were populated by proliferating MUTZ-3 progenitor cells, as confirmed by CD45$^+$ and Ki67$^+$ staining that appear co-localised with Vimentin$^+$ FRCs (Fig. 2C). These data suggest that FRCs are needed for MUTZ-3 progenitor cells to survive in this 3D matrix.

FRCs skew the differentiation of DCs in the 3D FRC-DC organotypic model

Given the ability of FRCs to promote the survival of both MUTZ-3 progenitor cells and MUTZ-3 DCs in the 3D hydrogel, we next decided to characterise *in vitro* the influence of FRCs on DC phenotype to replicate the native effects of FRCs on local differentiation of DC precursors/progenitors once in the HuLN. We added a standard *in vitro* DC-differentiation cytokine cocktail (*i.e.*, GM-CSF, IL-4 and TNFα) to the hydrogel co-cultures of FRCs and MUTZ-3 progenitor cells for one week at the start of the culturing period. Since MUTZ-3 progenitor cells were less viable when cultured alone in the 3D hydrogel without FRCs or any cytokine stimuli (Fig. 2A), separate stand-alone 2D cultures of MUTZ-3 progenitor cells were used as controls. Normally, MUTZ-3 DCs differentiate from MUTZ-3 progenitor cells in response to the cytokine stimuli by up-regulating CD1a and DC-SIGN, hallmarks of MUTZ-3-derived DC phenotype[29, 33].

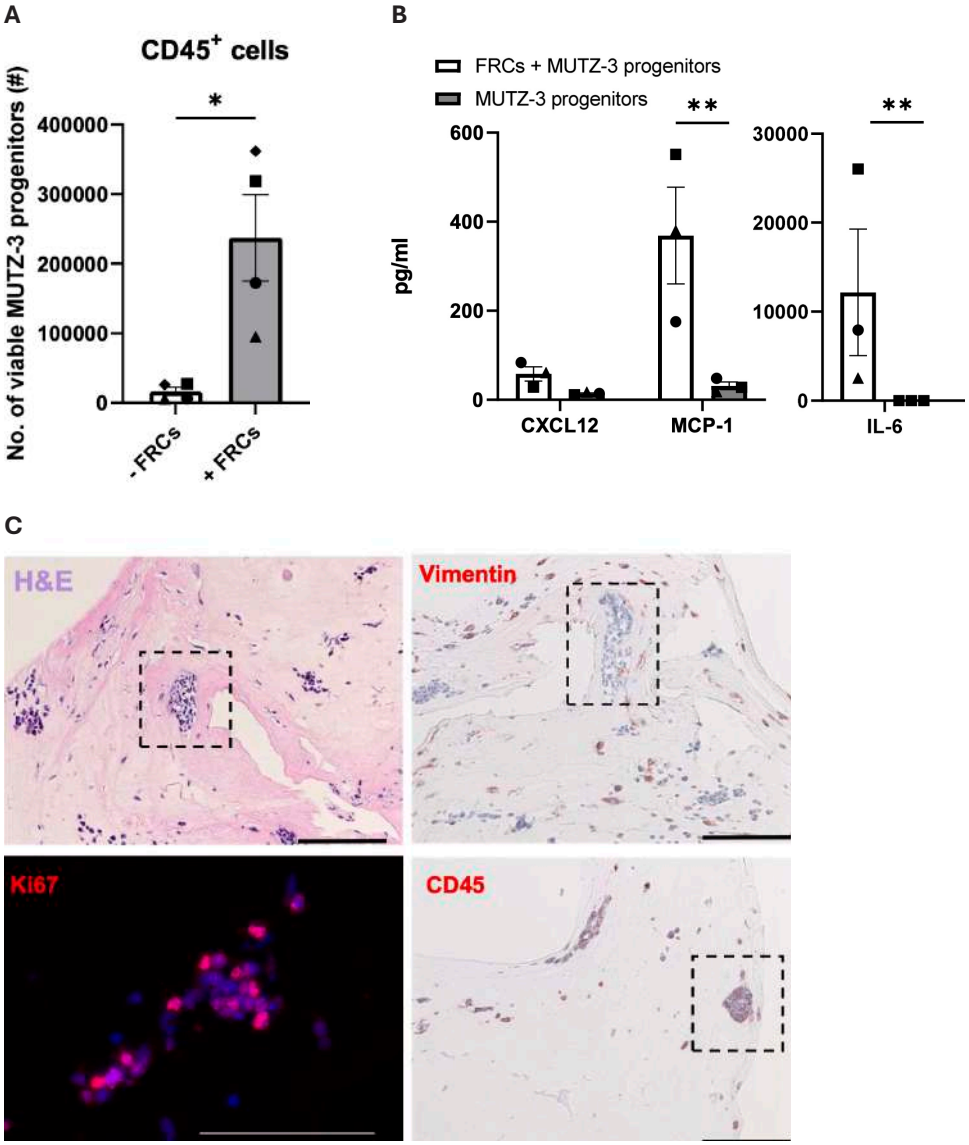

Fig. 2 - FRCs influence the survival and proliferation of MUTZ-3 progenitors inside the 3D FRC-DC organotypic model. (A) Viability of MUTZ-3 Progenitor cells harvested from hydrogel after one week -/+ FRCs. Each shape represents an independent experiment and a different FRC donor if applicable. Results are shown as mean ± SEM; *n* = 4 independent experiments performed in duplicate. **(B)** Cytokine / chemokine analytes detected in the hydrogel medium after a one week culture -/+ FRCs. Each shape represents an independent experiment and a different FRC donor if applicable. Results are shown as mean ± SEM; *n* = 3 independent experiments performed in duplicate. **(C)** Representative histological paraffin sections of a one week FRC - MUTZ-3 progenitor hydrogel co-culture. Haematoxylin and eosin (H&E) staining identifies MUTZ-3 progenitor cell nests, highlighted in black dashed box, and stained individually for proliferation marker Ki67, Vimentin and CD45 (red). Scale bar = 50 µm. *$p < 0.05$, **$p < 0.01$

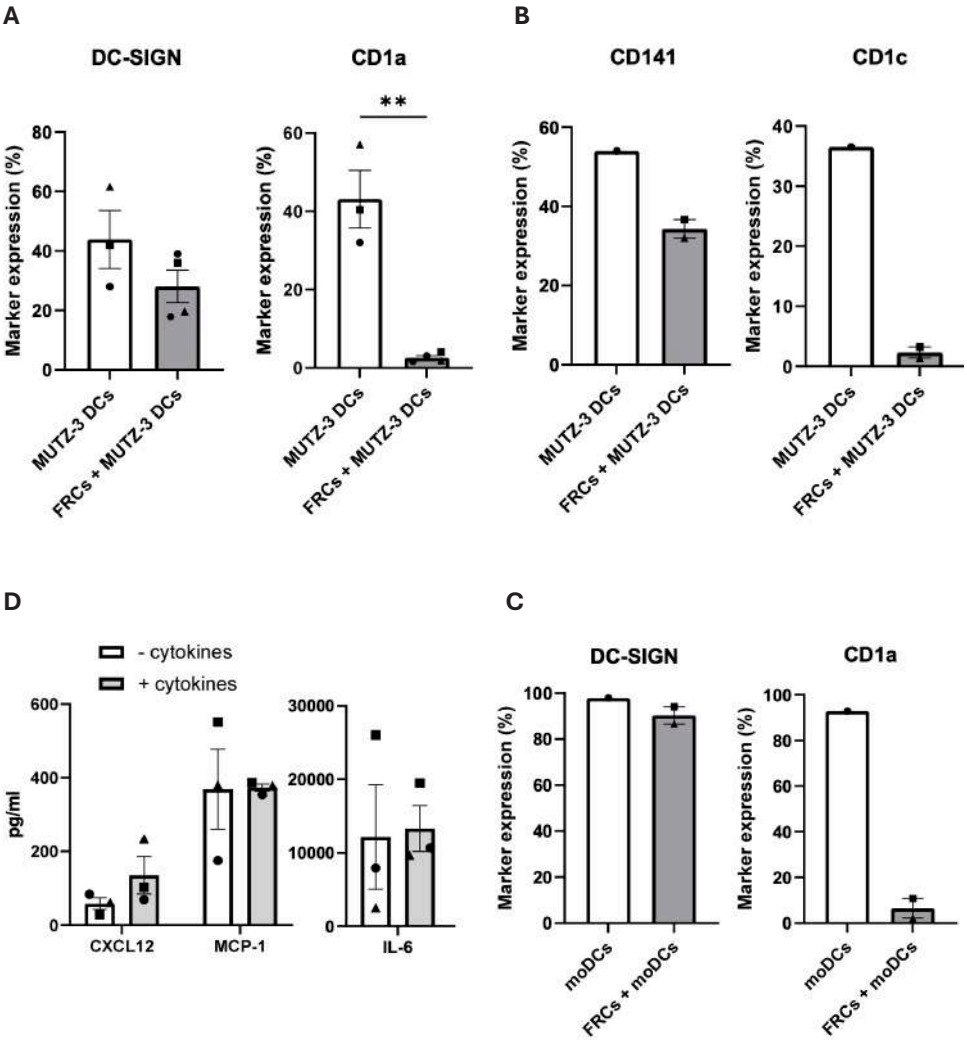

Fig. 3 - FRCs influence the differentiation of DCs inside the 3D FRC-DC organotypic model. Phenotype of differentiated MUTZ-3 DCs -/+ FRCs after a one week cytokine stimuli with GM-CSF (100 ng/ml), IL-4 (10 ng/ml) and TNFα (2.5 ng/ml). **(A)** Results for DC-SIGN and CD1a are shown as mean ± SEM; *n* = 4 independent experiments performed in duplicate. Each shape represents an independent experiment and a different FRC donor relative to one batch of MUTZ-3 DCs. **(B)** Results for CD141 and CD1c are shown as mean ± SEM; *n* = 2 independent experiments performed in duplicate. Each shape represents an independent experiment and a different FRC donor relative to one batch of MUTZ-3 DCs. **(C)** Cytokine / chemokine analytes detected in the FRC - MUTZ-3 DC hydrogel medium after a one week culture -/+ cytokines. Each shape represents an independent experiment and a different FRC donor. Results are shown as mean ± SEM; *n* = 3 independent experiments performed in duplicate. **(D)** Phenotype of differentiated moDCs -/+ FRCs after a one week cytokine stimuli with GM-CSF (100 ng/ml) and IL-4 (10 ng/ml). Each shape represents an independent experiment and a different FRC donor relative to one batch of moDCs. Results are shown as mean ± SEM; *n* = 2 independent experiments performed in duplicate. $^{**}p < 0.01$

However, the MUTZ-3 DCs that developed in the presence of FRCs and cytokines surprisingly only expressed DC-SIGN, while lacking CD1a expression (Fig. 3B and Fig. S1A). We next assessed the expression levels of CD141 and CD1c, markers associated with cDC1 and cDC2 subsets, respectively. In the 2D control setting without FRCs, MUTZ-3 progenitor cells exhibited a baseline expression of CD141 before cytokine stimuli, which increased along with CD1c expression during cell differentiation into MUTZ-3 DCs. Both markers were seen to be reduced on MUTZ-3 DCs when FRCs were present in 3D during the cytokine induced differentiation; CD1c to a greater extent than CD141 (Fig. 3B).
Further analysis into other MUTZ-3 DC markers revealed heterogeneous expression profiles after cytokine exposure (Fig. S1B). In the condition where FRCs were present compared to without, the $CD1a^-$ MUTZ-3 DC population was completely absent as expected and the $DC\text{-}SIGN^+$ population of MUTZ-3 DCs showed a slightly more prominent expression of the co-stimulatory molecule CD86 and CLEC2, the ligand of PDPN on FRCs. The $DC\text{-}SIGN^-$ MUTZ-3 DCs with FRCs had higher $HLA\text{-}DR^+$ expression compared to $DC\text{-}SIGN^+$ populations, and these $HLA\text{-}DR^+DC\text{-}SIGN^-$ cells had a more pronounced CLEC2 abundance. Analysis of the hydrogel co-culture supernatants with FRCs revealed no effect of the cytokine differentiation cocktail on the secretion of the DC-associated proteins CXCL12, MCP-1 and IL-6 (Fig. 3C).
To determine whether the effects of FRCs on MUTZ-3 DC differentiation were specific to HuLN FRCs, the same experimental set up was performed in 3D using dermal fibroblasts or gut fibroblasts with MUTZ-3 progenitor cells. Subjecting the hydrogels to cytokine stimuli, we found MUTZ-3 DC differentiation to be consistently affected by all fibroblasts obtained from different anatomical locations. Most notably and in line with our current results, CD1a expression was absent on MUTZ-3 DCs with all fibroblasts compared to the MUTZ-3 DCs alone, and levels of DC-SIGN were unchanged between samples (Fig. S1C). Fibroblasts did not affect the expression levels of CD141 during cytokine-induced MUTZ-3 DC differentiation in any conditions. Additionally, there was no upregulation of CD1c on MUTZ-3 DCs when in the presence of all fibroblasts (Fig. S1C). Uniquely, without any cytokine stimuli, dermal fibroblasts did imprint an almost two-fold higher CD141 expression on MUTZ-3 progenitor cells compared to all other fibroblasts (Fig. S1D). All tissue stromal cells expressed PDPN to a certain extent, confirming a consistent fibroblast status (Fig. S1E).
Prompted by the observation that FRCs affected MUTZ-3 DC phenotypic differentiation, we further explored the possibility of a similar FRC-effect on primary moDCs. In place of MUTZ-3 progenitor cells, primary monocytes were used in the same experimental set up as detailed above. When examining the characteristics of DC phenotypes, we observed the absence of CD1a expression on the moDCs that had differentiated upon cytokine stimuli from monocytes in the presence of FRCs (Fig. 3D). Almost all resulting moDCs expressed high levels of DC-SIGN and CD141, irrespective of FRCs inclusion, while CD1c expression in moDCs was reduced by around 50% upon cytokine differentiation with FRCs compared to without FRCs (Fig. S1F).
These findings, consistent with our observations with MUTZ-3 DCs, demonstrate that primary FRCs can influence the differentiation of DCs into a $CD1a^-$ phenotype under cytokine stimulation within the 3D FRC-DC organotypic model, emphasising the role of primary FRCs in guiding DC differentiation.

HuLNs harbour similar DC and FRC subsets

We next investigated whether the cell characteristics of the 3D FRC-DC organotypic model were representative of cell profiles existing in HuLNs. Firstly, we analysed DC subsets in huLN cell suspensions using spectral flow cytometry. We observed a range of CD11c expression intensities among $CD11c^+$ cells and further examination of these $CD11c^+$ cells revealed a distinct cluster of DC-$SIGN^+$ cells, while $CD1a^+$ cells were completely absent (Fig. 4A and Fig. S2). Apparent clusters of the two major conventional DC subsets, cDC1 ($CD141^+$) and cDC2 ($CD1c^+$), were identified. However, these subsets did not exhibit a significant overlap with the DC-$SIGN^+$ cells, where only a small minor population showed potential CD141 positivity. The cluster of DC-$SIGN^+$ cells exhibited diverse expression patterns of HLA-DR with limited expression of CD86 and lacked expression of the maturation marker CD83, indicating immature cell types.

$GREM1^+$ FRCs are responsible *in vivo* for DC maintenance within HuLNs[17]. Therefore, we next analysed the cultured FRC donors used for the 3D FRC-DC organotypic model for expression of GREM1. Indeed, *GREM1* mRNA could be detected across all cultured FRC donors at variable expression levels, while this was absent in MUTZ-3 DCs (Fig. 4B). In addition, a large portion of FRCs expressed PDPN and CD90 with a subset expressing CD146 (Fig. 4C), which are all markers of FRCs residing in the paracortex area[28, 34].

In summary, these results highlight that DCs and FRCs used for co-culture in the 3D FRC-DC organotypic model correlate to true cell profiles that are found in the native HuLN.

$CD1a^-$ MUTZ-3 DCs function as antigen presenting cells

Since FRCs exhibit the ability to direct MUTZ-3 DC differentiation towards a $CD1a^-$ cell upon cytokine stimuli in the 3D FRC-DC organotypic model, we next investigated the functionality of these skewed $CD1a^-$ cells. Specifically, we assessed their capability to induce T cell proliferation in a MLR. Hereto, we generated the $CD1a^-$ MUTZ-3 DCs in the 3D FRC-DC organotypic model, digested the hydrogel to a single cell suspension and co-cultured this cell suspension in a 2D plate with $CD4^+$ T cells. As a control, normal $CD1a^+$ MUTZ-3 DCs were generated in 2D without FRCs and then co-cultured with T cells. In order to account for the effect of FRCs on T cells in the MLR, FRCs were added in two separate conditions; co-cultured with T cells alone or together with normal MUTZ-3 DCs ($CD1a^+$). After three and six days, the levels of T cell proliferation were assessed through flow cytometry, revealing T cell division across all biological conditions by day six (Fig. 5A). Our findings revealed that the $CD1a^-$ MUTZ-3 DCs retained the ability to induce T cell proliferation. However, this capability was not statistically significant but always lower for each donor compared to that of the normal MUTZ-3 DCs ($CD1a^+$). Across all experimental conditions, the impact of FRCs on the MLR was minimal. Specifically, co-culture of FRCs with T cells resulted in only 5% of T cell proliferation, indicating a limited effect on promoting T cell proliferation.

To further characterise the MLR experiment, secretion of immune response-related analytes was assessed in supernatants derived from the four conditions mentioned above. The relative expression levels for each analyte across all supernatant samples collected at day three and six were presented

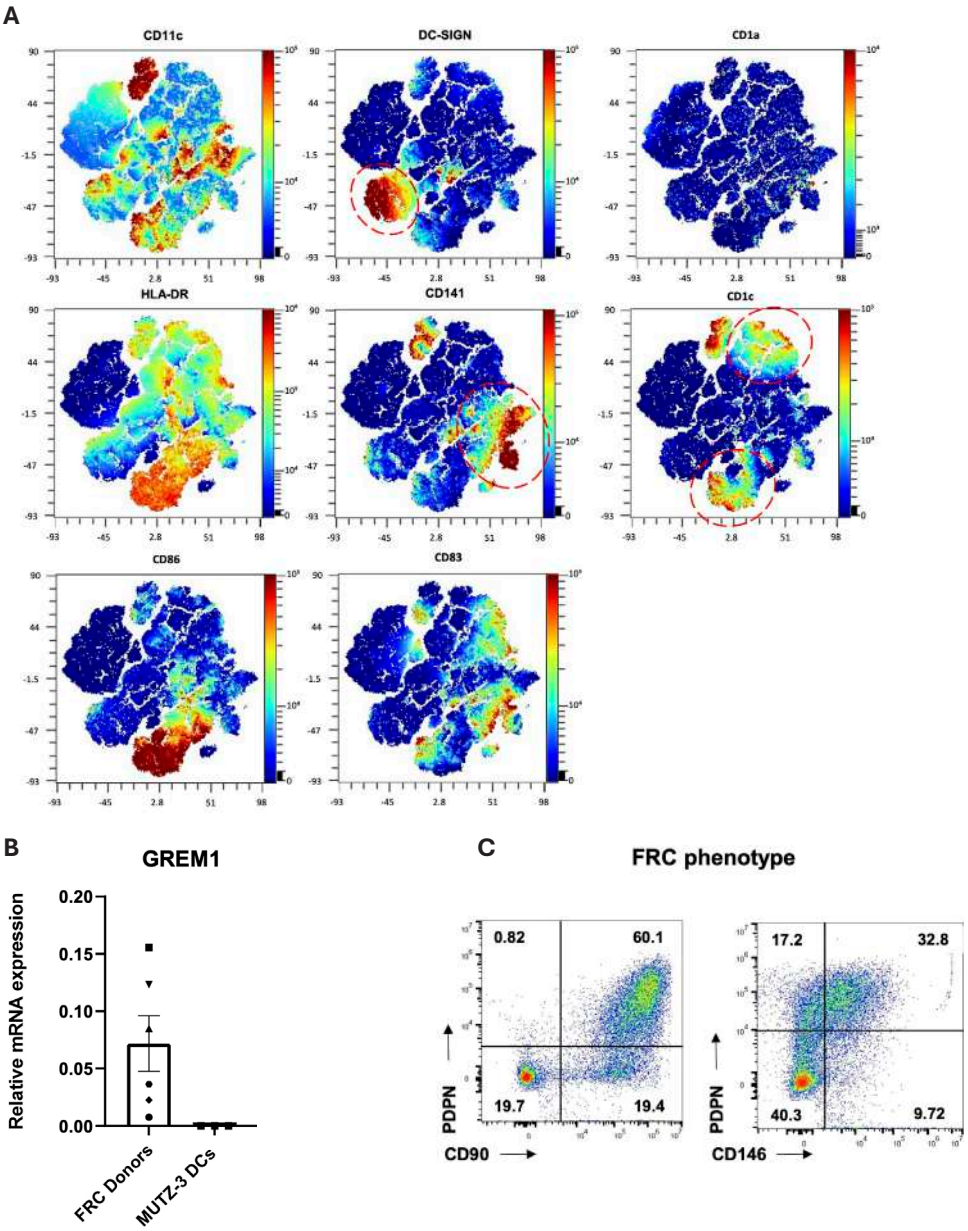

Fig. 4 - HuLNs harbour the DC and FRC subsets that have been generated with the 3D FRC-DC organotypic model. (A) High dimensional analysis show extensive distribution of markers on CD11c cells from HuLNs. The t-SNE plots are an overlay of 3 independent donors. Red dashed gates highlight the CD1c, CD141 and DC-SIGN subsets. **(B)** mRNA expression of GREM1, relative to housekeeping gene, confirmed on all FRC donors, represented by shapes, and not detected in the MUTZ-3 DC cell line. **(C)** Flow cytometry analysis of cultured FRC donors used for the 3D FRC-DC organotypic model, gated for PDPN, CD90 and CD146 expression. Results are shown as one representative dot plot; *n* = 3 independent experiments.

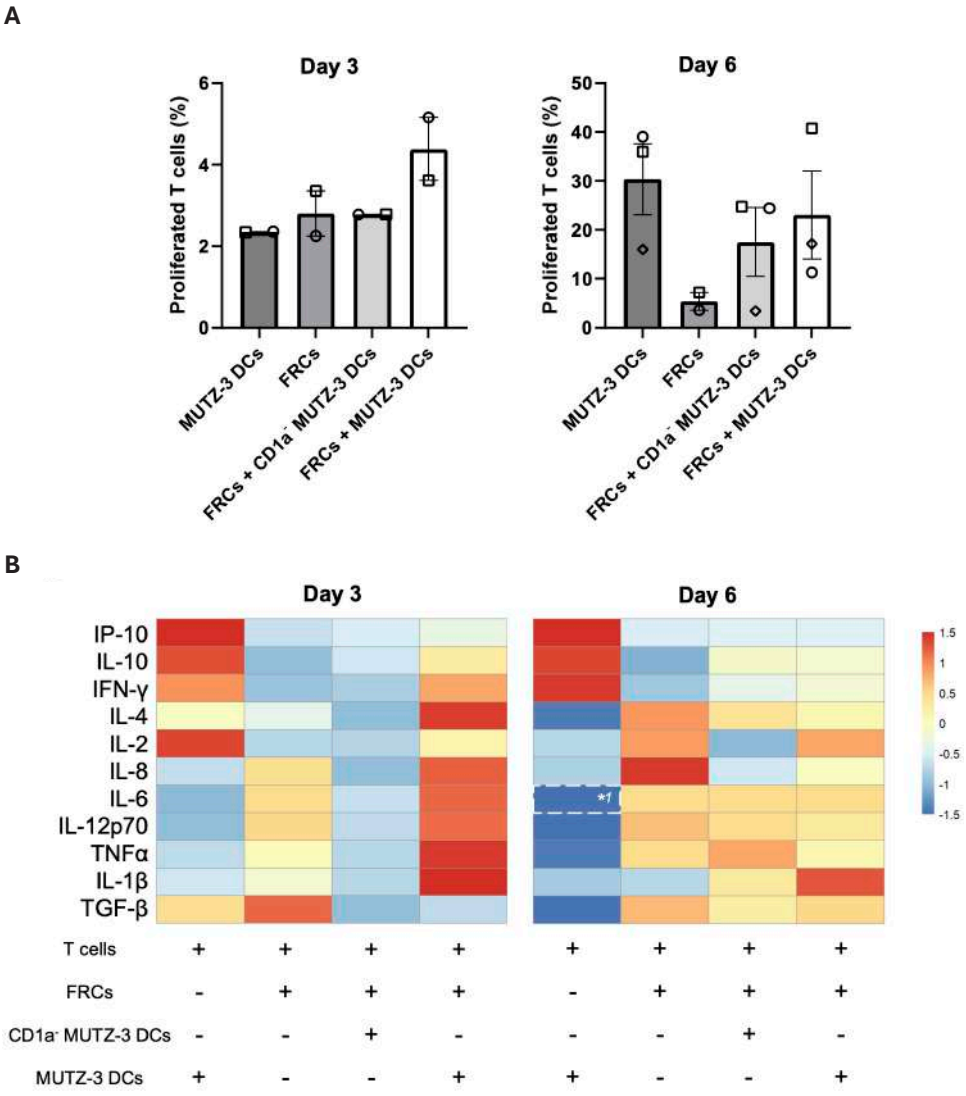

Fig. 5 - Assessment of phenotypically different MUTZ-3 DCs on their T cell stimulation potential. CD1a- MUTZ-3 DCs were first generated in the 3D FRC-DC organotypic model for seven days, isolated from the hydrogel to form a single cell suspension, and then co-cultured with CFSE-labelled CD4 T cells for a further six days in a 2D plate. MUTZ-3 DCs (CD1a+) were generated without FRCs in 2D, and FRCs from 3D were added into their respective conditions. **(A)** Proliferation of T cells was measured based on CFSE levels on CD3 T cells. Each shape represents an independent experiment and a different FRC donor if applicable. Results are shown as mean ± SEM; $n = 2$ independent experiments for day three, $n = 3$ independent experiments for day six, all performed in duplicate. **(B)** Protein concentrations of analytes detected in the MLR displayed in a heatmap scaled by individual cytokine / chemokine rows. Results are shown as mean of $n = 2$ independent experiments performed in duplicate. *1 White dashed box denotes an analytes significant difference in one biological condition compared to all of the other conditions. *$p < 0.05$

in a heatmap to visualise the expression patterns (Fig. 5B and Fig. S3A). In the control condition where no FRCs were present (MUTZ-3 DCs + T cells), the highest secretion of IFNγ, CXCL10/IP-10 and IL-10 was detected at both day three and six, indicating an optimal climate for T cell activation (Fig. 5B). In the same condition, IL-2 and IL-4 levels were elevated at day three, but diminished by day six, implying a rapid kinetic of DC-induced T cell activation. When T cells were co-cultured with FRCs only (FRCs + T cells), levels of IL-8, IL-6, TNFα, TGF-β and IL-12p70 were found at day three, suggesting their secretion by FRCs, which were also detected by day six, along with higher levels of IL-2 and IL-4. This group of cytokines were more synergistically acute at day three in the condition containing all three cell types (FRCs + MUTZ-3 DCs + T cells) compared to the other biological conditions, which was then reduced at day six to a more balanced homeostatic spectrum of analytes within this sample.
We did not find any cytokines or chemokines in the culture supernatant of the $CD1a^-$ MUTZ-3 DCs at day three. By day six, the FRC-affiliated analytes were recorded in this sample, along with minimal IL-4, IFNγ and IL-10 proteins that suggest a subdued T cell activation compared to the other conditions with MUTZ-3 DCs. Of note, IL-1β was detected in abundance consistently at day three and six for MUTZ-3 DCs + FRCs, compared to $CD1a^-$ MUTZ-3 DCs where IL-1β was only up-regulated to a lesser extent at day six, insinuating more of a pro-inflammatory capacity of the MUTZ-3 DCs.
In conclusion, these findings suggest that $CD1a^-$ MUTZ-3 DCs that are developed in the presence of FRCs in the 3D FRC-DC organotypic model retain their ability to activate T cells, albeit with differences in their cytokine/chemokine secretion profiles compared to normal $CD1a^+$ MUTZ-3 DCs.

Discussion

In HuLNs, FRCs are necessary to support the localisation and functional abilities of DCs and their respective subsets[16, 17]. Here, we report the development and characterisation of a novel 3D FRC-DC organotypic model of the HuLN paracortex, where we demonstrate the influence of primary FRCs on DC function and set the foundations for a HuLN *in vitro*.
Our model's functional ability was validated by investigating DC phenotype development and we showed that FRCs had the ability to skew the differentiation of DCs based primarily on the expression of the CD1a marker and their secreted factors in the MLR. Human fibroblasts have previously demonstrated diverse modulation of DC behaviour, either exhibiting suppressive properties when originating from lung/gingiva tissue[35, 36] or of more complementary nature for DC maturation when from skin tissue[37]. Here, the use of HuLN FRCs regulated final DC differentiation to a resulting phenotype similar to that of LN-resident DCs[38, 39, 40].
Migratory DCs arrive into the LN as a fully mature cell after differentiating in peripheral tissue, yet resident DCs in HuLNs can be differentiated *in situ* based on the cytokine environment. The specific factors responsible for the FRC regulation of DC differentiation were not fully explored in this study, yet the high levels of IL-6 detected in the 3D FRC-DC organotypic model have a potential determinant since it has been shown in mouse studies that IL-6 can inhibit DC maturation[41]. The Notch signalling pathway also represents a potential mechanism underlying this phenomenon, warranting further

investigation. Notch ligands have been shown in mice to control lymphocyte and myeloid cell development[42], e.g. Jagged-1 on bone marrow stroma restricts DC differentiation[43], and Notch ligand-expressing fibroblasts can form special immune niche in lymphoid organs[44]. In human datasets, an array of Notch ligands have been found on FRCs[17] but this has not been characterised in further detail. The lack of CD1a expression suggests differentiation of DC precursors in the presence of FRCs towards non-migratory DCs because $CD1a^+$ DCs are characterised as migratory peripheral DCs and non LN-resident[45, 46, 47]. We found no $CD1a^+$ DCs when we traced back the cell profile to the primary cell suspensions from the native HuLNs, indicating a potentially non-inflamed HuLN. However, we did identify $CD11c^+HLA\text{-}DR^+DC\text{-}SIGN^+$ cells, which exhibited a similar phenotype to the MUTZ-3 DCs generated in our 3D FRC-DC organotypic model. Nevertheless, these native cells appeared phenotypically distinct from the populations of cDC1 ($CD141^+$) and cDC2 ($CD1c^+$) cells present in primary HuLNs. Consistent expression of $CD141^+$ on MUTZ-3 DCs in our 3D FRC-DC organotypic model does correlates to the native tissue, as $CD141^+$ DCs have been found localised in the T cell-rich paracortex area[48].

We investigated whether this unique FRC-skewing effect on DCs was specific for LN FRCs in comparison to other tissue fibroblasts. It was revealed that dermal- and gut-derived fibroblasts also restricted CD1a upregulation on MUTZ-3 DCs during differentiation. However, it was seen specifically for dermal fibroblasts that they could further induce MUTZ-3 progenitor cells expression of CD141, a marker associated with skin resident DCs[37, 49]. These observations suggest that variations in the properties of tissue fibroblasts can exert both common and distinct effects on the development of DCs. These stromal elements should be kept in mind when designing such organotypic models that include immune cells. The functionality of these FRC-skewed $CD1a^-$ MUTZ-3 DCs was confirmed in a T cell MLR. These $CD1a^-$ MUTZ-3 DCs furthermore lacked the high affinity scavenger receptor CD163, associated with development towards macrophage lineage[50], indicating their differentiation towards resident DCs.

We found FRCs to be critical for culturing DCs long-term in this 3D environment, evident through the increased viability of MUTZ-3 DCs and proliferation of MUTZ-3 progenitors. Analytes FLT3L, CXCL12 and MCP-1 were detected in the FRC-DC hydrogel supernatant, which are homeostatic signals promoting DC attraction and survival[17, 51, 52, 53]. However, we believe DC survival requires the physical presence of FRCs in the hydrogel since we tested FRC-cultured conditioned medium on MUTZ-3 DCs alone in the hydrogel (data not shown), which did not improve their viability upon culture harvesting. Therefore, we conclude that it is beneficial to study DCs in 3D with a stromal cell component, such as an FRC.

We selected a type I collagen-fibrin hydrogel as the foundation for our 3D FRC-DC organotypic model. This choice was based on the abundance of type I collagen in the native HuLNs[54] and the specific practical properties that fibrin has for *in vitro* organ models[55]. The ECM of HuLNs includes a distributed plethora of proteoglycans, glycoproteins and collagens that undergo extensive remodelling during the initiation of an immune response[56] and can actively dictate immune cell functioning[57]. Recapitulating the intricate complexity of the native ECM protein network presents a technical challenge in enhancing this 3D FRC-DC organotypic model, where future improvements may involve manipulating decellularized tissue as a suitable ECM-substitute[55, 58]. Nonetheless, we have demonstrated here

with the ECM composition in our 3D FRC-DC organotypic model a platform where both FRCs and DCs exhibit characteristics of their cellular subsets that are present within the HuLN.

The limitations of our research include the comprehensive use of the MUTZ-3 cell line to act as a DC cell, while only correlating some of our major findings with moDCs (Fig. 3D). The MUTZ-3 cells are a robust DC-alternative for experimental studies that can reduce the donor variation exhibited with primary DCs. From extensive characterisation and comparison to multiple DC subtypes, they display clear transcriptional[29, 33] and functional similarities of moDCs to a certain extent[59], such as their differentiation, maturation[60, 61] and ability to induce T cell proliferation[62,63,64]. Furthermore, MUTZ-3 cells have already demonstrated their functional DC properties in organotypic models, such as reconstructed human skin and oral mucosa models[25, 26, 27, 65, 66]. These models feature mainly the Langerhans cell version of the MUTZ-3, where these cells have responded to the exposure of chemical allergens by indication of migration, maturation and in some cases differentiation towards macrophages in the model, demonstrating their fit for purpose in tissue-engineering studies. The use of isolated primary DCs/myeloid cells subsets and future inclusion of T cells within the 3D matrix could improve the model further when *i.e.,* niche-associated interactions between FRCs and different DC subsets are subject of study; as cDC1 and cDC2 could be studied for specifically following CD8 and CD4 responses, respectively. From the stromal cell perspective, the expression of *GREM1* mRNA on all our donor FRCs used in the 3D model further validates the physiological relevance for DC maintenance. Likewise, the surface expression of molecules CD90, CD146 and PDPN on the FRCs correspond to FRCs found specifically in the native T cell area, which are in contact with DCs[34, 67]. Although it should be noted that not all FRCs express these markers since different FRC subsets exist in various locations throughout the native HuLN [5]. Nevertheless, the cell types we used represent an appropriate comparison of the model to the human tissue and reinforces its biological potential as a prospective HuLN *in vitro*.

In conclusion, this study showcases the early construction of an *in vitro* HuLN, termed a 3D FRC-DC organotypic model, that reveals the influence of FRCs on the characterisation and study of DCs. This model forms a more physiologically relevant microenvironment to study immune cells within lymphoid organs, further validating its potential use in systemic immunological research and as a future application for microfluidic (multi)-organ-on-chip models.

Acknowledgements

The authors would like to thank and acknowledge the expert help of the Microscopy & Cytometry Core Facility at Amsterdam UMC (location Vrije Universiteit Amsterdam). We thank Kim Ober and Dr. Monique Verstegen from the Erasmus MC, Rotterdam for sample logistics.

Contributions

Conceptualization: AIM, JJK, CMdW, SG and REM; Methodology: AIM, SWS, JJK, CMdW, SG and REM; Investigation: AIM; Validation: AIM, SWS, AJA, JJK and CMdW; Software: AM and MdK; Data curation: AIM; Writing-original draft preparation: AIM; Writing-review and editing: AIM, JJK, CMdW, SG and REM; Supervision: JJK, CMdW, SG and REM; Funding acquisition: SG and REM; Ethical approval and donor information: LJWvdL and HPR. All authors have read and agreed to the published version of the manuscript.

Ethical statement

HuLNs were obtained from donors during liver transplant procedures performed at the Erasmus MC, Rotterdam, The Netherlands, in accordance to the Medical Ethical Committee (Medisch Ethische Toetsings Commissie; METC) of Erasmus MC (MEC-2014-060). All patients (liver transplant recipients) gave written informed consent to use their donor tissue.

References

[1] Roozendaal R, Mebius RE, Kraal G. The conduit system of the lymph node. Int Immunol. 2008;20:1483-7.

[2] Krishnamurty AT, Turley SJ. Lymph node stromal cells: Cartographers of the immune system. Nat Immunol. 2020;21:369-80.

[3] Bajenoff M, Egen JG, Koo LY, Laugier JP, Brau F, Glaichenhaus N, Germain RN. Stromal cell networks regulate lymphocyte entry, migration, and territoriality in lymph nodes. Immunity. 2006;25:989-1001.

[4] Roozendaal R, Mebius RE. Stromal cell-immune cell interactions. Annu Rev Immunol. 2011;29:23-43.

[5] Rodda LB, Lu E, Bennett ML, Sokol CL, Wang X, Luther SA, et al. Single-cell rna sequencing of lymph node stromal cells reveals niche-associated heterogeneity. Immunity. 2018;48:1014-28 e6.

[6] Grasso C, Pierie C, Mebius RE, van Baarsen LGM. Lymph node stromal cells: Subsets and functions in health and disease. Trends Immunol. 2021;42:920-36.

[7] Acton SE, Astarita JL, Malhotra D, Lukacs-Kornek V, Franz B, Hess PR, et al. Podoplanin-rich stromal networks induce dendritic cell motility via activation of the c-type lectin receptor clec-2. Immunity. 2012;37:276-89.

[8] Girard JP, Moussion C, Forster R. Hevs, lymphatics and homeostatic immune cell trafficking in lymph nodes. Nat Rev Immunol. 2012;12:762-73.

[9] Acton SE, Onder L, Novkovic M, Martinez VG, Ludewig B. Communication, construction, and fluid control: Lymphoid organ fibroblastic reticular cell and conduit networks. Trends Immunol. 2021;42:782-94.

[10] Collin M, Bigley V. Human dendritic cell subsets: An update. Immunology. 2018;154:3-20.

[11] Gerner MY, Kastenmuller W, Ifrim I, Kabat J, Germain RN. Histo-cytometry: A method for highly multiplex quantitative tissue imaging analysis applied to dendritic cell subset microanatomy in lymph nodes. Immunity. 2012;37:364-76.

[12] Gerner MY, Casey KA, Kastenmuller W, Germain RN. Dendritic cell and antigen dispersal landscapes regulate t cell immunity. J Exp Med. 2017;214:3105-22.

[13] Baptista AP, Gola A, Huang Y, Milanez-Almeida P, Torabi-Parizi P, Urban JF, Jr., et al. The chemoattractant receptor ebi2 drives intranodal naive cd4(+) t cell peripheralization to promote effective adaptive immunity. Immunity. 2019;50:1188-201 e6.

[14] van de Ven R, van den Hout MF, Lindenberg JJ, Sluijter BJ, van Leeuwen PA, Lougheed SM, et al. Characterization of four conventional dendritic cell subsets in human skin-draining lymph nodes in relation to t-cell activation. Blood. 2011;118:2502-10.

[15] Segura E, Soumelis V. Of human dc migrants and residents. Immunity. 2017;46:342-4.

[16] Novkovic M, Onder L, Cupovic J, Abe J, Bomze D, Cremasco V, et al. Topological small-world organization of the fibroblastic reticular cell network determines lymph node functionality. PLoS Biol. 2016;14:e1002515.

[17] Kapoor VN, Muller S, Keerthivasan S, Brown M, Chalouni C, Storm EE, et al. Gremlin 1(+) fibroblastic niche maintains dendritic cell homeostasis in lymphoid tissues. Nat Immunol. 2021;22:571-85.

[18] Ozulumba T, Montalbine AN, Ortiz-Cardenas JE, Pompano RR. New tools for immunologists: Models of lymph node function from cells to tissues. Front Immunol. 2023;14:1183286.

[19] Goyal G, Prabhala P, Mahajan G, Bausk B, Gilboa T, Xie L, et al. Ectopic lymphoid follicle formation and human seasonal influenza vaccination responses recapitulated in an organ-on-a-chip. Adv Sci (Weinh). 2022;9:e2103241.

[20] Wagar LE, Salahudeen A, Constantz CM, Wendel BS, Lyons MM, Mallajosyula V, et al. Modeling human adaptive immune responses with tonsil organoids. Nat Med. 2021;27:125-35.

[21] Belanger MC, Ball AG, Catterton MA, Kinman AWL, Anbaei P, Groff BD, et al. Acute lymph node slices are a functional model system to study immunity ex vivo. ACS Pharmacol Transl Sci. 2021;4:128-42.

[22] Knoblich K, Cruz Migoni S, Siew SM, Jinks E, Kaul B, Jeffery HC, et al. The human lymph node microenvironment

unilaterally regulates t-cell activation and differentiation. PLoS Biol. 2018;16:e2005046.
[23] Braham MVJ, van Binnendijk RS, Buisman AM, Mebius RE, de Wit J, van Els C. A synthetic human 3d in vitro lymphoid model enhancing b-cell survival and functional differentiation. iScience. 2023;26:105741.
[24] Kwee BJ, Akue A, Sung KE. On-chip human lymph node stromal network for evaluating dendritic cell and t-cell trafficking. bioRxiv. 20232023.03.21.533042.
[25] Kosten IJ, Spiekstra SW, de Gruijl TD, Gibbs S. Mutz-3 derived langerhans cells in human skin equivalents show differential migration and phenotypic plasticity after allergen or irritant exposure. Toxicol Appl Pharmacol. 2015;287:35-42.
[26] Koning JJ, Rodrigues Neves CT, Schimek K, Thon M, Spiekstra SW, Waaijman T, et al. A multi-organ-on-chip approach to investigate how oral exposure to metals can cause systemic toxicity leading to langerhans cell activation in skin. Front Toxicol. 2021;3:824825.
[27] Kosten IJ, Buskermolen JK, Spiekstra SW, de Gruijl TD, Gibbs S. Gingiva equivalents secrete negligible amounts of key chemokines involved in langerhans cell migration compared to skin equivalents. J Immunol Res. 2015;2015:627125.
[28] Fletcher AL, Malhotra D, Acton SE, Lukacs-Kornek V, Bellemare-Pelletier A, Curry M, et al. Reproducible isolation of lymph node stromal cells reveals site-dependent differences in fibroblastic reticular cells. Front Immunol. 2011;2:35.
[29] Masterson AJ, Sombroek CC, De Gruijl TD, Graus YM, van der Vliet HJ, Lougheed SM, et al. Mutz-3, a human cell line model for the cytokine-induced differentiation of dendritic cells from cd34+ precursors. Blood. 2002;100:701-3.
[30] Michielon E, Lopez Gonzalez M, Burm JLA, Waaijman T, Jordanova ES, de Gruijl TD, Gibbs S. Micro-environmental cross-talk in an organotypic human melanoma-in-skin model directs m2-like monocyte differentiation via il-10. Cancer Immunol Immunother. 2020;69:2319-31.
[31] Roet JEG, Mikula AM, Kok Md, Chadick CH, Vallejo JJG, Roest HP, et al. Unbiased method for spectral analysis of cells with great diversity of autofluorescence spectra. bioRxiv. 20232023.07.28.550943.
[32] Renier N, Wu Z, Simon DJ, Yang J, Ariel P, Tessier-Lavigne M. Idisco: A simple, rapid method to immunolabel large tissue samples for volume imaging. Cell. 2014;159:896-910.
[33] Larsson K, Lindstedt M, Borrebaeck CA. Functional and transcriptional profiling of mutz-3, a myeloid cell line acting as a model for dendritic cells. Immunology. 2006;117:156-66.
[34] Eom J, Park SM, Feisst V, Chen CJ, Mathy JE, McIntosh JD, et al. Distinctive subpopulations of stromal cells are present in human lymph nodes infiltrated with melanoma. Cancer Immunol Res. 2020;8:990-1003.
[35] Freynet O, Marchal-Somme J, Jean-Louis F, Mailleux A, Crestani B, Soler P, Michel L. Human lung fibroblasts may modulate dendritic cell phenotype and function: Results from a pilot in vitro study. Respir Res. 2016;17:36.
[36] Seguier S, Tartour E, Guerin C, Couty L, Lemitre M, Lallement L, et al. Inhibition of the differentiation of monocyte-derived dendritic cells by human gingival fibroblasts. PLoS One. 2013;8:e70937.
[37] Saalbach A, Klein C, Sleeman J, Sack U, Kauer F, Gebhardt C, et al. Dermal fibroblasts induce maturation of dendritic cells. J Immunol. 2007;178:4966-74.
[38] Engering A, van Vliet SJ, Hebeda K, Jackson DG, Prevo R, Singh SK, et al. Dynamic populations of dendritic cell-specific icam-3 grabbing nonintegrin-positive immature dendritic cells and liver/lymph node-specific icam-3 grabbing nonintegrin-positive endothelial cells in the outer zones of the paracortex of human lymph nodes. Am J Pathol. 2004;164:1587-95.
[39] Askmyr D, Abolhalaj M, Gomez Jimenez D, Greiff L, Lindstedt M, Lundberg K. Pattern recognition receptor expression and maturation profile of dendritic cell subtypes in human tonsils and lymph nodes. Hum Immunol. 2021;82:976-81.
[40] Min J, Yang D, Kim M, Haam K, Yoo A, Choi JH, et al. Inflammation induces two types of inflammatory dendritic cells in inflamed lymph nodes. Exp Mol Med. 2018;50:e458.

[41] Park SJ, Nakagawa T, Kitamura H, Atsumi T, Kamon H, Sawa S, et al. Il-6 regulates in vivo dendritic cell differentiation through stat3 activation. J Immunol. 2004;173:3844-54.

[42] Kirkling ME, Cytlak U, Lau CM, Lewis KL, Resteu A, Khodadadi-Jamayran A, et al. Notch signaling facilitates in vitro generation of cross-presenting classical dendritic cells. Cell Rep. 2018;23:3658-72 e6.

[43] Cheng P, Nefedova Y, Corzo CA, Gabrilovich DI. Regulation of dendritic-cell differentiation by bone marrow stroma via different notch ligands. Blood. 2007;109:507-15.

[44] Fasnacht N, Huang HY, Koch U, Favre S, Auderset F, Chai Q, et al. Specific fibroblastic niches in secondary lymphoid organs orchestrate distinct notch-regulated immune responses. J Exp Med. 2014;211:2265-79.

[45] van Pul KM, Vuylsteke R, van de Ven R, Te Velde EA, Rutgers EJT, van den Tol PM, et al. Selectively hampered activation of lymph node-resident dendritic cells precedes profound t cell suppression and metastatic spread in the breast cancer sentinel lymph node. J Immunother Cancer. 2019;7:133.

[46] van Pul KM, Fransen MF, van de Ven R, de Gruijl TD. Immunotherapy goes local: The central role of lymph nodes in driving tumor infiltration and efficacy. Front Immunol. 2021;12:643291.

[47] Angel CE, Chen CJ, Horlacher OC, Winkler S, John T, Browning J, et al. Distinctive localization of antigen-presenting cells in human lymph nodes. Blood. 2009;113:1257-67.

[48] Jongbloed SL, Kassianos AJ, McDonald KJ, Clark GJ, Ju X, Angel CE, et al. Human cd141+ (bdca-3)+ dendritic cells (dcs) represent a unique myeloid dc subset that cross-presents necrotic cell antigens. J Exp Med. 2010;207:1247-60.

[49] Saalbach A, Klein C, Schirmer C, Briest W, Anderegg U, Simon JC. Dermal fibroblasts promote the migration of dendritic cells. J Invest Dermatol. 2010;130:444-54.

[50] Hoves S, Krause SW, Schutz C, Halbritter D, Scholmerich J, Herfarth H, Fleck M. Monocyte-derived human macrophages mediate anergy in allogeneic t cells and induce regulatory t cells. J Immunol. 2006;177:2691-8.

[51] Ugur M, Labios RJ, Fenton C, Knopper K, Jobin K, Imdahl F, et al. Lymph node medulla regulates the spatiotemporal unfolding of resident dendritic cell networks. Immunity. 2023;56:1778-93 e10.

[52] Hernandez-Lopez C, Valencia J, Hidalgo L, Martinez VG, Zapata AG, Sacedon R, et al. Cxcl12/cxcr4 signaling promotes human thymic dendritic cell survival regulating the bcl-2/bax ratio. Immunol Lett. 2008;120:72-8.

[53] Tiberio L, Del Prete A, Schioppa T, Sozio F, Bosisio D, Sozzani S. Chemokine and chemotactic signals in dendritic cell migration. Cell Mol Immunol. 2018;15:346-52.

[54] Sixt M, Kanazawa N, Selg M, Samson T, Roos G, Reinhardt DP, et al. The conduit system transports soluble antigens from the afferent lymph to resident dendritic cells in the t cell area of the lymph node. Immunity. 2005;22:19-29.

[55] van Tienderen GS, van Beek MEA, Schurink IJ, Rosmark O, Roest HP, Tieleman J, et al. Modelling metastatic colonization of cholangiocarcinoma organoids in decellularized lung and lymph nodes. Front Oncol. 2022;12:1101901.

[56] Morgado FN, da Silva AVA, Porrozzi R. Infectious diseases and the lymphoid extracellular matrix remodeling: A focus on conduit system. Cells. 2020;9.

[57] Sutherland TE, Dyer DP, Allen JE. The extracellular matrix and the immune system: A mutually dependent relationship. Science. 2023;379:eabp8964.

[58] Choi YS, Jeong E, Lee JS, Kim SK, Jo SH, Kim YG, et al. Immunomodulatory scaffolds derived from lymph node extracellular matrices. ACS Appl Mater Interfaces. 2021;13:14037-49.

[59] Rasaiyaah J, Noursadeghi M, Kellam P, Chain B. Transcriptional and functional defects of dendritic cells derived from the mutz-3 leukaemia line. Immunology. 2009;127:429-41.

[60] Lundberg K, Albrekt AS, Nelissen I, Santegoets S, de Gruijl TD, Gibbs S, Lindstedt M. Transcriptional

profiling of human dendritic cell populations and models--unique profiles of in vitro dendritic cells and implications on functionality and applicability. PLoS One. 2013;8:e52875.

[61] Santegoets SJ, van den Eertwegh AJ, van de Loosdrecht AA, Scheper RJ, de Gruijl TD. Human dendritic cell line models for dc differentiation and clinical dc vaccination studies. J Leukoc Biol. 2008;84:1364-73.

[62] Santegoets SJ, Schreurs MW, Masterson AJ, Liu YP, Goletz S, Baumeister H, et al. In vitro priming of tumor-specific cytotoxic t lymphocytes using allogeneic dendritic cells derived from the human mutz-3 cell line. Cancer Immunol Immunother. 2006;55:1480-90.

[63] Santegoets SJ, Masterson AJ, van der Sluis PC, Lougheed SM, Fluitsma DM, van den Eertwegh AJ, et al. A cd34(+) human cell line model of myeloid dendritic cell differentiation: Evidence for a cd14(+) cd11b(+) langerhans cell precursor. J Leukoc Biol. 2006;80:1337-44.

[64] Santegoets SJ, Bontkes HJ, Stam AG, Bhoelan F, Ruizendaal JJ, van den Eertwegh AJ, et al. Inducing antitumor t cell immunity: Comparative functional analysis of interstitial versus langerhans dendritic cells in a human cell line model. J Immunol. 2008;180:4540-9.

[65] Ouwehand K, Spiekstra SW, Waaijman T, Breetveld M, Scheper RJ, de Gruijl TD, Gibbs S. Ccl5 and ccl20 mediate immigration of langerhans cells into the epidermis of full thickness human skin equivalents. Eur J Cell Biol. 2012;91:765-73.

[66] Ouwehand K, Oosterhoff D, Breetveld M, Scheper RJ, de Gruijl TD, Gibbs S. Irritant-induced migration of langerhans cells coincides with an il-10-dependent switch to a macrophage-like phenotype. J Invest Dermatol. 2011;131:418-25.

[67] Park SM, Angel CE, McIntosh JD, Brooks AE, Middleditch M, Chen CJ, et al. Sphingosine-1-phosphate lyase is expressed by cd68+ cells on the parenchymal side of marginal reticular cells in human lymph nodes. Eur J Immunol. 2014;44:2425-36.

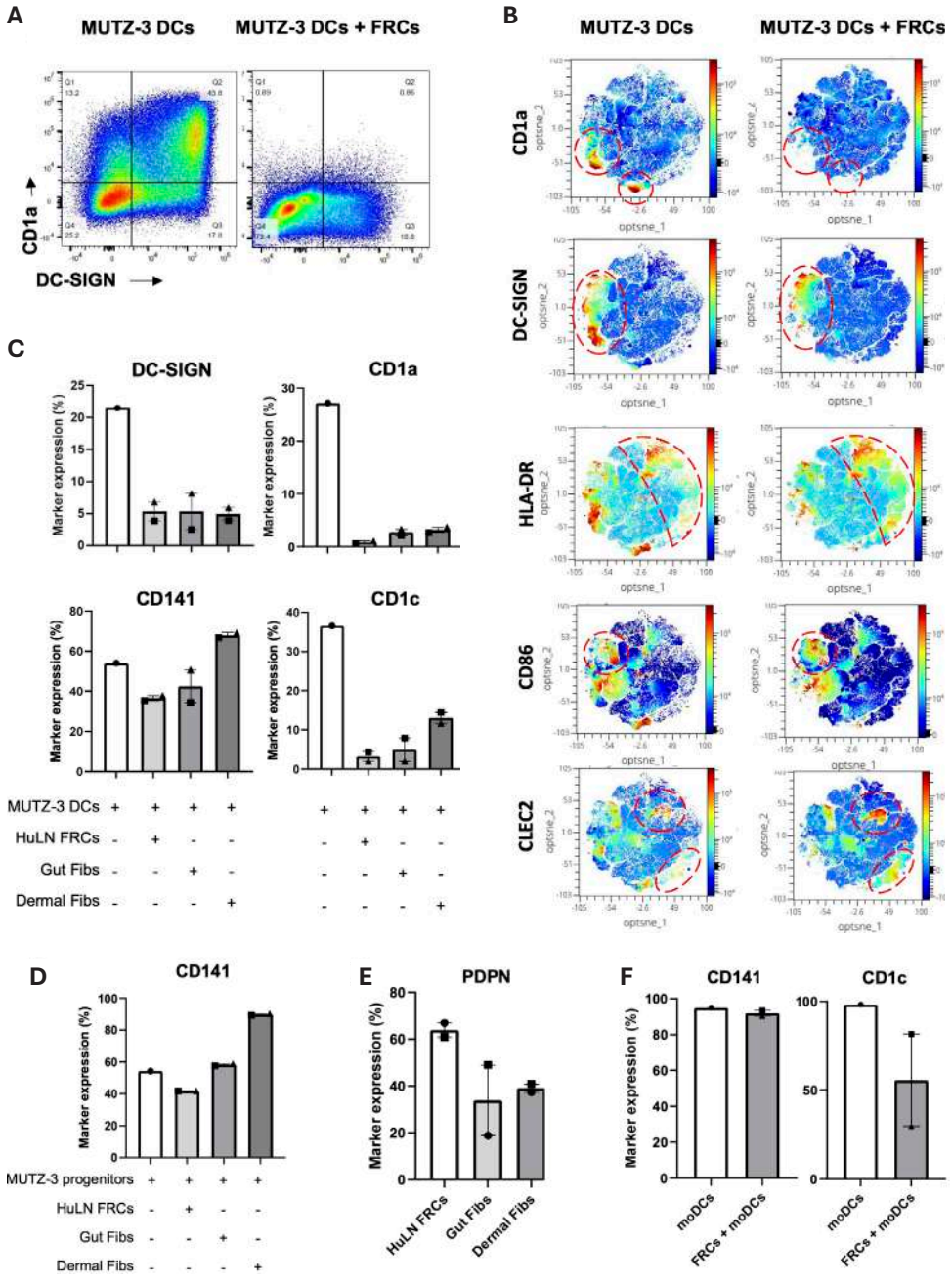

Fig. S1 - Characterization of FRC-DC interactions in 3D. (A) Representative flow cytometry dot plots of DC-SIGN and CD1a expression on MUTZ-3 DCs -/+ FRCs during their cytokine differentiation. **(B)** High dimensional analysis show extensive heterogeneous distribution of CD45+ MUTZ-3 DCs markers differentiated with or without FRCs, highlighted using red dashed boxes. The t-SNE graphs are representative plots from MUTZ-3 DCs -/+ one FRC donor. **(C)** Phenotype of MUTZ-3 DCs differentiated in 3D hydrogel under cytokine stimuli with different tissue fibroblasts.

Results for DC-SIGN, CD1a, CD141 and CD1c are shown as mean ± SEM; *n* = 2 independent experiments performed in duplicate. Each shape represents an independent experiment and a different FRC donor relative to one batch of MUTZ-3 DCs. Fibs; Fibroblasts **(D)** Expression of CD141 on MUTZ-3 progenitors under no cytokine stimuli with different tissue fibroblasts in 3D hydrogel. Results are shown as mean ± SEM; *n* = 2 independent experiments performed in duplicate. Each shape represents an independent experiment and a different FRC donor relative to one batch of MUTZ-3 progenitors. **(E)** Expression of PDPN on the different tissue fibroblasts gated as CD45-. Results are shown as mean ± SEM; *n* = 2 independent experiments performed in duplicate. Each shape represents an independent experiment and a different fibroblast donor. **(F)** Expression of CD141 and CD1c on differentiated moDCs -/+ FRCs after a one week cytokine stimuli. Results are shown as mean ± SEM; *n* = 2 independent experiments performed in duplicate. Each shape represents an independent experiment and a different FRC donor relative to one batch of moDCs.

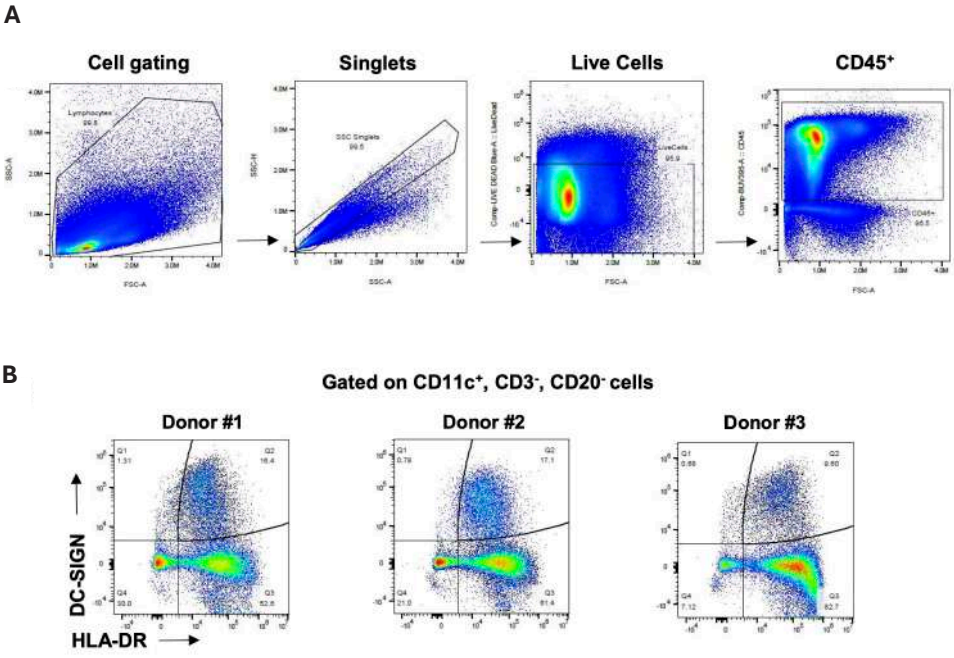

Fig. S2 - Gating strategy for HuLN DC subsets. (A) Representative gating strategy of flow cytometry dot plots to identify CD11c cells from HuLN cell suspensions. **(B)** Individual dot plots of three HuLN donors gated on CD45+CD11c+, excluding CD3+ and CD20+ cells, revealed HLA-DR+ DC-SIGN+ cells.

A

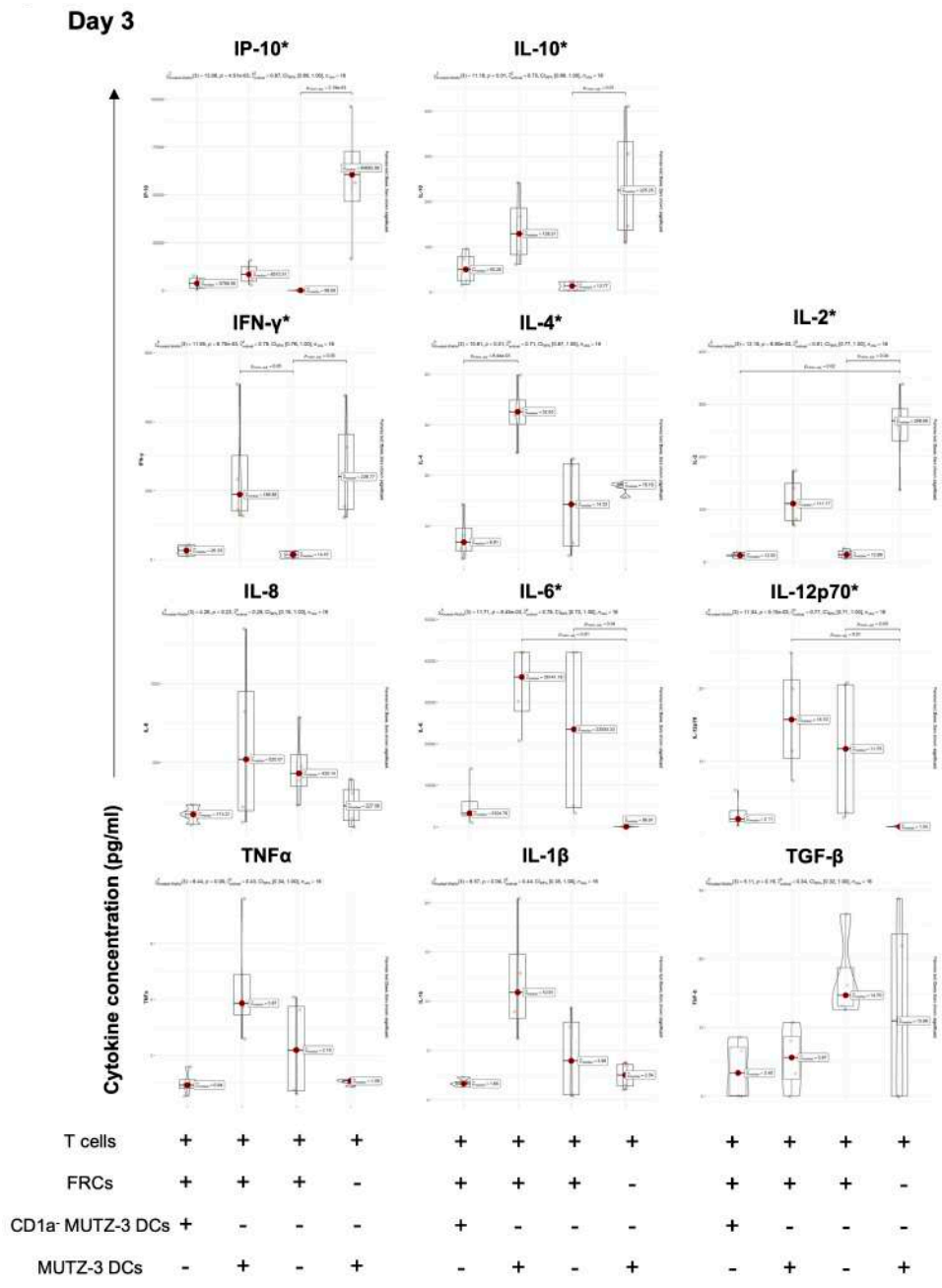
Day 3
IP-10*
IL-10*
IFN-γ*
IL-4*
IL-2*
IL-8
IL-6*
IL-12p70*
TNFα
IL-1β
TGF-β
Cytokine concentration (pg/ml)
T cells + + + + + + + + + + + +
FRCs + + + - + + + - + + + -
CD1a- MUTZ-3 DCs + - - - + - - - + - - -
MUTZ-3 DCs - + - + - + - + - + - +

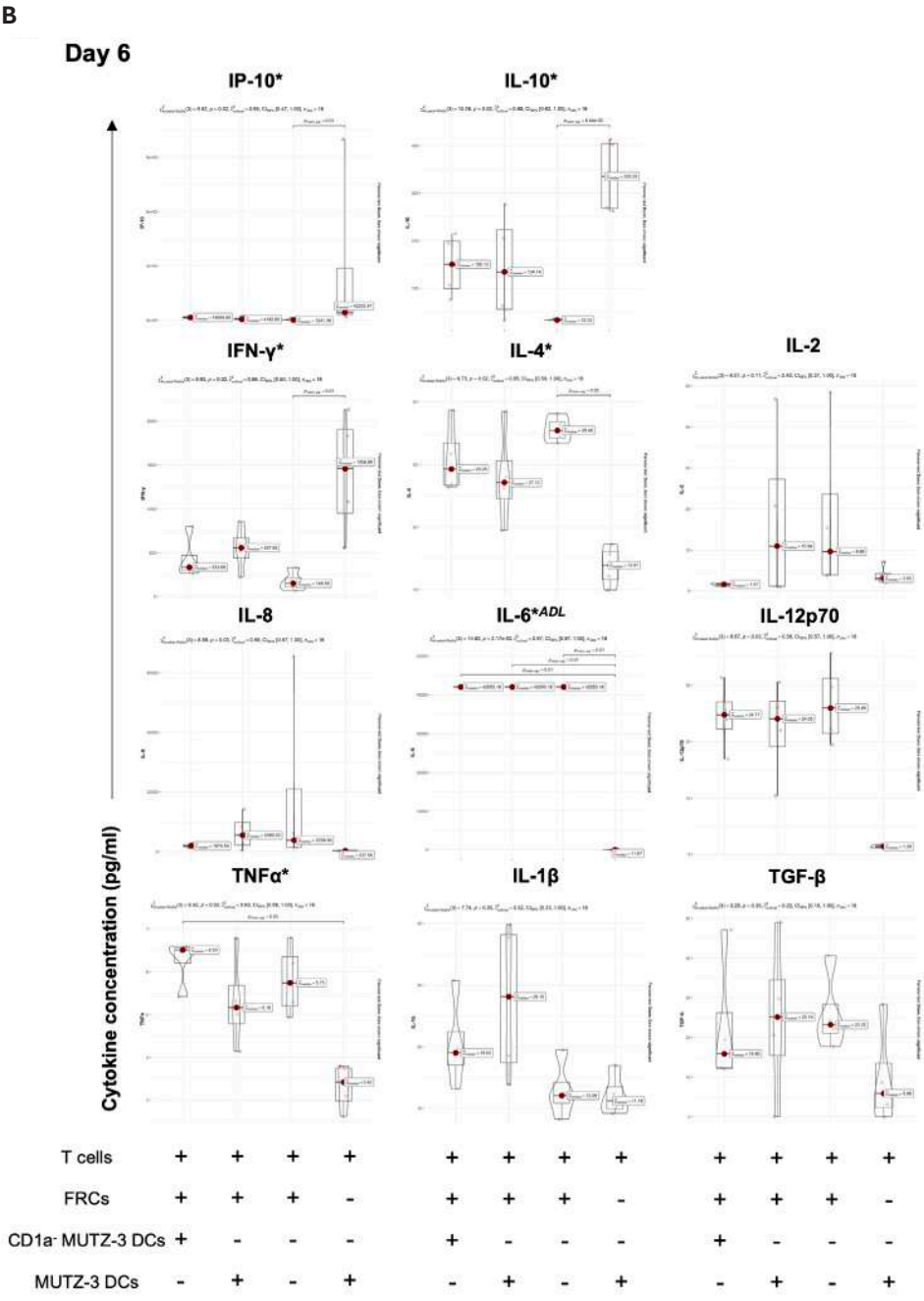

Fig. S3 - Overview of analyte concentrations per condition from T cell MLR. Individual cytokine / chemokine concentration values displayed in a ggstatsplot for all data; *n* = 2 independent experiments performed in duplicate. **(A)** Day three. **(B)** Day six. Analyte name with a * depicts a significant difference occurring between one or more biological conditions within said analyte. *ADL* = at detection limit for full assay saturation of analytes protein concentration. *$p < 0.05$, **$p < 0.01$

5

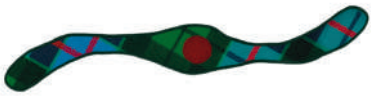

Functional Organotypic Human Lymph Node Model With Native Immune Cells Benefits From Fibroblastic Reticular Cell Enrichment

Andrew I. Morrison[1,2], Jesse E. Kuipers[1], Henk P. Roest[3], Luc J.W. van der Laan[3], Charlotte M. de Winde[1,2,4], Jasper J. Koning[1,2], Susan Gibbs[1,2,5], Reina E. Mebius[1,2]

[1] Amsterdam UMC location Vrije Universiteit Amsterdam, Molecular Cell Biology & Immunology, De Boelelaan 1117, Amsterdam, The Netherlands.

[2] Amsterdam institute for Infection and Immunity, Amsterdam, The Netherlands.

[3] Erasmus MC Transplant Institute, University Medical Center Rotterdam, Department of Surgery, Dr. Molewaterplein 40, 3015GD, Rotterdam, The Netherlands.

[4] Cancer Center Amsterdam, Amsterdam, The Netherlands.

[5] Department Oral Cell Biology, Academic Centre for Dentistry Amsterdam (ACTA), University of Amsterdam and Vrije Universiteit, Amsterdam, The Netherlands.

Scientific Reports 2025. Apr;15(1):12233 DOI: 10.1038/s41598-025-95031-9

Abstract

Lymphoid organ function depends on fibroblastic reticular cells (FRCs), the non-hematopoietic mesenchymal stromal cells that crucially support immune activity in human lymph nodes (LNs). The in vitro study of human immunology requires physiological LN models, yet the inclusion of FRCs in current models is lacking. Here, we created an organotypic LN hydrogel model, containing native immune cells from LN tissue and *ex vivo* cultured autologous FRCs. During a one-week culture period, enrichment of FRCs into the LN model benefited the viability of all immune cell populations, particularly B cells, and promoted the presence of certain subsets including CD4+ naïve T cells and unswitched (US) memory B cells. FRCs enhanced the production of immune-related cytokines and chemokines, such as B cell activating factor from the TNF family (BAFF), CXC motif chemokine ligand 12 (CXCL12), CC motif chemokine ligand 19 (CCL19) and interleukin-6 (IL-6). Functionality of the LN model was assessed through T cell activation by CD3 stimulation or initiation of an allogenic reaction with different maturation statuses of monocyte-derived dendritic cells (moDCs). Interestingly, T cell expansion was restricted in FRC-enriched LN models, reflecting an intrinsic characteristic of LN FRCs. As such, this organotypic LN model highlights the influence of FRCs on immune cells and allows an opportunity to further study antigen-induced immune responses, e.g. vaccine or immunotherapy testing.

Introduction

Lymph nodes (LNs) are a critical component of human immunology. Situated throughout the body, they act mechanistically to drain and filter interstitial fluid from all tissue and organs, while screening harmful pathogens, non-self-antigens, and allowing the removal of toxic metabolites. LNs facilitate the interaction between innate and adaptive immune cells, where incoming and resident immune cells are supported by the non-hematopoietic LN stromal cells (LNSCs)[1]. Not only do LNSCs provide structural support to the LN interior, they also regulate the crosstalk between the arrival of naïve immune cells from the blood circulation and migratory immune cells from the lymphatic vasculature[2]. In search of their cognate antigen, the guidance of immune cell migration and survival is enabled through LNSC-derived chemokines and cytokines, respectively, and LNSCs provide an anchorage point for immune cells via specific cell-cell adhesion molecular interactions[3,4].

Typically, LNSCs make up less than 5% of all cells within human LNs[5] and are categorised into different subtypes. The endothelial cells are $CD31^+$ and classified based on their podoplanin (PDPN) expression as lymphatic endothelial cells (LECs, $PDPN^+$) or blood endothelial cells (BECs, $PDPN^-$)[6]. The $CD31^-$ LNSCs are mesenchymal stromal cells, or fibroblastic reticular cells (FRCs), initially defined as $PDPN^+$ but new insights in humans have revealed a heterogenous profile of mesenchymal stromal cells with overlapping phenotypes between $PDPN^-$ and $PDPN^+$ FRCs[5,7,8]. FRCs create a three-dimensional (3D) reticular network[9] and are composed of distinctive subsets with unique functions depending on their location within LNs[10,11]. FRCs have a distinguished role in regulating immune activity in the LN[12], such as exhibiting control of T cell proliferation via multiple mechanisms[7]. In disease conditions, FRC function can become dysregulated, as observed in autoimmune disorders[13] or within the tumour microenvironment[14]. This highlights the importance of FRCs in dictating immune responses.

Given the central position that LNs play in health and disease, the appeal of generating *in vitro* models of human LNs has now been recognised. Not only is there a global need for better human disease models due to the limitations of animal models like species differences and poor translational capabilities[15,16], but there is also a demand to further understand the human immune system[17] and LN pathology[18]. One of first reported human LN models made use of an *in vitro* bioreactor with peripheral blood mononuclear cells (PBMCs) to study cellular immunity[19]. Since then, this approach has evolved into a variety of static and dynamic human LN models, each featuring distinct elements and focusing on several aspects of immune functionality. This includes the use of PBMC-derived immune cells cultured in 3D models demonstrating naïve B cell class switching[20], B cell follicle formation, and antibody secretion under flow[21,22]. Encouraging progress has also been made with the use of lymphoid tissue-derived cell suspensions in transwells to robustly recapitulate vaccine responses[23,24] and study immuno-oncology therapies[25]. However, focus on the cell-mediated branch of adaptive immunity, the use of native LN-derived cells in 3D, and the influence of LNSCs in LN models have yet to be addressed. Such insights are crucial given the multitude of central LNSC functions, ranging from organogenesis[26], guiding homeostatic and allostatic immune cell activity[12,27,28], and even aiding with the formation of tertiary lymphoid organ structures[29].

Hereto, in this study, the physiological relevance of a 3D LN model, pre-established by our group and originally composed of FRCs and DCs[30], was improved to recapitulate a more LN-like environment

through the inclusion of immune cells and FRCs. This advanced LN model made use of a 3D collagen-based hydrogel and LN-derived cell suspensions, with an enrichment of donor matched FRCs from *ex vivo* cultures[5]. In order to simulate the native immunocompetent properties required for an *in vitro* human LN model, characterisation of immune cell populations and the cytokine/chemokine landscape was performed to address the influence of additional FRCs in the LN model. Then, to demonstrate cell-mediated LN functionality, we investigated the capacity to induce T cell activation in FRC-enriched and non-enriched LN models, either through direct T cell receptor (TCR) triggering or via the addition of allogeneic dendritic cells (DCs).

Methods

Human tissue collection

Human LNs were obtained from donors and patients during liver transplant procedures performed at the Erasmus MC, Rotterdam, The Netherlands. The use of biopsies for research purposes is in accordance with the ethical standard of the Helsinki Declaration of 1975. The use of the tissue for research purposes was approved by the Medical Ethical Committee (Medisch Ethische Toetsings Commissie; METC) of Erasmus MC (MEC-2014-060). All confirmed methods of research were accepted and performed in accordance with the relevant guidelines and regulations. All patients (liver transplant recipients) gave written informed consent to use their donor tissue. Donor livers and patient explant livers had their LNs resected along the hepatic artery and portal vein in the porta hepatis. LNs were transported in Belzer UW Cold Storage Solution (Bridge to Life Ltd., London, England, UK) and processed within 72 hours of surgery. LN origin characteristics are shown in Table S1.

Enzymatic digestion of human lymph nodes

Isolation of immune and stromal cells from human LNs was achieved through enzymatic tissue digestion, as previously described[5,31]. Briefly, LNs were digested in 4 × 10-minute cycles in an enzyme mixture containing RPMI-1640 with 2.4 mg/ml Dispase II, 0.6 mg/ml Collagenase P and 0.3 mg/ml DNase I (all from Sigma-Aldrich, St. Louis, MO, USA). Ice cold phosphate-buffered saline (PBS), supplemented with 2% foetal calf serum (FCS) (HyClone; GE Healthcare, Chicago, IL, USA) and 5 mM ethylenediaminetetraacetic acid (EDTA), was used to stop the digestion cycle and to wash the isolated cells by centrifugation at 300 G for 4 minutes at 4°C. Cell pellet was re-suspended in 1 ml of DMEM (Gibco, Grand Island, NY, USA) with 10% FCS, strained through a 100 µM filter, and counted. The LN cell suspensions were either cryopreserved or cultured as described below.

Culture of primary fibroblastic reticular cells

FRCs were cultured as previously described[5]. Briefly, LN cell suspensions were seeded at a density of 1.25×10^6 cell suspension per cm^2 on culture flasks, pre-coated with 2 $\mu g/cm^2$ collagen from calf skin (Sigma-Aldrich). Culture media comprised of DMEM (Gibco) with 10% FCS (HyClone; GE

Healthcare), 2% Penicillin/Streptomycin/Glutamine (PSG) and 1% Insulin/Transferrin/Selenium (ITS) (Gibco). Upon confluence, cells were passaged and harvested with 0.5% Trypsin containing 5 mM EDTA. FRCs were used up to passage six for all individual experiments.

Generation of monocyte-derived dendritic cells

Human $CD14^+$ monocytes were isolated from PBMCs using $CD14^+$ magnetic activated cell sorting beads (#130-050-201, Miltenyi Biotec, Bergisch Gladbach, Germany) as previously described[30]. For use in the T cell functional experiments, monocyte-derived dendritic cells (moDCs) were generated to either a conventional or mature phenotype[32]. Cell culture medium was composed of RPMI-1640 with HEPES and L-glutamine (Gibco), supplemented with 10% FCS, 100 IU/ml sodium-penicillin and 100 µg/ml streptomycin (all Gibco). For conventional moDCs, moDCs were harvested after three days in culture media supplemented with 100 ng/ml rhGM-CSF (Biosource, International Inc) and 10 ng/ml IL-4 (BioVision). For maturation of moDCs, 100 ng/ml IL-6, 50 ng/ml TNF-α, 25 ng/ml IL-1β, 1 µg/ml PGE2 was added to the above culture conditions at day two and harvested at day three.

Construction of organotypic 3D LN model

A schematic illustration for the generation of the organotypic 3D LN model can be found in Fig. 1A. The LN model was constructed in 24-well transwells (0.4 µm pore size; Corning, NY, USA) by mixing rat-tail collagen type I (3 mg/ml end concentration) in Hank's Balanced Salt Solution (HBSS without Ca and Mg, Gibco) with fibrinogen from human plasma (Enzyme research laboratories, cat no: FIB 1, South Bend, IN, USA) (1 mg/ml end concentration). Cell suspensions were adjusted to a total final concentration of 10×10^6 cells per ml of hydrogel, with final hydrogel volumes ranging between 200 µl and 250 µl. In FRC-enriched models, FRCs accounted for 1% of the final cell concentration. Thrombin (0.5 U/ml; Merck KGaA, Darmstadt, Germany) was added to each hydrogel to allow for fibrin formation and hydrogel polymerisation at 37°C and 5% CO_2 for 1.5 hours. Complete LN model medium, composed of RPMI-1640 with HEPES and L-glutamine, 10% FCS, 2% PSG, 1% ITS, 1X non-essential amino acids (NEAA) (Gibco), 1X sodium pyruvate (Gibco) and 1X normocin (Invivogen, Toulouse, France), was added both above and below the hydrogel. A 50% medium refreshment took place every three/four days, while collected culture supernatant was stored at -20°C for future analysis. At the end of the culture period, hydrogels were either fixed for 3D imaging or enzymatically digested to a single cell suspension for analysis by flow cytometry using 0.2 mg/ml Collagenase P and 0.1 mg/ml DNase I for 1 hour at 37°C, after which the reaction was stopped with PBS containing 2% FCS and 5 mM EDTA.

Flow Cytometry

Cell suspensions were stained in a 96-well U bottom plate at 4°C for flow cytometry analysis. Cells were firstly washed with FACS buffer containing PBS, 0.1% bovine serum albumin (BSA) and 0.05% NaN_3, and stained with a fixable viability dye (eFluor™ 780, #65-0865-14, Invitrogen) for 10 minutes at 4°C. Fc-receptor blocking was performed using 10% normal human serum, and cells were subsequently incubated with directly-labeled antibodies against cell surface markers, diluted in blocking buffer.

After staining, cells were washed two times with FACS buffer and fixed with 2% paraformaldehyde (PFA) (VWR, Radnor, PA, USA) for 10 minutes at room temperature (RT). Cells were then washed with 0.5% saponin buffer, and intracellular antibody staining was performed. An overview of all antibodies used can be found in Table 1. Samples and single stains on beads were acquired on an Aurora 5-laser Flow Cytometer (Cytek; Fremont, CA, USA). Autofluorescence (AF) correction of cells was performed as previously described[33]. Data analysis was conducted using OMIQ (Boston, MA, USA).

Table 1 **Overview of antibodies.** FACS: Flow cytometry

Antigen	Label	Clone	Catalog	Assay
CD3		T3b	N/A	T cell functionality
CD3	PE-Cy5	UCHT1	Biolegend; 300410	FACS
CD3	PE-Dazzle594	SK7	Biolegend; 344844	FACS
CD4	BUV563	SK3	BD biosciences; 612912	FACS
CD8	Alexa Fluor 532	RPA-T8	Invitrogen; 58-0088-42	FACS
CD11c	cFluor BYG710	Bu15	Cytek biosciences; RC-00181	FACS
CD14	cFluor V450	M5E2	Cytek biosciences; R7-20003	FACS
CD19	BUV496	HIB19	BD biosciences; 741141	FACS
CD20	Pacific Blue	2H7	Biolegend; 302320	FACS
CD21	BUV395	B-ly4	BD biosciences; 740288	FACS
CD24	PE-CF594	ML5	BD biosciences; 562405	FACS
CD25	PE-Cy7	M-A251	Biolegend; 356108	FACS
CD27	PE	M-T271	Biolegend; 356406	FACS
CD38	BV605	HB-7	Biolegend; 356642	FACS
CD45	cFluor V547	HI30	Cytek biosciences; R7-20011	FACS
CD45	BV570	HI30	Biolegend; 304034	FACS
CD45RO	BUV805	UCHL1	BD biosciences; 748367	FACS
CD62L	Alexa Fluor 488	DREG-56	Biolegend; 304816	FACS
CD69	BUV737	FN50	ThermoFisher; 367-0699-42	FACS
HLA-DR	BUV395	L243	BD biosciences; 564040	FACS
IgD	AF700	IA6-2	Biolegend; 348230	FACS
Ki-67	BV650	B56	BD biosciences; 563757	FACS
CD3	Alexa Fluor 488	UCHT1	Biolegend; 300454	3D imaging
CD45		2B11 + PD7/26	Dako; GA751	3D imaging

Vimentin	Alexa Fluor 488 / 647	O91D3	Biolegend; 677807	3D imaging
Goat anti-Mouse IgG1	Alexa Fluor 647	Polyclonal	ThermoFisher; # A-21240	3D imaging

Staining and 3D imaging of LN model

Hydrogels pieces were fixed by directly adding 4% PFA (Electron Microscopy Sciences, Hatfield, PA, USA) and incubated for 30 mins at RT on a rocker. Hydrogels were then preserved in PBS with 0.05% NaN_3 until antibody staining. Prior to immunostaining, hydrogels were washed with 0.2% Triton in PBS. Next, hydrogels were incubated with an unconjugated antibody, diluted in 0.2% Triton in PBS, for overnight static staining at 4°C. The following day, hydrogels were washed twice with 0.2% Triton in PBS and then incubated with a secondary antibody at RT on a rocker for 2 hours. Next, hydrogels were washed twice with 0.2% Triton in PBS and directly-labeled antibodies were added for an overnight incubation at 4°C. An overview of all antibodies used can be found in Table 1. The following day after hydrogel washing, DAPI (Invitrogen) was added for 1 hour at RT, followed by two washing steps and then stored at 4°C until analysis. LN models were imaged by confocal microscopy using a Nikon AXR (Nikon, Tokyo, Japan). Images were analysed using Imaris software version 10.1.0 (Oxford Instruments, Oxfordshire, UK).

Cytokine/Chemokine detection in LN model supernatant

Supernatants from 3D LN models were harvested at either day three and six for T cell functionality experiments, or after one-week for all other experiments. Media was collected from above and below the hydrogels, pooled, and analysed for the presence of cytokines and chemokines using cytokine bead arrays (CBAs) (Human Essential Immune Response and Custom LEGENDplex panel; BioLegend, San Diego, CA, USA), according to the manufacturer's instructions. Acquisition was performed on an AttuneNxT (Thermofisher, Waltham, MA, USA) and analysis was conducted using the LEGENDplex Data Analysis Software Suite (BioLegend).

Functional T cell activation

The proliferation and activation of T cells inside the organotypic LN model was performed by using an anti-CD3 antibody or inducing an allogenic reaction. For CD3 stimulation, 10 ng/ml of anti-CD3 antibody (clone T3b; in-house made) was administered per 0.5 million T cells, directly before LN hydrogel casting. For an allogenic response, conventional or mature moDCs were included during hydrogel casting of the LN model. The number of moDCs added per model was set at 1 moDC for every 3 T cells, based on an estimation of lymphocyte numbers per donor. The LN models were cultured for six days for T cell activation.

Statistical analysis

All data are presented as mean ± standard error of the mean (SEM). The number of human LN donors is described in each figure legend and a donor shape is used consistently throughout the manuscript (Table S1). Statistical analysis was conducted using GraphPad Prism 9 software version 9.5.1 (GraphPad Software Inc., La Jolla, CA, USA). Statistical test indicated in figure legends. Differences were significant when $p < 0.05$. For correlation analyses, the base R cor() function and the corrplot() function of the corrplot package were used under R version 4.3.2.

Results

Enrichment with FRCs benefit immune cell viability in LN model

The organotypic 3D human LN model was generated by combining cryopreserved LN cell suspensions with or without *ex vivo* cultured FRCs, which were donor matched, in a collagen-based hydrogel for one week of culture (Fig. 1A). The number of FRCs used to enrich the LN model was equivalent to 1% of the total cell concentration per model. Typically, the population of immune cells in LN tissue is mostly comprised of lymphocytes, and flow cytometry analysis confirmed this composition in the LN cell suspensions used for creating the LN model, albeit with a biological variation in the percentage of T and B cells between donors (Fig. 1B). This cellular ratio remained present after culture of the LN model either with or without enriched FRCs, as well as a continuous low percentage of myeloid cells (Fig. 1B and Fig. S1A). Interestingly though, the absolute number of immune cells, particularly B cells, were found to be increased within FRC enriched-LN models, relative to the non-enriched LN models (Fig. 1C), suggesting a FRC-value to immune cell viability. Furthermore, the FRCs used for these LN models were previously characterised *ex vivo* where most cells were $PDPN^+$ in culture[5]. As such, the presence of $CD45^-$ $PDPN^+$ cells were found in the LN models, with more than 1% detected in the FRC-enriched LN models from all viable cells (Fig. 1C), which is above the percentage of FRCs administered at the start of the enriched LN model cultures.

Confocal imaging of the FRC-enriched LN models at a 3D level revealed elongated FRC morphology (Fig. 1Ei), a hallmark topology of native FRCs in human LNs for supporting immune cell activity[2,34]. As the bulk of immune cells ($DAPI^+CD45^+$ cells) were comprised of mainly lymphocytes, these were found randomly distributed throughout the hydrogel (Fig. 1Ei). Likewise, T cells ($DAPI^+CD3^+$ cells) and FRCs could be detected in the same area (Fig. 1Eii). In non-enriched LN models, lymphocytes were also evenly dispersed within the hydrogel, with pre-existing FRCs from the LN cell suspensions visible too, albeit with a fainter staining intensity (Fig. S1B).

As such, these results suggest that addition of FRCs promotes native lymphocyte survival in a 3D human LN model, based on the relative increase in immune cell numbers, specifically B cells.

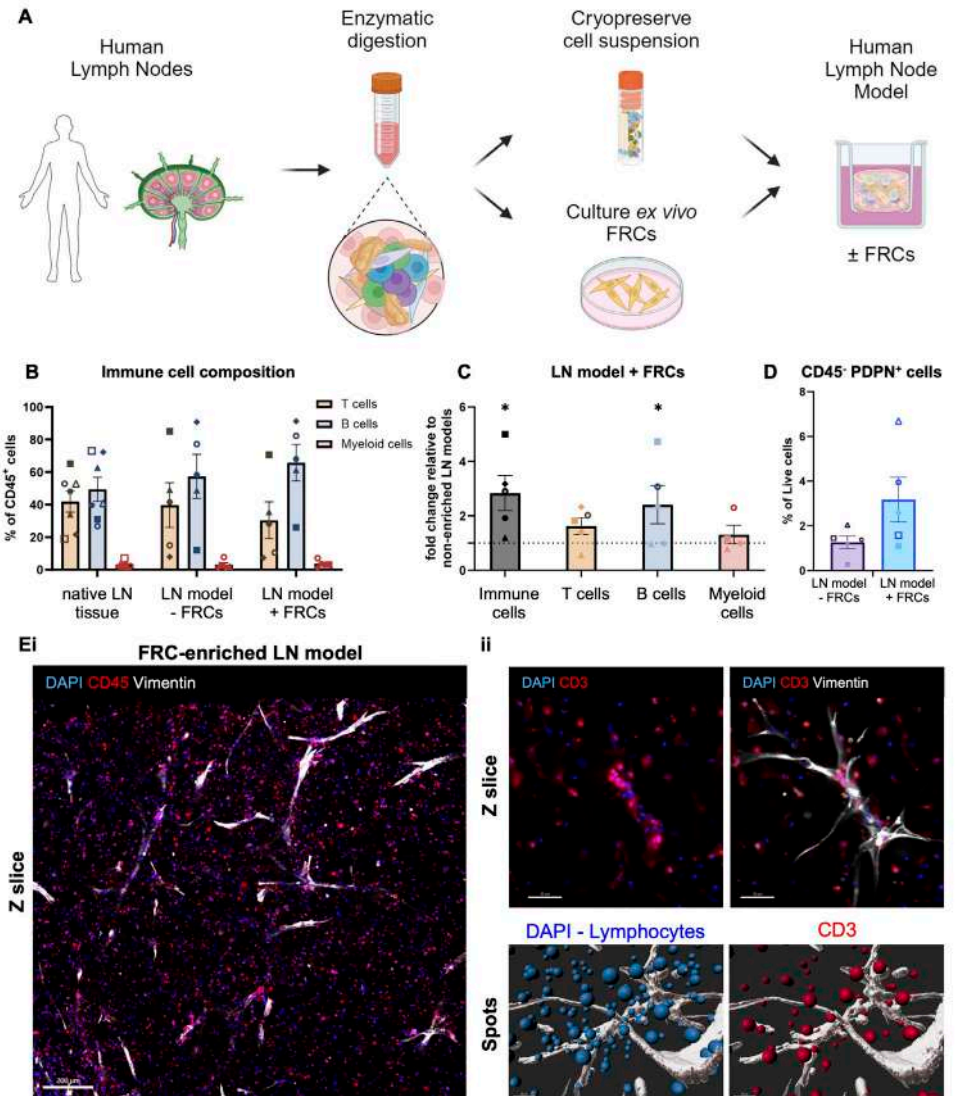

Fig. 1 - Set-up and general characterisation of the LN model. (A) Schematic illustrative workflow for generating the 3D LN model. Created with Biorender.com. **(B-D)** Flow cytometry analysis of **(B)** immune cell composition from starting native LN cell suspension and in the LN model (± enriched *ex vivo* FRCs) after a one week culture. **(C)** Fold change in number of immune cells ($CD45^+$), T cells ($CD3^+$), B cells ($CD19^+CD20^+$) and myeloid cell (sum of $CD11c^+$ and $CD14^+$ cells) with FRCs, relative to non-enriched LN models set at 1. **(D)** Composition of $CD45^-PDPN^+$ stromal cells within LN model ± FRCs. Shapes represent different donors and columns mean ± SEM; n = ≥5 independent experiments. Ordinary two-way ANOVA (*$p < 0.05$). **(E)** Representative 3D image of FRC-enriched LN model. **(i)** Z-slice from a 200 µm thick Z-stack, with DAPI nuclei (blue), CD45 (red) and vimentin (white) staining. Scale bar is 200 µm. **(ii)** Upper panels - magnified Z-slice of DAPI (blue), CD3 (red) and vimentin (white) immunofluorescent staining to identify T cells ($DAPI^+CD3^+$), other lymphocytes ($DAPI^+CD3^-$), and FRCs ($DAPI^+$vimentin$^+$). Scale bar is 50 µm. Lower panels - rendered spots of $DAPI^+$ lymphocytes with a ≤ 7 µm diameter, and T cells ($CD3^+$) in close-proximity to a surface rendered FRC. Scale bar is 30 µm.

FRCs maintain native immune subsets in LN model

Within human LNs, a plethora of immune cell subsets exist at a homeostatic level, anticipating antigen challenge and cues to mount a rapid immune response. For optimal immune activity, such immune cell subsets require the support of FRCs[35,36]. To address whether specific lymphocyte subsets were able to survive in the LN model, we looked further into the present T and B subtypes to assess whether there was a selective FRC-effect.

T cells are composed of multiple subsets that allow an efficient immune reaction to pathogenic threat after antigen encounter in the human LN. Therefore, flow cytometry characterisation was performed of $CD4^+$ and $CD8^+$ T cells within the FRC-enriched and non-enriched LN models for the following populations, central memory (T_{CM}; $CD62L^+CD45RO^+$), effector memory (T_{EM}; $CD62L^-CD45RO^+$), naïve ($T_{naïve}$; $CD62L^+CD45RO^-$) and effector (T_{EFF}; $CD62L^-CD45RO^-$) T cells (Fig. S1C). Intriguingly, FRCs significantly increased the number of $CD4^+$ naïve T cells to more than two fold on average compared to the LN models without FRCs (Fig. 2A). The addition of FRCs to the LN models did not appear to substantially alter the composition ratio of T cell subtypes, with the naïve populations forming the majority of the T cells (Fig. 2B).

When B cells are exposed to antigens in human LNs, the secretion of neutralising antibodies and the formation of memory cells begins for long-term immunity. To decipher the B cell subsets present in our LN model with or without enriched FRCs, we used the universal CD27 versus IgD gating strategy consensus[37] to classify memory ($CD27^+IgD^-$) or naïve ($CD27^-IgD^+$) $CD19^+CD20^+$ B cells (Fig. S1D). Such subtyping also revealed the populations of unswitched (US) memory B cells ($CD27^+IgD^{lo}$) and double negative (DN) B cells ($CD27^-IgD^-$), the latter a heterogenous mix of atypical/exhausted memory cells and activated plasmablast precursors[38,39]. Surprisingly, FRC-enriched LN models had on average six times more US memory B cells compared to non-enriched LN models (Fig. 2C). While the other B cell subsets were present in the LN models, this FRC-selective effect on US memory B cells was remarkable, given the majority of B cells were comprised of memory B cells (Fig. 2D). Additionally, germinal centre (GC) B cells were identified in FRC-enriched LN models, based on a $CD27^+CD38^+$ phenotype, and thus maintaining their representation in the $CD27^+$ memory B cell fraction (Fig. 2E). No plasmablasts or pre-GC B cells were detected in the LN model, irrespective of FRC enrichment (data not shown).

The small minority of myeloid cells, capable of antigen presentation and pathogen elimination in human LNs, found within the LN model were not investigated further for macrophage or DC subset phenotyping due to low cell frequencies (Fig.1C). Together, this data indicates that in our LN model, FRCs improve the final lymphocyte numbers and have a selective preference for certain subtypes that are relevant for LN functioning. This implies that with FRCs, a more immune-competent human LN *in vitro* model has been generated.

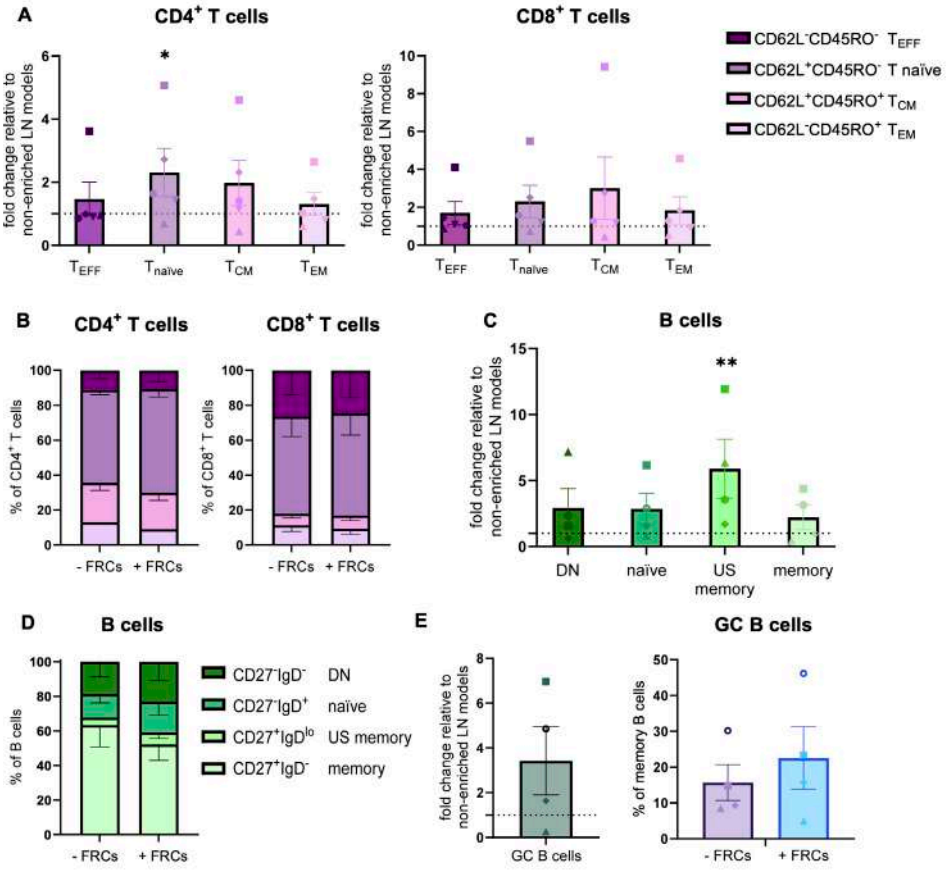

Fig. 2 - Native immune subsets benefit from addition of FRCs. LN model after a one week culture ± enriched *ex vivo* FRCs **(A-B)** $CD3^+$ T cells in LN model ± FRCs. **(A)** Relative fold change in number of effector (T_{EFF}, $CD62L^-CD45RO^-$), naïve (T naïve, $CD62L^+CD45RO^-$), central memory (T_{CM}, $CD62L^+CD45RO^+$) and effector memory (T_{EM}, $CD62L^-CD45RO^+$) cells within the $CD4^+$ and $CD8^+$ T cell population in LN model with FRCs relative to the non-enriched LN models, which is set to 1. **(B)** Average proportion of $CD4^+$ and $CD8^+$ subsets within the LN model ± FRCs. Shapes represent different donors and columns mean ± SEM; n = 5 independent experiments. Ordinary two-way ANOVA (*$p < 0.05$). **(C-E)** $CD19^+CD20^+$ B cells in LN model ± FRCs. **(C)** Relative fold change in number of double negative (DN) ($CD27^-IgD^-$), naïve ($CD27^-IgD^+$), unswitched (US) memory ($CD27^+IgD^{lo}$) and memory ($CD27^+IgD^-$) B cells in LN models with FRCs, relative to the non-enriched LN models , which is set to 1. **(D)** Average proportion of B cell subsets in LN model ± FRCs. **(E)** Germinal centre (GC) B cells gated as $CD19^+CD20^+CD27^+IgD^-CD38^+$ cells. Average donor fold change in GC B cell numbers in LN model with FRCs (+FRCs), with non-enriched LN models (-FRCs) set to 1, and percentage of GC B cells within memory B cell population ($CD27^+IgD^-$). Shapes represent different donors and columns mean ± SEM; n = 4 independent experiments. Ordinary two-way ANOVA (**$p < 0.01$).

FRCs provide immune relevant factors

Considering the well-characterised ability of FRCs to secrete immune-related molecules in human LNs for lymphocyte functioning[40], it was of interest to determine the cytokines and chemokines present in the LN model supernatant after one week (Fig. 3). Since FRCs increased B cell numbers significantly in the LN models, B cell-acting factors were examined. This included the survival proteins; a proliferation inducing ligand (APRIL) and B cell activating factor from the TNF family (BAFF), as well as the chemoattractant molecules CXC motif chemokine ligand 12 (CXCL12) and CXCL13. From this, only BAFF and CXCL12 were elevated with FRC enrichment. Likewise, inflammatory mediators of lymphocyte activity, interleukin-4 (IL-4), IL-6 and IL-10, were all significantly prominent in FRC-enriched LN models. Furthermore, other LN relevant analytes CXCL10 and IL-8, as well as protein cues for immune cell migration, like CC motif chemokine ligand 19 (CCL19) and monocyte chemoattractant protein 1 (MCP-1), were detected in LN models, with only CCL19 augmented in FRC-enriched LN models. A complete overview on the relationship between these immune factors and immune cell subsets was visualised in a correlation heat plot made for both LN models (Fig. S2). Collectively, these data suggests that the FRC-enriched LN models have an enhanced presence of pleiotropic molecular signals that are LN-specific for lymphocyte survival, homing and functioning.

Local T cell response is restrained by FRCs in LN model

The first trigger for initiation of the cell-mediated adaptive immune response in human LNs is T cell activation. This fundamental process is governed by FRCs, who not only guide immune cells into the LN paracortex, but physically facilitate the antigen presentation and subsequent immune activation[41]. Therefore, as a proof-of-concept for immunological LN functionality, we next assessed the capacity of the LN model to support *in situ* the stimulation of T cells.

Hereto, native LN T cells within the LN cell suspension were provided with an anti-CD3 antibody upon casting of the hydrogel. This meant that the co-stimulatory signals derived from CD80/CD86 expressing antigen-presenting cells (APCs) could only be provided when within the proximity of the T cells. Such APC phenotypes were confirmed present within the fresh LN cell suspensions used in the LN models (Fig. S3A). Performing flow cytometry analysis of the LN model after six days of culture, quantification of the total absolute number of T cells revealed an average 1.5-fold increase after the addition of anti-CD3 to the LN model without FRC enrichment (Fig. 4A). This was not observed in the FRC-enriched LN models with anti-CD3 stimulation. There were no apparent differences in the relative numbers of individual T cell subsets after CD3 stimulation in the LN models, with or without FRC enrichment (Fig. 4B).

Upon phenotyping functional markers on all T cells in general, no significant changes were observed across activation markers $CD25^+$, $CD69^+$ and $HLA\text{-}DR^+$, and the proliferation marker $Ki67^+$ on T cells after CD3 stimulation, independent of FRCs (Fig. 4C). To further examine T cell status, the supernatant of the LN model was sampled at day three and six to investigate cytokines related to T cell activity (Fig. 4D). Most strikingly, IFNγ peaked on day three when anti-CD3 was administered to the non-enriched LN models. Contrarily, no IFNγ was detected in FRC-enriched LN models after CD3 stimulation. Similarly,

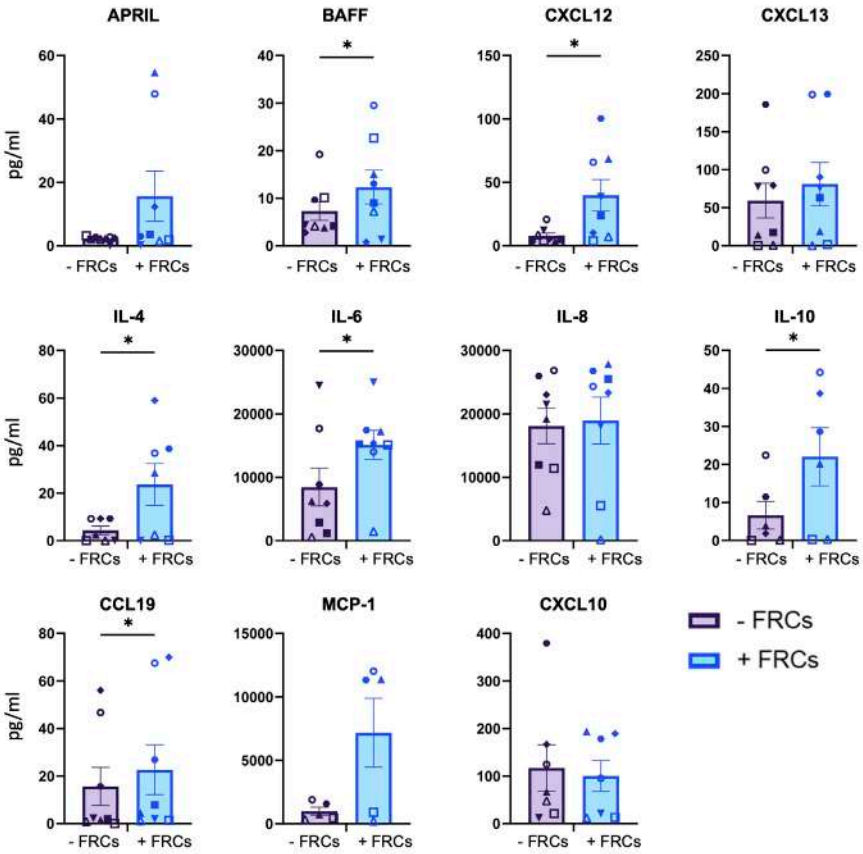

Fig. 3 - FRCs secrete soluble factors for immune cells. Cytokine bead array of LN model supernatant after a one week culture ± enriched *ex vivo* FRCs. Shapes represent different donors and columns mean ± SEM; n ≥ 5 independent experiments. Paired *t*-test ($^{*}p < 0.05$).

this pattern was also seen for IL-2 on day six, and TNFα levels were close to zero throughout all conditions. In order to address whether different T cell subsets specifically correlated with the presence or absence of FRCs after CD3 stimulation, we performed correlation analysis of both conditions. This showed that a negative correlation of $T_{naïve}$ cells and the expression of CD25 and Ki67 in the condition without FRCs, suggesting T cell activation and expansion, was absent in the presence of FRCs (Fig. 4E). Furthermore, in LN models enriched with FRCs, a positive correlation was observed between $T_{naïve}$ cells and memory T cells, which was not observed in the absence of FRCs. This indicates that there may be an FRC-influence on naïve and memory T cell dynamics after CD3 stimulation.

Furthermore, the data indicates that T cells are within enough proximity to APCs in the LN model since they are responsive to CD3 stimulation. In addition, FRCs appear to restrict and regulate T cell activity through reducing T cell proliferation and cytokines associated with T-cell activation, aligning with the specific features of human FRCs[7]. While in addition, providing the special microenvironment that promotes the presence of naïve and memory T cells.

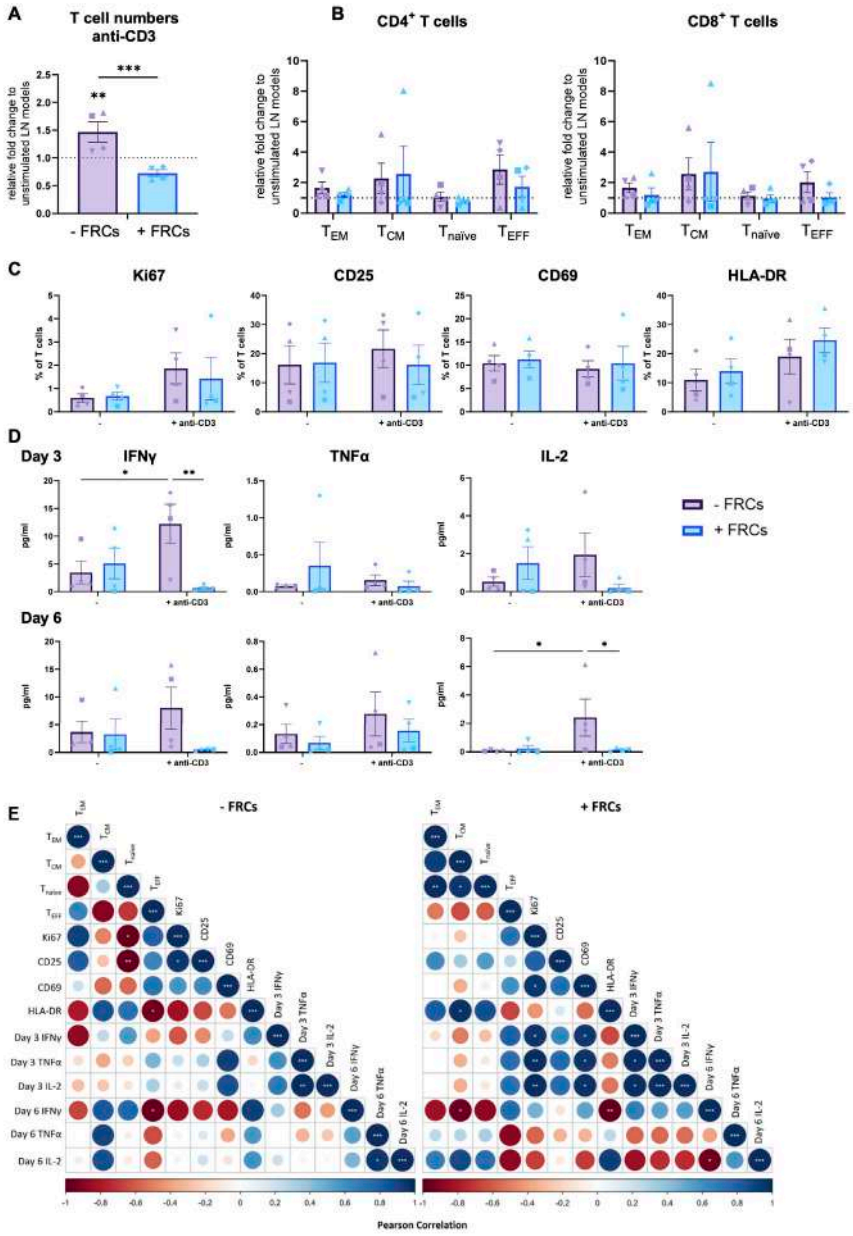

Fig. 4 - TCR triggering results in T cell activation. (A) Relative donor fold change in T cell numbers after a six day co-culture with anti-CD3 ± FRCs in LN model, with no anti-CD3 stimuli set to 1. **(B)** Relative fold change per donor in number of $CD4^+$ and $CD8^+$ T cell subsets between LN models ± FRCs after anti-CD3 stimulation, with no anti-CD3 stimuli set to 1. **(C)** Expression of proliferation (Ki67) and activation markers (CD25, CD69, HLA-DR) on T cells ± anti-CD3 and ± FRCs in LN model. **(D)** Cytokine analysis of media from LN model at day three and six ± anti-CD3 and ± FRCs. Shapes represent different donors and columns mean ± SEM; n = 4 independent experiments. Ordinary two-way ANOVA (*$p < 0.05$, **$p < 0.01$, ***$p < 0.001$). **(E)** Pearson correlation plots of T cell subsets, activation markers and cytokines ± FRCs after CD3 stimulation (*$p < 0.05$, **$p < 0.01$, ***$p < 0.001$).

Allogeneic immune activation demonstrates T cell functionality in LN model

Since the results above suggest that T cells can become activated and proliferate in the non-enriched LN models after direct CD3 stimulation, it was next of interest to recapitulate a more potent physiological response to boost T cell activity. As such, the influx of DCs into the human LN during an immune response was simulated by inducing an allogenic reaction, where DCs were mixed into the LN models at the start of the culture period. Prior to this, the DCs were differentiated from blood-isolated monocytes into either conventional moDCs (Fig. S3B) or mature DCs (Fig. S3C), characterised by expression levels of CD86, CD80 and HLA-DR.

After a six day co-culture of moDCs in the LN model, quantification of total absolute T cell numbers showed that cell numbers were not influenced by FRCs (Fig. 5A). However, when focusing on T cell subsets, T_{EM} cells were significantly increased at the cost of $T_{naïve}$ cells in FRC-enriched cultures after moDC stimulation (Fig. 5B). Signs of T cell proliferation and activation was evident through Ki67 and HLA-DR upregulation on T cells in the non-enriched LN models, respectively (Fig. 5C). Interestingly in FRC-enriched cultures, IL-2 was detected on both days after moDC inclusion, with TNFα and IFNγ measurably present only on day six, and the latter more pronounced than in non-enriched FRC LN cultures (Fig. 5D). Again, correlation analysis revealed that $T_{naïve}$ cells were positively correlated with T_{CM}, and T_{CM} with T_{EM}, in the FRC-enriched LN models (Fig. 5E), which was not seen in the absence of FRCs. This suggests FRCs may promote the memory T cell pool after moDC stimulation.

The addition of mature DCs resulted in a significant increase in the number of T cells in the non-enriched LN models (Fig. 6A). T cell numbers in FRC-enriched LN models were unchanged, indicating a clear restrictive effect of FRCs on T cell proliferation with no variation throughout T cell subsets (Fig. 6B). Addition of mature DCs showed a further upregulation of Ki67 and HLA-DR independent of FRC enrichment (Fig. 6C). Upregulation of CD69, responsible for lymphocyte retention within lymph nodes[42], was selectively observed only in FRC-enriched LN models (Fig. 6C). IL-2 significantly peaked on day six in non-enriched LN models after mature DC inclusion, with slight donor variation across the other analytes (Fig. 6D). Correlation plots unveiled that without the addition of FRCs, T_{CM} cells positively associated with all activation markers (Fig. 6E), indicating a more active response to mature DC stimulation, not seen in the presence of FRCs. Yet again, only in the FRC-enriched LN models, $T_{naïve}$ cells were positively correlated with both central and effector memory T cells.

Given these results, native LN T cells retain the capacity to respond to specific T cell activation signals in the LN model *in vitro*, with the most intense response observed with stimuli derived from the mature HLA-mismatched APCs. Therefore, this demonstration of cell-mediated immune functionality within a physiological relevant *in vitro* human LN, and the enriched-FRC dampening effects on T cell numbers and selective promotion of $T_{naïve}$ and memory T cells, provides potential for future development into assays that could study antigen-specific adaptive immune activities.

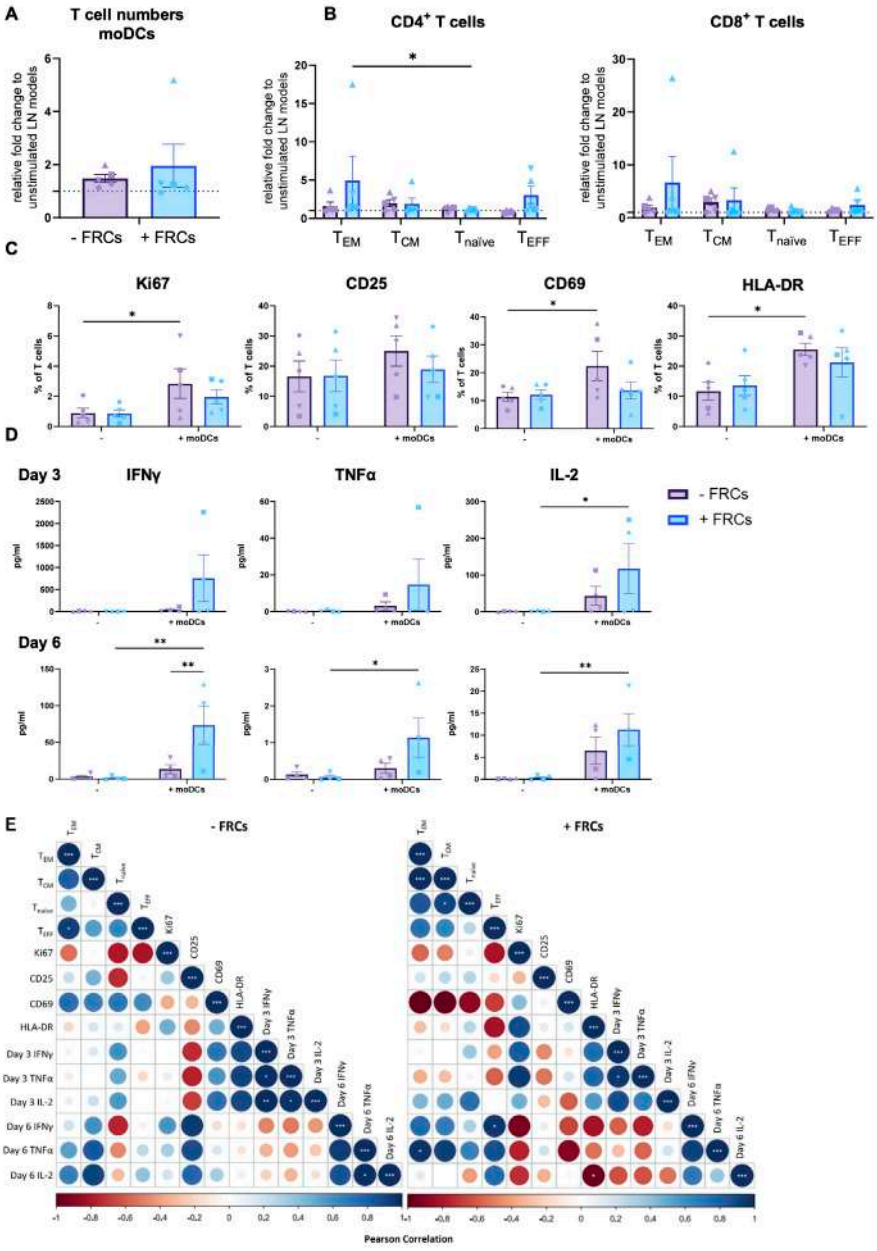

Fig. 5 - Addition of allogenic moDCs results in further T cell activation. (A) Relative donor fold change in T cell numbers after a six day co-culture with moDCs ± FRCs in LN model, with no moDCs set to 1. **(B)** Relative fold change per donor in number of $CD4^+$ and $CD8^+$ T cell subsets between LN models ± FRCs with moDCs. **(C)** Expression of proliferation (Ki67) and activation markers (CD25, CD69, HLA-DR) on T cells with ± moDCs and ± FRCs in LN model. **(D)** Cytokine analysis of media from LN model at day three and six with ± moDCs and ± FRCs. Shapes represent different donors and columns mean ± SEM; n ≥ 4 independent experiments. Ordinary two-way ANOVA (*$p < 0.05$, **$p < 0.01$). **(E)** Pearson correlation plots of T cell subsets, activation markers and cytokines ± FRCs after moDC stimulation (*$p < 0.05$, **$p < 0.01$, ***$p < 0.001$).

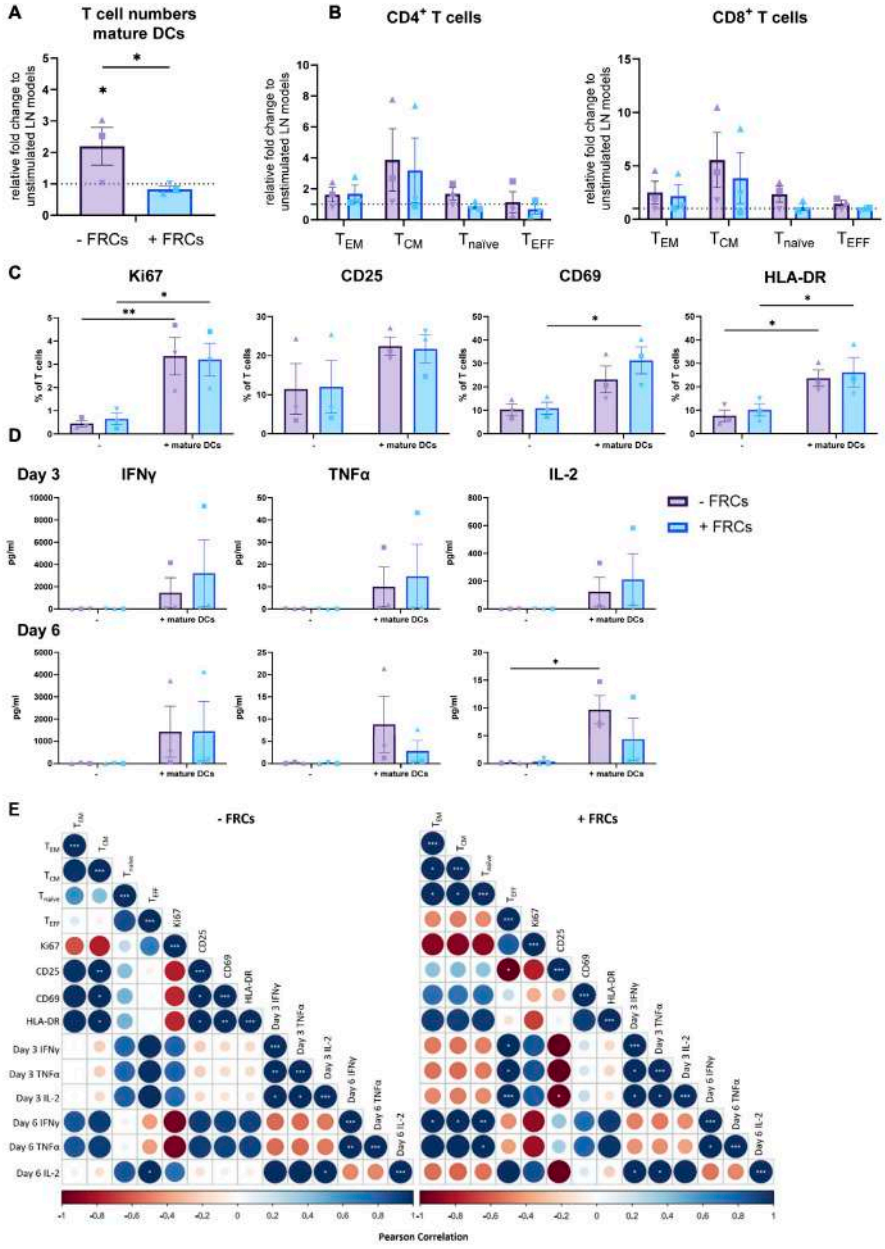

Fig. 6 - Addition of allogenic mature DCs further enhances T cell activation. (A) Relative donor fold change in T cell numbers after a six day co-culture with mature DCs ± FRCs in LN model, with no mature DCs set to 1. **(B)** Relative fold change per donor in number of $CD4^+$ and $CD8^+$ T cell subsets between LN models ± FRCs with mature DCs. **(C)** Expression of proliferation (Ki67) and activation markers (CD25, CD69, HLA-DR) on T cells with ± mature DCs and ± FRCs in LN model. **(D)** Cytokine analysis of media from LN model at day three and six with ± mature DCs and ± FRCs. Shapes represent different donors and columns mean ± SEM; n = 3 independent experiments. Ordinary two-way ANOVA ($^*p < 0.05$, $^{**}p < 0.01$). **(E)** Pearson correlation plots of T cell subsets, activation markers and cytokines ± FRCs after mature DC stimulation ($^*p < 0.05$, $^{**}p < 0.01$, $^{***}p < 0.001$).

Discussion

Although FRCs have been shown to have a vital role in directing immune activity in human LNs[12], current LN models that study immune events have yet to address or emphasise their importance. In this study, we thus aimed to develop and characterise a functional 3D immunocompetent human LN *in vitro* and explored the effects of enriching the models with *ex vivo* cultured FRCs. Our work expanded upon the first generation of a LN model, using only FRCs and DCs that was developed by us[30], which laid the foundations of the *in vitro* organotypic human LN presented in this manuscript. Here, we show that all relevant native LN immune cells are found back in the LN model after seven days of culture. Furthermore, enrichment with FRCs promoted a homeostatic LN environment with the presence of both T- and B-lymphocytes, especially B cells, while creating an environment during activation in which memory T cells positively correlate with the presence of naïve T cells. The LN model allowed for T cell activation by APCs, where enrichment of FRCs had a suppressive effect in this process.

In order to decide on the extent of FRC-enrichment into LN models, we settled on 1% of the total cell number per LN model, which is just over twice the number of FRCs found within native LN tissue[5]. This was to ensure that a sufficient cell number was included to study FRC influence on immune cells, while also maintaining a cellular composition close to the physiological ratio. Increasing percentages of FRCs in the LN model was investigated, but this resulted in hydrogel contraction (data not shown), a phenomenon previously described for human FRCs[31], which hinders downstream analysis due to the limited material availability. Furthermore, an increase of FRCs was observed in the collagen-based hydrogel, and therefore we avoided culturing for longer than one week to limit FRC overgrowth and the risk of hydrogel contraction.

Since our aim was to determine the effects of FRC incorporation into human LN models, it was useful to understand the type of cellular material available in order to generate a model that closely represents the physiological situation. It is well documented that FRCs are a heterogenous pool of fibroblasts that have a unique profile and function corresponding to their anatomical region in LNs[10]. The *ex vivo* cultured FRCs used for enriching the LN models in this current study were previously characterised by our group. This revealed homogeneity amongst donors of multiple FRC subsets exhibiting $PDPN^+$, $CD90^+$, $CD146^+$ and $BST1^+$ phenotypes[5], as well as *GREM1* mRNA[30], the DC-supporting FRC subset in human LNs[43]. This phenotypic profile mostly resembles FRCs found throughout the LN paracortex where T cells and DCs reside. This previous characterisation of *ex vivo* cultured FRCs also did not identify follicular DCs (FDCs), the B cell follicle-stroma, based on absent $CD21^+$ stromal cells.

Existence of FDCs have been reported to require interaction with B lymphocytes[44], and therefore FDCs or B cell area-like stromal cells may hypothetically exist in our LN model given the abundance of viable B cells. Although if so, it is not clear whether this may arise from a differentiation of enriched FRCs towards B cell area stromal cells, outgrowth of FDCs from the LN cell suspensions or the presence of marginal reticular cells (MRCs). MRCs are the FRCs found under the subcapsular sinus reported to express BAFF[45] and exist as a potential origin for FDC differentiation[46]. Therefore, while out of scope of this present study, the further characterisation of FRC subsets inside the LN model would be of interest to next examine, providing circumvention of the challenges with panel

design against FRC autofluorescence[33]. This will allow elucidation of whether specific FRC subsets become enriched as a result of native LN immune cell crosstalk within a 3D environment, which would otherwise be absent in *ex vivo* cultures. With the flexibility of this LN model, addition of FRC subsets from LN tissue, or genetically altered FRCs, can result in a versatile approach to study in depth their contribution to immune cell activity.

In line with this, B cell-related factors, namely APRIL, BAFF, CXCL13 and IL-6, were more concentrated in FRC-enriched LN models. These factors are known to be stromal-derived[40], but can also be secreted by myeloid cells which were present in low abundance within the LN models, regardless of FRC enrichment. Likewise, migratory chemokines MCP-1, CXCL12 and CCL19 are secreted by stromal cells, with the latter two elevated in FRC-enriched LN models. Inflammatory mediators IL-4, IL-8 and IL-10 were also present, which can originate from multiple immune cells of myeloid- and lymphocyte-descent, with IL-10 also acting as a B cell survival agent and higher in FRC-enriched LN models. All of these factors are relevant for optimal and efficient LN activity, but still it was not possible to identify other LN-relevant immune factors like IL-7 and CCL21 in our LN model. It is unclear whether the inability to detect soluble factors is due to consumption by cells in the hydrogel, trapping of the factors within the hydrogel of the LN model, or not produced at all. Recent advancements in tissue engineering technology can enable us to overcome and elucidate these quantification disputes to sample *in situ* the local microenvironment[47].

Not only is understanding FRC characteristics relevant for LN models, such organotypic model development requires proof-of-concept studies which in our case reflects a degree of LN functionality. As such, to evaluate the functionality of the LN model, the capacity of T cell stimulation was investigated. This mimicked the first step of a cell-mediated adaptive immune response in LNs, where DCs arrive bearing a foreign peripheral antigen to interact and activate T cells, a process facilitated by FRCs[41] and resulting in production of immune cells derived factors IL-2, TNFα and IFNγ. The LN models with enriched FRCs demonstrated a restriction on the total numbers of T cells, which is a hallmark of both mouse[48-51] and human FRCs[7]. Knoblich et al., identified four different molecular mechanisms used by FRCs to block T cell proliferation, making use of sliced tonsil tissue or two-dimensional (2D) HLA-mismatched FRC-T cell co-cultures, stimulated over a 24-96 hour period. Our findings were similar to Knoblich, as with our LN model we could also demonstrate FRC-dampening of T cell expansion after stimulation. This held true for the allogenic responses, particularly with mature DCs expressing the highest co-stimulatory molecules and most representative to the native LN response, but FRCs still allowed the eliciting of T cell functions after stimulation, like cytokine secretion. While donor variation is likely explained by the different degrees of biological HLA-mismatch, our correlation analysis further helped highlight the potential FRC-modulation of T cell activity. It's remarkable that in all three activation schemes, a positive correlation between $T_{naïve}$ and T_{CM} was seen in the FRC-enriched cultures, while additionally also seen between $T_{naïve}$ and T_{EM} in two of the three stimuli. This suggests that FRCs could be promoting memory T cell formation. Other correlation patterns showing FRC involvement in T cell dynamics, such as the potential relationship between CD25 and IL-2 signalling[52], could warrant further investigation to decipher mechanistic understanding of FRC behaviour behind cell mediated immunity in LNs.

The potential of this functional FRC-enriched LN model has early promise for true recapitulation of human LN biology given the immune cells and molecular signals present, as well as a capacity for T cell functionality. The enriched FRC-regulation of T cell activity may not be ideal when prompting immune activity, but could be practical to use as a system when trying to overcome this FRC suppression for e.g., targeting FRCs therapeutically to improve immunotherapies. Similarly, this model can be incorporated into humoral immune studies, especially given that FRCs supported B cells in our model. Lymphoid organ models of humoral immunity have been widely characterised already in response to vaccination dynamics and donor characteristics[23-25,53], but this has yet to be achieved with native LN material, LNSCs and a 3D environment which is valuable given they contain the necessary tissue-specific properties. Numerous other applications can make use of FRC-enriched LN models, such as investigating tolerogenic responses in autoimmunity[13], FRCs-influence in anti-tumour immunity[54] and organ-specific immune responses from LNSC imprinting[55].

Ultimately, there are still outstanding factors required for closer representation to the dynamic *in vitro* LN-like microenvironment. This includes core physiological parameters like flow, shear stress, mechanical forces, and nutrient gradients. These principles are lacking in our static LN model and it therefore would be appealing to incorporate the LN model into microfluidic organ-on-chip (OoC) devices[17,56]. This could augment key events related to optimal LN functioning, such as immune cell clustering and production of soluble factors, like IL-7 and CCL21 that were not present in our LN model and need fluid flow for detection[57]. Complimentary, this LN model was developed using a hydrogel that allows flexible implementation into multi-OoC devices, presenting the ability to link the LN model with other organ models, such as the skin or intestine. This can simulate lymphatic organ drainage, immune cell trafficking and metabolite diffusion, which are all necessary components of human immunology. In time, such multi-OoCs will provide us with the opportunity to truly create the systemic bridge from the innate to the adaptive immune response *in vitro*.

Current limitations of our LN model include a biological donor heterogeneity of immune cells, as well as lower cell density compared to what is found in the native LN. Our LN model cell density is around 50 times less dense than a recently reported lymphoid organ model with PBMCs in a 3D hydrogel, in which compact lymphocyte clusters could be observed[22]. The source of our tissue material is a limiting factor for scaling up the cell density, and it remains to be determined if efficient nutrients and oxygen can be supplied to all immune cells in such a high cell-concentrated LN model. Future improvements could be made with the use of donor matched PBMCs to increase the pool of naïve lymphocytes. This in turn could allow the assessment of antigen-specific autologous responses in different donors. This may include e.g. vaccination, immunotherapy testing or detection of antigen-specific lymphocytes. Future technical modifications can also be attempted to manipulate the extracellular matrix (ECM) environment, either by integrating other ECM proteins to be more physiological[58] or by using a synthetic-based scaffold to reduce contraction[20]. This could allow longer culture periods, especially to study adaptive immune response kinetics, and potentially enhance the cellular organisation of the LN model. Likewise, use of an open or porous ECM/synthetic scaffold may help bypass the challenges with *in situ* sampling of the model`s local microenvironment, as alluded to above. With such alterations, care must still be taken to ensure that physiological properties of the LN environment are preserved.

In summary, the LN is an integral part of human immunology, and with such an organotypic 3D LN model containing FRCs that increased the physiological recapitulation of the LN microenvironment, there is now a system that can be manipulated further to study immune responses.

Acknowledgements

The authors would like to thank and acknowledge the expert help of the Microscopy & Cytometry Core Facility, and the Antibody Conjugate Facility, at Amsterdam UMC (location Vrije Universiteit Amsterdam). We appreciate and give thanks to our bioinformatician Mike de Kok for his timely advice with the correlation plots. We thank Alberta Paul (Cytek) for advice on the T cell functional antibody panel design for multispectral flow cytometry. We extend our gratitude to Kim Ober and Dr. Monique Verstegen from the Erasmus MC, Rotterdam for sample logistics. The presented work was funded by the European Union's Horizon 2020 research and innovation programme under grant agreement No. 847551 ARCAID. LJWvdL is supported by funding from the Convergence Health Technology Flagship grant (Organ Transplantation) and Medical Delta program grant (Regenerative Medicine 4D). CMdW is supported by Cancer Center Amsterdam (Grant No. CCA2019-9-57 and CCA2020-9-73), and the Dutch Cancer Foundation (KWF; Young Investigator Grant no. 2022-4 EXPL/14641). JJK is supported by the LymphChip consortium, NWA-ORC programme of the Dutch Research Council (NWO; project no. 1292.19.019).

Author Contributions

Conceptualisation: **AIM** and **REM**; Methodology: **AIM**, **JEK**, **CMdW, JJK, SG** and **REM**; Investigation: **AIM** and **JEK**; Validation: **AIM**; Software: **AIM**; Data curation: **AIM**; Writing-original draft preparation: **AIM**; Writing-review and editing: **AIM**, **JJK**, **CMdW**, **SG** and **REM**; Supervision: **CMdW, JJK, SG** and **REM**; Funding acquisition: **SG** and **REM**; Ethical approval and sample information: **HPR** and **LJWvdL**. All authors have read and agreed to the published version of the manuscript.

References

[1] Krishnamurty, A. T. & Turley, S. J. Lymph node stromal cells: cartographers of the immune system. ***Nat Immunol*** 21, 369-380 (2020). https://doi.org/10.1038/s41590-020-0635-3

[2] Bajenoff, M. ***et al.*** Stromal cell networks regulate lymphocyte entry, migration, and territoriality in lymph nodes. ***Immunity*** 25, 989-1001 (2006). https://doi.org/10.1016/j.immuni.2006.10.011

[3] Girard, J. P., Moussion, C. & Forster, R. HEVs, lymphatics and homeostatic immune cell trafficking in lymph nodes. ***Nat Rev Immunol*** 12, 762-773 (2012). https://doi.org/10.1038/nri3298

[4] Roozendaal, R. & Mebius, R. E. Stromal cell-immune cell interactions. ***Annu Rev Immunol*** 29, 23-43 (2011). https://doi.org/10.1146/annurev-immunol-031210-101357

[5] Roet, J. E. G. ***et al.*** Human lymph node fibroblastic reticular cells maintain heterogeneous characteristics in culture. ***iScience*** 27, 110179 (2024). https://doi.org/10.1016/j.isci.2024.110179

[6] Turley, S. J., Fletcher, A. L. & Elpek, K. G. The stromal and haematopoietic antigen-presenting cells that reside in secondary lymphoid organs. ***Nat Rev Immunol*** 10, 813-825 (2010). https://doi.org/10.1038/nri2886

[7] Knoblich, K. ***et al.*** The human lymph node microenvironment unilaterally regulates T-cell activation and differentiation. ***PLoS Biol*** 16, e2005046 (2018). https://doi.org/10.1371/journal.pbio.2005046

[8] Eom, J. ***et al.*** Distinctive Subpopulations of Stromal Cells Are Present in Human Lymph Nodes Infiltrated with Melanoma. *Cancer Immunol Res* 8, 990-1003 (2020). https://doi.org/10.1158/2326-6066.CIR-19-0796

[9] Acton, S. E., Onder, L., Novkovic, M., Martinez, V. G. & Ludewig, B. Communication, construction, and fluid control: lymphoid organ fibroblastic reticular cell and conduit networks. *Trends Immunol* 42, 782-794 (2021). https://doi.org/10.1016/j.it.2021.07.003

[10] Rodda, L. B. *et al.* Single-Cell RNA Sequencing of Lymph Node Stromal Cells Reveals Niche-Associated Heterogeneity. *Immunity* 48, 1014-1028 e1016 (2018). https://doi.org/10.1016/j.immuni.2018.04.006

[11] Grasso, C., Pierie, C., Mebius, R. E. & van Baarsen, L. G. M. Lymph node stromal cells: subsets and functions in health and disease. *Trends Immunol* 42, 920-936 (2021). https://doi.org/10.1016/j.it.2021.08.009

[12] Li, L., Wu, J., Abdi, R., Jewell, C. M. & Bromberg, J. S. Lymph node fibroblastic reticular cells steer immune responses. *Trends Immunol* 42, 723-734 (2021). https://doi.org/10.1016/j.it.2021.06.006

[13] Hahnlein, J. S. *et al.* Human Lymph Node Stromal Cells Have the Machinery to Regulate Peripheral Tolerance during Health and Rheumatoid Arthritis. *Int J Mol Sci* 21 (2020). https://doi.org/10.3390/ijms21165713

[14] Radtke, A. J. *et al.* Multi-omic profiling of follicular lymphoma reveals changes in tissue architecture and enhanced stromal remodeling in high-risk patients. *Cancer Cell* 42, 444-463 e410 (2024). https://doi.org/10.1016/j.ccell.2024.02.001

[15] Marx, U. *et al.* Biology-inspired microphysiological systems to advance patient benefit and animal welfare in drug development. *ALTEX* 37, 365-394 (2020). https://doi.org/10.14573/altex.2001241

[16] Langhans, S. A. Three-Dimensional in Vitro Cell Culture Models in Drug Discovery and Drug Repositioning. *Front Pharmacol* 9, 6 (2018). https://doi.org/10.3389/fphar.2018.00006

[17] Morrison, A. I., Sjoerds, M. J., Vonk, L. A., Gibbs, S. & Koning, J. J. In vitro immunity: an overview of immunocompetent organ-on-chip models. *Front Immunol* 15, 1373186 (2024). https://doi.org/10.3389/fimmu.2024.1373186

[18] Ozulumba, T., Montalbine, A. N., Ortiz-Cardenas, J. E. & Pompano, R. R. New tools for immunologists: models of lymph node function from cells to tissues. *Front Immunol* 14, 1183286 (2023). https://doi.org/10.3389/fimmu.2023.1183286

[19] Giese, C. *et al.* Immunological substance testing on human lymphatic micro-organoids in vitro. *J Biotechnol* 148, 38-45 (2010). https://doi.org/10.1016/j.jbiotec.2010.03.001

[20] Braham, M. V. J. *et al.* A synthetic human 3D in vitro lymphoid model enhancing B-cell survival and functional differentiation. *iScience* 26, 105741 (2023). https://doi.org/10.1016/j.isci.2022.105741

[21] Goyal, G. *et al.* Ectopic Lymphoid Follicle Formation and Human Seasonal Influenza Vaccination Responses Recapitulated in an Organ-on-a-Chip. *Adv Sci (Weinh)* 9, e2103241 (2022). https://doi.org/10.1002/advs.202103241

[22] Jeger-Madiot, R. *et al.* Modeling memory B cell responses in a lymphoid organ-chip to evaluate mRNA vaccine boosting. *J Exp Med* 221 (2024). https://doi.org/10.1084/jem.20240289

[23] Wagar, L. E. *et al.* Modeling human adaptive immune responses with tonsil organoids. *Nat Med* 27, 125-135 (2021). https://doi.org/10.1038/s41591-020-01145-0

[24] Kastenschmidt, J. M. *et al.* Influenza vaccine format mediates distinct cellular and antibody responses in human immune organoids. *Immunity* 56, 1910-1926 e1917 (2023). https://doi.org/10.1016/j.immuni.2023.06.019

[25] Kastenschmidt, J. M. *et al.* A human lymphoma organoid model for evaluating and targeting the follicular lymphoma tumor immune microenvironment. *Cell Stem Cell* 31, 410-420 e414 (2024). https://doi.org/10.1016/j.stem.2024.01.012

[26] Koning, J. J. & Mebius, R. E. Stromal cells and immune cells involved in formation of lymph nodes and their niches. *Curr Opin Immunol* 64, 20-25 (2020). https://doi.org/10.1016/j.coi.2020.03.003

[27] Harle, G., Kowalski, C., Garnier, L. & Hugues, S. Lymph Node Stromal Cells: Mapmakers of T Cell Immunity. *Int J Mol Sci* 21 (2020). https://doi.org/10.3390/ijms21207785

[28] Acton, S. E. *et al.* Dendritic cells control fibroblastic reticular network tension and lymph node expansion. *Nature* 514, 498-502 (2014). https://doi.org/10.1038/nature13814

[29] Gago da Graca, C., van Baarsen, L. G. M. & Mebius, R. E. Tertiary Lymphoid Structures: Diversity in Their Development, Composition, and Role. *J Immunol* 206, 273-281 (2021). https://doi.org/10.4049/jimmunol.2000873

[30] Morrison, A. I. *et al.* An Organotypic Human Lymph Node Model Reveals the Importance of Fibroblastic Reticular Cells for Dendritic Cell Function. *Tissue Eng Regen Med* 21, 455-471 (2024). https://doi.org/10.1007/s13770-023-00609-x

[31] Fletcher, A. L. *et al.* Reproducible isolation of lymph node stromal cells reveals site-dependent differences in fibroblastic reticular cells. *Front Immunol* 2, 35 (2011). https://doi.org/10.3389/fimmu.2011.00035

[32] Obermaier, B. *et al.* Development of a new protocol for 2-day generation of mature dendritic cells from human monocytes. *Biol Proced Online* 5, 197-203 (2003). https://doi.org/10.1251/bpo62

[33] Roet, J. E. G. *et al.* Unbiased method for spectral analysis of cells with great diversity of autofluorescence spectra. *Cytometry A* 105, 595-606 (2024). https://doi.org/10.1002/cyto.a.24856

[34] Katakai, T., Hara, T., Sugai, M., Gonda, H. & Shimizu, A. Lymph node fibroblastic reticular cells construct the stromal reticulum via contact with lymphocytes. *J Exp Med* 200, 783-795 (2004). https://doi.org/10.1084/jem.20040254

[35] Link, A. *et al.* Fibroblastic reticular cells in lymph nodes regulate the homeostasis of naive T cells. *Nat Immunol* 8, 1255-1265 (2007). https://doi.org/10.1038/ni1513

[36] Cremasco, V. *et al.* B cell homeostasis and follicle confines are governed by fibroblastic reticular cells. *Nat Immunol* 15, 973-981 (2014). https://doi.org/10.1038/ni.2965

[37] Sanz, I. ***et al.*** Challenges and Opportunities for Consistent Classification of Human B Cell and Plasma Cell Populations. *Front Immunol* 10, 2458 (2019). https://doi.org/10.3389/fimmu.2019.02458

[38] Wei, C., Jung, J. & Sanz, I. OMIP-003: phenotypic analysis of human memory B cells. *Cytometry A* 79, 894-896 (2011). https://doi.org/10.1002/cyto.a.21112

[39] Kaminski, D. A., Wei, C., Qian, Y., Rosenberg, A. F. & Sanz, I. Advances in human B cell phenotypic profiling. *Front Immunol* 3, 302 (2012). https://doi.org/10.3389/fimmu.2012.00302

[40] Fletcher, A. L., Acton, S. E. & Knoblich, K. Lymph node fibroblastic reticular cells in health and disease. *Nat Rev Immunol* 15, 350-361 (2015). https://doi.org/10.1038/nri3846

[41] Brown, F. D. & Turley, S. J. Fibroblastic reticular cells: organization and regulation of the T lymphocyte life cycle. *J Immunol* 194, 1389-1394 (2015). https://doi.org/10.4049/jimmunol.1402520

[42] Shiow, L. R. *et al.* CD69 acts downstream of interferon-alpha/beta to inhibit S1P1 and lymphocyte egress from lymphoid organs. *Nature* 440, 540-544 (2006). https://doi.org/10.1038/nature04606

[43] Kapoor, V. N. *et al.* Gremlin 1(+) fibroblastic niche maintains dendritic cell homeostasis in lymphoid tissues. *Nat Immunol* 22, 571-585 (2021). https://doi.org/10.1038/s41590-021-00920-6

[44] Koning, J. J. & Mebius, R. E. Interdependence of stromal and immune cells for lymph node function. *Trends Immunol* 33, 264-270 (2012). https://doi.org/10.1016/j.it.2011.10.006

[45] Heesters, B. A. *et al.* Characterization of human FDCs reveals regulation of T cells and antigen presentation to B cells. *J Exp Med* 218 (2021). https://doi.org/10.1084/jem.20210790

[46] Jarjour, M. *et al.* Fate mapping reveals origin and dynamics of lymph node follicular dendritic cells. *J Exp Med* 211, 1109-1122 (2014). https://doi.org/10.1084/jem.20132409

[47] Michielon, E. *et al.* Integration of line-field confocal optical coherence tomography and in situ microenvironmental mapping to investigate the living microenvironment of reconstructed human skin and melanoma models. *J Dermatol Sci* 115, 85-93 (2024). https://doi.org/10.1016/j.jdermsci.2024.07.001

[48] Siegert, S. *et al.* Fibroblastic reticular cells from lymph nodes attenuate T cell expansion by producing nitric oxide. *PLoS One* 6, e27618 (2011). https://doi.org/10.1371/journal.pone.0027618

[49] Lukacs-Kornek, V. *et al.* Regulated release of nitric oxide by nonhematopoietic stroma controls expansion of the activated T cell pool in lymph nodes. *Nat Immunol* 12, 1096-1104 (2011). https://doi.org/10.1038/ni.2112

[50] Khan, O. *et al.* Regulation of T cell priming by lymphoid stroma. *PLoS One* 6, e26138 (2011). https://doi.org/10.1371/journal.pone.0026138

[51] Denton, A. E., Roberts, E. W., Linterman, M. A. & Fearon, D. T. Fibroblastic reticular cells of the lymph node are required for retention of resting but not activated CD8+ T cells. *Proc Natl Acad Sci U S A* 111, 12139-12144 (2014). https://doi.org/10.1073/pnas.1412910111

[52] Kim, D. *et al.* Lymph node fibroblastic reticular cells regulate differentiation and function of CD4 T cells via CD25. *J Exp Med* 219 (2022). https://doi.org/10.1084/jem.20200795

[53] Mitul, M. T. *et al.* Tissue-specific sex differences in pediatric and adult immune cell composition and function. *Front Immunol* 15, 1373537 (2024). https://doi.org/10.3389/fimmu.2024.1373537

[54] Onder, L. *et al.* Fibroblastic reticular cells generate protective intratumoral T cell environments in lung cancer. *Cell* 188, 430-446 e420 (2025). https://doi.org/10.1016/j.cell.2024.10.042

[55] Zou, M., Wiechers, C. & Huehn, J. Lymph node stromal cell subsets-Emerging specialists for tailored tissue-specific immune responses. *Int J Med Microbiol* 311, 151492 (2021). https://doi.org/10.1016/j.ijmm.2021.151492

[56] Hammel, J. H., Zatorski, J. M., Cook, S. R., Pompano, R. R. & Munson, J. M. Engineering in vitro immune-competent tissue models for testing and evaluation of therapeutics. *Adv Drug Deliv Rev* 182, 114111 (2022). https://doi.org/10.1016/j.addr.2022.114111

[57] Tomei, A. A., Siegert, S., Britschgi, M. R., Luther, S. A. & Swartz, M. A. Fluid flow regulates stromal cell organization and CCL21 expression in a tissue-engineered lymph node microenvironment. *J Immunol* 183, 4273-4283 (2009). https://doi.org/10.4049/jimmunol.0900835

[58] Choi, Y. S. *et al.* Immunomodulatory Scaffolds Derived from Lymph Node Extracellular Matrices. *ACS Appl Mater Interfaces* 13, 14037-14049 (2021). https://doi.org/10.1021/acsami.1c02542

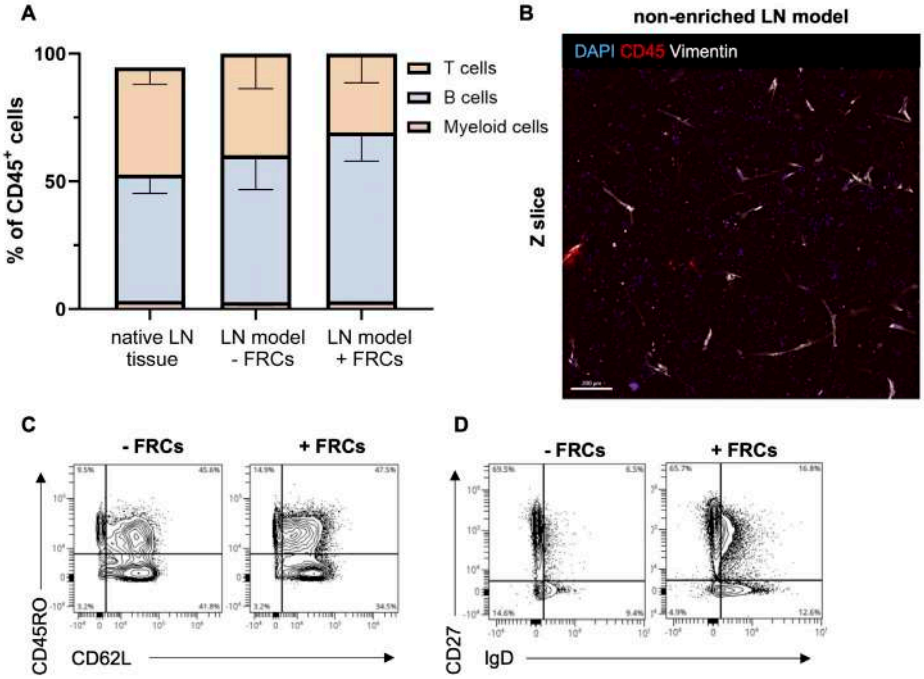

Fig. S1 - Characterisation of LN model ± FRCs. (A) Average donor fold change in number of T cells ($CD3^+$), B cells ($CD19+CD20^+$) and myeloid cells (sum of $CD11c^+$ and $CD14^+$) in native LN tissue and LN models with FRCs (+FRCs). n = ≥5 independent experiments. **(B)** Representative 3D image of a non-enriched LN model; Z-slice from a 200 µm thick Z-stack, with DAPI nuclei (blue), CD45 (red) and vimentin (white) staining. Scale bar is 200 µm. **(C)** Representative contour plot gating strategy for effector (T_{EFF}, $CD62L^-CD45RO^-$), naïve ($T_{naïve}$, $CD62L^+CD45RO^-$), central memory (T_{CM}, $CD62L^+CD45RO^+$) and effector memory (T_{EM}, $CD62L^-CD45RO^+$) phenotype within the $CD3^+$ gated T cells. **(D)** Representative contour plot gating strategy for DN ($CD27^-IgD^-$), naïve ($CD27^-IgD+$), US memory ($CD27+IgD^{lo}$) and memory ($CD27^+IgD^-$) B cells.

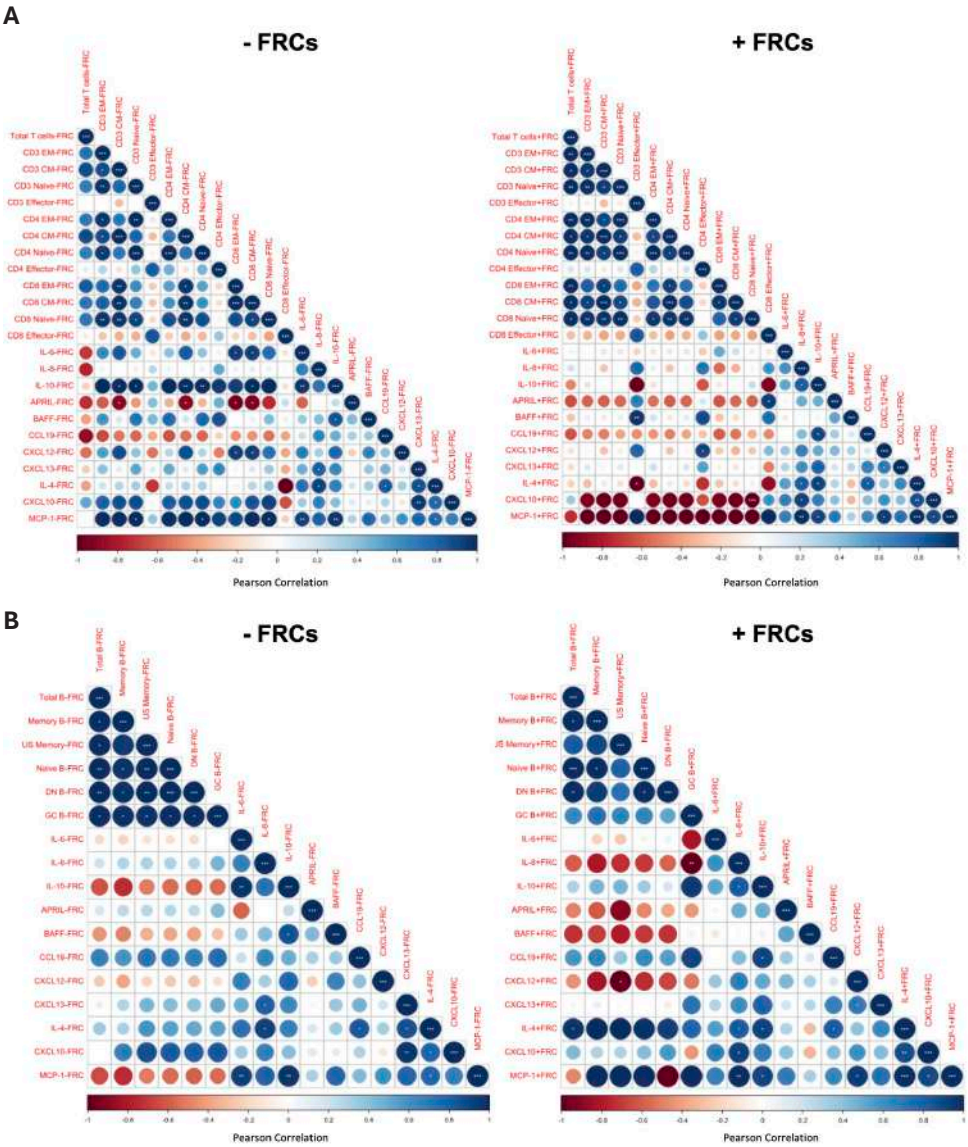

Fig. S2 - Correlation plots of LN model secretome ± FRCs with immune cell subsets. (A) T cell and **(B)** B cell subsets from figure 1 and 2 correlated with figure 3 chemokines and cytokines. Legend maps negative correlation (-1) to positive correlation (+1). (*p < 0.05, **p < 0.01, ***p < 0.001).

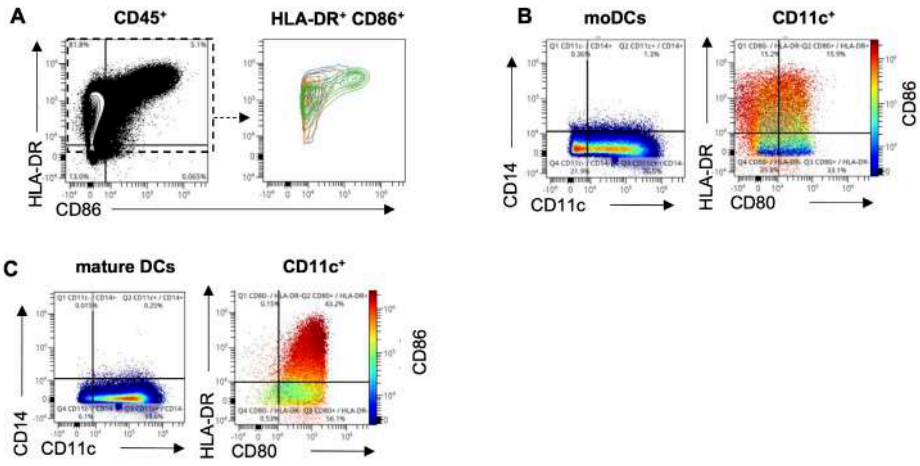

Fig. S3 - Phenotype of co-stimulatory molecules on antigen presenting cells used in T cell stimulation of LN models. (A) Representative FACS plot of CD45$^+$ native LN cell suspensions with the percentage of HLA-DR$^+$ and CD86$^+$ cells. Contour coloured plots overlay n = 3 donors. **(B)** FACS plot of CD11c$^+$ moDC phenotype for CD80, HLA-DR and CD86 (red) levels. **(C)** FACS plot of CD11c$^+$ mature DC phenotype for CD80, HLA-DR and CD86 (red) levels.

Table S1 **Human lymph node donor characteristics.** F: Female, M: Male, DBD: Donation after Brain Death, DCD: Donation after Circulatory Death, PSC: Primary sclerosing cholangitis.

#	Donor	Sex	Age	HLA-type	Symbol
1	DBD	F	16	A1 A19 A32 B15 B62 B16 B39 Bw6 Cw3 Cw9 Cw12 DR5 DR5 DR11 DR12 DR52 DQ3 DQ3 DQ7 DQ7	◆
2	DBD	F	59	A3 A28 A68 B12 B44 B70 B72 Bw4 Bw6 Cw2 Cw5 DR3 DR17 DR4 DR52 DR53 DQ2 DQ3 DQ7 DQA-03 DQA-05 DP-0401 DPA-01	■
3	DCD	F	46	A1 A11 B17 B57 B35 Bw4 Bw6 Cw4 Cw6 DR1 DR7 DQ1 DQ5 DQ3 DQ9 DQA-01 DQA-02 DP-0201 DPA-01	○
4	DCD	M	50	A1 A19 A33 B14 B65 B40 B61 Bw6 Cw2 Cw8 DR3 DR17 DR6 DR13 DR52 DQ1 DQ6 DQ2 DQA-01 DQA-05 DP-0201 DP-10 DPA-01 DPA-02	⬢
5	DBD	F	68	A2, A68 (28), Bw4, Bw6, B7, B53, Cw4, Cw7, DP-0401, DR52, DPA-01, DQ6 (1), DQ4, DQA-01, DQA-04, DR13 (6), DR8	▲
6	DCD	F	53	A1, A2, Bw4, Bw6, B57 (17), B60 (40), Cw10 (3), Cw7, DP-03, DP-0401, DR51, DPA-01, DQ6 (1), DQA-01, DR15 (2)	▼
7	Patient: PSC	F	51	A1 B8 C7 DRB1 3 DRB3 DQB1 2	△
8	DCD	M	16	A2 A3 B7 B12 B44 Bw4 Bw6 Cw5 Cw7 DR2 DR15 DR4 DR51 DR53 DQ1 DQ6 DQ3 DQ7	□

6

Integration of lymphatic vasculature to a human lymph node-on-chip enhances physiological immune properties

Andrew I. Morrison[1,2†], Jonas Jäger[1,2†], Charlotte M. de Winde[1,2,3], Henk P. Roest[4], Luc J.W. van der Laan[4], Susan Gibbs[1,2,5], Jasper J. Koning[1,2], Reina E. Mebius[1,2]

[1] Amsterdam UMC location Vrije Universiteit Amsterdam, Molecular Cell Biology & Immunology, De Boelelaan 1117, Amsterdam, The Netherlands.
[2] Amsterdam institute for Immunology and Infectious diseases, Amsterdam, The Netherlands.
[3] Cancer Center Amsterdam, Amsterdam, The Netherlands
[4] Erasmus MC Transplant Institute, University Medical Center Rotterdam, Department of Surgery, Dr. Molewaterplein 40, 3015GD, Rotterdam, The Netherlands.
[5] Department Oral Cell Biology, Academic Centre for Dentistry Amsterdam (ACTA), University of Amsterdam and Vrije Universiteit, Amsterdam, The Netherlands.

[†]Equal contribution

Submitted to *Materials Today Bio*.
BioRxiv DOI: 10.1101/2025.03.20.644364

Abstract

To study systemic human innate and adaptive immune responses in detail, competent *in vitro* lymph node (LN) models with LN stromal cells (LNSCs) are required to recapitulate the physiological microenvironment. The multicellular organisation of LNs possesses a challenge for designing such microphysiological systems (MPS), particularly with the structural complexity of LNs and the lymphatic vasculature. Here, we established an organotypic LN model with integrated lymphatics in an organ-on-chip (OoC) platform containing a printed sacrificial structure, and studied the influence of a perfused lymphatic endothelial cell (LEC)-lined channel on the LN-on-chip microenvironment. Upon one-week of culture under lymphatic flow, LECs lined the tubular structure forming a lymphatic vessel through the LN model, and stable metabolic conditions within the LN-on-chip were confirmed. Interestingly, LECs in the LN-on-chip displayed the phenotype found in human LNs with upregulation of LEC-specific LN markers, such as atypical chemokine receptor 4 (ACKR4). The presence of the LEC-lined perfused vessel in the LN-on-chip resulted in the increase of native immune cells, most notably B cells, and the secretion of survival and migratory signals, namely interleukin-7 (IL-7) and CC motif chemokine ligand 21 (CCL21). Likewise, LECs promoted the abundance of immune cell clusters closer to the vessel. As such, these features represent an enhanced physiological microenvironment to allow for immune cell migration and interactions for efficient LN functioning. This approach paves the way for LN integration into multi-OoC (MOC) platforms to investigate immunological crosstalk between tissue-derived factors, immune cell trafficking and organ-specific adaptive immune responses.

Introduction

Lymph nodes (LNs) play an integral part in systemic immunology. Their localisation throughout the human body is tailored towards the efficient drainage of interstitial fluid from all tissues and organs, allowing the screening of pathogens, removal of toxins and the migration of cells to initiate the adaptive immune response. Such immune responses occur due to the highly dynamic and architectural structure of the multicellular LN microenvironment. This organisation is regulated by LN stromal cells (LNSCs) from non-hematopoietic origin[1]. Fibroblastic reticular cells (FRCs), a type of LNSC from the mesenchymal lineage, create the three-dimensional (3D) structural network throughout the LN[2] and promote crosstalk between dendritic cells (DCs), T cells and B cells for immune activity[3]. In addition to FRCs, the non-mesenchymal LNSCs are composed of endothelial cells (ECs), either blood ECs (BECs) or lymphatic ECs (LECs), with both cell types lining their respective vessels to regulate immune cell migration to and from the LN[1].

Upon inflammation in peripheral tissues and organs, antigen-induced activation of antigen presenting cells (APCs) can occur, resulting in their migration into the lymphatic vasculature. These are typically DCs, and once activated they upregulate C-C chemokine receptor type 7 (CCR7) to undergo chemotaxis along the afferent lymphatic vasculature into the LN, following a chemotactic gradient of LEC-secreted CC motif chemokine ligand 21 (CCL21) [4]. LECs establish this CCL21 gradient by expressing atypical chemokine receptor 4 (ACKR4) to scavenge CCL21 [5], thereby guiding DCs through the afferent lymphatics and facilitating their arrival into the LN subcapsular sinus (SCS) [6]. Here, DCs enter the LN parenchyma by undergoing transendothelial migration[7] , facilitated by additional chemotactic cues[8], including CCL19; the second ligand of CCR7[5,9].

The LECs of the LN are heterogenous and populate intertwined networks of sinus channels across the LN parenchyma. Six subsets of human LECs have been identified based on anatomical location[10], displaying unique cellular signatures compared to peripheral LECs [11,12]. These include ACKR4$^+$ SCS ceiling LECs, TNF receptor superfamily member 9$^+$ (TNFSRF9$^+$) SCS floor LECs, and macrophage receptor with collagenous structure$^+$ (MARCO$^+$) medullary LECs. Furthermore, distinct functional properties of LECs have been uncovered in mice, such as producing survival and proliferation signals[13], trapping and filtering lymph-borne molecules[14], and exhibiting antigen-presenting capabilities[15,16]. Therefore, LECs of the LN are essential for promoting the adaptive immune response.

To study the LN in health and disease, and recapitulate such an immunological cascade of events for an adaptive immune response *in vitro*, a biological system is required that can reflect the physiological LN environment. Therefore, recent interest has been made in developing LN models to study *in vitro* immunity. Such models are microphysiological systems (MPS), which have been developed in response to the need for better human models for drug testing, disease modelling and basic understanding of organ physiology[17,18]. LN models have currently demonstrated robust humoral immunity from vaccine and cancer therapy applications[19,20,21] but are suboptimal based on lack of LNSC inclusion. LNSCs have shown their value in 3D LN models[22,23,24], yet these static models lack key physiological elements like flow, which can induce specific cytokine and chemokine expression[25]. In this context, recent advances in the Organ-on-chip (OoC) field become apparent, particularly for using microfluidic devices to model human immunology[26]. LN-on-chips have shown early promise

with studying responses to vaccination using peripheral blood mononuclear cells (PBMCs)[27,28] and tonsil-derived cells[29], stromal-regulated immune cell migration[30,31] and cell-cell interactions[32,33]. However, LN-on-chip models that use native LN-derived cells and integrate lymphatic vasculature are currently non-existent.

To resemble the human LN function and architecture more closely, we have previously developed a static LN model with native immune cells and enriched with FRCs[23]. In this study, we take this LN model one step further and incorporated a perfused LEC-lined lymphatic vessel through the LN model using the TissUse's HUMIMIC Chip2 OoC device, modified with a sacrificial structure[34]. The influence of LECs and flow on the LN microenvironment was characterised over a one-week culture period. In contrast to a LN-on-chip without lymphatics, the LN-on-chip with integrated LECs showed increased lymphocytes, survival and migratory factors, as well as an abundance of immune cell clusters, which are all hallmarks of an optimal LN-like microenvironment. As such, this LN-on-chip demonstrates a degree of immunocompetency previously unobserved in static LN models.

Material and methods

Human tissue collection

Human LNs were obtained during liver transplant procedures of cadaveric donors at the Erasmus MC, Rotterdam, The Netherlands, in accordance with the Medisch Ethische Toetsings Commissie (METC) of Erasmus MC (MEC-2014-060). The use of biopsies for research purposes follows the ethical Helsinki Declaration of 1975 standards. All patients (liver transplant recipients) gave written informed consent to use their donor tissue. LNs were resected along the hepatic artery and portal vein in the porta hepatis. LNs were transported in Belzer UW Cold Storage Solution (Bridge to Life Ltd., London, England, UK) and processed within 72 hours of surgery. Donor details are in Table S1

Enzymatic digestion of human lymph nodes

Immune cells and LECs were isolated from human LN-tissue by enzymatic digestion, as previously described[35]. Briefly, 4 x 10-minute digestion cycles of LNs in an enzyme mixture containing RPMI-1640 with 2.4 mg/ml Dispase II, 0.6 mg/ml Collagenase P and 0.3 mg/ml DNase I (all from Sigma-Aldrich, St. Louis, MO, USA) was performed. Ice cold phosphate-buffered saline (PBS), supplemented with 2% foetal calf serum (FCS) (HyClone; GE Healthcare, Chicago, IL, USA) and 5 mM ethylenediaminetetraacetic acid (EDTA), was used to stop digestion and wash the isolated cells at 300 G centrifugation for 4 mins at 4 °C. Cell pellet was re-suspended in 1 ml of DMEM (Gibco, Grand Island, NY, USA) with 10% FCS, strained through a 100 µM filter, and counted. The LN cell suspensions were either cryopreserved or cultured as described below.

Culture of primary lymphatic endothelial cells

LN cell suspensions were seeded at a density of 1.25 x 10^6 cell suspension per cm^2 on culture flasks, coated with 2 µg/cm^2 gelatin (Sigma-Aldrich). For selective LEC outgrowth, culture media comprised

of Endothelial Cell Growth Medium MV2 (MV2; PromoCell, Heidelberg, Germany) with 10% FSC and 1% Penicillin/Streptomycin/Glutamine (PSG). After three days, lymphocytes were washed away with PBS, and upon confluence, cells were passaged and harvested with 0.5% Trypsin + 5 mM EDTA. LECs were used up to passage 4 for all individual experiments.

Microfluidic device

In this study, we made use of the HUMIMIC Chip2 24-well (TissUse, Berlin, Germany) with a printed sacrificial structure (single or bifurcated print) within the larger 14 mm diameter culture compartment (further referred to as the LN compartment) and aligned with the on-chip microcirculation (Figure 1B). The manufacturing details, characterisation of flow parameters and method of endothelialisation have been described previously for this chip[34]. Flow was applied during the experimental culture period in a counterclockwise circulation using a HUMIMIC Starter (TissUse) control unit, set at a 30 bpm frequency with ± 50 mbar to simulate lymphatic flow[34,36].

Construction of LN-on-chip model

The 3D LN model was constructed, as previously described[23], directly into the HUMIMIC Chip2's LN compartment (Figure 1A). This was performed by mixing human LN cell suspensions with a hydrogel composed of rat-tail collagen type I (3 mg/ml end concentration) in Hank's Balanced Salt Solution (HBSS without Ca and Mg, Gibco) and fibrinogen from human plasma (1 mg/ml end concentration; Enzyme research laboratories, cat no: FIB 1, South Bend, IN, USA). LN cell suspensions were adjusted to a concentration of 10 x 10^6 cells per ml of hydrogel, with a final hydrogel volume at either 300 or 350 µl. Thrombin (0.5 U/ml; Merck KGaA, Darmstadt, Germany) and aprotinin (50 KIU/ml; SERVA, Heidelberg, Germany) were added to the hydrogel for fibrinogen polymerisation and to prevent shrinkage respectively. Hydrogels were polymerised inside chips at 37 °C and 5% CO_2 for 30 mins, after which the sacrificial structure dissolved to leave a hollow channel. Complete MV2 medium was added to the vascular compartment (300 µl) and LN model medium, composed of RPMI-1640 with HEPES and L-glutamine (Gibco), 10% FCS (HyClone; GE Healthcare), 2% PSG, 1% ITS (Gibco), 1X non-essential amino acids (NEAA) (Gibco), 1X sodium pyruvate (Gibco) and 1X normocin (Invivogen, Toulouse, France), was added to the hydrogel compartment (500 µl). Both media contained 50 KIU/ml aprotinin (to reduce shrinkage). The chip was connected to the HUMIMIC Starter for an overnight incubation at 37 °C and 5% CO_2 in flow (± 500 mbar, 30 bpm) to remove remnants of the dissolved sacrificial structure in the lumen.

Lymphatic endothelial cell seeding

The next day, remaining residuals of the printed sacrificial structure were removed by a medium exchange of MV2 in the vascular compartment. LECs were then seeded at a total number of 5 x 10^5 cells to the vascular compartment and flushed through the vessel under the LN model via pressure differences applied with the compartment lids. Chips were incubated at 37 °C, 5% CO2 for 4 hours. After incubation, the vascular compartment was washed with MV2 medium. Next, 300 µl of fresh MV2

medium was added to the vascular compartment, and 500 µl of fresh LN model medium on top of the hydrogel, with 50 KIU/ml aprotinin (to reduce shrinkage) supplemented to both media from here onwards. LN-on-chip models without LEC endothelialisation followed the same procedure. Chips were then cultured under flow at 30 bpm ± 50 mbar for a seven-day period. A full medium exchange was performed on day 3 and 5 for both compartments, with each compartment supernatant stored separately at 4 °C and -20 °C for future analysis (Figure 1C). At the end of the culture period, medium from the two compartments was collected separately and the LN-on-chip was either fixed *in situ* for 3D imaging, or the LN hydrogel was removed for enzymatic digestion. Enzymatic digestion to a single cell suspension for analysis by flow cytometry was achieved using 0.2 mg/ml Collagenase P and 0.1 mg/ml DNase I for 1 hour at 37°C, after which the reaction was stopped with PBS containing 2% FCS and 5 mM EDTA.

Metabolic analysis

Levels of glucose, lactate, and lactate dehydrogenase (LDH) activity were analysed from chip supernatants on day 3, 5 and 7. This was performed using a Glucose Colorimetric Detection Kit (EIAGLUC, Thermo Fisher), Lactate Assay Kit (MAK064, Sigma-Aldrich) and Cytotoxicity Detection Kit PLUS (LDH) (04744934001, Roche, Basel, Switzerland), according to the manufacturer's instructions. MV2 and LN model medium were used as background controls in each analysis.

Flow Cytometry

Cell suspensions were stained in a 96-well U bottom plate at 4 °C for flow cytometric analysis. Cells were first washed with FACS buffer containing PBS, 0.1% bovine serum albumin (BSA) and 0.05% NaN_3, and stained with a fixable viability dye (eFluor™ 780; Invitrogen; #65-0865-14) for 10 mins at 4 °C. Fc-receptor blocking was performed using 10% normal human serum, and cells were then incubated with directly labelled antibodies. Post-staining, cells were washed two times with FACS buffer and fixed with 2% paraformaldehyde (PFA) (VWR, Radnor, PA, USA) for 10 mins at room temperature (RT). An overview of all antibodies used can be found in Table 1. Samples and single stains on beads were acquired on Aurora 5-laser Flow Cytometer (Cytek; Fremont, CA, USA). Autofluorescence (AF) correction of cells was performed as previously described[37]. Data analysis was conducted using OMIQ (Boston, MA, USA).

Table 1 **Overview of antibodies.** FACS: Flow cytometry, IHC: Immunohistochemistry

Antigen	Label	Clone	Catalog	Assay
ACKR4	BV650	13E11	BD biosciences; 747804	FACS
CD3	PE-Dazzle594	SK7	Biolegend; 344844	FACS
CD4	BUV563	SK3	BD biosciences; 612912	FACS

CD8	cFluor V610	SK1	Cytek biosciences; R7-20241	FACS
CD11c	cFluor BYG710	Bu15	Cytek biosciences; RC-00181	FACS
CD14	cFluor V450	M5E2	Cytek biosciences; R7-20003	FACS
CD19	cFluor R685	HIB19	Cytek biosciences; R7-20117	FACS
CD31	Alexa Fluor 488	WM59	Biolegend; 303109	FACS
CD45	cFluor V547	HI30	Cytek biosciences; R7-20011	FACS
CD45	BV570	HI30	Biolegend; 304034	FACS
MARCO	PE-Cy7	PLK-1	Invitrogen; 25-5447-42	FACS
TNFRSF9	PE	D2Z4Y	Cell signalling; 95663	FACS
PDPN	Alexa Fluor 647	NC-08	Biolegend; 337007	FACS
CD31		JC70A	Dako; m0823	3D imaging / IHC
CD45		2B11 + PD7/26	Dako; GA751	3D imaging
Vimentin	Alexa Fluor 488 / 647	O91D3	Biolegend; 677809/677807	3D imaging
Goat anti-Mouse IgG1	Alexa Fluor 488 / 647	Polyclonal	ThermoFisher; A-21121/A-21240	3D imaging

Immuno-fluorescent and -histochemical staining

The LN-on-chip hydrogel and channels were fixed in the chips by directly adding 4% PFA in PBS (Electron Microscopy Sciences, Hatfield, PA, USA) in PBS for 10 min under flow (± 500 mbar, 30 bpm) followed by 20 mins static at 37°C. Chips were then washed twice with PBS for 10 mins pumping at RT (± 500 mbar, 30 bpm). Hydrogels were then preserved in PBS with 0.02% NaN_3 before antibody staining or paraffin embedding. An overview of all antibodies used can be found in Table 1.
For *in situ* immunofluorescent chip staining, chips were pre-treated with 0.2% Triton in PBS, followed by incubation in the chip with an unconjugated antibody to both the vascular (100 µl) and LN (200 µl) compartment, diluted in 0.2% Triton in PBS. Unconjugated antibodies used were anti-CD31 (clone JC70A, Dako; m0823) and anti-CD45 (clone 2B11 + PD7/26, Dako; GA751). Staining was performed under flow (± 500 mbar, 30 bpm) for 30 mins at RT to ensure complete antibody coverage throughout the microfluidic circuit, then left overnight at 4 °C on a rocker to allow antibody diffusion through the hydrogel. The next day, chips were washed twice with 0.2% Triton in PBS and incubated with a secondary antibody conjugate at RT on a rocker for 2 hours. The secondary antibody conjugate used was goat anti-mouse IgG1 (Alexa Fluor 488/647, polyclonal, ThermoFisher; A-21121/A-21240). Afterwards, a directly labelled antibody, anti-Vimentin (Alexa Fluor 488/647, clone O91D3, Biolegend; 677809/677807) was added to the chip for an overnight incubation at 4 °C on a rocker. Before image acquisition, DAPI (Invitrogen) was added for 1 hour at RT, followed by two washing steps and storage at

4 °C until analysis. Chips were imaged by confocal microscopy using a Nikon AXR (Nikon, Tokyo, Japan). For paraffin embedding, hydrogels were removed from the chip and subsequently dehydrated, embedded in paraffin and cut at 5 µm sections for immuno-histochemical (IHC) analysis. For CD31 staining, sections were deparaffinised and immersed in 10 mM Tris/1 mM EDTA buffer (pH 9.0) for 15 mins at 100°C for antigen retrieval, followed by slowly cooling to RT. Sections were then washed with PBS and stained for 1 hour with anti-CD31 (clone JC70A, Dako; m0823). This was followed by incubation with BrightVision plus Poly-HRP-Anti-Mouse/Rabbit/Rat IgG (Immunologic, VWR International B.V., Breda, the Netherlands) and 3-amino-9-ethylcarbazole (AEC, Sigma-Aldrich) substrate, concluded with a hematoxylin counterstain. Sections were imaged using a Nikon Eclipse 80i microscope (Nikon, Tokyo, Japan) with NIS Elements 4.13 software (Nikon).

Image analysis

Immunofluorescent 3D images were analysed using Imaris (v10.1.0; Oxford Instruments, Oxfordshire, UK). Firstly, the vessel surface was rendered with machine learning segmentation (10 µm smoothness detail) based on DAPI for models without a LEC vessel, and Vimentin for models with a LEC vessel. Subsequently, spots were generated on $DAPI^{+}CD45^{+}$ cells to identify immune cells (4.5 µm approximate diameter). A cell cluster was defined as one cell with nine cell neighbours within an average distance of 20 µm between each cell. Then, the average distance of immune cells or clusters to the vessel surface was calculated.

Cytokine/Chemokine analysis

Chip supernatants were collected separately from the vasculature and hydrogel compartment and analysed for the presence of cytokines and chemokines. This was performed using either a cytokine bead array (CBA; Custom LEGENDplex panel, BioLegend) or an enzyme-linked immunosorbent assay (ELISA) for CCL21 (#ab193759, Abcam, Cambridge, UK), according to the manufacturer's instructions. CBA acquisition was performed on AttuneNxT (Thermofisher, Waltham, MA, USA) and protein concentrations were determined using the LEGENDplex Data Analysis Software Suite (BioLegend).

Statistical analysis

All data are presented as mean ± standard error of the mean (SEM). The number of human LN donors is described in each figure legend. Statistical analysis was conducted using GraphPad Prism 9 software version 9.5.1 (GraphPad Software Inc., La Jolla, CA). Statistical tests are indicated in figure legends. Differences were significant when $P < 0.05$.

Results

Development of metabolically stable LN-on-chip with integrated lymphatics

A schematic construction of the LN-on-chip with integrated lymphatics is illustrated in Figure 1. Briefly, the LN hydrogel model[23] was first cast into the LN compartment of the HUMIMIC Chip2, after which the hollow channel of the sacrificial printed structure was seeded either with or without donor-matched LECs. These two biological conditions allowed for studying the influence of LECs on the LN-on-chip microenvironment over seven days under flow. Conditioned media samples were collected from both the circulating lymphatic vasculature and above the LN hydrogel.

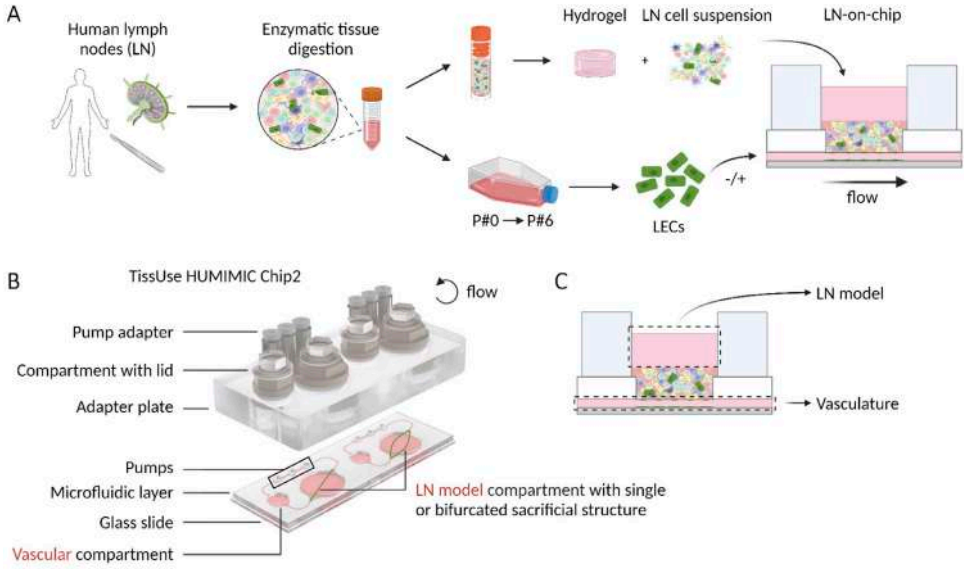

Fig. 1 - Generation of a vascularised lymph node model on-chip. (A) Procedure to isolate cells from a human LN. After enzymatic digestion, the LN cell suspension was cryopreserved and donor-matched LECs amplified until passage 6. Subsequently, the LN cell suspension was thawed, incorporated in a collagen/fibrin hydrogel, and added to a chip platform. Mimicking lymphatics, LECs lined a perfused channel underneath the LN model to generate a vascularised LN-on-chip. LN-on-chip models were compared with either an empty vessel or a vessel lined with LECs. **(B)** Explosion view of the HUMIMIC Chip2 chip platform used in this study. In the LN compartment, a sacrificial structure was incorporated to create a lymphatic channel containing LECs underneath the LN hydrogel. **(C)** Sampling in the vascular compartment and the LN compartment allows to separate circulating medium in the vasculature and static medium on top of the LN model. Created with BioRender.com

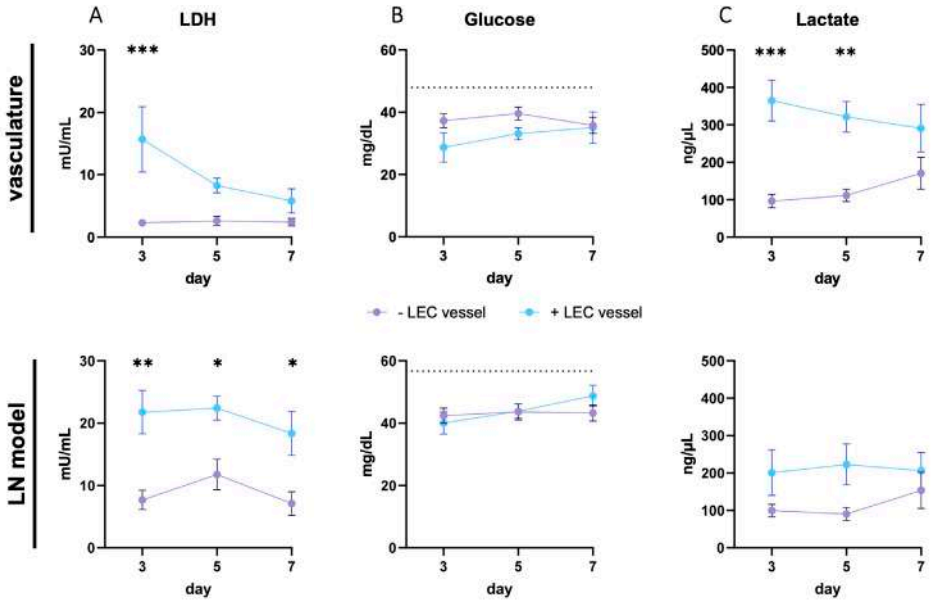

Fig. 2 - LN-on-chip is viable and metabolically stable for 7 days with and without a LEC vessel. (A) Lactate dehydrogenase (LDH), **(B)** Glucose (with initial levels from culture media indicated as dotted line), **(C)** Lactate concentrations in the culture medium, measured at day 3, 5 and 7 during the LN-on-chip culture period. Medium was sampled either from the perfused vasculature (upper graphs) or on top of the LN model (lower graphs). Shapes represent different donors as mean ± SEM; n = 4 independent experiments, each performed with intra-experimental duplicates. Significance indicated between ± LEC vessel per day with ordinary two-way ANOVA (*$p < 0.05$, **$p < 0.01$, ***$p < 0.001$).

To determine whether the LN-on-chip was viable and metabolically active, LDH, glucose and lactate concentrations were measured in the supernatant from both compartments at day three, five and seven of culture. A higher concentration of LDH was measured in both chip compartments at day three in the LN-on-chips with a LEC vessel, which then decreased over the seven days in the vasculature (Figure 2A and S1A). Glucose consumption from the initial cell culture medium remained similar for both conditions, with no clear changes over time (Figure 2B and S1B). More lactate was secreted in the models with a LEC vessel compared to without, which was higher in the vasculature compartment compared to the LN model (Figure 2C and S1C).
As such, these factors collectively showed that, within a one-week culture period under flow, a stable metabolic profile of a LN-on-chip with an integrated LEC vessel was generated.

LECs in LN-on-chip physiologically represent LN lymphatics

Next, to determine whether the unique properties of LN LECs were recapitulated in the LN model, morphology and phenotype of the LECs were characterised within the LN-on-chip. Upon confocal imaging of the endothelialised LN models, a uniform adherence of LECs along the inner layer of the vessel wall and a visibly distinct lumen structure was observed from CD31 and Vimentin staining (Figure 3A and 3B). These LN-derived LECs have also been previously described to express VE-cadherin$^+$

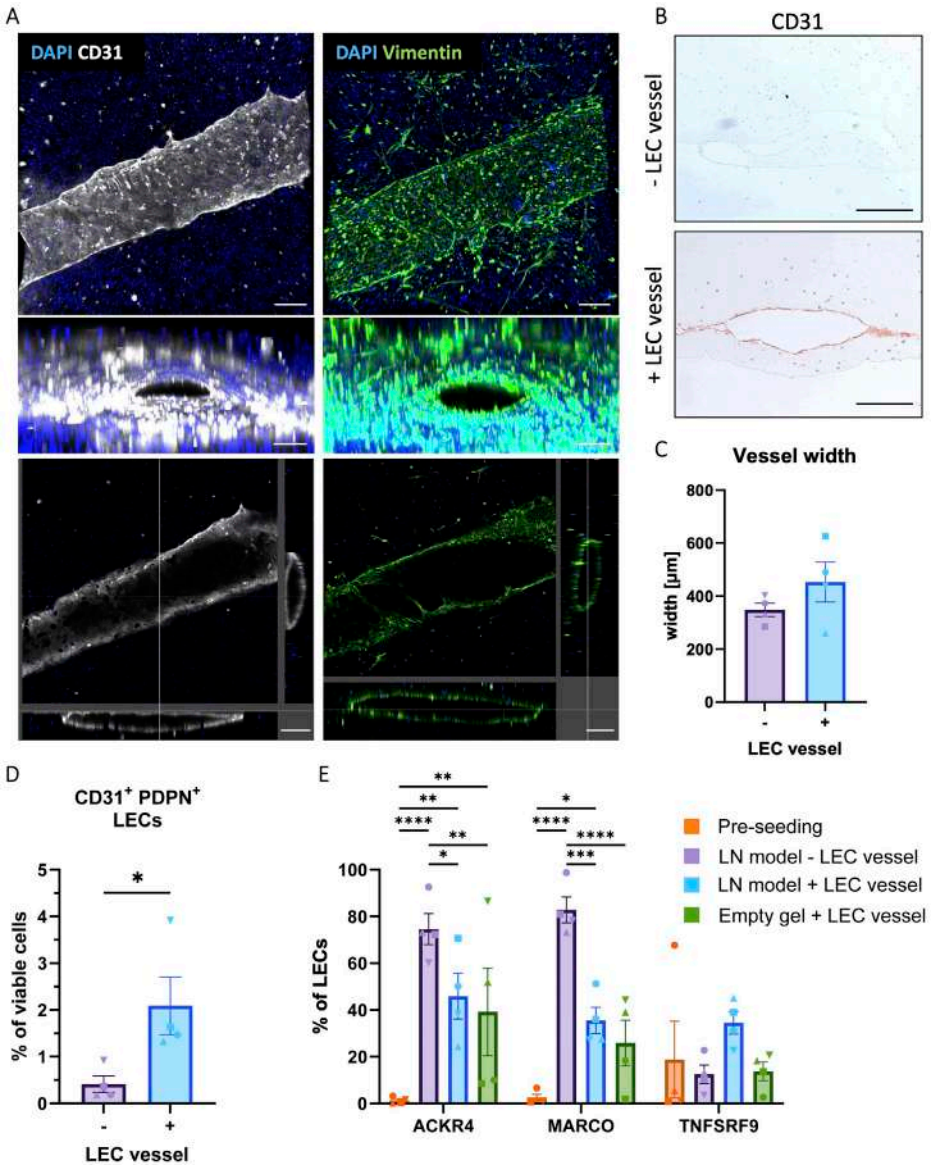

Fig. 3 - Lymphatic endothelial cells physiologically represent LN lymphatics on-chip. (A) LEC vessel staining for DAPI, Vimentin and CD31. Depicted are z-stacks with a top view and a cross section of the channel and a section view, indicating xy-, xz- and yz-cross sections. Scale bars: 200 µm**. (B)** Immunohistochemical staining for CD31, images -/+ LEC vessel show cross-sectional area of channel. Scale bars: 100 µm. **(C)** Width of the channel in the LN-on-chip model without or with (-/+) a LEC vessel. **(D)** Proportion of LECs in the LN-on-chip model -/+ LEC vessel. **(E)** Detailed characterisation for SCS ceiling (ACKR4), medullary (MARCO) and SCS floor (TNFSRF9) LEC markers before seeding in the chip, and after a seven-day culture period on-chip with LN model -/+ LEC vessel or + LEC vessel with an empty hydrogel. Representative gating strategy and histogram overlays for these three markers found in (Figure S2C and S2D). Shapes represent different donors and columns mean ± SEM; n = 4 independent experiments. Ordinary two-way ANOVA (*$p < 0.05$, **$p < 0.01$, ***$p < 0.001$, ****$p < 0.0001$).

tight junctions and permeable integrity when in a similar vessel-like setting[38]. The lumen structure remained present in vessels without LECs (Figure 3B and S2A), indicating vessel stability through the LN model regardless of LEC endothelialisation. The vessel width was slightly larger with LECs (453 µm ± 76 µm) compared to without LECs (348 µm ± 26 µm) (Figure 3C), with both mean measurements deviating above and below the initial 420 µm vessel width reported after printing[34], respectively.
The phenotype of the LECs from the LN-on-chip model was further investigated after digestion of the LN hydrogel to a single cell suspension using flow cytometry. Prior to LEC-endothelisation of LN-on-chip model, an average purity of 95% LECs across donors from *ex vivo* cultures was confirmed based on CD31 and podoplanin (PDPN) expression (Figure S2B). Within the LN-on-chip hydrogel model with an integrated LEC vessel, $CD31^+PDPN^+$ LECs were identified as constituting to approximately 2% of the total viable cells (Figure 3D). In the absence of a LEC vessel, 0.5% of total cells in the hydrogel were LECs, which is the physiological-like proportion within the native LN cell suspension[35].
To further characterise the LECs in the LN-on-chip model, we analysed the expression of specific markers associated with distinct LEC subsets found in human LNs, i.e. MARCO, ACKR4 and TNFSRF9[10]. Interestingly, compared to the LEC phenotype prior to endothelisation from *ex vivo* cultures, significantly more LECs expressed ACKR4 and MARCO observed in both LN-on-chip models with and without a LEC vessel (Figure 3E). It is worth noting that the small number of LECs in the total cell suspension from the LN model without a LEC vessel (0.5% in Figure 3D) had the highest expression of both markers.
To investigate whether expression of these LEC markers was due to flow and/or presence of immune cells within the LN model, an empty hydrogel with a LEC vessel was generated to simulate a flow-only condition. In the absence of the LN cell suspension, most LECs lost their $CD31^+PDPN^+$ phenotype (Figure S2B), but those remaining as LECs still expressed higher ACKR4 compared to cultured LECs (Figure 3E). No changes to TNFSRF9 expression were seen on LECs across all conditions.
In summary, these results highlight an intact LEC vessel in a LN model and demonstrate a more physiological LEC phenotype on-chip, with characteristics resembling SCS ceiling and medullary LECs.

LECs preserve B cells within LN-on-chip

To determine the composition of the native immune cells within the LN-on-chip, and whether this was influenced with the integration of a LEC vessel, general immune cell populations were phenotyped by flow cytometry analysis (Figure S2C). Most immune cells in the LN-on-chip models were found to be T- and B-lymphocytes, with a degree of donor heterogeneity (Figure 4A). T cells were comprised of more $CD4^+$ than $CD8^+$ T cells (Figure 4B), and the percentage of myeloid cells was 1% and 0.5% (-/+ vessel, respectively) of the overall immune cells. While the presence of the LEC vessel did not significantly alter the composition of immune cells, it did significantly increase the total number of immune cells after the seven-day culture (Figure 4C). This was most striking for the B cells, evident from the respective fold change increase compared to the same donors without a LEC vessel (Figure 4C). Henceforth, this shows that immune cell populations, and especially B cells, increase in number with the existence of a LEC-populated lymphatic vessel, indicating a successful generation of an immunocompetent LN-on-chip model.

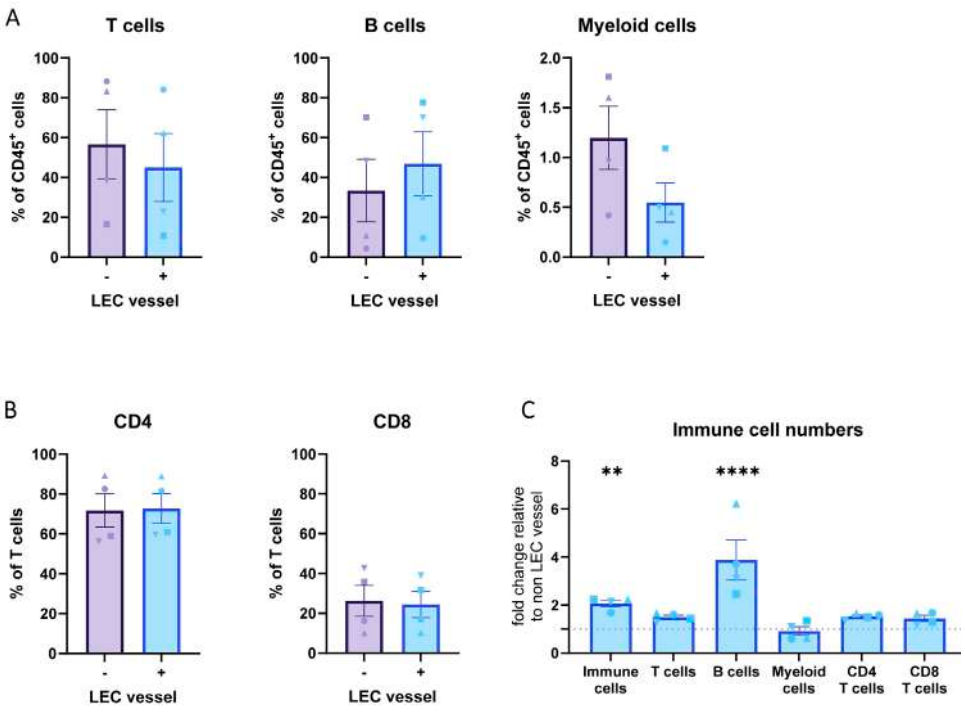

Fig. 4 - Consistent immune cell populations in LN-on-chip, independent of LEC vessel presence. A. Populations of $CD3^+$ T cells, $CD20^+$ B cells and $CD11c^+CD14^+$ myeloid cells within the $CD45^+$ immune cells after a 7 day culture on-chip -/+ LEC vessel. **(B)** Composition % of CD4 and CD8 T cells -/+ LEC vessel. **(C)** Fold change in number of immune cells in LN-on-chip model + LEC vessel, relative to - LEC vessel set at 1. Shapes represent different donors and columns mean ± SEM; n = 4 independent experiments. Ordinary two-way ANOVA (**$p < 0.01$, ****$p < 0.0001$).

LECs induce LN-relevant homeostatic factors within LN-on-chip

Since the ability of immune cell function in the LN requires LEC-secreted survival and migratory signals[7], cytokine and chemokine analysis of the LN-on-chip with and without a LEC vessel was performed at day three, five and seven from both the vasculature and the LN model compartment. LN-on-chips with a LEC vessel revealed an increased secretion of the survival cytokine IL-7 in both compartments on day three and five in the LN model (Figure 5A). The total cumulative secretion of IL-7 throughout the system across one-week was significantly higher in the LN model with a LEC vessel (Figure 5B). Higher concentrations of CCL21 were found in the vasculature at day three within LN-on-chip with a LEC vessel but decreased over time. Total CCL21 secretion was higher in the vasculature with a LEC vessel than no LEC vessel. Interestingly, homeostatic LN-relevant factor CXC motif chemokine ligand 12 (CXCL12) was highest on day five in the LN model with a LEC vessel, and total CXCL12 secretion was significantly more pronounced in the LN model with a LEC vessel compared to the vasculature and the LN model compartment without a LEC vessel. The B cell chemoattractant CXCL13 was found

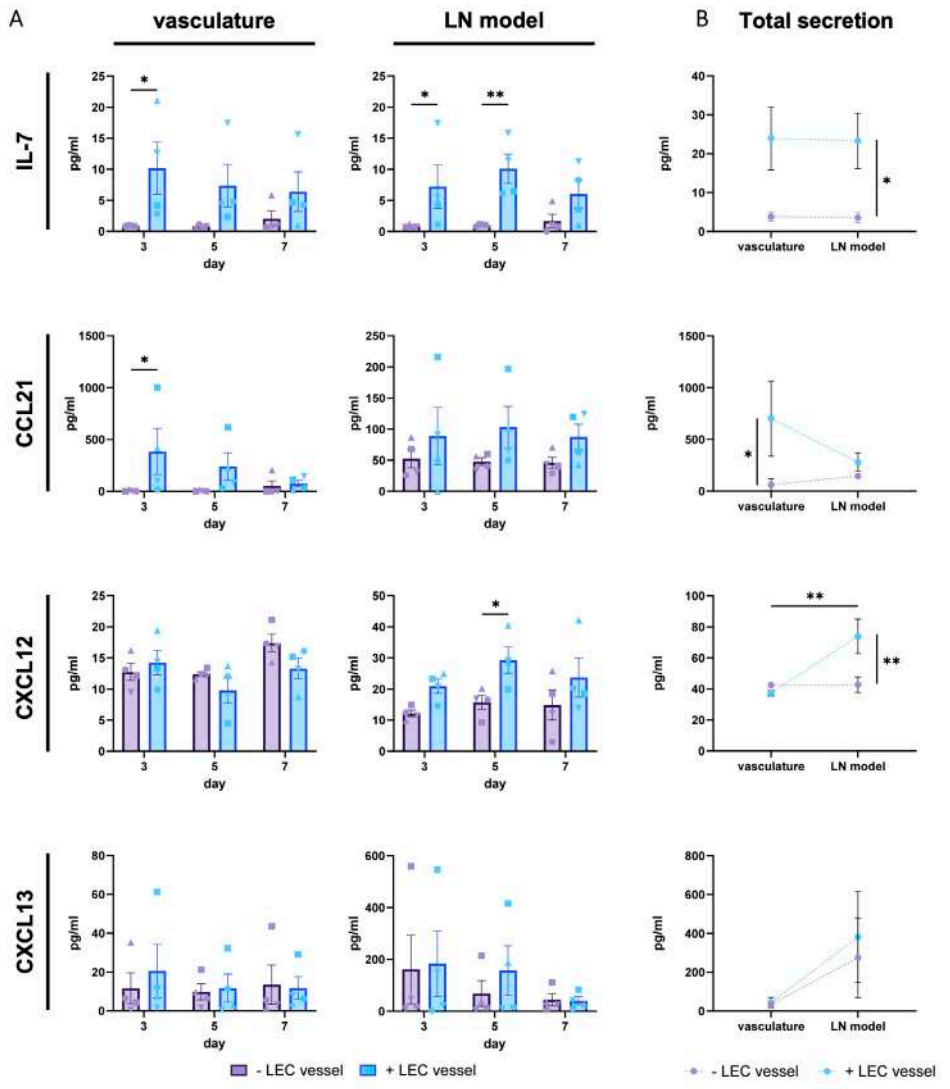

Fig. 5 - Addition of a LEC vessel results in increased IL-7 and CCL21 secretion in the vasculature. (A) LN-specific cytokine secretion**,** IL-7, CCL21, CXCL12 and CXCL13, into the vasculature (left graphs) and hydrogel (right graphs) supernatant of the chip throughout the culture period at day 3, 5 and 7. Compared are empty hydrogel channels with a lymphatic vessel. **(B)** Total cumulative cytokine secretion throughout the 7-day LN-on-chip culture period. Shapes represent different donors and columns mean ± SEM; n = 4 independent experiments of pooled intra-experimental duplicates. Significance of total secretion indicated between ± LEC vessel per compartment (vertical line) or between compartments + LEC vessel (horizontal line), with ordinary two-way ANOVA (*$p < 0.05$, **$p < 0.01$).

at a higher concentration in the LN model compartment compared to the vasculature, but there was no direct LEC-vessel influence.
This indicates that an integrated LEC vessel not only supports the production of survival and migratory signals in a LN-on-chip, but also the establishes compartmentalised microenvironments of lymphatics and LN, related to specific LN physiology.

LECs promote closer proximities of immune cell and cluster formation in LN-on-chip

LNs are structured to promote immune cell interactions, which is essential for optimal immune responses[39,40]. Therefore, the spatial distribution of immune cells in our LN-on-chip models around the lymphatic vessel was investigated. Images were acquired around the middle of the LN model, with a given field of view accounting for a fraction of the whole LN compartment. Here, many $CD45^+$ immune cells were found distributed throughout the model (Figure 6A), irrespective of a present LEC vessel (Figure S3A), with some immune cells observed in close vicinity to the lymphatic vessel in certain areas. Quantification revealed that the total number of immune cells in the whole field of view was indifferent between -/+ LEC vessel, yet the presence of a LEC vessel increased the total number of immune cells within < 200 µm proximity of the lymphatic vessel in all donors but one (Figure 6B). Immune cells found grouped together were further defined as an immune cell cluster, with the criteria for one immune cell to have nine neighbours within an average cell distance of 20 µm, that includes overlapping neighbours (Figure 6C, Figure S3B-D). The LN-on-chips with a LEC vessel provoked a higher abundance of immune cells clusters in all donors, and resulted in shorter distances of these clusters to the vessel surface in three out of four donors (Figure 6D).
Therefore, the addition of a LEC vessel seemed to benefit the organisation of the immune cells in proximity to each other and towards the lymphatics, thus in position for optimal immune activity.

Discussion

The *in vitro* study of systemic immunology requires physiologically relevant human LN models that contain LNSCs and recapitulate organ characteristics[26]. Here we used a commercially available chip system, the HUMIMIC Chip2 24-well with a sacrificial structure from TissUse, to generate a LN-on-chip model with integrated lymphatics. This was achieved by using donor-matched LECs to endothelialise a hollow channel through a LN hydrogel containing a native LN cell suspension. A one-week culture under flow displayed a stable metabolic profile, and LECs added to the LN-on-chip exhibited morphological and phenotypical features that were representative of LN LECs. In addition, LN-on-chip models with a LEC vessel provided the necessary components for LN functioning and immune cell interactions, such as compartmentalised migratory signals, survival factors and immune cell clusters in closer proximity to the lymphatic vessel.
The integration of vascularised organ models is currently a major target within the MPS field[41]. This allows for the delivery of nutrients, homeostatic factors, metabolites and removal of waste products, as well as mimicking processes such as cell trafficking, pharmacodynamics and tissue crosstalk[42,43].

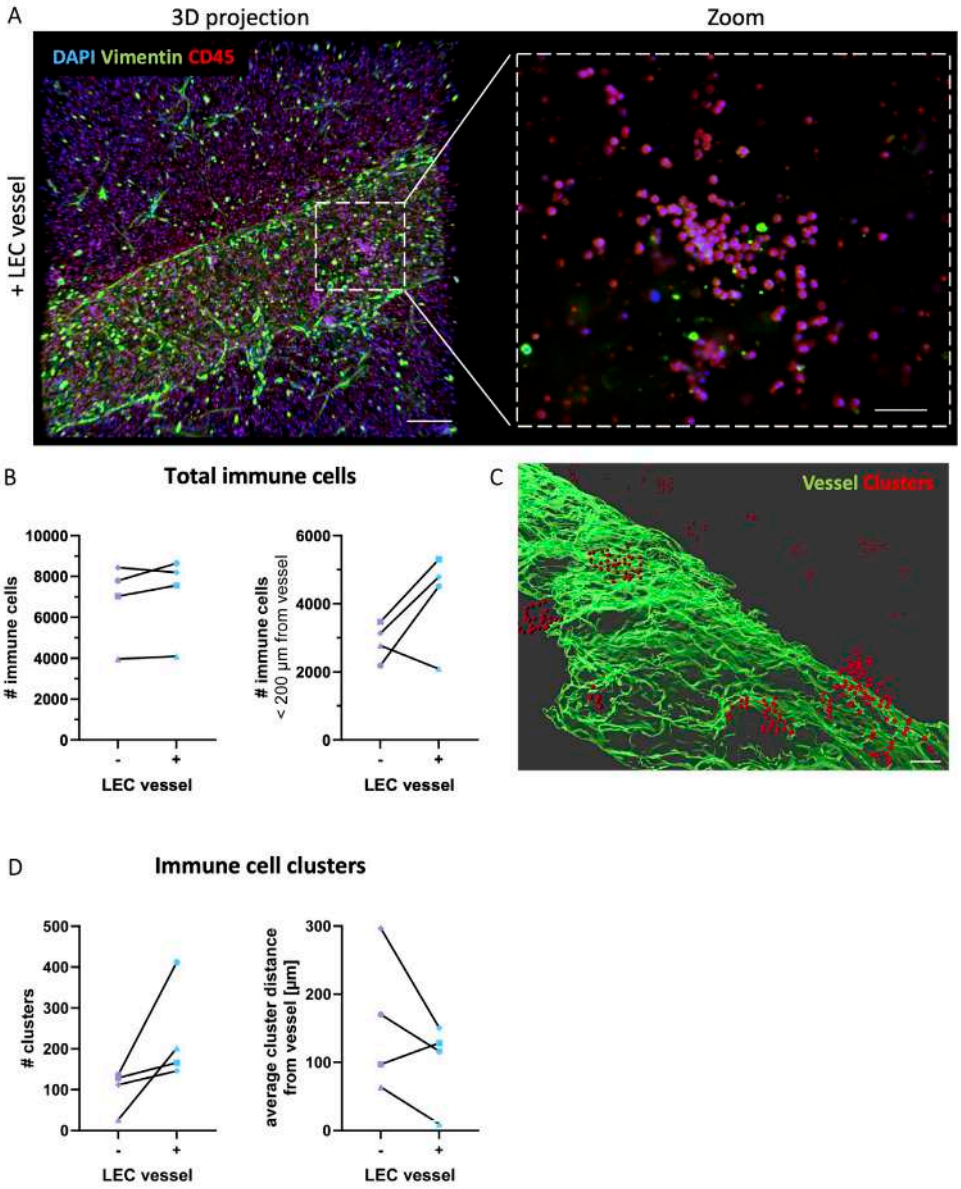

Fig. 6 - Vascularisation with LECs promotes immune cell clustering. (A) Staining of the LN-on-chip at day 7 for CD45 (red), vimentin (green) and DAPI (blue) shown as 3D projections + LEC vessel. Zoom magnification visualises immune cell clusters in a single z-plane. Scale bars: 200 µm in overviews, 50 µm in magnification. **(B)** Quantification of the total immune cells and within 200 µm of the vessel. **(C)** Surface rendering for the LEC vessel (green) and clustered immune cells (red) in close proximity of the vessel. Scale bar: 70 µm. **(D)** Quantified clustered immune cells and their shortest distance to the vessel surface. Details are shown in Figure S3.

Likewise, it can be used to investigate disease progression, such as tumour metastasis[44] and EC biology under flow[36,45,46]. Modelling vascularisation has been made possible through various microfabrication techniques, 3D-bioprinting, sacrificial moulds or by inducing cell self-organisation[47]. Regarding the function of the LN, numerous waterfall-like and blind-ended lymphatic channels are intricated through the LN parenchyma to filter the incoming lymph[7,48], which makes it difficult to accurately model LN lymphatics *in vitro*[49]. This complexity has hindered the development of immunocompetent human LN models since currently they do not address the inclusion of primary LECs and vasculature integration. Here, we began with mimicking lymphatic vasculature in a LN-on-chip model with a LEC-populated channel. As such, even without applying any stimuli to induce immune activity, our data provides evidence that inclusion of a LEC-lined vessel in the LN-on-chip model has a substantial effect on the LN microenvironment during homeostasis.

The organotypic LN model used in this study was comprised of a LN-derived cell suspension which contained both native immune and non-immune cells, such as FRCs and LECs[35]. In contrast to other studies which use PBMCs[27,28], tonsils[29,33] or cell lines[30,31,32,38] to model a LN-on-chip, we incorporated the cell suspension of native LNs. The static culture of the organotypic LN model was characterised previously by our group[23], which revealed the benefit of further enrichment with autologous FRCs for viability of lymphocyte subsets, and presence of survival and homeostatic factors. For this LN-on-chip study, the LN model was not further enriched with extra FRCs due to their contractile properties in hydrogel environments[50]. This decision aimed to prevent remodelling or disruption of the lymphatic vessel during the culture period, thus also limiting the culture length to one week. Henceforth, future studies should be aimed at including cultured FRCs and preventing shrinkage through use of other ECM-scaffolds[24,51,52]. Nevertheless, even without FRC enrichment, native immune cells were still observed to be present and maintained in a viable LN environment for the entire culture period, supported by the presence of LECs.

The presence of the lymphatic vessel proved valuable for lymphocytes, particularly for B cells since more cells were found in the hydrogel of the LN-on-chip. The high concentrations of B cell-related factors CXCL12 and CXCL13 most likely account for the maintenance of B cells, which were also originally found in our static LN models along with IL-6, a key B cell survival cytokine[23]. In parallel, the detection of IL-7 in the LEC-populated LN-on-chips was an interesting finding given its previous absence in our static LN models[23]. Both IL-7 and CCL21 are produced by LECs, but while CCL21 is highly enriched within the vasculature, the levels of IL-7 are comparable in both compartments. While IL-7 is most commonly known for naïve T cell survival[53,54], it can also influence B cells during LN organogenesis[55], as well as their development[56] and maturation[57]. The addition of LECs resulted in more CCL21 secreted into the system, with low levels of CCL21 found in the LN model which was also previously absent in static cultures. Flow has been reported to induce CCL21 expression in cultured FRCs[25], yet it remains to be determined here if LEC secretion of CCL21 is enhanced by flow. However, this would require testing in a different experimental set-up, as it is not feasible to maintain the LN-on-chip under static conditions due to rapid stagnation of culture medium, which reduces cell viability. Both IL-7 and CCL21 are crucial for optimal LN functioning *in vivo*, as knockout mouse models of these factors demonstrated severe depletion of lymphocytes and immune malfunctioning

under antigen challenge[58,59,60]. Furthermore, other LN-on-chip models lacking LECs failed to capture presence of IL-7 and CCL21 in the system[28,30,32]. Therefore, the emergence of these factors associated with the normal physiology of functional LNs, after the integration of a LEC vessel into a LN-on-chip, indicates an improved *in vitro* LN model to generate a supportive microenvironment for lymphocyte survival and potential migration ability.

Additionally, LECs promoted the clustering of immune cells in close proximity to the lymphatic vessel in the LN-on-chip, another physiological attribute for LN functioning[39,40]. In the native LN, naïve lymphocytes routinely survey soluble antigens or incoming APCs from afferent lymphatics. This requires numerous immune cell interactions for cognate antigen matching, so therefore the increased abundance of immune clusters facilitates such interactions and thus antigen-specific recognition by lymphocytes close to the lymphatic vessel. This is particularly relevant for *in vitro* model functionality in future experiments, as cell density can enhance the likelihood of antigen-specific immune responses[61]. Similar lymphocyte clustering has been observed with PBMCs in LN-on-chips, where flow was found to induce lymphocyte follicle formation and germinal centre characteristics without immune activation[27,28]. In our model, these immune cell clusters represent an early setting necessary for immune communication and activation. Details of lymphocyte characterisation and uncovering the mechanisms behind cluster formation, such as investigating chemoattractant-rich zones or lymphatic vessel hotspots of transendothelial migration[62,63], could be investigated further with longer culture periods.

The LECs in the LN-on-chip model displayed similar characteristics to LN lymphatics by retaining their $CD31^{+}PDPN^{+}$ phenotype and upregulating specific LN subset markers, such as ACKR4 for SCS ceiling LECs and MARCO for medullary LECs[10]. Since ACKR4 acts as a decoy receptor for CCL21 in the SCS ceiling LECs, its action is to generate a CCL21 gradient over the floor LECs, allowing DC entry into the LN parenchyma[5,6]. The function of $MARCO^{+}$ LECs in the LN medullary region are yet to be elucidated, but since MARCO recognises a plethora of ligands, it is hypothesised to crosstalk with macrophages for neutrophil recruitment[10]. It is unclear whether all the identified LEC subsets are present after enzymatic digestion of the LN tissue, but it was remarkable that the LECs regained LN-specific subset specifications when introduced in a LN-like microenvironmental setting. After culturing an endothelialised empty hydrogel-on-chip, in place of the LN model, most LECs lost their $CD31^{+}PDPN^{+}$ phenotype, indicating a possible mutual crosstalk between both stromal and hematopoietic cell types. In the absence of the LN model, flow alone could induce ACKR4 expression on LECs, which has been previously reported[64,65]. However, this may suggest that immune cell presence is additionally required for upregulation of MARCO, as medullary LECs are located in a region that is naturally rich in immune cells. Investigation into LEC culturing techniques may allow a future tailored approach to include specific LEC subsets into the LN-on-chip.

The choice in using the HUMIMIC Chip2 system to develop the LN-on-chip was due to the flexible ability to integrate a hydrogel-based organotypic model incorporating a customisable sacrificial printed structure[34]. In addition, the platform is versatile for use as a MOC, allowing medium to recirculate in a closed loop. This resulted in compartmentalised microenvironments, separating the circulating vasculature media and the media above the LN hydrogel. The measurements of biomarkers associated

with cellular health, such as glucose, lactate and LDH, are commonly used within the OoC field[66]. Detection of these markers across the culture period indicated the viability and metabolic activity of cells within the chip. The LN-on-chip models with a LEC vessel had higher rates of LDH production, glucose consumption and lactate secretion compared to absent LEC vessels, indicating greater metabolic activity or higher concentrations with a greater cell presence. Across the seven days, all values decreased or plateaued between conditions, implying stable metabolic models.

A compartmentalised difference of soluble factors was also observed for cytokines and chemokines. The addition of the LEC vessel to the LN-on-chip model resulted in IL-7 increase in both compartments, CCL21 abundance in only the circulating vasculature compartment and more CXCL12 secretion specific to the LN model compartment. Also, both with and without the LEC vessel, CXCL13 was found exclusively in the LN model compartment. It is worth noting that with this method of extrinsic sampling, it is unknown whether such factors are present in excess or absent due to cell consumption or confinement within the hydrogel. However, advancements of new tissue engineering technologies may allow the sampling of the hydrogel microenvironment *in situ*[67]. Nonetheless, it is interesting that such signalling molecules stay local to their physiological LN-microenvironment, e.g. CCL21 in the vasculature and CXCL13 in the LN. Moreover, this becomes particularly relevant when connecting a second organotypic model to the LN model in a MOC. It would be valuable to explore the dynamic evolutions of these soluble factors over longer culture periods between the different compartments. As such, this LN-on-chip with integrated lymphatics offers a versatile platform that can be manipulated for future experimental set-ups. One such example is the potential use of BECs instead of LECs to simulate blood vasculature. More so, this could also be used for functional experiments, including the migration of immune cells via the lymph or blood vasculature circuit to mimic incoming immune cell trafficking, as well as delivering soluble antigens or vaccines/immunotherapies to generate a local LN immune response. The current status of the LN-on-chip in terms of displaying a migratory-like LN microenvironment would indicate suitability for such experiments. This in turn will also allow the opportunity to generate a MOC to recapitulate a lymph-draining organ *in vitro*[26]. Integration of other organ models, such as skin and intestine, into a MOC with a LN model would allow the study of cross-organ communication and possible mechanisms behind immune-related disease pathophysiology. For example, immunocompetent models of healthy reconstructed human skin (RhS) are well-established within OoC systems[68,69,70]. Given the accurate representation of melanoma in RhS[71], these models could be implemented into a skin-draining LN-on-chip to study tumour metastasis and anti-tumour immunity.

There are certain limitations that exist with this present study. Firstly, this method is low-throughput with scarce donor material, which would make it challenging to scale up for high-throughput experiments, which is a benchmark for the OoC and MPS field. Additionally, the one-week OoC culture duration falls short of the recommended 28-day period for translational research, based on the organisation for economic co-operation and development (OECD) guidelines for animal tests[72,73]. As earlier alluded to, the nature of hydrogel contraction is a limiting factor for this and could be overcome by using other ECM-scaffolds for the LN model. Also, some of the biological parameters are less physiological compared to native tissue. For example, restrictions with vessel printing resolutions means the 450 µm average LEC vessel width is more comparable to the diameter of small veins and arteries[74], well-above

native lymphatic measurements[75]. However, during an immune response, these diameters rapidly change with LN swelling due to the influx of immune cells[76].
In summary, this human LN-on-chip with integrated lymphatics highlights the benefits of including LECs to generate a more physiological LN model. As such, this can be used and further advanced to recapitulate systemic human immunology.

Acknowledgements

The authors would like to thank and acknowledge the expert help of the Microscopy & Cytometry Core Facility (location Vrije Universiteit Amsterdam). We thank Kim Ober and Dr. Monique Verstegen (Erasmus MC, Rotterdam, The Netherlands) for sample logistics and Dr. Radjesh Bisoendial (Maasstad Hospital, Rotterdam, The Netherlands) for LEC-culturing recommendations. The presented work was funded by the European Union's Horizon 2020 research and innovation programme under grant agreement No. 847551 ARCAID. JJ is supported by SMART Organ-on-Chip consortium, NWO-TTW Perspective Programme of the Dutch Research Council (NWO; project no. P19-03). CMdW is supported by Cancer Center Amsterdam (Grant No. CCA2019-9-57 and CCA2020-9-73) and the Dutch Cancer Foundation (KWF; Young Investigator Grant no. 2022-4 EXPL/14641). LJWvdL is supported by funding from the Convergence Health Technology Flagship grant (Organ Transplantation). JJK is supported by the LymphChip consortium, NWA-ORC programme of the Dutch Research Council (NWO; project no. 1292.19.019).

CRediT authorship contribution statement

Andrew I. Morrison: Conceptualisation, Methodology, Investigation, Validation, Software, Data curation, Writing-original draft preparation, Writing-review and editing. **Jonas Jäger:** Methodology, Investigation, Validation, Software, Data curation, Writing-review and editing. **Charlotte M. de Winde:** Writing-review and editing, Supervision. **Henk P. Roest:** Resources. **Luc J.W. van der Laan:** Resources, Writing-review and editing. **Susan Gibbs:** Methodology, Writing-review and editing, Supervision, Funding acquisition. **Jasper J. Koning:** Methodology, Writing-review and editing, Supervision. **Reina E. Mebius:** Conceptualisation, Methodology, Writing-review and editing, Supervision, Funding acquisition

References

[1] Krishnamurty AT, Turley SJ. Lymph node stromal cells: cartographers of the immune system. Nat Immunol. 2020;21(4):369-80.

[2] Bajenoff M, Egen JG, Koo LY, Laugier JP, Brau F, Glaichenhaus N, et al. Stromal cell networks regulate lymphocyte entry, migration, and territoriality in lymph nodes. Immunity. 2006;25(6):989-1001.

[3] Li L, Wu J, Abdi R, Jewell CM, Bromberg JS. Lymph node fibroblastic reticular cells steer immune responses. Trends Immunol. 2021;42(8):723-34.

[4] Weber M, Hauschild R, Schwarz J, Moussion C, de Vries I, Legler DF, et al. Interstitial dendritic cell guidance by haptotactic chemokine gradients. Science. 2013;339(6117):328-32.

[5] Ulvmar MH, Werth K, Braun A, Kelay P, Hub E, Eller K, et al. The atypical chemokine receptor CCRL1 shapes functional CCL21 gradients in lymph nodes. Nat Immunol. 2014;15(7):623-30.

[6] Bastow CR, Bunting MD, Kara EE, McKenzie DR, Caon A, Devi S, et al. Scavenging of soluble and immobilized CCL21 by ACKR4 regulates peripheral dendritic cell emigration. Proc Natl Acad Sci U S A. 2021;118(17).

[7] Jalkanen S, Salmi M. Lymphatic endothelial cells of the lymph node. Nat Rev Immunol. 2020;20(9):566-78.

[8] Qu C, Edwards EW, Tacke F, Angeli V, Llodra J, Sanchez-Schmitz G, et al. Role of CCR8 and other chemokine pathways in the migration of monocyte-derived dendritic cells to lymph nodes. J Exp Med. 2004;200(10):1231-41.

[9] Luther SA, Bidgol A, Hargreaves DC, Schmidt A, Xu Y, Paniyadi J, et al. Differing activities of homeostatic chemokines CCL19, CCL21, and CXCL12 in lymphocyte and dendritic cell recruitment and lymphoid neogenesis. J Immunol. 2002;169(1):424-33.

[10] Takeda A, Hollmen M, Dermadi D, Pan J, Brulois KF, Kaukonen R, et al. Single-Cell Survey of Human Lymphatics Unveils Marked Endothelial Cell Heterogeneity and Mechanisms of Homing for Neutrophils. Immunity. 2019;51(3):561-72 e5.

[11] Petrova TV, Koh GY. Organ-specific lymphatic vasculature: From development to pathophysiology. J Exp Med. 2018;215(1):35-49.

[12] Malhotra D, Fletcher AL, Astarita J, Lukacs-Kornek V, Tayalia P, Gonzalez SF, et al. Transcriptional profiling of stroma from inflamed and resting lymph nodes defines immunological hallmarks. Nat Immunol. 2012;13(5):499-510.

[13] Hara T, Shitara S, Imai K, Miyachi H, Kitano S, Yao H, et al. Identification of IL-7-producing cells in primary and secondary lymphoid organs using IL-7-GFP knock-in mice. J Immunol. 2012;189(4):1577-84.

[14] Kahari L, Fair-Makela R, Auvinen K, Rantakari P, Jalkanen S, Ivaska J, et al. Transcytosis route mediates rapid delivery of intact antibodies to draining lymph nodes. J Clin Invest. 2019;129(8):3086-102.

[15] Cohen JN, Guidi CJ, Tewalt EF, Qiao H, Rouhani SJ, Ruddell A, et al. Lymph node-resident lymphatic endothelial cells mediate peripheral tolerance via Aire-independent direct antigen presentation. J Exp Med. 2010;207(4):681-8.

[16] Fletcher AL, Lukacs-Kornek V, Reynoso ED, Pinner SE, Bellemare-Pelletier A, Curry MS, et al. Lymph node fibroblastic reticular cells directly present peripheral tissue antigen under steady-state and inflammatory conditions. J Exp Med. 2010;207(4):689-97.

[17] Marx U, Akabane T, Andersson TB, Baker E, Beilmann M, Beken S, et al. Biology-inspired microphysiological systems to advance patient benefit and animal welfare in drug development. ALTEX. 2020;37(3):365-94.

[18] Langhans SA. Three-Dimensional in Vitro Cell Culture Models in Drug Discovery and Drug Repositioning. Front Pharmacol. 2018;9:6.

[19] Wagar LE, Salahudeen A, Constantz CM, Wendel BS, Lyons MM, Mallajosyula V, et al. Modeling human adaptive immune responses with tonsil organoids. Nat Med. 2021;27(1):125-35.

[20] Kastenschmidt JM, Schroers-Martin JG, Sworder BJ, Sureshchandra S, Khodadoust MS, Liu CL, et

al. A human lymphoma organoid model for evaluating and targeting the follicular lymphoma tumor immune microenvironment. Cell Stem Cell. 2024;31(3):410-20 e4.

[21] Kastenschmidt JM, Sureshchandra S, Jain A, Hernandez-Davies JE, de Assis R, Wagoner ZW, et al. Influenza vaccine format mediates distinct cellular and antibody responses in human immune organoids. Immunity. 2023;56(8):1910-26 e7.

[22] Morrison AI, Mikula AM, Spiekstra SW, de Kok M, Affandi AJ, Roest HP, et al. An Organotypic Human Lymph Node Model Reveals the Importance of Fibroblastic Reticular Cells for Dendritic Cell Function. Tissue Eng Regen Med. 2024;21(3):455-71.

[23] Morrison AI, Kuipers JE, Roest HP, van der Laan LJW, de Winde CM, Koning JJ, et al. Functional organotypic human lymph node model with native immune cells benefits from fibroblastic reticular cell enrichment. Sci Rep. 2025;15(1):12233.

[24] Braham MVJ, van Binnendijk RS, Buisman AM, Mebius RE, de Wit J, van Els C. A synthetic human 3D in vitro lymphoid model enhancing B-cell survival and functional differentiation. iScience. 2023;26(1):105741.

[25] Tomei AA, Siegert S, Britschgi MR, Luther SA, Swartz MA. Fluid flow regulates stromal cell organization and CCL21 expression in a tissue-engineered lymph node microenvironment. J Immunol. 2009;183(7):4273-83.

[26] Morrison AI, Sjoerds MJ, Vonk LA, Gibbs S, Koning JJ. In vitro immunity: an overview of immunocompetent organ-on-chip models. Front Immunol. 2024;15:1373186.

[27] Jeger-Madiot R, Planas D, Staropoli I, Debarnot H, Kervevan J, Mary H, et al. Modeling memory B cell responses in a lymphoid organ-chip to evaluate mRNA vaccine boosting. J Exp Med. 2024;221(10).

[28] Goyal G, Prabhala P, Mahajan G, Bausk B, Gilboa T, Xie L, et al. Ectopic Lymphoid Follicle Formation and Human Seasonal Influenza Vaccination Responses Recapitulated in an Organ-on-a-Chip. Adv Sci (Weinh). 2022;9(14):e2103241.

[29] Teufel C, Schlemmer A-S, Eiken AW, Wagoner ZW, Vöhringer D, Christ L, et al. Lymphoid-tissue-on-chip recapitulates human antibody responses in vitro. bioRxiv. 2025:2025.01.14.632762.

[30] Kwee BJ, Mansouri M, Akue A, Sung KE. On-chip human lymph node stromal network for evaluating dendritic cell and T-cell trafficking. Biofabrication. 2024;17(1).

[31] Fergusson JR, Siu JHY, Gupta N, Nee E, Reinke S, Ströbel T, et al. Ex vivo Model of Functioning Human Lymph Node Reveals Pivotal Role for Innate Lymphoid Cells and Stromal Populations in Response to Vaccine Adjuvant. bioRxiv. 2024:2024.08.21.608943.

[32] Birmingham KG, O'Melia MJ, Bordy S, Reyes Aguilar D, El-Reyas B, Lesinski G, et al. Lymph Node Subcapsular Sinus Microenvironment-On-A-Chip Modeling Shear Flow Relevant to Lymphatic Metastasis and Immune Cell Homing. iScience. 2020;23(11):101751.

[33] Zatorski JM, Raskovic D, Arneja A, Kiridena S, Ozulumba T, Hammel JH, et al. Initiation of primary T cell—B cell interactions and extrafollicular antibody responses in an organized microphysiological model of the human lymph node. bioRxiv. 2025:2025.01.12.632545.

[34] Jäger J, Berger P, Morrison AI, Erfurth H, Thon M, Dehne E-M, et al. A Sacrificial 3D Printed Vessel-on-Chip Demonstrates a Versatile Approach to Model Connective Tissue Pathology. bioRxiv. 2025:2025.02.06.636821.

[35] Roet JEG, Morrison AI, Mikula AM, de Kok M, Panocha D, Roest HP, et al. Human lymph node fibroblastic reticular cells maintain heterogeneous characteristics in culture. iScience. 2024;27(7):110179.

[36] Jäger J, Thon M, Schimek K, Marx U, Gibbs S, Koning JJ. Differential biomarker expression of blood and lymphatic vasculature in multi-organ-chips. Sci Rep. 2025;15(1):14492.

[37] Roet JEG, Mikula AM, de Kok M, Chadick CH, Garcia Vallejo JJ, Roest HP, et al. Unbiased method for spectral analysis of cells with great diversity of autofluorescence spectra. Cytometry A. 2024;105(8):595-606.

[38] Jouybar M, Mikula AM, Zuidmeer N, Konijn T, de Jonge AV, Roest HP, et al. Lymphoma-on-chip model reveals that lymph node stromal cells promote diffuse large B-cell lymphoma survival and migration. Materials Today Bio. 2025;31:101544.

[39] Cakala-Jakimowicz M, Kolodziej-Wojnar P, Puzianowska-Kuznicka M. Aging-Related Cellular, Structural and Functional Changes in the Lymph Nodes: A Significant Component of Immunosenescence? An Overview. Cells. 2021;10(11).
[40] Ozulumba T, Montalbine AN, Ortiz-Cardenas JE, Pompano RR. New tools for immunologists: models of lymph node function from cells to tissues. Front Immunol. 2023;14:1183286.
[41] Shelton SE. Vascular microphysiological systems. Curr Opin Hematol. 2024;31(3):155-61.
[42] Henderson AR, Choi H, Lee E. Blood and Lymphatic Vasculatures On-Chip Platforms and Their Applications for Organ-Specific In Vitro Modeling. Micromachines (Basel). 2020;11(2).
[43] Moses SR, Adorno JJ, Palmer AF, Song JW. Vessel-on-a-chip models for studying microvascular physiology, transport, and function in vitro. Am J Physiol Cell Physiol. 2021;320(1):C92-C105.
[44] Jouybar M, de Winde CM, Wolf K, Friedl P, Mebius RE, den Toonder JMJ. Cancer-on-chip models for metastasis: importance of the tumor microenvironment. Trends Biotechnol. 2024;42(4):431-48.
[45] de Graaf MNS, Cochrane A, van den Hil FE, Buijsman W, van der Meer AD, van den Berg A, et al. Scalable microphysiological system to model three-dimensional blood vessels. APL Bioeng. 2019;3(2):026105.
[46] Jouybar M, van der Kallen S, Sahebali S, Bouten C, den Toonder JMJ. The Impact of Channel Geometry and Flow Regime on Endothelial Orientation and Morphology in Vessel-on-Chip. Advanced Materials Technologies.n/a(n/a):2401994.
[47] Lim J, Fang HW, Bupphathong S, Sung PC, Yeh CE, Huang W, et al. The Edifice of Vasculature-On-Chips: A Focused Review on the Key Elements and Assembly of Angiogenesis Models. ACS Biomater Sci Eng. 2024;10(6):3548-67.
[48] Sainte-Marie G. The lymph node revisited: development, morphology, functioning, and role in triggering primary immune responses. Anat Rec (Hoboken). 2010;293(2):320-37.
[49] Margaris KN, Black RA. Modelling the lymphatic system: challenges and opportunities. J R Soc Interface. 2012;9(69):601-12.
[50] Fletcher AL, Malhotra D, Acton SE, Lukacs-Kornek V, Bellemare-Pelletier A, Curry M, et al. Reproducible isolation of lymph node stromal cells reveals site-dependent differences in fibroblastic reticular cells. Front Immunol. 2011;2:35.
[51] Choi YS, Jeong E, Lee JS, Kim SK, Jo SH, Kim YG, et al. Immunomodulatory Scaffolds Derived from Lymph Node Extracellular Matrices. ACS Appl Mater Interfaces. 2021;13(12):14037-49.
[52] Panocha D, Roet JEG, Kuipers JE, de Winde CM, Mebius RE. Lymph node fibroblast-produced extracellular matrix shapes immune function. Trends Immunol. 2025.
[53] Onder L, Narang P, Scandella E, Chai Q, Iolyeva M, Hoorweg K, et al. IL-7-producing stromal cells are critical for lymph node remodeling. Blood. 2012;120(24):4675-83.
[54] Surh CD, Sprent J. Homeostasis of naive and memory T cells. Immunity. 2008;29(6):848-62.
[55] Iolyeva M, Aebischer D, Proulx ST, Willrodt AH, Ecoiffier T, Haner S, et al. Interleukin-7 is produced by afferent lymphatic vessels and supports lymphatic drainage. Blood. 2013;122(13):2271-81.
[56] Kikuchi K, Lai AY, Hsu CL, Kondo M. IL-7 receptor signaling is necessary for stage transition in adult B cell development through up-regulation of EBF. J Exp Med. 2005;201(8):1197-203.
[57] Huang J, Long Z, Jia R, Wang M, Zhu D, Liu M, et al. The Broad Immunomodulatory Effects of IL-7 and Its Application In Vaccines. Front Immunol. 2021;12:680442.
[58] Chai Q, Onder L, Scandella E, Gil-Cruz C, Perez-Shibayama C, Cupovic J, et al. Maturation of lymph node fibroblastic reticular cells from myofibroblastic precursors is critical for antiviral immunity. Immunity. 2013;38(5):1013-24.
[59] Denton AE, Roberts EW, Linterman MA, Fearon DT. Fibroblastic reticular cells of the lymph node are required for retention of resting but not activated CD8+ T cells. Proc Natl Acad Sci U S A. 2014;111(33):12139-44.
[60] Link A, Vogt TK, Favre S, Britschgi MR, Acha-Orbea H, Hinz B, et al. Fibroblastic reticular cells in lymph nodes regulate the homeostasis of naive T cells. Nat Immunol. 2007;8(11):1255-65.

[61] Romer PS, Berr S, Avota E, Na SY, Battaglia M, ten Berge I, et al. Preculture of PBMCs at high cell density increases sensitivity of T-cell responses, revealing cytokine release by CD28 superagonist TGN1412. Blood. 2011;118(26):6772-82.

[62] Gronloh MLB, Arts JJG, van Buul JD. Neutrophil transendothelial migration hotspots - mechanisms and implications. J Cell Sci. 2021;134(7).

[63] van Steen ACI, Kempers L, Schoppmeyer R, Blokker M, Beebe DJ, Nolte MA, et al. Transendothelial migration induces differential migration dynamics of leukocytes in tissue matrix. J Cell Sci. 2021;134(21).

[64] Sabine A, Bovay E, Demir CS, Kimura W, Jaquet M, Agalarov Y, et al. FOXC2 and fluid shear stress stabilize postnatal lymphatic vasculature. J Clin Invest. 2015;125(10):3861-77.

[65] Friess MC, Kritikos I, Schineis P, Medina-Sanchez JD, Gkountidi AO, Vallone A, et al. Mechanosensitive ACKR4 scavenges CCR7 chemokines to facilitate T cell de-adhesion and passive transport by flow in inflamed afferent lymphatics. Cell Rep. 2022;38(5):110334.

[66] Shroff T, Aina K, Maass C, Cipriano M, Lambrecht J, Tacke F, et al. Studying metabolism with multi-organ chips: new tools for disease modelling, pharmacokinetics and pharmacodynamics. Open Biol. 2022;12(3):210333.

[67] Michielon E, Motta AC, Ogien J, Oranje P, Waaijman T, Thakoersing V, et al. Integration of line-field confocal optical coherence tomography and in situ microenvironmental mapping to investigate the living microenvironment of reconstructed human skin and melanoma models. J Dermatol Sci. 2024;115(2):85-93.

[68] Koning JJ, Rodrigues Neves CT, Schimek K, Thon M, Spiekstra SW, Waaijman T, et al. A Multi-Organ-on-Chip Approach to Investigate How Oral Exposure to Metals Can Cause Systemic Toxicity Leading to Langerhans Cell Activation in Skin. Front Toxicol. 2021;3:824825.

[69] Vahav I, Thon M, van den Broek LJ, Spiekstra SW, Atac B, Lindner G, et al. Proof-of-Concept Organ-on-Chip Study: Topical Cinnamaldehyde Exposure of Reconstructed Human Skin with Integrated Neopapillae Cultured under Dynamic Flow. Pharmaceutics. 2022;14(8).

[70] Michielon E, Boninsegna M, Waaijman T, Fassini D, Spiekstra SW, Cramer J, et al. Environmentally Controlled Microfluidic System Enabling Immune Cell Flow and Activation in an Endothelialised Skin-On-Chip. Adv Healthc Mater. 2024;13(29):e2400750.

[71] Michielon E, King LA, Waaijman T, Veth M, Spiekstra SW, van der Vliet HJ, et al. An organotypic human melanoma-in-skin model as an in vitro tool for testing Vgamma9Vdelta2-T cell-based immunotherapy. Immunooncol Technol. 2024;24:100724.

[72] Malik M, Yang Y, Fathi P, Mahler GJ, Esch MB. Critical Considerations for the Design of Multi-Organ Microphysiological Systems (MPS). Front Cell Dev Biol. 2021;9:721338.

[73] Mastrangeli M, Millet S, Orchid partners T, van den Eijnden-van Raaij J. Organ-on-chip in development: Towards a roadmap for organs-on-chip. ALTEX - Alternatives to animal experimentation. 2019;36(4):650-68.

[74] Camasao DB, Mantovani D. The mechanical characterization of blood vessels and their substitutes in the continuous quest for physiological-relevant performances. A critical review. Mater Today Bio. 2021;10:100106.

[75] Liao S, von der Weid PY. Lymphatic system: an active pathway for immune protection. Semin Cell Dev Biol. 2015;38:83-9.

[76] Tan KW, Yeo KP, Wong FH, Lim HY, Khoo KL, Abastado JP, et al. Expansion of cortical and medullary sinuses restrains lymph node hypertrophy during prolonged inflammation. J Immunol. 2012;188(8):4065-80.

A

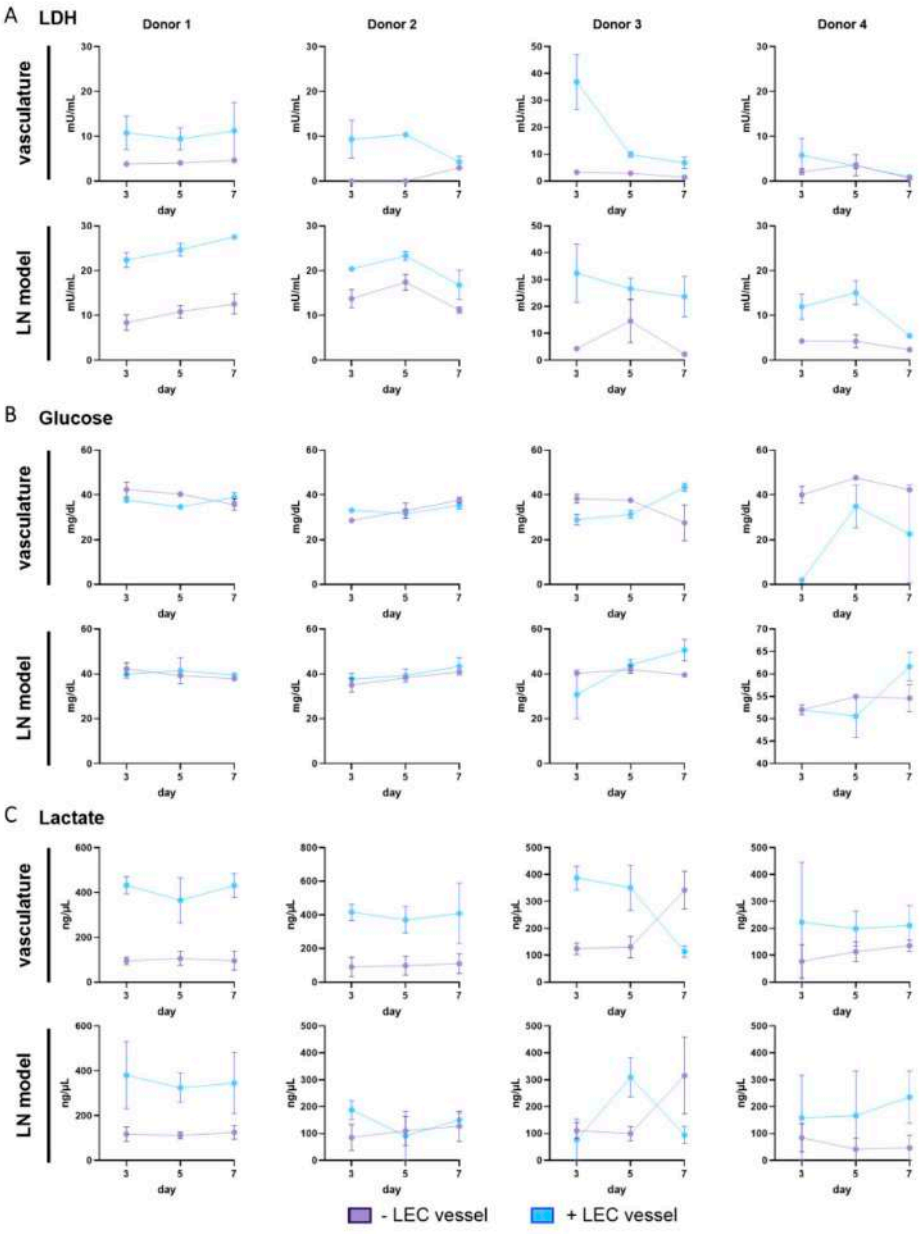

Fig. S1 - Metabolic readouts of individual donors. (A) LDH secretion **(B)** Glucose concentration and **(C)** Lactate secretion into culture supernatant of LN-on-chip cultures. Depicted are individual values for 4 different LN donors in duplicates.

B

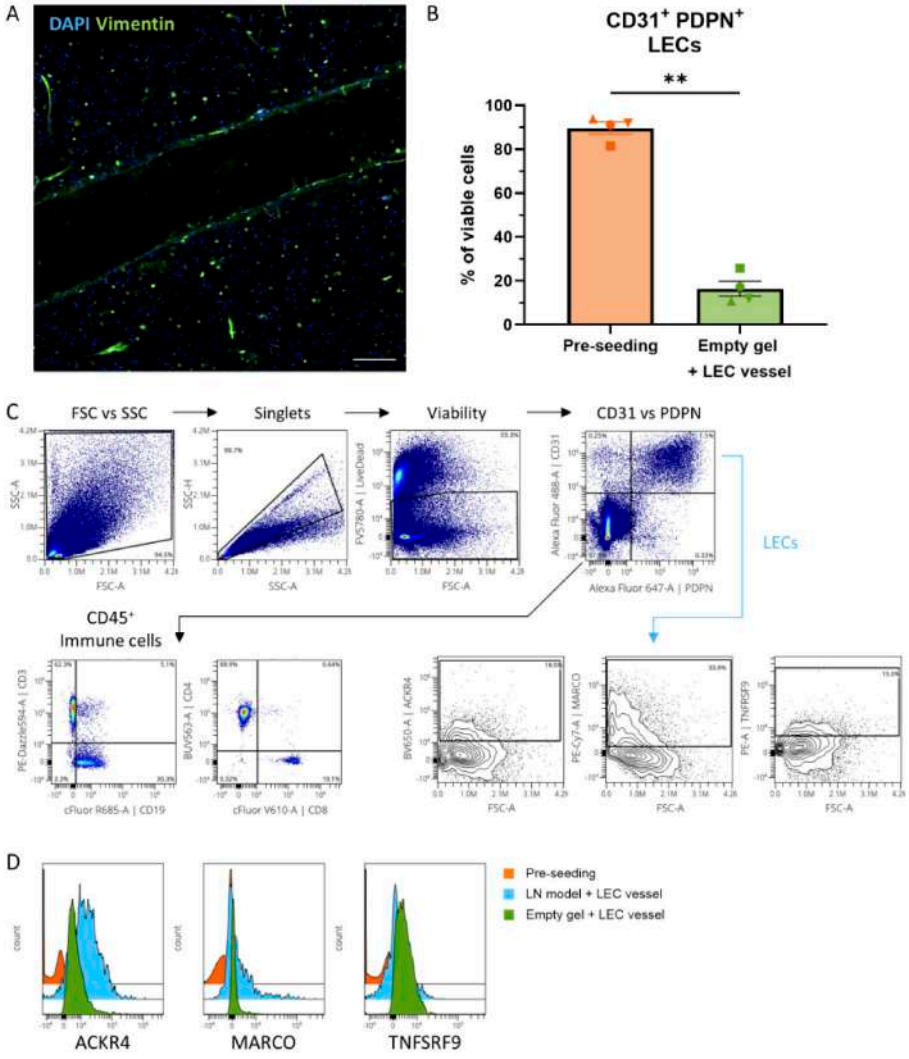

Fig. S2 - LEC characterization before seeding and in the chip. (A) Vimentin (green) and DAPI (blue) staining of a LN-on-chip with an empty vessel, imaged in the middle of the channel. Scale bar: 200 µm. **(B)** LEC phenotype from CD31 and PDPN marker expression of different donors used before seeding into the chip., and after chip culture through an empty hydrogel. **(C)** Representative gating strategy to identify different cells in LN model, where CD31⁺PDPN⁺ LECs are selected for further phenotyping (blue line), and CD31⁻PDPN⁻ cells are selected for immune cell gating (black line). **(D)** Representative histogram overlap of LEC phenotype for ACKR4, MARCO and TNFSRF9 across pre-seeding cultured LECs, LECs in the LN model + LEC vessel, and an empty hydrogel + LEC vessel.

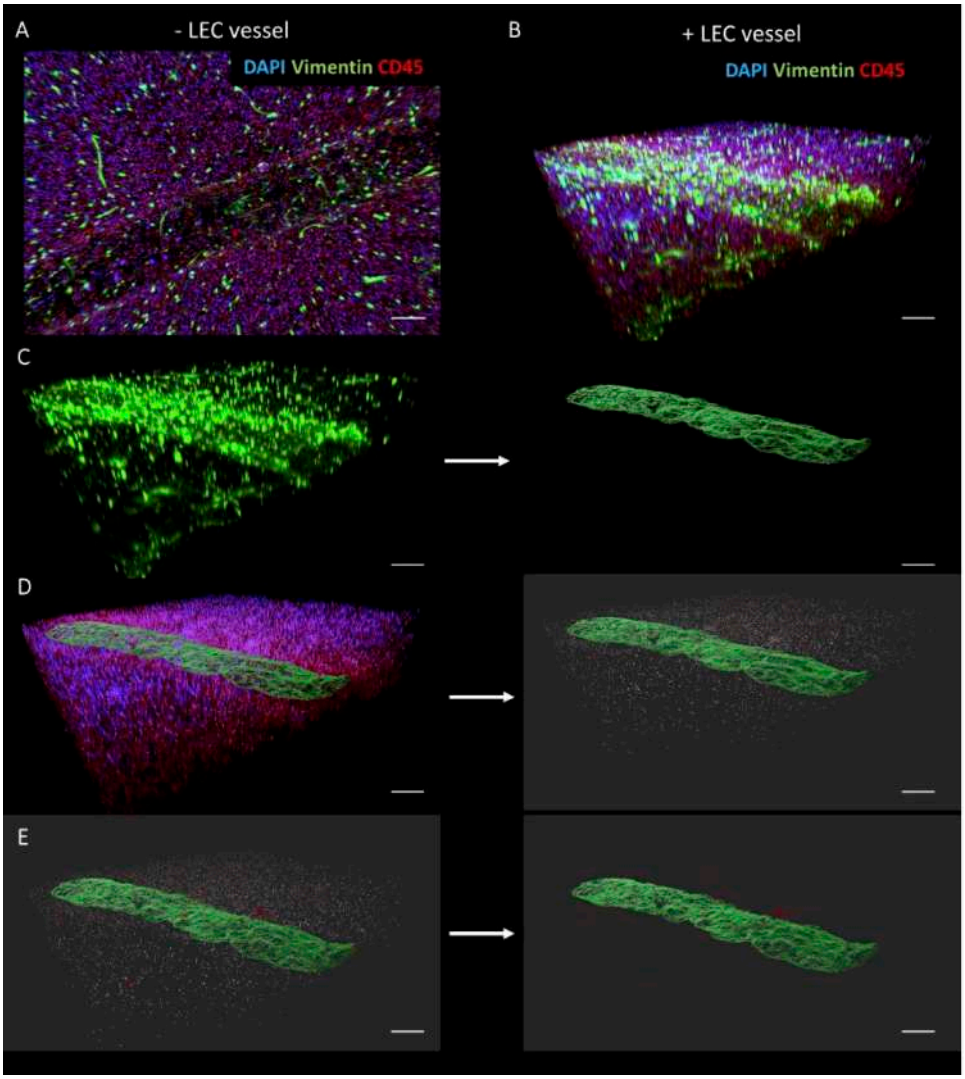

Fig. S3 - LN-on-chip renderings at day 7. (A) 3D projection of LN-on-chip without lymphatic vessel. **(B)**. 3D reconstruction of the LN-on-chip with lymphatic vessel stained with DAPI (blue), vimentin (green and CD45 (red)). **(C)**. Vessel surface rendering (green) based on vimentin. **(D)** Immune cell rendering (grey) of $DAPI^{+}CD45^{+}$ cells. **(E)** Immune cells clusters rendered (red) based on the following criteria: 9 closest neighbours within an average distance of 0-20 µm. Scale bars: 200 µm.

7

General Discussion

In humans, lymph nodes (LNs) are integrated within the lymphatic system for drainage and filtration of interstitial fluid from all tissues and organs. As such, this allows the removal of toxic and waste metabolites, including the detection of pathogenic material and activated immune cells bearing foreign antigens. The highly dense lymphocyte environment within LNs, compartmentalised into distinct regions, allows for efficient adaptive immune reactions to occur, facilitated by the LN stromal cells (LNSCs). This central hub for immune cell priming and specific memory responses makes the LN an integral part of systemic immunology in both health and disease. Therefore, LNs are an important organ to model *in vitro* for understanding the mechanisms behind immune functionality, including testing new drug therapies, vaccine responses, tissue-specific immune responses and uncovering potential novel disease pathophysiology.

Together, scientists in the tissue engineering and microphysiological systems (MPS) field strive for replacement of animal models with physiologically relevant human models[1,2]. The immune system remains a core discipline of this progress. However, the current advancements of human LN models over the last decade are still in their early infancy. Due to the diverse multicellular environment, intricate design and plethora of immune events emanating from LNs, it can be appropriate to apply the rhetorical question - "How simplistically complex should an organ model be?". Interestingly enough, there is a subjective paradoxical answer – "It depends!". The spectrum of human LN models can range from two cell co-cultures[3] up to models mimicking isolated LN regions like B cell follicles[4] or the subcapsular sinus (SCS)[5], and then even branching further into fully immunocompetent organoid-like LN environments[6]. Nevertheless, a desired criterium for setting up organ models *in vitro* is to have a system with the representative cell types and structures within a dynamic environment. Henceforth, this can then require the application of microfluidic organ-on-chip (OoC) devices, which have been summarised in **Chapter 2** for modelling the human immune system, aptly opening this thesis to the ultimate goal of *in vitro* immunity.

Hereto, this thesis aimed to construct a physiological human LN *in vitro*, with a focus on incorporating LNSCs as the foundation for a properly functioning LN. The work has been developed to investigate the contribution of LNSCs, particularly fibroblastic reticular cells (FRCs), to LN functioning and for incorporation into OoC microfluidic devices as a platform for multi-OoC (MOC). Accordingly, the work of this thesis can be split into three main objectives:

Goals

1. Isolate, culture and characterise mesenchymal stromal cells from human LN tissue,
2. Develop a functional three-dimensional (3D) LN model with integrated LNSCs,
3. Bring the LN model into an OoC environment.

With the use of LNSCs as a foundation for developing the LN model, there remains a number of outstanding points of discussion that are a prevalent theme across all research chapters in this thesis. These topics are examined below and include the material used for the LN models, such as the relevant cell types and 3D environments, as well as the depth of LN functionality that can recapitulate physiological immune activity.

LNSC heterogeneity for LN models

LNSCs have a valuable contribution to LN biology, globally defined as the "cartographers of the immune system"[7]. Most of the research performed to uncover LNSC functions has made use of mouse models, for which translation of subsequent findings to human LNSCs has seen a mixed degree of overlap and distinct differences. For a general comparison, mice have 22 LNs occurring at the same location in their body[8], whereas humans have several hundred[9,10], making it difficult to characterise the nature of every single human LN. Both species have LNSCs categorised into four major subtypes, *i.e.* the mesenchymal FRCs and double negative cells (DNCs), and the endothelial-derived blood endothelial cells (BECs) and lymphatic endothelial cells (LECs), yet discrepancies exist when comparing heterogenous subdivisions of these cell profiles at a deeper level. For example, in the mesenchymal subsets, murine FRCs are strictly defined as podoplanin$^+$ (PDPN$^+$) and composed of up to twelve clusters from single-cell RNA sequencing (scRNAseq) analysis[11,12]. In contrast, recent human studies have revealed that not all human FRCs have a homogeneous PDPN$^+$ expression, indicating some are within the originally-defined DNCs and as thus galvanised an existing dissensus on the nomenclature centred around human PDPN FRC classification[11,13-19]. Nevertheless, there are currently at least five recognised subtypes of FRCs identified across the LN, such as T cell zone FRCs (TRCs), B cell zone FRCs (BRCs), follicular dendritic cells (FDCs), marginal reticular cells (MRCs) and pericytes[11,20]. However, FRCs from both species still exhibit functionally similar features, such as their influence on immune cells to guide migration and promote survival via chemokines and cytokines, respectively, mediate leukocyte differentiation and restrict T cell division, albeit through different molecular mechanisms[16,21-24].

Therefore, in order to develop stromal-competent *in vitro* LN models, not only is it important to elucidate the function of subset-specific LNSCs, but also to understand the contents of the available tissue material and the extent at which LNSCs can be isolated and cultured before bringing into these LN models. As such, in **Chapter 3**, we characterised human mesenchymal stromal cells *ex vivo* after isolation from healthy, resting human LN tissue and subsequent culture on collagen-coated flasks. This revealed that the original FRC-defining marker PDPN in mice was not exclusive to all FRCs in humans. We found that other markers like CD90, BST1 and CD146, were expressed more widely on FRCs compared to PDPN. Throughout culture, four new FRC clusters emerged, with an increased PDPN expression, in addition to the four preserved from fresh isolation. The homogeneity amongst donors reassuringly indicated the reliability of our method, providing novel insights into the possibilities around isolating and culturing human FRCs subsets. In this study, we did not accurately define the exact types of FRCs present, as this would require further transcriptome, secretome and functional experiments per individual FRC cluster to match with existing scRNAseq data. Based on the membrane markers we used, it can be broadly speculated that a mix of TRCs, BRCs and MRCs were present, as no FDCs were found amongst the FRCs and pericytes were lost along culture too. Such information is highly relevant going forth when using FRCs as a foundation for the LN models. This can allow physiological relevance, tailored hypotheses and aid with setting up specific experimental designs to study the relationship between FRCs and immune cells. This was evident in **Chapter 4**,

where FRCs were deemed important for dendritic cell (DC) phenotype and survival in a 3D hydrogel environment. These FRCs expressed the mRNA for *GREM1*, defined as the DC-supporting FRC subset in LNs[12] which are also known to be *VCAM1*$^{+}$[11], and therefore these FRCs could match with cluster 10 of cultured FRCs from **Chapter 3**. It is however not yet clear whether all or just a subset of FRCs in the model were *GREM1*$^{+}$. These FRCs not only enhanced DC survival in 3D but also influenced their phenotype in response to differentiation stimuli, shaping it into a profile reminiscent of LN-resident DCs[25,26]. Such a phenomenon could be due to mechanisms within the Notch signalling pathway, with Notch ligands having the ability to control immune cell development and found in plentiful on human FRC datasets[12,27]. Although as of yet, the relevance of this pathway has been unexplored between human LN FRC and DC interactions. These findings indicated that the practicalities for studying immune cells in a hydrogel environment required the presence of FRCs. Likewise, in **Chapter 5**, we enriched a complete LN-cell suspension with additional FRCs in a 3D hydrogel, and discovered that this enrichment benefited the resulting number of immune cells and affected the lymphocyte composition. FRCs were seen to selectively retain more B cells than T cells, secreting B cell-related factors like CXC motif chemokine ligand 13 (CXCL13) and B cell activating factor from the TNF family (BAFF), which are common traits of BRCs, MRCs and FDCs[20]. CC motif chemokine ligand 19 (CCL19) was also found elevated in FRC-enriched models, which is a characteristic of TRCs[20].
It is unknown to what extent FRCs have the ability to reprogram intrinsically and differentiate between subsets based on their surrounding microenvironment. This also includes the rate of FRC maturation and terminal senescence, as many of the isolated FRCs in **Chapter 3** were identified as CD34^{+}, suggesting an immature phenotype[12]. FRCs were found to proliferate when placed in the 3D collagen environment, either from *ex vivo* cultures or from starting LN cell suspensions, leading to unwanted hydrogel contraction around 10-14 days, a previously documented phenomenon[28]. Compared to the profile of FRCs grown in standard two-dimensional (2D) cultures from **Chapter 3**, it was not investigated if the collagen hydrogel or presence of native LN immune cells provoked selective outgrowth of different FRC subsets in 3D. It is worth experimenting in the future if different extracellular matrix (ECM) proteins could lead to the development of different FRC subsets, given the plethora of ECM proteins found throughout the LN[29,30]. As such, advances in purification of FRC subsets from LN tissue are appealing to allow a versatile approach for selecting specific FRC subsets that can be strategically incorporated into LN models. This can be highly relevant for a multitude of reasons, e.g. a more general approach to ensure all FRC subtypes are present for a LN model or if one wished to study immune events related to only the B cell follicles, FDCs and BRCs could be used for 3D co-cultures with B cells.

In order to strengthen the stromal-competency of LN models, it was of interest to include and address the role of LECs. Hereto, LECs were introduced into the LN model as a lymphatic vessel-on-chip in **Chapter 6**. As a result, LECs were found to enhance the LN microenvironment by secreting interleukin-7 (IL-7) and CCL21. These factors are attributes of TRCs, although we did not detect this in the other LN models discussed in **Chapters 4** and **5**. Human LECs have been categorised into six major subsets throughout the LN lymphatics[31]. In the developed LN-on-chip, it was discovered that LECs could recapitulate expression of these subset defining markers, like ACKR4 and MARCO reported

on SCS-ceiling and medullary LECs, respectively. Profiling of fresh LEC subsets and phenotypic changes across *ex vivo* culture were not performed, so future studies would be welcomed to better characterise LEC populations. Likewise, once in *in vitro* models, it could be investigated whether LEC subsets follow spatial cues for marker expression, e.g. ACKR4^{+} LECs found on the vessel ceiling and TNFSRF9^{+} LECs located on the vessel floor.

In summary, the intricate composition of LNSC heterogeneity is an important aspect to consider and address for developing human LN models. It is presumed that future research into LNSCs will uncover more subsets and their functions, thereby providing new challenging opportunities to accurately model the LNSCs in different areas of human LNs.

Physiological relevance of LN models

Recapitulating the degree of organ physiology has certain underlying principles that must be acknowledged for *in vitro* LN models. Such parameters have been reviewed in the secondary lymphoid organ section of **Chapter 2** for LN-on-chip models. We believe our approach to develop LN models with LNSCs cements us in a strong position over other recently published LN models (**Table 1, Chapter 1**) to truly recreate the LN microenvironment. There are only a handful of static and dynamic LN models that have incorporated LNSCs, but each model has its limitations, including our own.

Firstly, enriching the full LN models with FRCs or LECs in **Chapter 5** (Fig. 1D) and **Chapter 6** (Fig. 3D), respectively, slightly unbalanced the physiological ratio of LNSCs present in the native human LN[18]. This could have been due to proliferation of immune or stromal cells, but this enrichment was done to allow for enough stromal involvement and to ensure plenty of 'natural' stromal-derived factors were available for immune cells. This was deemed more beneficial for creating an organic-like system without supplementing extra growth factors to the LN model media, like the addition of BAFF seen in other studies that lacked stromal cells[6].

The LN model presented in this thesis was developed in a collagen-based hydrogel. Given this collagen environment and the fact that the native LN paracortex is rich in FRC-deposited collagenous fibres, our LN model could be deemed more physiological compared to other lymphoid organ models, which are cultured on transwells and do not address ECM-components[6,32-34]. The collagen was isolated from rat tails, with additives such as fibrin (and aprotinin) included into the hydrogel to limit contraction. Collagen is just one out of a plethora of ECM proteins in human LNs that also contain laminins, proteoglycans and fibronectins[29]. ECM proteins in LNs are a dynamic and multifunctional scaffold that provides structural support to the LN interior, while also serving as a source of immune factors and anchorage point for cell migration[35,36]. Primarily produced by FRCs[37], ECM proteins also undergo remodelling during LN activation[38]. Therefore, the ECM-microenvironment is another component to acknowledge when designing LN models. Experimenting with a single protein or a combination of ECM proteins may further support the physiological relevance of the LN environment, dependent on the research goal. For example, decellularised LN tissue could be used as a potential scaffold for a LN model containing all native ECM components[39,40]. Otherwise, integration of certain laminin isoforms, such as laminin α-5 found in the B cell follicles[41] or laminin α-4 in the T cell area[42], would be of interest when modelling these LN regions in isolation.

These biological ECM-derivates mentioned above are used widely amongst lab groups for designing LN model microenvironments[43], but others have also taken the approach to use synthetic-based scaffold, such as PEG-4MAL, which showcased already to support B cell functioning in certain LN models[4,44]. The use of a scaffold may help circumvent the challenges with hydrogels, such as cell-induced contraction and access to LN interior for microenvironment sampling. Recently, the latter has been made possible by the company IMcoMET (Rotterdam, The Netherlands), who have developed a M-Duo Technology® that features a needle-pair system that can extract *in situ* the soluble microenvironment[45]. This would prove useful to help answer in real-time the much debated question about the LN model secretome – whether undetected factors are simply absent, trapped in the hydrogel or already consumed by the residing cells. Nonetheless, it remains to be determined whether cell seeding and LN stability are possible when using synthetic scaffolds, with care taken not to deviate from the native properties of LNs with the introduction of artificial features.

Another crucial factor in developing LN models is the source of cellular material. Medical agreements and ethical laws can sometimes be a hurdle for universal access to human LN materials, so lab groups are often limited by the available resources. In the LN models presented in this thesis, all components are from primary origin, specifically native liver-draining LNs from deceased humans, but otherwise healthy as they are donors for liver transplantation. This makes our LN model more physiological, especially as existing LN models use either cell lines, PBMCs or tonsil-derived cell suspensions[43,46,47]. Cell lines miss the diversity of native LN cells, while PBMCs lack tissue-specific immune cells and stromal populations. It is commonly known that lymphoid organs can generate site-specific immune responses, like mucosal- or tolerogenic-associated events[48,49]. Inversely, tissue-derived factors are also thought to imprint LNSCs[50]. For example, in mouse gut-draining LNs, diet-derived vimentin A induced mesenteric FRCs to synergistically increase levels of retinoic acid (RA)[51], which is required for Treg induction[52], FDC development[53] and supports IgA production[54]. Furthermore, LN transplant experiments performed in mice[55] have revealed that the LN microenvironment can partially retain its capacity to elicit location-specific immune responses. For example, LNSCs from mesenteric LNs grafted into the knee joint, still had the ability to upregulate the gut-homing molecule integrin α4β7[56]. Therefore, given these unique imprinting abilities of tissue-derived factors on LNSC properties, it would be fascinating to see how this unfolds in humans and the possibilities to model *in vitro*.
Similarly, it is desirable to use donor-matched immune cells to create an autologous system, otherwise the presence of T cells can lead to unwanted allogenicity through mismatching between the human leukocyte antigen (HLA) types[57]. Due to the mechanisms that have evolved with human immunity, T cells via their TCR will recognise non-self-antigens and trigger an allogenic reaction. This is a challenge with organ transplantation and finding HLA-matched donors, potentially leading to graft-*versus*-host disease. Consequently, the route of using induced pluripotent stem cells (iPSC) as an endless cell source would be appealing to overcome this hurdle for autologous LN models. Research has shown steady progress in creating general iPSC-derived immune cells types, like T and B lymphocytes, myeloid cells and natural killer (NK) cells[58]. However, the replication of mature and tissue-specific immune cell subsets, a diverse antigen receptor repertoire, and generating iPSC-derived LNSCs, remain significant challenges that would be difficult to reproduce. Although, the potential for

advancement in this area is highly promising and it is rather exciting to see how far the field can go. In conclusion, factors such as the ECM-microenvironment and source of cellular material are crucial parameters to take into account when mimicking physiologically-relevant human LN models. The LN model in this thesis made use of a collagen-based hydrogel, a core ECM-protein in LNs, and native LN-derived immune and stromal cells, thereby encouragingly showcasing a physiological-like *in vitro* LN model with potential for future application.

Antigen-specific LN functionality

The main attraction for modelling the human LN *in vitro* is the ability to generate and study human immune responses. LN models replicating immune activities could be used for proof-of-principle experiments for immunotherapies/vaccination studies before entering the clinic or to investigate the off-target organ toxicity of drug candidates. The degree of immune functionality is subjective and can be evaluated at various levels, such as simplistic changes in cell surface marker expression or as detailed as antigen-specific readouts. We explored this to a certain extent during development of the LN model. In **Chapter 4**, we found that in the 3D hydrogel with FRCs, precursor DCs/monocytes had the ability to differentiate under cytokine stimuli to what resembled a LN-resident DC phenotype, based on the absence of CD1a and CD1c marker expression[25,26,59].

On a more functional level, we unearthed in **Chapter 5** that the LN model allowed the capacity for T cells to proliferate and become activated during an allogenic response. In turn, this was suppressed by the enriched FRCs in the LN model, a native phenomenon reported previously in literature[16], and therefore highlighting a physiologically-relevant readout. With the LN-on-chip in **Chapter 6**, we did not actively test LN functionality but passively found LECs to promote an increased clustering of immune cells in closer proximity to the lymphatic vessel. As a result, this LN model in both static and dynamic settings had the ability to generate a certain degree of functional LN properties. However, there remains one outstanding parameter to be addressed – whether antigen-specific LN immune responses can be generated.

One side of immune activity is humoral immunity (antibody production), studied by vaccinating or exposing viral antigens directly to LN models. The majority of LN models have already reported this. Most notably, the Lisa Wagar group in the USA, generated static transwell-based tonsil suspension models, termed “organoids”, that could demonstrate antigen-specific lymphocyte and antibody responses to the influenza virus[6,32]. The Wagar group could also model follicular lymphoma treatments[33] and uncover sex-specific lymphocyte responses, such as uncovering that paediatric female tonsils contained more responsive memory B cells compared to males[34]. Other LN models that demonstrated antigen-specific immune responses included the use of PBMCs-on-chip from the OoC company Emulate. Here, flow was applied to an empty channel above a hydrogel containing a high cell density of PBMCs, which interestingly induced follicle formation in the hydrogel. Moreover, antibody secretion and memory B cell responses to the influenza virus, influenza vaccine and COVID-19 mRNA vaccines were also recapitulated[60,61]. In our model, we opted for a cell-mediated LN response by stimulating an allogenic reaction in **Chapter 5** using different maturation statuses of monocyte derived DCs (moDCs). FRC-enriched LN models restricted T cell division after moDC

inclusion, which may not be ideal when prompting immune activity, but could be practical to use as a system when trying to overcome this FRC suppression.

Of note, efforts were made to set-up an assay for the detection of antigen-specific T cells using an adapted published protocol (Fig. 1A)[62]. This would be highly relevant for the human LN model to advance our understanding of immune mechanisms, improve therapeutic interventions and support precision medicine approaches. This was performed by priming LN cell suspensions with specific peptides in a conventional static 2D culture. These included the major histocompatibility complex (MHC) class I influenza A and the melanoma-related MART-1 peptides, as well as MHC class I and II SARS-CoV-2 peptides. Donors were selected based on HLA-type and available COVID-19 vaccination status, if applicable. Unfortunately, almost all of these attempts were unsuccessful at identifying expansion of antigen-specific T cells from tetramer staining and/or intracellular cytokine production in 2D cultures, irrespective of FRC addition. This only appeared possible for one donor upon detection of COVID-19-specific $CD8^+$ T cells in culture with FRCs after tetramer staining (Fig. 1B), yet it was hard to perceive accurately given the low number of events. As a result, it was decided against pursuing such an assay in a 3D environment given the low frequency of cells found in a conventional 2D culture setting. This finding led to the hypothesis that the source of our liver-draining LN material might not contain enough antigen-specific T cells and therefore we may possibly need the naïve pool of lymphocytes from PBMCs, or stimulation with liver-related immune peptides, to increase the chances of antigen-specific T cell detection in our LN model. This relates back to the importance of working within the boundaries of the available LN tissue material. Likewise, vaccination experiments for antibody secretion and antigen-specific B cells would be of interest to try and investigate further in the future, but this would require a longer culture period of up to three weeks for plasmablast formation, which is currently challenging given our experiences with hydrogel contraction after 10-14 days of culture.

In summary, our LN model has demonstrated various aspects of LN functionality, such as DC differentiation, active T cell proliferation and immune cell clustering. This functionality has been influenced by the presence of LNSCs, whether through enhancement or regulation of immune activity, which are all physiological hallmarks of native LNSC characteristics.

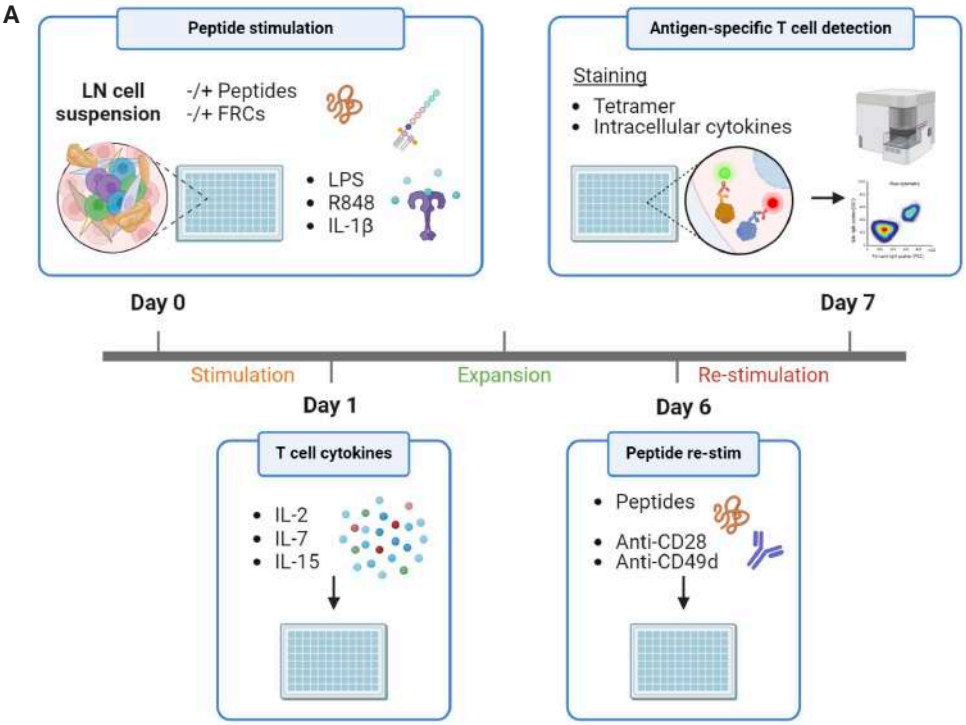

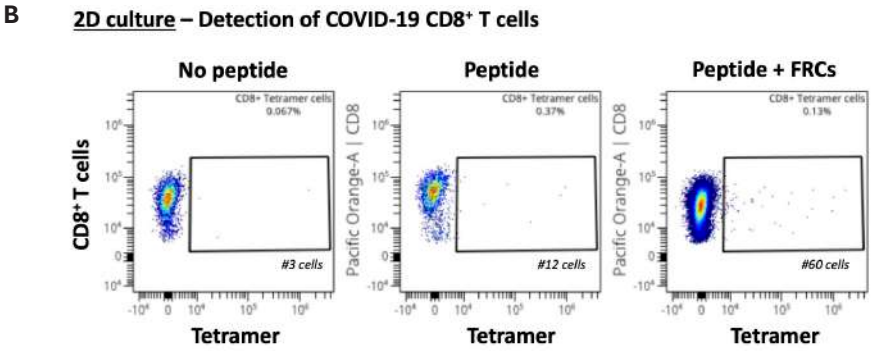

Fig. 1 - Detection of antigen-specific T cells in human LN material. (A) Schematic illustration of assay workflow adapted and modified from Cimen Bozkus *et al.*[62]. Human LN cell suspensions were seeded in 96-well plates and stimulated with adjuvants; lipopolysaccharide (LPS), TLR-7/8 agonist (R848) and IL-1β, either ± peptides and ± 1% FRCs. The following day, and every 2-3 days after, cultures were treated with cytokines IL-2, IL-7 and IL-15 to support T cell expansion. Upon day 6, cultures were re-stimulated overnight with the peptide along with the co-stimulatory agents anti-CD28 and anti-CD49d. Next day, cultures were harvested for tetramer and intracellular cytokine staining for antigen-specific T cell detection via flow cytometry. Created with BioRender.com**. (B)** Representative flow cytometry plots for detection of COVID-19 specific CD8⁺ T cells via tetramer staining in human LN cell suspensions. Three culture conditions were examined in a conventional 2D setting; no peptide and peptide administered ± 1% FRCs.

Organ-draining LN-on-chip

The ultimate goal of this thesis was to construct a human LN model that could be incorporated into an OoC device. Henceforth, **Chapter 6** fittingly concludes the experimental research by bringing the LN model into the HUMIMIC Chip2 from TissUse (Berlin, Germany) and generate a lymphatic vessel using autologous LECs. To our knowledge, this is the first LN-on-chip model that contains both a native LN cell suspension and vascularisation with donor-matched LECs. Published LN-on-chip models, reviewed in **Chapter 2**, mainly feature PBMCs or cell lines used in commercial or in house-produced chips, with to date only two setups containing LNSCs to induce immune cell chemotaxis[63,64]. Integrating LECs in a vessel was of interest for enhancing the physiological relevance, since LECs line the lumen of the lymphatics. As a result, we witnessed the upregulation of markers and soluble factors associated with native LN lymphatics. Immune cell clusters were found in a higher abundance near the lymphatic vessel, a topographic result that was previously not observed in static LN models. This was particularly appealing as flow had been already indicated to induce cell clustering in the Emulate chips[60] and now in our LN model we observed more clusters when LECs were additionally present. It is unknown whether this was due to dense areas of LEC-derived survival and/or migratory signals attracting immune cells. Either way, these clusters may indicate a more optimal cellular organisation for immune activity, as it increases the chances of immune cell interactions and for APCs to find their cognate antigen. As the LN drains all tissues and organs to trigger tissue-specific immune responses, this approach offers the potential integration with other organ models into a MOC, thereby simulating an organ-draining LN.

Appropriately, a skin-draining LN-on-chip experiment was piloted using one skin donor and two LN donors as proof-of-concept that a tissue-draining LN can be incorporated and modelled in a MOC setup (Fig. 2A). A reconstructed human skin model (RhS) was cultured in the HUMIMIC Chip3 compartment with a LN model in the adjacent compartment, connected by a LN-derived LEC populated lymphatic vessel through the LN model (Fig. 2B), similar to the experimental setup in **Chapter 6**. Compared to the controls of each LN or RhS model cultured in isolation, five days of RhS-LN co-culture under flow revealed stable lactate dehydrogenase (LDH) release, indicating promising co-culture viability (Fig. 2C). The secretome of the RhS-LN-on-chip, averaged out from all compartments in the chip, notably had a synergistic increase of B cell-related factors CXCL13 and BAFF, as well as IL-6, IL-10 and interferon gamma (IFNγ) (Fig. 2D). Interestingly, BAFF was also found in the chip containing only the RhS model, with comparable levels to the RhS-LN model, and this is most likely derived from the keratinocytes present in the RhS model[65]. In turn, there was an improved percentage of B cells within the LN model when the RhS was cultured in the neighbouring compartment (Fig. 2E). Since this skin-draining LN-on-chip led to a viable five day co-culture, with benefits for an increased B:T cell ratio observed in the LN environment, it therefore shows early compatible potential for developing the logistics behind combining two organotypic models from unmatched donors into the one MOC device. Henceforth, it would be possible to proceed with combining other organs to study tissue-specific immune events, such as a melanoma-RhS model for tumour metastasis[66,67] or stromal-competent intestine models[68] for tolerogenic immune responses.

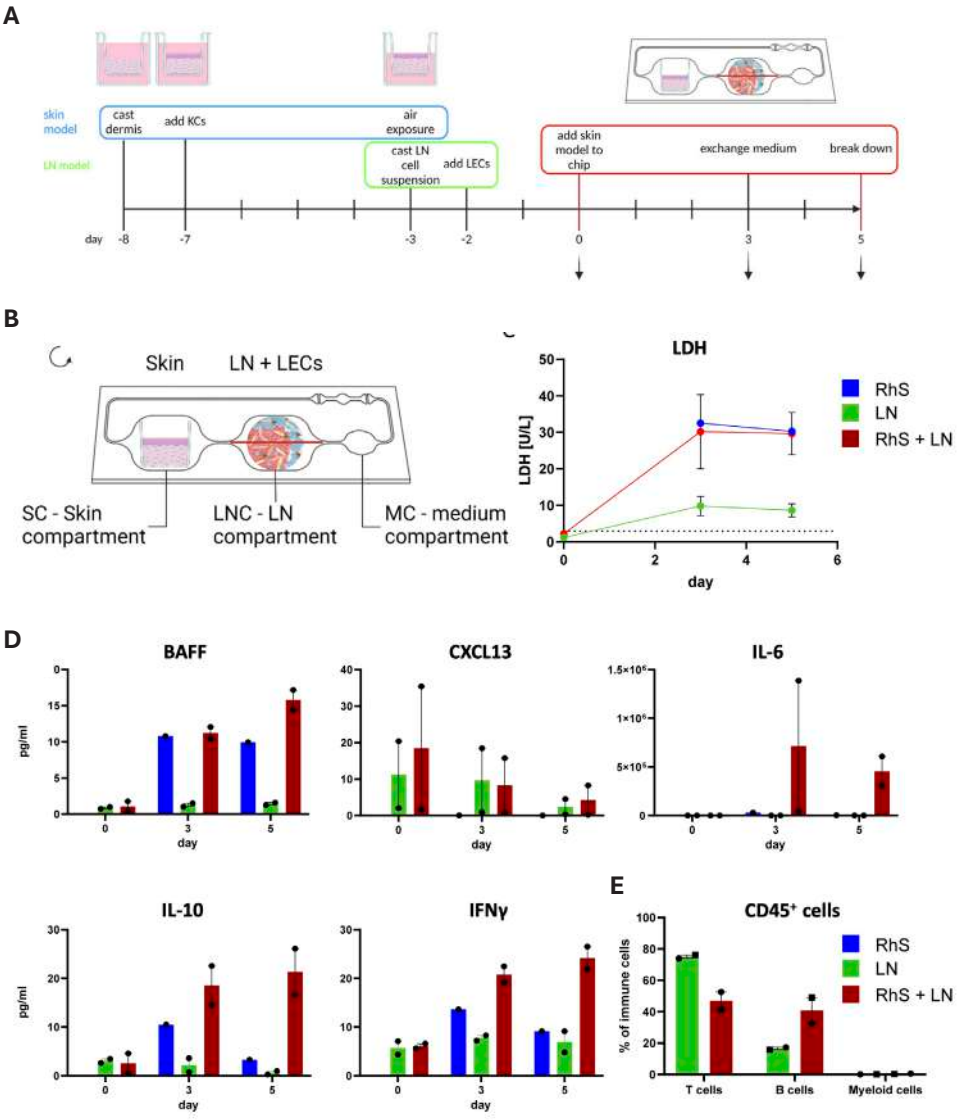

Fig. 2 - Generation of a skin-LN-on-chip with integrated lymphatics. A. Procedure and timeline of combining the RhS with our LN model on chip. Downward arrows signify supernatant collection and media refreshment. **(B)** Overview of the HUMIMIC Chip3 chip platform and culture compartments, with arrow indicating direction of flow. **(C)** Secretion of LDH in RhS-LN models. Setups include chip models with either RhS only (blue), LN only (green) and RhS + LN (red). Concentrations are an average across all chip compartments. **(D).** Secretome of RhS-LN model over chip culture period. Concentrations are an average across all chip compartments. **(E)** Flow cytometry percentage of immune cells in LN model at the end of chip culture period. All data are mean ± SEM; n = 2 independent LN donors and n = 1 RhS donor. LN; Lymph node, RhS; Reconstructed human skin.

Concluding remarks

In summary, the work presented in this PhD thesis aimed to develop a physiologically relevant model of a stromal-competent human LN *in vitro*. These results have sought to bridge the gaps in OoC LN models such as the lack of LNSCs and native tissue material (**Chapter 2**), and further expanded upon prior knowledge of human FRC subsets (**Chapter 3**). Henceforth, building the foundation of a 3D LN *in vitro* began with a two-cell model comprised of FRCs and DCs (**Chapter 4**), with subsequent immunocompetent evolutions through incorporation of FRCs and LN-derived immune cells in both static (**Chapter 5**) and dynamic environments, including the integration of LN lymphatics (**Chapter 6**). A summarised overview of the LN models presented in this thesis are found in **Table 1** below. The current status of this LN model has shown a multitude of potential, with FRCs and LECs demonstrating their influence for immune cell activity, as well as exhibiting general immune-related functionality. These findings lay the groundwork and are highly applicable for future research into human LN models, but some notable improvements still need to be addressed. These include prolongation of the culture period up to the desired 28 days for translational MPS research[69,70], as well as recapitulation of antigen-specific immune readouts. Moreover, no model to date has demonstrated a full visual reflection of the organisational human LN architecture, which one day could be as groundbreaking as when the structure of DNA was first discovered. Moving forward, exploring combinations of LN-on-chip with other organotypic models will enhance our understanding of tissue-specific immune events in both health and disease[71]. Thereby, creating such a physiological relevant application for studying systemic human immunology will become a major milestone on the human quest for reducing animal experiments and recreating *in vitro* immunity.

Table 1 **Overview of our human LN models.** ECM; extracellular matrix, FRCs; fibroblastic reticular cells, LECs; lymphatic endothelial cells, LN; Lymph node, OoC; Organ-on-chip, 3D; three-dimensional.

Complexity	Model	Features	Source	Limitations
3D cultures	FRCs + DCs (**Chapter 4**)	FRCs promote DC survival, and influence their proliferation and differentiation	Liver LNs	No adaptive immune cells Static
	LN model (**Chapter 5**)	FRCs enriched in LN model promote B cell survival and immune factors FRCs restrict T cell proliferation	Liver LNs	Only cell-mediated immune responses Static
Full LN OoC	LN-on-chip with lymphatics (**Chapter 6**)	LEC-populated vessel enhances a migratory LN-like microenvironment LECs promote immune cell numbers and clustering	Liver LNs	No functional adaptive immune responses

References

[1] Marx, U. *et al.* Biology-inspired microphysiological systems to advance patient benefit and animal welfare in drug development. *ALTEX* 37, 365-394 (2020). https://doi.org/10.14573/altex.2001241

[2] Pamies, D. *et al.* Recommendations on fit-for-purpose criteria to establish quality management for microphysiological systems and for monitoring their reproducibility. *Stem Cell Reports* 19, 604-617 (2024). https://doi.org/10.1016/j.stemcr.2024.03.009

[3] Morrison, A. I. *et al.* An Organotypic Human Lymph Node Model Reveals the Importance of Fibroblastic Reticular Cells for Dendritic Cell Function. *Tissue Eng Regen Med* 21, 455-471 (2024). https://doi.org/10.1007/s13770-023-00609-x

[4] Braham, M. V. J. *et al.* A synthetic human 3D in vitro lymphoid model enhancing B-cell survival and functional differentiation. *iScience* 26, 105741 (2023). https://doi.org/10.1016/j.isci.2022.105741

[5] Birmingham, K. G. *et al.* Lymph Node Subcapsular Sinus Microenvironment-On-A-Chip Modeling Shear Flow Relevant to Lymphatic Metastasis and Immune Cell Homing. *iScience* 23, 101751 (2020). https://doi.org/10.1016/j.isci.2020.101751

[6] Wagar, L. E. *et al.* Modeling human adaptive immune responses with tonsil organoids. *Nat Med* 27, 125-135 (2021). https://doi.org/10.1038/s41591-020-01145-0

[7] Krishnamurty, A. T. & Turley, S. J. Lymph node stromal cells: cartographers of the immune system. *Nat Immunol* 21, 369-380 (2020). https://doi.org/10.1038/s41590-020-0635-3

[8] Van den Broeck, W., Derore, A. & Simoens, P. Anatomy and nomenclature of murine lymph nodes: Descriptive study and nomenclatory standardization in BALB/cAnNCrl mice. *J Immunol Methods* 312, 12-19 (2006). https://doi.org/10.1016/j.jim.2006.01.022

[9] Hoorweg, K. & Cupedo, T. Development of human lymph nodes and Peyer's patches. *Semin Immunol* 20, 164-170 (2008). https://doi.org/10.1016/j.smim.2008.02.003

[10] Santambrogio, L. *Immunology of the Lymphatic System*. (Springer New York, NY).

[11] Rodda, L. B. *et al.* Single-Cell RNA Sequencing of Lymph Node Stromal Cells Reveals Niche-Associated Heterogeneity. *Immunity* 48, 1014-1028 e1016 (2018). https://doi.org/10.1016/j.immuni.2018.04.006

[12] Kapoor, V. N. *et al.* Gremlin 1(+) fibroblastic niche maintains dendritic cell homeostasis in lymphoid tissues. *Nat Immunol* 22, 571-585 (2021). https://doi.org/10.1038/s41590-021-00920-6

[13] Grasso, C. *et al.* Identification and mapping of human lymph node stromal cell subsets by combining single-cell RNA sequencing with spatial transcriptomics. *bioRxiv*, 2023.2008.2018.553530 (2023). https://doi.org/10.1101/2023.08.18.553530

[14] Abe, Y. *et al.* A single-cell atlas of non-haematopoietic cells in human lymph nodes and lymphoma reveals a landscape of stromal remodelling. *Nat Cell Biol* 24, 565-578 (2022). https://doi.org/10.1038/s41556-022-00866-3

[15] Eom, J. *et al.* Distinctive Subpopulations of Stromal Cells Are Present in Human Lymph Nodes Infiltrated with Melanoma. *Cancer Immunol Res* 8, 990-1003 (2020). https://doi.org/10.1158/2326-6066.CIR-19-0796

[16] Knoblich, K. *et al.* The human lymph node microenvironment unilaterally regulates T-cell activation and differentiation. *PLoS Biol* 16, e2005046 (2018). https://doi.org/10.1371/journal.pbio.2005046

[17] Severino, P. *et al.* Human Lymph Node-Derived Fibroblastic and Double-Negative Reticular Cells Alter Their Chemokines and Cytokines Expression Profile Following Inflammatory Stimuli. *Front Immunol* 8, 141 (2017). https://doi.org/10.3389/fimmu.2017.00141

[18] Roet, J. E. G. *et al.* Human lymph node fibroblastic reticular cells maintain heterogeneous characteristics in culture. *iScience* 27, 110179 (2024). https://doi.org/10.1016/j.isci.2024.110179

[19] Park, S. M. *et al.* Sphingosine-1-phosphate lyase is expressed by CD68+ cells on the parenchymal side of marginal reticular cells in human lymph nodes. *Eur J Immunol* 44, 2425-2436 (2014). https://doi.org/10.1002/eji.201344158

[20] Fletcher, A. L., Acton, S. E. & Knoblich, K. Lymph node fibroblastic reticular cells in health and disease. *Nat Rev Immunol* 15, 350-361 (2015). https://doi.org/10.1038/nri3846

[21] Denton, A. E., Roberts, E. W., Linterman, M. A. & Fearon, D. T. Fibroblastic reticular cells of the lymph node are required for retention of resting but not activated CD8+ T cells. *Proc Natl Acad Sci U S A* 111, 12139-12144 (2014). https://doi.org/10.1073/pnas.1412910111

[22] Khan, O. *et al.* Regulation of T cell priming by lymphoid stroma. *PLoS One* 6, e26138 (2011). https://doi.org/10.1371/journal.pone.0026138

[23] Siegert, S. *et al.* Fibroblastic reticular cells from lymph nodes attenuate T cell expansion by producing nitric oxide. *PLoS One* 6, e27618 (2011). https://doi.org/10.1371/journal.pone.0027618

[24] Lukacs-Kornek, V. *et al.* Regulated release of nitric oxide by nonhematopoietic stroma controls expansion of the activated T cell pool in lymph nodes. *Nat Immunol* 12, 1096-1104 (2011). https://doi.org/10.1038/ni.2112

[25] Angel, C. E. *et al.* Distinctive localization of antigen-presenting cells in human lymph nodes. *Blood* 113, 1257-1267 (2009). https://doi.org/10.1182/blood-2008-06-165266

[26] van Pul, K. M., Fransen, M. F., van de Ven, R. & de Gruijl, T. D. Immunotherapy Goes Local: The Central Role of Lymph Nodes in Driving Tumor Infiltration and Efficacy. *Front Immunol* 12, 643291 (2021). https://doi.org/10.3389/fimmu.2021.643291

[27] Fasnacht, N. *et al.* Specific fibroblastic niches in secondary lymphoid organs orchestrate distinct Notch-regulated immune responses. *J Exp Med* 211, 2265-2279 (2014). https://doi.org/10.1084/jem.20132528

[28] Fletcher, A. L. *et al.* Reproducible isolation of lymph node stromal cells reveals site-dependent differences in fibroblastic reticular cells. *Front Immunol* 2, 35 (2011). https://doi.org/10.3389/fimmu.2011.00035

[29] Sixt, M. *et al.* The conduit system transports soluble antigens from the afferent lymph to resident dendritic cells in the T cell area of the lymph node. *Immunity* 22, 19-29 (2005). https://doi.org/10.1016/j.immuni.2004.11.013

[30] Panocha, D., Roet, J. E. G., Kuipers, J. E., de Winde, C. M. & Mebius, R. E. Lymph node fibroblast-produced extracellular matrix shapes immune function. *Trends Immunol* (2025). https://doi.org/10.1016/j.it.2025.02.002

[31] Takeda, A. *et al.* Single-Cell Survey of Human Lymphatics Unveils Marked Endothelial Cell Heterogeneity and Mechanisms of Homing for Neutrophils. *Immunity* 51, 561-572 e565 (2019). https://doi.org/10.1016/j.immuni.2019.06.027

[32] Kastenschmidt, J. M. *et al.* Influenza vaccine format mediates distinct cellular and antibody responses in human immune organoids. *Immunity* 56, 1910-1926 e1917 (2023). https://doi.org/10.1016/j.immuni.2023.06.019

[33] Kastenschmidt, J. M. *et al.* A human lymphoma organoid model for evaluating and targeting the follicular lymphoma tumor immune microenvironment. *Cell Stem Cell* 31, 410-420 e414 (2024). https://doi.org/10.1016/j.stem.2024.01.012

[34] Mitul, M. T. *et al.* Tissue-specific sex differences in pediatric and adult immune cell composition and function. *Front Immunol* 15, 1373537 (2024). https://doi.org/10.3389/fimmu.2024.1373537

[35] Iliopoulou, M. *et al.* Extracellular matrix rigidity modulates physical properties of subcapsular sinus macrophage-B cell immune synapses. *Biophys J* 123, 2282-2300 (2024). https://doi.org/10.1016/j.bpj.2023.10.010

[36] Song, J. *et al.* Extracellular matrix of secondary lymphoid organs impacts on B-cell fate and survival. *Proc Natl Acad Sci U S A* 110, E2915-2924 (2013). https://doi.org/10.1073/pnas.1218131110

[37] Martinez, V. G. *et al.* Fibroblastic Reticular Cells Control Conduit Matrix Deposition during Lymph Node Expansion. *Cell Rep* 29, 2810-2822 e2815 (2019). https://doi.org/10.1016/j.celrep.2019.10.103

[38] Najibi, A. J. *et al.* Durable lymph-node expansion is associated with the efficacy of therapeutic vaccination.

Nat Biomed Eng 8, 1226-1242 (2024). https://doi.org/10.1038/s41551-024-01209-3

[39] Choi, Y. S. *et al.* Immunomodulatory Scaffolds Derived from Lymph Node Extracellular Matrices. *ACS Appl Mater Interfaces* 13, 14037-14049 (2021). https://doi.org/10.1021/acsami.1c02542

[40] van Tienderen, G. S. *et al.* Modelling metastatic colonization of cholangiocarcinoma organoids in decellularized lung and lymph nodes. *Front Oncol* 12, 1101901 (2022). https://doi.org/10.3389/fonc.2022.1101901

[41] Song, J. *et al.* The extracellular matrix of lymph node reticular fibers modulates follicle border interactions and germinal center formation. *iScience* 26, 106753 (2023). https://doi.org/10.1016/j.isci.2023.106753

[42] Simon, T. *et al.* Differential Regulation of T-cell Immunity and Tolerance by Stromal Laminin Expressed in the Lymph Node. *Transplantation* 103, 2075-2089 (2019). https://doi.org/10.1097/TP.0000000000002774

[43] Ozulumba, T., Montalbine, A. N., Ortiz-Cardenas, J. E. & Pompano, R. R. New tools for immunologists: models of lymph node function from cells to tissues. *Front Immunol* 14, 1183286 (2023). https://doi.org/10.3389/fimmu.2023.1183286

[44] Zhong, Z. *et al.* Human immune organoids to decode B cell response in healthy donors and patients with lymphoma. *Nat Mater* (2024). https://doi.org/10.1038/s41563-024-02037-1

[45] Michielon, E. *et al.* Integration of line-field confocal optical coherence tomography and in situ microenvironmental mapping to investigate the living microenvironment of reconstructed human skin and melanoma models. *J Dermatol Sci* 115, 85-93 (2024). https://doi.org/10.1016/j.jdermsci.2024.07.001

[46] Shou, Y., Johnson, S. C., Quek, Y. J., Li, X. & Tay, A. Integrative lymph node-mimicking models created with biomaterials and computational tools to study the immune system. *Mater Today Bio* 14, 100269 (2022). https://doi.org/10.1016/j.mtbio.2022.100269

[47] Morrison, A. I., Sjoerds, M. J., Vonk, L. A., Gibbs, S. & Koning, J. J. In vitro immunity: an overview of immunocompetent organ-on-chip models. *Front Immunol* 15, 1373186 (2024). https://doi.org/10.3389/fimmu.2024.1373186

[48] Brandtzaeg, P. Potential of nasopharynx-associated lymphoid tissue for vaccine responses in the airways. *Am J Respir Crit Care Med* 183, 1595-1604 (2011). https://doi.org/10.1164/rccm.201011-1783OC

[49] Macpherson, A. J. & Smith, K. Mesenteric lymph nodes at the center of immune anatomy. *J Exp Med* 203, 497-500 (2006). https://doi.org/10.1084/jem.20060227

[50] Zou, M., Wiechers, C. & Huehn, J. Lymph node stromal cell subsets-Emerging specialists for tailored tissue-specific immune responses. *Int J Med Microbiol* 311, 151492 (2021). https://doi.org/10.1016/j.ijmm.2021.151492

[51] Molenaar, R. *et al.* Expression of retinaldehyde dehydrogenase enzymes in mucosal dendritic cells and gut-draining lymph node stromal cells is controlled by dietary vitamin A. *J Immunol* 186, 1934-1942 (2011). https://doi.org/10.4049/jimmunol.1001672

[52] Erkelens, M. N. & Mebius, R. E. Retinoic Acid and Immune Homeostasis: A Balancing Act. *Trends Immunol* 38, 168-180 (2017). https://doi.org/10.1016/j.it.2016.12.006

[53] Koning, J. J. *et al.* Development of follicular dendritic cells in lymph nodes depends on retinoic acid-mediated signaling. *Development* 148 (2021). https://doi.org/10.1242/dev.199713

[54] Bos, A., van Egmond, M. & Mebius, R. The role of retinoic acid in the production of immunoglobulin A. *Mucosal Immunol* 15, 562-572 (2022). https://doi.org/10.1038/s41385-022-00509-8

[55] Mebius, R. E., Brevé, J., Kraal, G. & Streeter, P. R. Developmental regulation of vascular addressin expression: a possible role for site-associated environments. *International Immunology* 5, 443-449 (1993). https://doi.org/10.1093/intimm/5.5.443

[56] Molenaar, R. *et al.* Lymph node stromal cells support dendritic cell-induced gut-homing of T cells. *J Immunol* 183, 6395-6402 (2009). https://doi.org/10.4049/jimmunol.0900311

[57] Mosaad, Y. M. Clinical Role of Human Leukocyte Antigen in Health and Disease. *Scandinavian Journal of Immunology* 82, 283-306 (2015). https://doi.org/https://doi.org/10.1111/sji.12329

[58] Jiang, J. H., Ren, R. T., Cheng, Y. J., Li, X. X. & Zhang, G. R. Immune cells and RBCs derived from human induced pluripotent stem cells: method, progress, prospective challenges. *Front Cell Dev Biol* 11, 1327466 (2023). https://doi.org/10.3389/fcell.2023.1327466

[59] van Pul, K. M. *et al*. Selectively hampered activation of lymph node-resident dendritic cells precedes profound T cell suppression and metastatic spread in the breast cancer sentinel lymph node. *J Immunother Cancer* 7, 133 (2019). https://doi.org/10.1186/s40425-019-0605-1

[60] Goyal, G. *et al*. Ectopic Lymphoid Follicle Formation and Human Seasonal Influenza Vaccination Responses Recapitulated in an Organ-on-a-Chip. *Adv Sci (Weinh)* 9, e2103241 (2022). https://doi.org/10.1002/advs.202103241

[61] Jeger-Madiot, R. *et al*. Modeling memory B cell responses in a lymphoid organ-chip to evaluate mRNA vaccine boosting. *J Exp Med* 221 (2024). https://doi.org/10.1084/jem.20240289

[62] Cimen Bozkus, C., Blazquez, A. B., Enokida, T. & Bhardwaj, N. A T-cell-based immunogenicity protocol for evaluating human antigen-specific responses. *STAR Protoc* 2, 100758 (2021). https://doi.org/10.1016/j.xpro.2021.100758

[63] Kwee, B. J., Mansouri, M., Akue, A. & Sung, K. E. On-chip human lymph node stromal network for evaluating dendritic cell and T-cell trafficking. *Biofabrication* 17 (2024). https://doi.org/10.1088/1758-5090/ad80ce

[64] Hammel, J. H. *et al*. Engineered human lymph node stroma model for examining interstitial fluid flow and T cell egress. *bioRxiv*, 2024.2012.2003.622729 (2024). https://doi.org/10.1101/2024.12.03.622729

[65] Alexaki, V. I. *et al*. B-cell maturation antigen (BCMA) activation exerts specific proinflammatory effects in normal human keratinocytes and is preferentially expressed in inflammatory skin pathologies. *Endocrinology* 153, 739-749 (2012). https://doi.org/10.1210/en.2011-1504

[66] Michielon, E. *et al*. A Reconstructed Human Melanoma-in-Skin Model to Study Immune Modulatory and Angiogenic Mechanisms Facilitating Initial Melanoma Growth and Invasion. *Cancers (Basel)* 15 (2023). https://doi.org/10.3390/cancers15102849

[67] Michielon, E. *et al*. An organotypic human melanoma-in-skin model as an in vitro tool for testing Vgamma9Vdelta2-T cell-based immunotherapy. *Immunooncol Technol* 24, 100724 (2024). https://doi.org/10.1016/j.iotech.2024.100724

[68] Asal, M. *et al*. Integration of Stromal Cells and Hydrogel Below Epithelium Results in Optimal Barrier Properties of Small Intestine Organoid Models. *Biomedicines* 12 (2024). https://doi.org/10.3390/biomedicines12122913

[69] Mastrangeli, M., Millet, S., Orchid Partners, T. & Van den Eijnden-van Raaij, J. Organ-on-chip in development: Towards a roadmap for organs-on-chip. *ALTEX* 36, 650-668 (2019). https://doi.org/10.14573/altex.1908271

[70] Malik, M., Yang, Y., Fathi, P., Mahler, G. J. & Esch, M. B. Critical Considerations for the Design of Multi-Organ Microphysiological Systems (MPS). *Front Cell Dev Biol* 9, 721338 (2021). https://doi.org/10.3389/fcell.2021.721338

[71] Weisberg, S. P., Ural, B. B. & Farber, D. L. Tissue-specific immunity for a changing world. *Cell* 184, 1517-1529 (2021). https://doi.org/10.1016/j.cell.2021.01.042

Appendices

Acknowledgements

Reina, I would like to thank you from the bottom of my heart for all you have done for me over the last few years. I have learnt so much from you - not just from your scientific brilliance, patience, humour and endless citations of papers from memory, but also from who you are as a person and your approach to life. It has shaped and matured me into who I am today, and I am grateful for it. **Sue**, thank you for all you have taught me over the years and allowing me to cement myself into the SkinLab. You have created a wonderful work environment and I appreciate all of the opportunities you have given me - whether that be conference trips, teaching me how to sell my research, keeping projects moving forward, and the annual lab visits to Efteling.

Lotte, I really appreciate all of your efforts that have guided me through my PhD. I think I have learnt more from you than you will ever know. I can now clearly define and address a research hypothesis, defend my work after the times you've played 'Devil's advocate', but most importantly I've learnt from you how to make science more fun! You have such a promising academic career ahead of you, and I can't wait to see it unfold. **Jasper**, aka 'Mr. Microscopy'. Firstly, I'm deeply thankful for you picking me up at the airport on my first day here in NL during COVID times, it feels like a lifetime ago. Thank you for all the wisdom, mentoring and fun you have provided me during my PhD, especially your approval for small office pranks. I enjoyed working with you, even if it was shorter than we had hoped. I'd like to think we are the pioneers of *in vitro* immunity, and wish you all the best for the future!

I'd like to thank my defence committee members, Prof. Dr. **Tanja de Gruijl**, Dr. **Lisa van Baarsen**, Prof. Dr. **Andries van der Meer**, Dr. **Tom Cupedo**, Dr. **Mariateresa Coppola** and Prof. Dr. **Jaap van Buul**, for taking the time to read my thesis. I look forward to our discussion on defence day!

To my PhD room. **Jonas**, JJ, thank you firstly for being my paranymph. I think it was fate that we had our interviews back to back on the same day. Little did I know that we would go on to embrace our PhDs side by side for the next 5 years, which has been an absolute pleasure. Thank you for showing me how to take life less seriously and enjoy the little things. I still can't believe the amount of nonsensical knowledge and inappropriateness you come out with, but I guess it is needed to balance out your intelligence. From international trips, bouncing PhD retreats, and Friday afternoon grafts to get our chip projects on the international stage - it has been a blast, danke schön. **Melis**, my energetic honeybee desk-neighbour. You were my ARCHAID partner, my OurDomain buddy, and the person I was always escaping COVID from. At times I have felt like your guardian, mostly without a choice, but I am proud to see the person you have become today through all of life's challenges. Thanks for always bringing contagious laughter, sharing all the never ending stories, and brightening up the room whenever you walked in, especially after visiting the dentist. I am looking forward to seeing you on a theatre stage again soon, maybe performing Jurassic Park with the lads from Berlin? You are loved, and not just by Oli, teşekkür ederim. **Elisabetta**, the first nickname we gave you was 'sweetheart', and I don't know why it disappeared...maybe when you passively became one of the bro's after we became aware you were not so innocent after all. Either way, I think it still holds true to this day. I owe a lot to you, you showed me the scientific ropes and were always willing to help with anything,

including these beautiful thesis illustrations! Thanks for always being there and having a rational answer to everything (except for your use of commas and American English). You make the most unreal pizza, organise the best social events, and make me feel part of your lovely family too, grazie mille.

To my friends in Group Reina. **Eelco**, one of the good guys! It has been a pleasure spending time with you, hearing stories of your bouldering adventures and watching you make the most audacious group picture for the MCBI calendar. I will miss your delicious brownies. **Mike**, my fellow laddie! I am grateful for your patience with all the times I have pestered you with statistics and R stuff, but I am also grateful to call you a dear friend. Your lab meeting presentations have been majestic, you always make an effort to include everyone, and your performance as a zombie is the best I've ever seen. Please never change! **Ola**, my dear Scottish-adopted expat! I literally can't thank you enough for your support, kindness and the fun times we had together. I don't think I've laughed so hard before in that lab meeting when Francis Bourgeois was brought up. Remember to take it easy (but not with your party costumes), you're one of a kind! **Tanja**, I have never quite met a personality like yours. My first impression of you during my interview was that we were going to have a good time, and boy did you make sure we did! Thanks for your humour, energy and positive outlook on life. I hope my Chippendale picture stays on your locker forever.
Janna, we started our PhD journey together and I wish to thank you for being such a lovely and sweet person. I have thoroughly enjoyed tackling the challenges of working with FRCs alongside you, as well as experiencing our first conferences together and battling the AII PhD Retreat committee when we were exiled for our honesty. If you ever decide to sell your knitting items one day at Pipoos, I will be your first customer! Keep being you. **Daphne**, I first met you as a Master's student and now look at you now, my fellow human LN modeller! We've come a long way, but thanks for being the best taxi driver with the fast food pit stops, all the lad-banter you have provided, and your unwavering support even up until today, I deeply appreciate it. You will go far, DP! **Elham**, I am glad you could be integrated into our group. Thank you for being such a nice person, educating me on B cells, and introducing me to Iranian food. **Kerem**, it was short but sweet, just tone it down with the dangerous homemade experiments, yeh? **Jesse**, it was an honour to supervise and watch you flourish into the friend you are today! **Amelie, Estefany, Eline** and **Catarina,** thank you for welcoming me into the lab and all the help you have provided.

To my friends in SkinLab. **Joline**, you are such a wonderful person! Even though I think the only time we properly worked together was handling the buffy coats, I always enjoyed your company in the lab and learnt so much about Dutch life from you. Being a Runescape girl, you have my uttermost respect, and I'm grateful for you allowing me to join your personal family moments too. **Maria**, you were the one who taught me how to make a hydrogel during the lab fasting competition, which I think went splendidly looking at where we are now, right!? Thanks for being a great teacher, I have learnt a lot about life from you, but also for always being up for a laugh and a prank. Be careful next time you enter any doors in Milan or have an unusual looking tea cup! **Rico**, I was so happy you joined the lab after hearing you supported Ajax during your interview. We have had such great memories in the Arena, and long may it continue! Thanks for being a chill guy, but also for demonstrating the balance between

partying hard and training more...I wish I had your discipline. **Sander**, my mutz maestro! I have to say I have loved hearing your life stories, especially on a Friday afternoon. Your positivity and laughter always makes me smile, and I am indebted to your scientific knowledge. Thank you for always shining brightly. **Sanne**, is there anything you can't do? Thank you for always offering to help with and perform lab work at the highest standard, but an even greater thanks for your post-weekend football analytics. It has been a pleasure and I am especially grateful for you introducing me to football in Friesland. **Taco**, you are a legend, no other words needed. My PhD would not be the same without you, I can't thank you enough for all the experiences and comfort you have provided. Educating me on the history of Dutch football, helping simplify lab experiments, motivating me to take up endurance running, as well as showing me the simple things in life! I'm eternally grateful. **Ibrahim**, the freshest guy I know! Thank you for being so kind, supportive in life decisions, and also having incredible ball-knowledge. The world needs more people like you, and I will miss you. **Lin**, thank you for being so wise and witty, I'm glad our paths crossed along our time at SkinLab. **Yan**, apart from trying to poison me with jelly beans, you have been great fun over the years, thank you.
Britt, my Britty! Your socially welcoming nature to everything in life is so admirable, and it has been an honour to go through my PhD at the same time as you. I appreciate all the Dutch words you have taught me, both good and bad. Thank you for being the light of the party (lowkey ref to the AII retreat fluorochrome party btw), bringing people up when they're down, and for being someone I can speak to about anything. You're a star. **Lisa-Lee**, my fraud of a captain! I'm glad to have experienced many core memories with you; the boating trip, Dam tot Damloop disaster, Amsterdam half-marathon (hopefully soon to be full one) and all the dog picnics. I don't think you realise how funny you are, but thanks for being a great friend! **Joey**, my og bulky boi! A big thank you for all the beer recommendations. I have also enjoyed your dark sense of humour and medical internship stories over the years, if only I still played an instrument we could have slap'd da bass together! **Roland**, my Bumbi! The newest member to the wolf pack, but certainly not the least. Your determination to succeed in life is laudable, which motivates and aligns with my own internal values too. Thanks for always being there, and also for the somewhat nonsense chats too. **Mirthe**, it was a joy to supervise you and your literature review. **Caroline**, **Judith**, **Maaike** and **Stephanie**, thanks for your warm welcomes into the lab, it has been a pleasure to have met you all.

To my ARCAID fellows. **Ana**, thank you señorita for designing this wonderful thesis cover, I love it! I have very much enjoyed our coffee catch ups in the neighbourhood and are glad to have met you, gracias. **Aoife,** my Irish Brexiteer, it has always been a delight spending time with you. Thanks for the fun, home comforts, and solid advice on pretty much all life matters. **Dimitrios**, it was a pleasure discussing football and big CYTOF panels with you. **Giulia,** you are always so bubbly and radiate happiness to everyone, thank you! **Sona,** it has always been an honour to be in your company and to navigate all the unemployment benefits. Thanks for being so lovely! **Utkarsh**, you are such a gentleman and a lucky married man. **Adrian, Agner, Aiarpi, Armando, Chiara, Eva, Fatemeh, Ihsan, Marina, Fatemeh** and **Sofia**, thanks for the ride!

To my friends in MCBI. **Alsya**, you are such an amazing person! I have learnt so much from you and grateful for the moments we spent together, I'd love to collaborate with you again in the future. I also wish for your dear Manchester United to bring you more hope, but not at the expense of Liverpool. **Aru**, thank you for always smiling and being so lovely, every time I see you makes me happy. Your courage to stand up and ask a question at our first NVVI inspired me to believe that I too can do anything. **Celine**, thanks for teaching me how to dance, even if I did not have much say in it. Your friendship has been a delight, and it has been a joy to see the transitional era from your creation of a murder-scene looking bathroom floor into a fit, gezellig stay-at-home girl. **Gizem**, you are so kind and friendly, thanks for making my day better whenever I see you. **Irene**, I think I actually met you on my first day back in summer of 2020. Thanks for all the fun and personal chats. Your fitness accomplishments are incredibly inspiring, and maybe one day I'll join you on that litter picking boat in the North Sea. **Cora**, **Eleonora**, **Leonie**, **Reece**, **Rianne** and **Nadia**, thanks for the laughs you brought to every social event, it was fun!

To my friends. **Aidan**, I am grateful for the day I met you backflipping alone in the corner of ASV. I appreciate your friendship and empathy with PhD life, you're gonna make it dude. Let's do that Hyrox together soon! **Ally**, thank you for all the faith you have put in our friendship. From mini-golf dates to deep life chats, I've cherished every moment of it. **Bea**, I am glad to have met you. You mean a lot to me and are such a strong person. Thanks not only for the continuous fun times but for reminding me to see my own self-worth. **Jackson**, my bro over the pond. Thank you for always making me believe in myself. I will always admire what you do in life, and miss you a lot. **Robbie**, I will always value our friendship since childhood, and wish to thank you for being there for me over the years. **Roberto**, my scouse mate! It has always been a blessing to spend time with you since the first month I arrived in Amsterdam. We've both changed a lot since then, but you make life for the better. **Ryan**, we've had some insane memories over the course of our lives, and I'm deeply grateful for having you as a friend, thank you and mon' the bonnie Scotland. **Sofia**, thank you so much for formatting this thesis, you are a wonderful person!

To my family. **Mum**, thank you for being my rock over the last few years. You gave me the strength and courage to keep going, and I don't know where I'd be without you. **Dad**, your support has been invaluable to me, even if it has come from more or less serious chats. You've taught me patience, and I am proud to be your son. **Stuart**, thank you for being my paranymph. We've both gone through a lot since I started my PhD, yet your ridiculous philosophy to 'wake up and smell the roses' has surprisingly worked for the best. I look up to you, not just from a physical point of view. Thanks for being only a call away, here's to more European football adventures in the future!

This thesis is also dedicated to those I have loved and lost.

Andrew

Curriculum vitae

Andrew Ingram Morrison was born on Tuesday 13th February 1996 in Kirkcaldy, Scotland. His scientific curiosity began one day in a high school biology class where his much valued teacher, Mrs Gordon, informed him that human cells had the ability to talk to each other. Fast forward six years later to 2013, Andrew was enrolled at the University of Aberdeen to study an integrated masters in Immunology and Pharmacology. This five-year degree offered a one-year industrial placement, where Andrew embarked on an adventure to Basel, Switzerland, and joined the lab of Dr. Christine Guntermann at Novartis. His master's thesis focused on developing a cellular assay of the IL-17A signalling pathway that could be used to screen potential drugs for autoimmune diseases.

Upon returning to Aberdeen, he graduated in 2018. This was, of course, endorsed by the legendary Prof. Dr. Steve Tucker, who supervised Andrew in his final degree lab project. This project investigated the glycosylation of POPDC1, a membrane protein that has a role in breast cancer metastasis.
After graduation, Andrew returned to Switzerland, and Novartis in Basel, where he completed a postgraduate internship in the group of Dr. Danilo Guerini. This work uncovered the protein degraders responsible for the anti-cancer drug-induced disappearance of STING, a pleiotropic mediator of inflammation within immune cells.

It was at this point that Andrew decided to pursue a new challenge, a PhD. Embracing his desire to stay abroad, he soon found himself in Amsterdam, The Netherlands, perfectly timed with the outbreak of the COVID-19 pandemic. Andrew started (remotely) his PhD in 2020 under the supervision of Prof. Dr. Reina Mebius and Prof. Dr. Sue Gibbs, where his work aimed to develop a human lymph node-on-chip. The results of this project are described in this thesis, titled "Modelling stromal-competent human lymph nodes *in vitro*".
Andrew is currently employed as a junior PostDoc at Leiden University Medical Centre, where he will continue his lymphoid organ-on-chip work to study nasal vaccines, led by Dr. Mariateresa Coppola under Prof. Dr. Maria Yazdanbakhsh.

List of publications

Andrew I. Morrison, Aleksandra M. Mikula, Sander W. Spiekstra, Michael de Kok, Alsya J. Affandi, Henk P. Roest, Luc J.W. van der Laan, Charlotte M. de Winde, Jasper J. Koning, Susan Gibbs, Reina E. Mebius. An Organotypic Human Lymph Node Model Reveals the Importance of Fibroblastic Reticular Cells for Dendritic Cell Function. Tissue Eng Regen Med 21(3):455-471 (December 2023). DOI: 10.1007/s13770-023-00609-x.

Andrew I. Morrison, Mirthe J. Sjoerds, Leander A. Vonk, Susan Gibbs, Jasper J. Koning. In vitro immunity: an overview of immunocompetent organ-on-chip models. Front Immunol 21:15:1373186 (May 2024). DOI: 10.3389/fimmu.2024.1373186.

Merve Mutlu, Isabel Schmidt, **Andrew I. Morrison**, Benedikt Goretzki, Felix Freuler, Damien Begue, Oliver Simic, Nicolas Pythoud, Erik Ahrne, Sandra Kapps, Susan Roest, Debora Bonenfant, Delphine Jeanpierre, Thi-Thanh-Thao Tran, Rob Maher, Shaojian An, Amandine Rietsch , Florian Nigsch, Andreas Hofmann, John Reece-Hoyes, Christian N. Parker, Danilo Guerini. Small molecule induced STING degradation facilitated by the HECT ligase HERC4. Nat Commun 29;15(1):4584 (May 2024). DOI: 10.1038/s41467-024-48922-w.

Janna E.G. Roet, **Andrew I. Morrison**, Aleksandra M. Mikula, Michael de Kok, Daphne Panocha, Henk P. Roest, Luc J.W. van der Laan, Charlotte M. de Winde, Reina E. Mebius. Human lymph node fibroblastic reticular cells maintain heterogeneous characteristics in culture. iScience. 27(7):110179 (June 2024). DOI: 10.1016/j.isci.2024.110179.

Jonas Jäger, Phil Berger, **Andrew I. Morrison**, Hendrik Erfurth, Maria Thon, Eva-Maria Dehne, Susan Gibbs, Jasper J. Koning. A Sacrificial 3D Printed Vessel-on-Chip Demonstrates a Versatile Approach to Model Connective Tissue Pathology. BioRxiv (February 2025). DOI: 10.1101/2025.02.06.636821.

Andrew I. Morrison, Jonas Jäger, Charlotte M. de Winde, Henk P. Roest, Luc J.W. van der Laan, Susan Gibbs, Jasper J. Koning, Reina E. Mebius. Integration of lymphatic vasculature to a human lymph node-on-chip enhances physiological immune properties. BioRxiv (March 2025). DOI: 10.1101/2025.03.20.644364

Andrew I. Morrison, Jesse E. Kuipers, Henk P. Roest, Luc J.W. van der Laan, Charlotte M. de Winde, Jasper J. Koning, Susan Gibbs, Reina E. Mebius. Functional organotypic human lymph node model with native immune cells benefits from fibroblastic reticular cell enrichment. Scientific Reports. 10;15(1):12233 (April 2025). DOI: 10.1038/s41598-025-95031-9.